Ministry of Sciences and Higher Education of the Russian Federation
Russian Academy of Sciences,
Department of Nanotechnologies and Information Technologies
Scientific Council of the DNIT RAS
"Fundamentals of Hardware Components for Computing and Control Systems and Related Materials"
Valiev Institute of Physics and Technology of the Russian Academy of Sciences

Proceedings of the International Conference «MICRO- AND NANOELECTRONICS – 2021» ICMNE – 2021

Book of Abstracts

October 4–8, 2021
Moscow – Zvenigorod, Russia

MAKS PRESS

MOSCOW – 2021

УДК 621
ББК 32.85
М59

Под редакцией:
В. Ф. Лукичева, чл.-корр. РАН;
К. В. Руденко, д-р физ.-мат. наук

Составитель:
В. П. Кудря, канд. физ.-мат. наук

Микро- и наноэлектроника – 2021: Труды международной конференции (4–8 октября,
М59 2021, г. Звенигород, РФ): Сборник тезисов / Под ред. В. Ф. Лукичева, К. В. Руденко; сост. В. П. Кудря. – Москва : МАКС Пресс, 2021. – 214 с.
ISBN 978-5-317-06675-8
https://doi.org/10.29003/m2433.ICMNE-2021

Сборник содержит тезисы докладов, представленных на Международной конференции «Микро- и наноэлектроника – 2021» (ICMNE-2021), включающая расширенную сессию «Квантовая информатика» (QI-2021). Тематика конференции охватывает большинство областей физики микро- и наноразмерных приборов, а также микро- и наноэлектронных технологий, и концентрируется на освещении последних достижений в этой сфере. Она продолжает серию всероссийских (с 1994 года) и международных конференций (с 2003 года).

Ключевые слова: нанотранзисторы, затворные стеки, квантовые компьютеры, МЭМС, магнитные материалы, оптоэлектроника.

УДК 621
ББК 32.85

Micro- and Nanoelectronics – 2021: Proceedings of the International Conference (October 4–8, 2021, Zvenigorod, Russia): Book of Abstracts / Ed. by V. F. Lukichev and K. V. Rudenko. Compiler V. P. Kudrya. – Moscow : MAKS Press, 2021. – 214 p.
ISBN 978-5-317-06675-8
https://doi.org/10.29003/m2433.ICMNE-2021

The Book of Abstracts contains the abstracts of the papers presented at the biannual International Conference “Micro- and Nanoelectronics – 2021” (ICMNE-2021) including the extended Session “Quantum Informatics” (QI-2021). The Conference topics cover the most of the areas dedicated to the physics of integrated micro- and nanoelectronic devices and related micro- and nanotechnologies. The Conference is focused on recent progress in those areas. It continues the series of the AllRussian Conferences (since 1994) and the International Conferences (since 2003).

Keywords: nanoscale transistors, gate stacks, quantum computers, MEMS, magnetic materials,optoelectronics.

ISBN 978-5-317-06675-8

OXFORD INSTRUMENTS

Oxford Instruments Plasma Technology

Process tools and leading-edge processes for the precise, controllable and repeatable etching, deposition and growth of micro- and nano-structures

ALE
Atomic Layer Etching

ALD
Atomic Layer Deposition

CNT

CVD
Chemical Vapour Deposition

ICP CVD

Bosch

RIE
Reactive Ion Etching

IBE
Ion Beam Etching

ICP RIE

IBD
Ion Beam Deposition

PECVD

DSE

TechnoInfo

Your partner in nanoscience research

Crestec Corporation CRESTEC

Advanced technologies in electron beam lithography and unique solutions

CABL-AP / CABL-UH

High resolution nanolithography systems

- acceleration voltage up to **130 kV**
- minimum line width is **5 nm**
- beam diameter < **1,6 nm**
- wafer diameter up to **200 мм**
- **TFE** electron emitter **(ZrO/W)**
- single-stage acceleration capability up to 130kV to minimize EOC size
- field sizes 30um, 60um, 120um, 300um, 600um, 1000um, 1500 um
- ultra-stable write capability is achieved using dual thermal controllers
- Vector scan (R,f) or (x,y)
- Raster scan and Spot scan
- small footprint
- low cost of clean room facilities and ownership

Ion Beam Services

High end equipment for ion beam and plasma immersion ion implantation to both the production and R&D purposes

ibs Innovative Ion Implant

IMC-200, FLEXION 200/400

Ion Beam implantation

- wafer diameter up to **200 mm**
- ion energy up to **1.2 MeV**
- single or multi-charged ions
- beam current up to **3000 uA**
- doses up to **10E18**
- **temperature range -150... 650 C**
- manual or cassette loading

PULSION

Plasma immersion ion implantation

- wafer diameter up to **460 mm**
- ion energy **from 30 eV to 30 KeV**
- current up to **300 uA**
- conformal 3D implantation
- simultaneous implantation of the full wafer
- manual or cassette loading

- more than **60 species** are available for implantat

www.technoinfo.ru / sales@technoinfo.ru / +7(499) 270-66-26

Technoinfo Ltd.
Official distributor of Thermo Fischer Scientific
in Russia and CIS

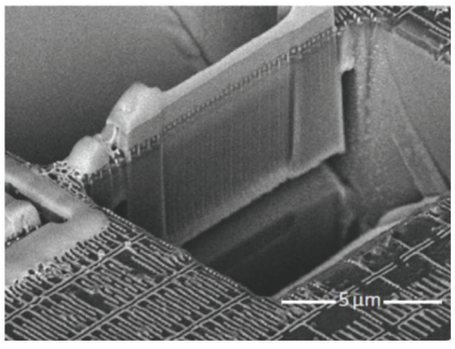

Helios DualBeam fully automated lamella preparation with AutoTEM 5 software, including unattended lift-out, transfer to TEM grid, and final thinning down to 15 nm.

The latest Thermo Fisher Scientific electron microscopy technological innovations for micro- and nanoelectronics.

Scientists and engineers constantly face new challenges that require highly localized characterization of increasingly complex samples with ever smaller features. The latest technological innovations of Thermo Fisher Scientific's DualBeam™ and TEM microscopes, in combination with the easiest to use, most comprehensive software and application expertise, allow for the fastest and easiest preparation and investigation of HR-S/TEM samples for a wide range of materials as well as high resolution artefact-free large volume 3D imaging and analysis.

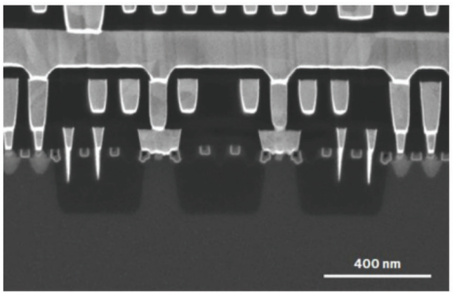

Thermo Fisher Scientific advanced focused ion beam technology allows for precise high-resolution cross-sectioning and imaging with superior material contrast.

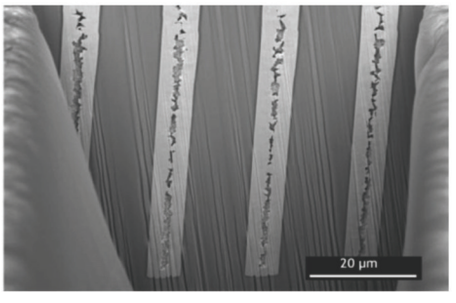

TSV large area cross section Ga-FIB: 65 nA, 4 hours, no polishing.

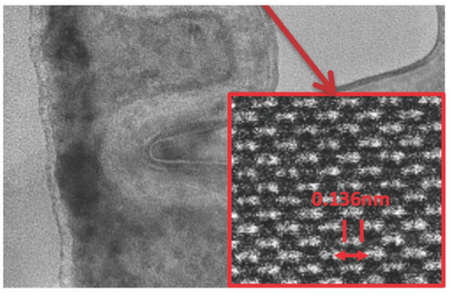

HRTEM large field of view image of transistor device. The inserts show Si dumbbells resolved in 110 orientation. Thermo Fisher Scientific Talos F200X with standard Ceta 16Mpx CMOS-camera.

SCANNING ELECTRON MICROSCOPES

- Axia
- Prisma
- Apreo 2
- Verios 5

DUALBEAM MICROSCOPES

- Scios 2
- Helios 5
- Helios Hydra
- Helios Laser FIB/Plasma FIB

TRANSMISSION ELECTRON MICROSCOPES

- Talos F200 i/E/X
- Spectra 200/300/Ultra
- Metrios AX

www.technoinfo.ru

Technoinfo Ltd.
9 b2a Kutuzovsky prt, off 77
Moscow, Russia 121248

НИКС
КОМПЬЮТЕРНАЯ КОМПАНИЯ

БИЗНЕС, ОСНОВАННЫЙ НА НАУЧНОМ ПОДХОДЕ

Спонсор конференций ICMNE2003, Qi2004, ICMNE2005, 2007, 2009, 2012, 2014, 2016, 2018

Год основания: **1991**

Профиль: **компьютеры,**
- комплектующие,
- программное обеспечение,
- бизнес-анализ

Учредители: **выпускники МФТИ**

Сотрудники: **600 человек,**
- из них 20% выпускников МФТИ и других физико-математических вузов России

Годовой оборот: **$80млн**

Сайт: www.nix.ru
- **150 тыс. уникальных посетителей в день**

Компьютерный супермаркет НИКС в рамках собственного проекта NANOSOFT® занимается всесторонней поддержкой российской науки и образования, исследований в области квантовой информатики. На гранты нашей компании многие талантливые студенты, преподаватели и российские учёные смогли успешно развивать свою научную деятельность.

NANOSOFT.RU

ваш шанс на прорыв в будущее

Nanosoft® - собственная программа Компьютерного супермаркета НИКС по поддержке российских ученых, занимающихся теоретическими и экспериментальными исследованиями квантовых приборов и нанотехнологий.

http://www.nanosoft.ru, science@nix.ru

TABLE OF CONTENTS

How to search for necessary abstract?

Every Abstract has its own identification number (for instance, L1-04, O1-07, P2-28, and so on), which is printed at the page bottom. This number corresponds to the one in the *Conference Programme*. If you do not know the number of the paper, but know at least one of the authors it is possible to find the Abstract using the *Author Index* located in the end of the *Book of Abstracts*.

Как отыскать интересующие Вас тезисы доклада?

Каждый доклад имеет собственный идентификационный номер (например, L1-04, O1-07, P2-28 и т.д.), который указан внизу страницы. Этот номер совпадает с номером, присвоенным докладу в *Программе конференции*. Если Вы не знаете номера доклада, но Вам известен хотя бы один из авторов, вы можете воспользоваться *Авторским указателем*, расположенным в конце *Сборника тезисов.*

Nanoelectronic devices for the ultimate integration of ICs with high performance and very low power consumption

Francis Balestra
Univ. Grenoble Alpes, CNRS, Grenoble INP, IMEP-LAHC, 38000 Grenoble, France

Micro-andNano-electronics have made dramaticprogress in the last decades. However, we face significant issues of increased power consumption and heating, performance saturation, high variability, and reliability. In this respect, new devices using innovative materials, circuit design techniques and system architecturescould offer solutions for substantial technological advances and performance over the coming decades.

This paper presents promising solutions in the CMOS and Beyond-CMOS fields. For NanoCMOS, MultiGate devices could affordhigherperformance and lowerpower logic applications, using advanced materials such as 1D or 2D structures, andmaterial substitution to avoid those critical for sustainable electronics.

Beyond-CMOS solutions could be needed in the next decades, especially for ultra-low powerand autonomous applications, and integrated infuture Nanosystemswith increased functionalities. In this regard, small slope switchescould allow to go beyond CMOS performance, for instance using tunnel transport with alternative materials, or Negative Capacitance FETs, or hetero-and hybrid-structures (TFET/NCFET, FET with phase change materials or nanofilaments, multi-materials, etc.) [1-20].

Wealsoneed disruptive materials and devices for brain-inspired computingschemes, which could allow to reduce substantially energy and area of future ICs for a number of artificial intelligence applications.

These disruptive concepts will be able to reach the ambitious targets of the IRDS Roadmap for the next 2 decades [21].

1. F. Balestra, Nanoscale CMOS: Innovative Materials, Modeling and Characterization, Francis Balestra Ed., ISTE-Wiley (2010).
2. F. Balestra, Beyond CMOS Nanodevices (tomes 1 & 2), Francis Balestra Ed., ISTE-Wiley (2014).
3. F. Balestra, Challenges for high performance and very low power operation at the end of the Roadmap, Solid-State Electronics, Volume 155, May 2019, pp. 27-31.
4. F. Balestra, Tunnel FETs for ultra low Power Nanoscale Devices, ISTE Open Science, Nanoelectronic Devices, Volume 18- 1, DOI : 10.21494/ISTE.OP.2018.0219.
5. F. Balestra, Challenges to Nano-scale Device World, ECS Transactions 66(5): 211-222, 2015.
6. F. Balestra, Advanced technologies for future materials and devices, Chapter in Springer Handbook of Semiconductor Devices, to be published, 2021.
7. F. Andrieu, Proc. Symp. of VLSI Technology (2010).
8. F. Balestra, Double-gate silicon-on-insulator transistor with volume inversion: A new device with greatly enhanced performance, IEEE Electron Dev. Lett., EDL-8: 410 (1987).
9. E. Rauly, Solid-State Electronics 43, p. 2033 (1999).
10. S.B. Deasy et al, Science, Vol. 354, Issue 6308, pp. 99-102, 2016.
11. W. Chung, IEDM 2017, p. 365.
12. A. Saeidi, IEEE EDL, VOL. 38, No. 10, p.1487, Oct. 2017.
13. M.H. Lee, IEDM 2018, p. 735.
14. Z. Yu, IEDM 2018, p. 524.
15. A. Saeidi, IEDM 2018, p. 304.
16. E.A. Casu., IEDM 2016, p. 19.3.1.
17. S. Lim, IEDM 16, p. 34.7.1.
18. C.-H. Yeh et al, IEDM 2019.
19. W. Cao, IDEM 2014.
20. Asselberghs, IEDM 2020.
21. International Roadmap for Devices and Systems, 2021.

SoC edge node devices combining SOI CMOS and sensors

Yakov Roizin
Tower Semiconductor, Migdal HaEmek, Israel, yakovro@towersemi.com

Embedded sensors of different types, such as sensors of UVC (<280nm) radiation, LWIR (long wave infra-red) thermometers, smart gas sensors and BioFets are becoming increasingly ubiquitous in different emerging applications, and, in particular, those sparked by Covid-19 pandemic. Tower Semiconductor RF SOI CMOS platform is used in high volume manufacturing of products requiring efficient isolation, such as cellular switches and low-noise amplifiers. In addition to active devices on fully depleted or partially depleted SOI, the process options include silicided and unsilicided polysilicon resistors, metal-insulator-metal capacitors and low loss inductors with thick Al and Cu layers. In combination with MEMS elements and wafer bonding, the RF SOI CMOS platform can be efficiently used for the development of novel sensors. Examples of the developed devices are discussed in the presentation.

UVC sanitizers killing SARS-CoV-2 viruses became popular for disinfecting the cabins of airplanes and cars and are already used by several airline and car rental companies. Such systems require UVC sensors for the control of sterilization efficiency and safety. A promising approach in the design of UVC sensors is using silicon detection layers with thicknesses of hundreds of Angstroms. UV component of light is efficiently absorbed in the thin silicon of SOI, while the device layers are almost transparent to visible and IR light. We suggested several novel UV sensors having high responsivity in UVC but not sensitive to UVB/ UVA/VIS/IR. The developed sensors comprise strings of connected in series sensitive vertical p-n junctions. The generated voltage can reach tens of volts under UV irradiation, while the footprint of devices is small. Further innovation is differential circuits that employ sensors with and without polysilicon filters absorbing UVC part of radiation. In combination with UVC transparent inter-metal and passivation dielectrics, high sensitivity and selectivity to UVC is achieved.

The small-size LWIR sensors for application as body thermometers in ultra-thin mobile devices are fabricated by bonding a SOI wafer with sensors on the membrane and a dummy wafer. Strings of serially connection vertical diodes are used in this design as linear temperature sensitive elements. The hollow for thermal isolation under the membrane at the SOI wafer is formed by an original dry etching technology. The dummy wafer contains a hollow from the opposite side of the membrane. An identical string of diodes on the bulk part of the SOI acts as a reference element. The bonded wafers are thinned and the remaining silicon bulk is used as a filter for blocking visible and UV radiation in temperature measurements.

The same basic RF SOI technology allows to fabricate sensors with open surfaces for gas and liquids sensing. The surface is covered by ~40A thermal dioxide and can be functionalized with different receptors, depending on the tested analyzes, e.g. viral RNA or host antibody proteins in liquids, or receptors interacting with specific volatile organic compounds. The developed devices employ the principle of junction field effect transistor. Applying voltage to the side gates allows to decrease the width of the conducting channel in the device layer of SOI to a level when this channel can be considered an electrically formed nanowire (EFN). The device works in the subthreshold region and is thus extremely sensitive to the value of the electrical potential at its open surface. The EFN channel can be confined at a distance from the top and bottom surfaces of the SOI silicon layer. Thus, noises connected with traps at the device level surfaces are significantly reduced, resulting in increased sensitivity.

An important feature of the discussed embedded sensor platforms is the possibility to design IP blocks with artificial intelligence (AI). Floating gate non-volatile memory cells originally designed for digital data storage, were converted into two-terminal analog devices operated in the energy-efficient sub-threshold regime. In comparison with other memories targeting AI applications, the developed memristors are fabricated within the commercial CMOS technology with enhanced reliability. The analog memristors are tuned using optimized switching voltages and times to achieve 65 discrete resistive levels. AI enabled edge devices with IP blocks for initial signal processing and communication allow to meet aggressive power consumption and cost requirements of the modern sensor systems.

Advanced Modeling of Emerging MRAM: From Finite Element Methods to Machine Learning Approaches

J. Ender[1,2], S. Fiorentini[1], R.L. de Orio[2], T. Hadámek[1], M. Bendra[1,2], W. Goes[3], S. Selberherr[2], V. Sverdlov[1,2]

1. Christian Doppler Laboratory for Nonvolatile Magnetoresistive Memory and Logic at the
2. Institute for Microelectronics, TU Wien, Gußhausstr. 27-29, 1040 Vienna, Austria
3. Silvaco Europe, Cambridge, United Kingdom, E-Mail: {sverdlov}@iue.tuwien.ac.at

Emerging magnetoresistive random access memories (MRAM) are nonvolatile and offer high speed and endurance. They are promising for stand-alone and embedded applications in the automotive industry, microcontrollers, internet of things, frame buffer memory, and slow SRAM. The MRAM cell usually includes a CoFeB reference layer (RL) and a free magnetic layer (FL), separated by an MgO tunnel barrier (TB). To increase the interface-induced perpendicular magnetic anisotropy, the FL is capped with a second MgO layer. Making the FL composed of several pieces separated by MgO layers further increases the perpendicular anisotropy. To benefit from the shape anisotropy and to increase the perpendicular anisotropy even further, the FL is elongated along the easy axis [1]. This allows to reduce the cell diameter to just 2.3 nm, which makes shape-anisotropy MRAM cells promising for ultra-dense memory applications.

To design ultra-scaled MRAM cells it is necessary to accurately model the torques acting on the textured magnetization in elongated composite magnetic layers with several MgO inclusions between the parts. The magnetization dynamics are then governed by the Landau-Lifshitz-Gilbert (LLG) equation supplemented with the corresponding torques. The torques are determined by the electric current generated nonequilibrium spin accumulation which depends on the magnetization. Therefore, the LLG and the spin-charge transport equations are coupled and must be solved self-consistently. To solve numerically this coupled system of partial differential equations, we use the finite element method (FEM). We implemented the solver with open-source C++ FEM libraries.

The computationally most expensive part is the demagnetizing field calculation which is performed by a hybrid finite element-boundary element method. This restricts the computational domain to ferromagnets only. Advanced compression algorithms for large, dense matrices are used to optimize the performance of the demagnetizing field calculations in complex structures [2]. To evaluate the torques acting on the magnetization, we employ the drift-diffusion approach for coupled spin and charge transport commonly applied in nanoscale metallic spin valves. For the computations of the torques acting in a magnetic tunnel junction (MTJ), an essential part of the cell of modern spin-transfer torque memories, we introduced a magnetization-dependent resistivity of the TB [3]. We investigated the dependence of the resulting torques on system parameters and show that this approach produces the torque magnitude expected in MTJs. We showed that a full three-dimensional solution of the equations is necessary to accurately model the torques acting on the magnetization. The use of a unique set of equations for the whole memory cell, including the FL, RL, contacts, and the TB, constitutes the advantage of our approach to rigorously describe the switching process of nonvolatile spin-transfer torque memories [4]. We also investigated the temperature at the free layer (FL) during switching. To incorporate the temperature increase due to the electric current, we solve the heat transport equation coupled to the electron, spin, and magnetization dynamics, and we demonstrated that the FL temperature is highly inhomogeneous due to a non-uniform magnetization of the FL during switching [5].

Spin-orbit torque (SOT) MRAM is fast-switching and thus well suitable for caches. By means of micromagnetic simulations we demonstrated the purely electrical switching of a perpendicular FL by the SOTs created by two orthogonal short current pulses. The second, reduced current pulse can be applied to many cells in an array, while maintaining deterministic switching [6]. To further optimize the pulse sequence, we used a machine learning approach based on reinforcement learning [7]. We demonstrated that a neural network trained on a fixed material parameter set optimally applies pulses and achieves switching for a wide range of material parameter variations as well as for sub-critical current values of the first pulse and second pulse.

1. B. Jinnai *et al., Proc. of the IEDM,* pp. 24.6.1-24.6.4 (2020).
2. J. Ender *et al., Proc. SISPAD,* pp. 213-2016 (2020).
3. S. Fiorentini *et al. , Solid-State Electron. ,* **186**, p. 108103 (2021).
4. S. Fiorentini *et al., 2021 SISPAD,* accepted (2021).
5. T. Hadámek *et al., 2021 EUROSOI-ULIS,* accepted (2021).
6. R. Orio *et al., Solid-State Electron.,* **185**, p. 108075 (2021).
7. J. Ender *et al., 2021 SISPAD,* accepted (2021).

Ion-based quantum computations: from single- to muli-qubit systems

N. Kolachevsky
P.N. Lebedev Physical Institute of Russian Academy of Sciences, Leninsly prosp. 53, Moscow, Russia

One of the mainstreams of today's quantum technologies is the development of quantum computers and corresponding computational methods. First prototypes based on multiple entangled two-level quantum systems (qubits) already demonstrate certain advantages over classical digital computers in performing several specific algorithms. A quantum two-level system, being the basic unit of a quantum computer, can be implemented by different physical methods. Among the most developed ones are superconducting junctions, ions, neutral atoms, and photon states. In this talk I will focus on the ion-based platform which possesses the longest qubit coherence times [1], high qubit state preparation and readout fidelities [2], as well as high fidelity of quantum gates [3]. Today ion quantum computers have won leadership in the quantum volume parameter, which jointly characterizes the number of qubits and the fidelity of operations.

We discuss the methods of trapping and cooling of ion chains, as well as encoding of quantum information in electronic states of the ion. One of the cornerstones of quantum computation is implementation of two-qubit gates. The entanglement of ions can be performed via common quantized vibrational modes in the parabolic potential of the Paul trap. The size of the quantum register based on this architecture demonstrated to-the-date is of 53 qubits [15]. Significant results in this field are achieved also by the industrial giant Honeywell.

One of the projects of "Leading Research Centers" in Russia is focused on development of a 5-qubit ion processor based on $^{171}Yb^{+}$ ions and a corresponding software platform for quantum computing. We will discuss current progress, namely ion state manipulation and readout, single-qubit operations [5], as well as some ideas how to scale up the ion quantum computer and increase the rate and fidelity of operations.

Research is supported by the Leading Research Center on Quantum Computing (Agreement # 014/20).

1. Wang Y., Um M., Zhang J. et al. Nature Photonics, **11**, 646, 2017.
2. Harty T.P., Allcock D.T.C., Ballance et al. Phys. Rev. Lett., **113**, 220501, 2014.
3. Gaebler J.P., Tan T.R., Lin Y. et al. Phys. Rev. Lett., **117**, 060505, 2016.
4. Zhang J., Pagano G., Hess P.W. et al. Nature, **551** (7682), 601-604, 2017.
5. Zalivako I.V., Semerikov I.A., Borisenko A.S. et al. JETP Letters, **114** (2), 53, 2021.

Towards quantum computation and simulations with single rubidium Rydberg atoms in an array of optical dipole traps

I.I. Ryabtsev[1,2], I.I. Beterov[1,2], E.A. Yakshina[1,2], D.B. Tretyakov[1,2], V.M. Entin[1,2], N.V. Alyanova[2], K.Yu. Mityanin[2], I.N. Ashkarin[1,2], K.-L. Pham[3], S. Lepoutre[3], P. Pillet[3], P. Cheinet[3]

1. Rzhanov Institute of Semiconductor Physics, Novosibirsk, Russia, E-mail address: ryabtsev@isp.nsc.ru

2. Novosibirsk State University, Novosibirsk, Russia

3. Laboratoire Aime Cotton, CNRS, Univ. Paris-Sud, Universite Paris-Saclay, Orsay, France

Single neutral atoms trapped in arrays of optical dipole traps are perspective variant of implementing quantum computation and simulations [1, 2]. In the case of alkali-metal atoms, the two working levels of a qubit are two hyperfine sublevels of the ground state. Their initialization is obtained by optical pumping, and one-qubit gates are realized with individually-addressed Raman or microwave transitions between two levels. Entangled states and two-qubit gates can be generated using a temporary excitation of ground-state atoms to a strongly interacting Rydberg state. In this talk, we will present our recent experimental results on implementing one-qubit gates for two Rb atoms in two traps and theoretical results on a new scheme of three-qubit Toffoli gate based on a three-body Förster resonance of a new kind. Both results are aimed at quantum information processing with neutral atoms.

First, we report the results of experiments on implementing individually addressable one-qubit quantum gates on a microwave transition with two ^{87}Rb atoms in two optical dipole traps [3, 4]. The addressing was carried out using additional focused laser light, which results in a differential light shift of the microwave transition frequency. In the absence of addressing in each of the atoms, Rabi oscillations were obtained on the microwave clock transition $5S_{1/2}$ ($F = 2$, $m_F = 0$) $\rightarrow$ $5S_{1/2}$($F = 1$, $m_F = 0$) between two working levels of qubits with a frequency of up to 5.1 kHz, a contrast up to 98%, and a coherence time up to 4 ms. When addressing was turned on, the probability of a microwave transition in the addressed atom was suppressed to an average value of less than 5%. The Rabi oscillations remaining in the other atom had the same contrast and corresponded to the implementation of individually addressable basic one-qubit quantum operations (Hadamard gate and NOT gate) from different initial states of a qubit with an average fidelity of (92 ± 3) %. After renormalising this fidelity to the error in the preparation and measurement of quantum states of qubits, an estimate of (97 ± 3) % is obtained for the fidelity of individual qubit rotations.

Second, we have performed extended numerical calculations of the new three-body Förster resonance for Rb Rydberg atoms $3\times70P_{3/2}(|M|=1/2)\rightarrow70S_{1/2}+71S_{1/2}+70P_{1/2}$ [5] in the full model, taking into account all the Zeeman sublevels of the Rydberg states, as well as their finite radiation lifetimes. For spatially localized atoms, the calculations predict the presence of population and phase oscillations of collective three-body states. Using them, a new scheme for performing a three-qubit quantum Toffoli gate was developed. The scheme from our previous joint work [6] was taken as a basis. This scheme, however, required laser excitation of three atoms into three different Rydberg states. In the new scheme, all three atoms are excited to the same Rydberg state, which greatly simplifies the experimental implementation. Numerical simulations have shown that the maximum fidelity of the Toffoli gate can reach 98.5%.

This work was supported by the Russia-France cooperation grant ECOMBI (CNRS grant No. PRC2312 and RFBR grant No. 19-52-15010). The Russian team was also supported by the Novosibirsk State University. The French team was also supported by the EU H2020 FET Proactive project RySQ (grant No. 640378).

1. M. Saffman, J. Phys. B, **49**, p. 202001, 2016.
2. I.I. Ryabtsev et al., Physics − Uspekhi **59**, pp. 196-208, 2016.
3. I.I. Beterov et al., JETP **132** (3), pp. 341-353, 2021.
4. I.I. Beterov et al., Quantum Electronics **51** (6), pp. 464-472, 2021.
5. P. Cheinet et al., Quantum Electronics **50** (3), pp. 213-219, 2020.
6. I.I. Beterov et al., Phys. Rev. A **98**, p. 042704, 2018.

Quantum Technologies: State of Art and Prospects

S. Kulik[1, 2]

1. Chair of Quantum Electronics, Faculty of Physics, M.V. Lomonosov State University, 119991, Moscow, Leninskie gory 1, building 35, Russia, sergei.kulik@physics.msu.ru.

2. Quantum Technology Centre of MSU, 119991, Moscow, Leninskie gory 1, building 2, Russia.

The report examines the main trends in the development of end-to-end technology "quantum technologies". The technologies include three sub-technologies: quantum computing, quantum communication, and quantum sensors.

In the Quantum Computing section, the emphasis is placed on physical platforms on the basis of which it is possible to build quantum computing devices. Three out of about a dozen represented in the world are developing in the Russian Federation. These are calculations based on superconducting structures, neutral atoms and ions, and photonic integrated circuits. The two platforms developed at the Center for Quantum Technologies of Moscow State University are discussed in most detail: rubidium atoms in micro-dipole traps and photonic chips.

The section "Quantum Communications" is devoted to the main trends in the development, first of all, of systems of quantum cryptography with an emphasis on network technologies. The technologies for creating completed products such as backbone quantum encoders, quantum telephony systems and atmospheric quantum communications, including space communications are considered in more detail.

The Quantum Sensors section covers about 20 developments in quantum devices that are promising for use in geological exploration, navigation, medicine, and other industries.

The Conclusion presents the conclusions and prospects for the development of the industry.

Many-spin entanglement in multiple quantum NMR in simple spin models

S. Doronin[1], I. Lazarev[1,2], E. Fel'dman[1]
1. Institute of Problems of Chemical Physics of Russian Academy of Sciences, Chernogolovka, Russia, efeldman@icp.ac.ru
2. Faculty of Fundamental Physical-Chemical Engineering, Lomonosov Moscow State-University, Moscow, Russia, the.ilia.lazarev@gmail.com

Entanglement [1] is an important concept in quantum mechanics. In particular, it is responsible for the superiority of quantum computers over their classical counterparts. Quantum superiority [2], recently demonstrated on a programmable superconducting processor, is related to the concept of entanglement, which is absent in classical physics. Pair entanglement is the most familiar while many-particle entanglement is its most general extension.

Multiple quantum (MQ) NMR [3] allows us to clarify deeper connections between MQ coherences and entanglement. Those connections are closely related to the spread of MQ correlations inside a many-spin system in the evolution process. As a result, it is possible to extract information about many-spin entanglement and an entanglement witness from the second moment of the distribution of the intensities of MQ NMR coherences. It is also important that there are relationships between the second moment of MQ NMR coherences on the one hand and the quantum Fisher information [4] and the Wigner-Yanase skew information [5] on the other hand. In particular, it was shown that the second moment of MQ NMR provides a lower bound on the quantum Fisher information [6], and yields the Wigner-Yanase skew information [5]. As a result, it is possible to extract information about the number of entangled spins in the system and even to investigate the dependence of the number of the entangled spins on the temperature [4, 6].

We investigated the dependence of the number of the entangled spins on the temperature in two simple models [5, 7]. The first model is a non-spherical nanopore filled with a gas of spin-carrying atoms (molecules) in a strong external magnetic field [4]. The dipole-dipole interactions (DDIs) of spin-carrying atoms (molecules) do not average out to zero due to molecular diffusion and the residual averaged DDIs are determined by only one coupling constant, which is the same for all pairs of interacting spins. This means that MQ NMR dynamics of such a system can be investigated exactly at arbitrary temperatures. We investigated the number k of the entangled spins and obtained that the system exhibits k-spin entanglement with k growing as the temperature decreases.

We investigated also many-spin entanglement in a zigzag spin chain in MQ NMR [7]. We studied the dependence of many-spin entanglement on the chain length and the temperature. Although entanglement is absent in the initial state of the system, many-spin entanglement emerges in the evolution process.

This work was carried out as a part of the state task (state registration no. AAAA-A19-119071190017-7). The work was also partially supported by the Russian Foundation for Basic Research (project 20-03-00147).

1. M.A. Nielsen, I.L. Chuang. *Quantum Computation and Quantum Information.* Cambridge University Press, Cambridge, 2009.
2. F. Arute, R. Babbush, J.C. Bardin, et al. "Quantum supremacy using a programmable superconducting processor*"*, Nature (London, U.K.), **574**, pp. 505-510, 2019.
3. J. Baum, M. Munovitz, A.N. Garroway, A. Pines. "Multiple-quantum dynamics in solid state NMR". J. Chem. Phys. **83**, pp. 2015-2025, 1985.
4. S. Doronin, E. Fel'dman, I. Lazarev. "Many-particle entanglement in multiple quantum nuclear magnetic resonance spectroscopy ". Phys.Rev. A **100**, 022330, 2019.
5. S. Doronin, E. Fel'dman, I. Lazarev. *"*Multiple quantum NMR in solids as a method of determination of Wigner-Yanase skew information". Phys. Lett. A **406**, 127458, 2021.
6. M. Gartner, P. Hauke, A.M. Rey. "Relating Out-of-Time-Order Correlations to Entanglement via Multiple-Quantum Coherences". Phys. Rev. Lett. **120**, 040402, 2018.
7.G. Bochkin, S. Vasil'ev, S. Doronin, E. Kuznetsova, I. Lazarev,· E. Fel'dman. "Many-Spin Entanglement in Zigzag Spin Chain in Multiple Quantum NMR". Appl. Magn. Res. **51**, pp. 667-678, 2020.

Quantum design of interference transistors based on resonance coalescence effect

N.M. Shubin[1,2,3], A.A. Gorbatsevich[1,2,3], G.Ya. Krasnikov[3]

1. P.N. Lebedev Physical Institute of the Russian Academy of Sciences, 119991, Moscow, Russia.
2. National Research University of Electronic Technology, 124498, Zelenograd, Moscow, Russia.
3. JSC Molecular Electronics Research Institute, Zelenograd, 124460 Moscow, Russia.

The progressive development of integrated circuits (IC) technology leads to the continuous decrease of the individual transistor characteristic size, which can be comparable to single molecules in the near future. At the same time, modern experimental technology makes it routinely possible to connect single organic molecules (objects of about 1 nm size) to two or even three electrodes and measure their electrical characteristics [1]. Therefore, molecular electronics seems quite promising as a perspective advance of the IC basic elements.

Quantum interference plays a crucial role in electron transport through single molecules [1]. Recently, it was shown that the interference phenomenon of resonance coalescence could be exploited to provide an efficient mechanism of current switching [2]. Realizing such a mechanism requires two molecular orbitals (MO) with close energies found in, e.g., diradicals [3]. However, the influence of outer MOs on this mechanism, and the operating principle of a complementary switch needed for CMOS-like architecture remain an unstudied problem. In the present study, we provide a comprehensive theoretical analysis of the resonance coalescence effect in the context of single-molecule switches applications.

First of all, we show that taking into account outer MOs (beyond two-level approximation) gives rise to a 'background' transmission, which, if non-zero, essentially decreases the efficiency of current switching. At the same time, the balanced contribution of symmetric and antisymmetric MOs provides zero 'background' transmission. Moreover, under certain conditions, outer MOs may increase the logarithmic transconductance compared to the idealized two-level case. Due to the Coulson-Rushbrooke pairing theorem, MOs of opposite parity cannot be balanced in alternant diradicals, such as e.g., trimethylenemethane and divinylcyclobutadiene studied in Ref. [2]. Thus, we get that non-alternant diradicals may be preferable as a basis for quantum interference transistors.

Chemical modification of molecules with diradical character can change the mutual arrangement of MOs, which may lead, in particular, to the dramatic change of the conductance [4]. We show that by varying the energy split between two close MOs, one may observe resonance coalescence at two exceptional points (EPs) in the parameter space. Thus, we propose a realization of complementary pair of quantum interference transistors, which differ by a slight chemical modification providing their operation at these EPs.

We believe that the results of our study can contribute to the development of design rules for promising basic elements of molecular electronics.

We acknowledge the Russian Science Foundation (project No. 21-19-00808) and the Ministry of Science and Higher Education of the Russian Federation (contract No. 075-03-2020-216, code 0719-2020-0017) for support.

1. F. Evers. "Advances and challenges in single-molecule electron transport" Rev. Mod. Phys., **92**, pp. 035001, 2020.
2. A.A. Gorbatsevich, G.Ya. Krasnikov, and N.M. Shubin. "PT-symmetric interference transistor". Sci. Rep., **8**, pp. 15780, 2018.
3. M. Abe. "Diradicals". Chem. Rev., **113**, pp. 7011-7088, 2013.
4. N. M. Shubin et al. "Interacting resonances and antiresonances in conjugated hydrocarbons: exceptional points and bound states in the continuum". Phys. Chem. Chem. Phys., Advance Article, 2021.

Single-electron single-atom transistor based on arsenic dopants in silicon

M.A. Kolpakov[1,2], S.A. Dagesyan[1,2], D.E. Presnov[1,2,3], V.V. Shorokhov[1,2], V.A. Krupenin[1,2], O.V. Snigirev[1,2]

1. Department of Physics, Moscow State University, Moscow, 119991 Russia, kolpacov1973@gmail.com
2. MSU Quantum Technology Center, Moscow, 119991 Russia, artem.trifonov@physics.msu.ru
3. Skobeltsyn Institute of Nuclear Physics, Moscow State University, Moscow, 119191 Russia, denis.presnov@physics.msu.ru

The recent nanofabrication development creates a possibility to design novel nanoscale electronic devices. One of them is single-atom single-electron transistor (SASET) where electron transport is provided by tunneling through a single dopant atom [1]. Single atom devices are very promising for a quantum computing applications [2]. SASET fabrication is a complex task. It requires the ability to manipulate by position of individual dopants. We obtained single dopant structure by sequential reduction of an overdoped silicon nanowire by series of short isotropic reactive-ion etchings similar with [3]. We used arsenic dopants with a greater charging energy than has phosphorus dopants used in [3].

Obtained structures were analyzed by measuring its electrical characteristics in a liquid helium and then in a dry dilution refrigerator within the temperature range from 4.2 K down to about 15 mK. Electrical characteristics were analyzed in a form of IV-curves and differential stability diagrams: conductance as a function of both source-drain and gate voltage.

The influence of impurity atom electron discrete energy spectrum on the electric transport through the device was revealed in a form of multiple horizontal regions on IV-curves and diagonal lines on differential stability diagrams. However, at a temperature of 4.2 K, these effects were strongly blurred by thermal fluctuations. Sample cooling in dilution refrigerator experiment showed sharpening of these effects but only until reaching 2 K. Further cooling even in millikelvin range had no effect on electrical characteristics. This may indicate a local overheating of the nanoscale region near the transistor. To minimize this effect, a new sample design was proposed. In the new samples, the thickness of transistor electrodes was increased and their length was reduced. Instead of chromium, a combination of titanium-gold-titanium was used providing better heat removal.

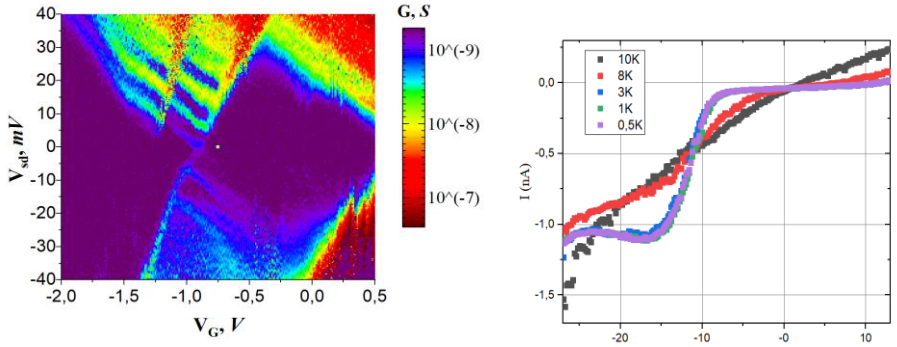

Fig. 1. Electrical characteristics of obtained SASET.

This research was performed according to the Development program of the Interdisciplinary Scientific and Educational School of Lomonosov Moscow State University «Photonic and quantum technologies. Digital medicine».

1. Fuechsle, Martin, et al. "A single-atom transistor." Nature nanotechnology, 7.4, pp. 242-246, 2012.
2. Koch, Matthias, et al. "Spin read-out in atomic qubits in an all-epitaxial three-dimensional transistor." Nature nanotechnology, 14.2, pp. 137-140, 2019.
3. Dagesyan S.A., et al. "Sequential reduction of the silicon single-electron transistor structure to atomic scale." Nanotechnology 28.22, 225304, 2017.

Investigation of electron transport in nanostructures based on metal-organic frameworks

S.A. Pankratov[1,2], I.V. Bozhev[1,2], V.V. Shorokhov[1,2], V.A. Krupenin[1,2], P.O. Mikhailov[1,2], I.O. Salimova[3], E.K. Beloglazkina[3], D.E. Presnov[1,2,4]

1. Faculty of Physics, Moscow State University, 119991 Moscow, Russia, pankratov.sa18@physics.msu.ru
2. MSU Quantum Technology Centre, Moscow, 119991, Russia shorokhov@phys.msu.ru
3. Faculty of Chemistry, Moscow State University, 119991 Moscow, Russia, bel@org.chem.msu.ru
4. Nuclear Physics Institute, Moscow State University, 119991 Moscow, Russia, denis.presnov@physics.msu.ru

The use of atomic or molecular structures as active components of electronic systems has led to the emergence of a new class of nanoelectronic devices [1, 2]. In particular, structures based on metal-organic frameworks (MOFs) – porous crystalline materials composed of metal ions interconnected by organic ligands, are of great interest. This is primarily due to the ability to create devices with well-defined properties on the basis of MOFs. Previously it was shown that devices based on MOFs demonstrate controllability and single-electron phenomena [2].

In this work, we investigated the conductivity of planar MOF polymers at room temperature. For this, the structures of eight metal electrodes converging in a region of 100 nm were fabricated on a thermally oxidized (500 nm) silicon substrate. The electron beam lithography was used to pattern the electrodes structure in the positive PMMA resist. Width of the electrodes in the central part was ~ 50 nm. The Au film 20 nm thick with an underlying 5 nm Ti layer was used as the electrode material.

A terpyridine ligand with anchor sulfur-containing group (A) was chemisorbed onto the sample surface between gold electrodes. The $Cu(ClO_4)_2 \cdot 6H_2O$ salt was chosen as a metal source, which forms the required bis-ligand coordination compounds with terpyridine [3]. A nonconducting (tetramethylene) (B) and a conjugated conducting linker (C) were used in this work. Further, two MOF synthetic strategies were proposed.

The first method was step by step coordination of organic and metal chain parts on the surface. The second one consisted of mixing solutions of ligands B, C and the salt solution in DMF, followed by sample immersion into the resulting “mixture”.

Investigations of I-V characteristics between each pair of electrodes have shown that the samples, prepared by first method, have resistances of hundreds of GΩ. Hysteresis I-V curves, caused by continuous charge redistribution within the MOF, were also observed in these samples. The second-type samples demonstrate coulomb blockade curves (see Fig. 1), which indicates the single-electron charge transport nature in these structures.

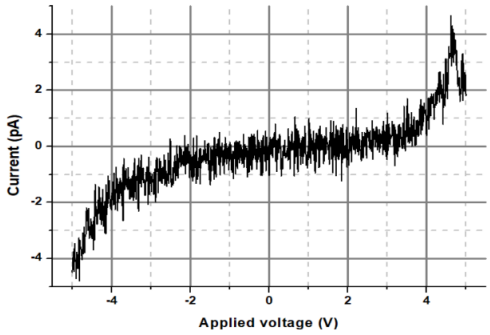

Fig. 1. The I-V curve of an experimental structure.

To create more homogeneous and reproducible structures, it is necessary to reduce the distance between the electrodes and use a more conductive polymer, which can be achieved by reducing the linkers length.

The proposed structure, in which metal intercalations form a homogeneous planar network of charge centers, and the electrodes are input and output terminals, allows creating tunable reservoir neural network and realize various logical elements on the physical basis of MOF.

This research was supported by the Interdisciplinary Scientific and Educational School of Moscow State University «Photonic and Quantum Technologies. Digital Medicine».

1. S.A. Dagesyan, V.V. Shorokhov, D.E. Presnov, et al., “Sequential reduction of the silicon single-electron transistor structure to atomic scale”. Nanotechnology, **28**, 225304, 2017.
2. J. Park, A.N. Pasupathy, J.I. Goldsmith, et al., “Coulomb blockade and the Kondo effect in single-atom transistors”. Nature, **417**, 722–725, 2002.
3. I.O. Salimova, A.V. Berezina, E.S. Barskaya, et al., “Syntheses of terpyridine-pyridylbenzothiazole linked ditopic ligands and their copper (II) complexes”. Polyhedron, **179**, 114403, 2020.

Tristate Transistors. Base Parameters and Impurities Distribution

S. Krivelevich
Valiev Institute of Physics and Technology of Russian Academy of Sciences, Yaroslavl Branch, Yaroslavl, Russia, s.krivelevich@mail.ru

Over the years, the development of micro (nano) electronics has been associated with an increase in the number of transistors in a single processor. An increase in the number of transistors is associated with an increase in the packing density and a decrease in the size of an individual transistor. A further reduction in the linear dimensions of an individual valve will lead to insoluble contradictions caused by technological limitations and fundamental laws of nature. It is possible to create gates with more than two stable logical states. In tristate transistors, a variant is possible in which the values of the output resistances in all three states differ by about an order of magnitude. In this case, electronic circuits allow the implementation of logic of the form "0-1-2". However, tristable gates, as far as the authors of this work know, are practically not described in the literature. One of the options for creating such valves is considered in this work.

A class of gates with three stable state characteristics can be based on bipolar field devices, which are used as transistors. Each bipolar field effect transistor contains two pairs of electrodes: two electrodes are used to modulate the conductivity of the active region of the transistor ("emitter and collector"), and two electrodes are used to "measure" the conductivity of the active region ("source and drain"). Each transistor must also contain an injecting (extracting) p-n junction. With a large forward bias of the p-n junction, the transistor enters the saturation mode with a low resistance of the active region. When the reverse bias is applied, the transistor goes into a quasi-stable depletion mode. In this mode, the resistance of the active region slowly increases with an increase in the absolute value of the reverse voltage. A further increase in the absolute value of the reverse bias leads to a sharp increase in the resistance of the active region, and the transistor goes into a complete depletion mode.

The technology for creating the considered tristate transistors is a classic "silicon" technology that includes standard processes for creating local doped and hidden insulating regions.

A feature of the described structures is that on the volt-resistive characteristic there must be a flat section corresponding to the state of a logical unit. To create such a flat section on the volt-resistive characteristic, it is necessary to form a special donor impurity distribution in the active region of the transistor. This distribution can be obtained as a solution to the inverse problem based on the Poisson equation. It should contain at least two substantially uniformly doped regions and a region with a predetermined distribution of dopant concentration gradients.

The standard technology for the creation of silicon device structures involves the widespread use of epitaxy and ion implantation. Modeling shows that distributions close to the specified distributions can also be obtained using epitaxy and precision ion implantation. A necessary condition for obtaining the specified distributions of the dopant is the variation of the energy of the implanted ions. At the acceptable values of the doping level the thickness of the entire active region of a tristable transistor will be several tens of nanometers. The main task arising in the development of the technological process for the formation of a given distribution profile, in this case, is to obtain a function of the density of the ion flux at given values of the ion energy from time to time. Strict requirements are imposed on the accuracy of reproduction of the distribution functions for dopants. Therefore, it can be argued that the ion doping process cannot be carried out manually. It should be automated.

Optical device fabrication technology with advanced electron beam lithography systems

M. Shibata
CRESTEC CORPORATION, Tokyo, Japan, shibata@crestec8.co.jp

Optical communication is one of the most active technologies that generate revolutions in many fields such as fifth and sixth generation mobile communication systems, cloud services, medical sensing and light detection and ranging (LiDAR). The key device for them is distributed feedback laser diode (DFB-LD). CRESTEC CORPORATION has contributed production of DFB-LDs since 1999 by developing Electron Beam Lithography (EBL) systems, which play an important role in fabricating grating structure of DFB-LDs.

The core technology for patterning of DFB-LDs is Field Size Modulation function (FSM), which enables pitch resolution down to 0.0012 nanometer. Since the grating pitch corresponds to laser frequency, precisely tuned lasers can be manufactured. With FSM the minimum writing position step can be controlled arbitrarily by finely tuning the writing field size.

Lately requirements for longer cavity lengths have been increased to get higher power lasers mainly for laser processing and LiDAR. To meet the requirements EBL systems with large writing field size is essential because pitch error is inevitable at field stitching point for EBL systems with smaller field size. We have developed EBL systems with 1500 micrometer field with beam energy of 50 keV (Fig. 1) and 2400 micrometer with 30 keV, respectively.

At the same time, requirements for chirped pitch control have been expanded to fabricate tunable laser diode. We also have developed this function to freely control grating pitch inside a chip.

The authors would like to discuss the core technologies for grating pattern fabrication for DFB-LDs.

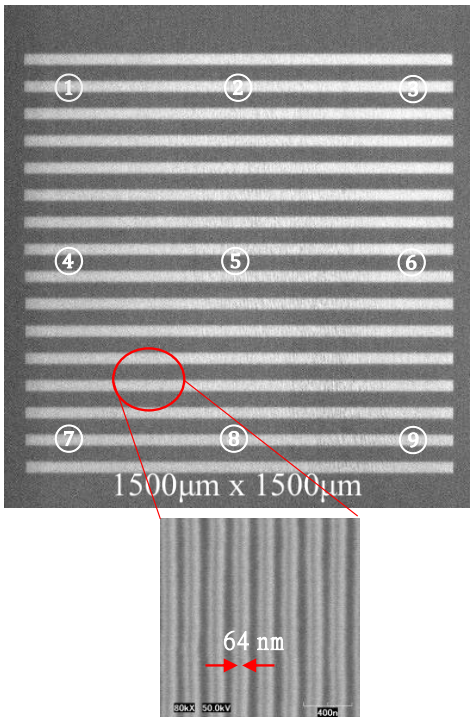

Position	Line width
	(nm)
1	67.2
2	64.0
3	67.2
4	64.0
5	64.0
6	67.2
7	64.0
8	64.0
9	67.2
Average	65.4
Max-Min	3.2
Accuracy	2.6
SD	1.6

Fig. 1. Line width uniformity of 1500 micrometer grating patterns.

Comprehensive simulation of thermally amplified e-beam lithography

F. Sidorov, A. Rogozhin, E. Zhikharev
Valiev Institute of Physics and Technology of RAS, Moscow 117218, Russia

Method of thermally amplified e-beam lithography proposed by Bruk et al. [1] is based on chain depolymerization reaction, which takes place in positive polymer resists during e-beam exposure at temperatures above glass transition. This method could be effectively applied for the formation of three-dimensional structures with well-rounded profile, but its lateral resolution is low (about 300 nm). For the optimization thermally amplified e-beam lithography parameters, the comprehensive simulation of this process was carried out.

Major processes, affecting the structure profile in thermally amplified e-beam lithography, are primary and secondary electron scattering, e-beam induced scission of resist molecules, thermal depropagation of resist and resist thermal reflow [2]. The former is induced by high temperature and reduction in the resist viscosity due to the changes in resist molecular weight distribution, caused by main-chain scissions. For the simulation of e-beam scattering in resist and substrate the actual models based on the energy loss function (for inelastic scattering) and the Mott differential cross sections (for elastic scattering) were used [3, 4]. Temperature dependence of e-beam induced main-chain scission rate was determined by simulation of radiation chain-scission yield [5]. A kinetic model of resist depolymerization was used for modeling of resist molecular distribution at different exposure stages (Fig. 1a), which allowed to simulate local resist viscosity reduction during the process. Finite element modeling package “Surface Evolver” was applied for the profile simulation of thermal reflow, taking into account non-uniform resist viscosity distribution [6]. The whole exposure period was divided into 1-10 second intervals and processes mentioned above were simulated successively for each interval, which allowed to simulate structure profile after exposure (Fig. 1b).

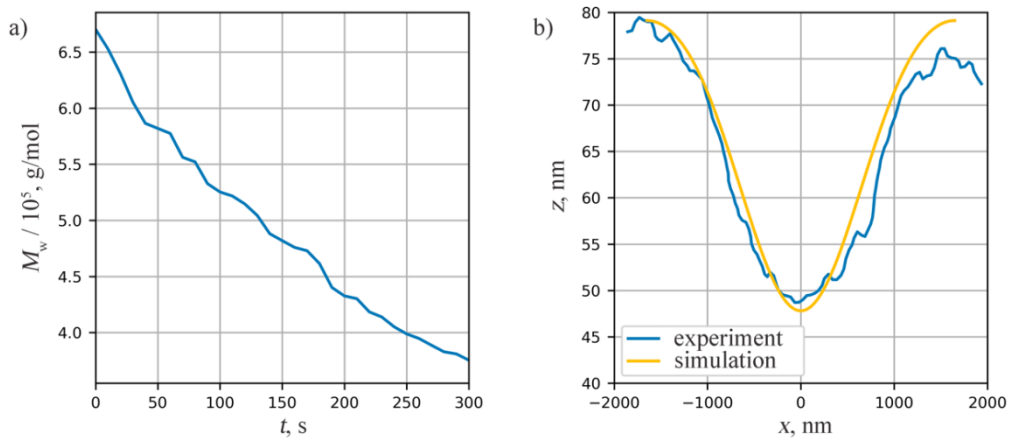

Fig. 1. Mass-average polymer weight time dependence in the center of line (a) and resulting line profile obtained using thermally amplified e-beam lithography (b). E-beam current density is 1.9 nA/cm^2, the exposure time is 320 s, the resist (PMMA) layer thickness is 80 nm, the sample temperature is 125 °C.

1. M.A. Bruk et al. “Method of masking pattern formation in positive e-beam resist layers”. Russ. Bull. Invent. N9. Russian Federation patent 2478226, 2013.
2. A. Rogozhin et al. “Nanophotonic structure formation by the dry e-beam etching of the resist: resolution limitation origins”. Computer Optics, **41**, 4, 2017.
3. M. Dapor. “Energy loss of fast electrons impinging upon polymethylmethacrylate”. Nucl. Instr. Meth. Phys. Res. B, **352**, pp. 190-194, 2015.
4. A. Valentin et al. “Geant4 physics processes for microdosimetry simulation: Very low energy electromagnetic models for electrons in silicon”. Nucl. Instr. Meth. Phys. Res. B, **288**, 66-73, 2012.
5. F. Sidorov and A. Rogozhin. “Detailed Monte-Carlo simulation of PMMA chain scissions in e-beam lithography”, JOP Conf. Ser., **1410**, 012234, 2019.
6. K. Brakke. “The Surface Evolver”. Experimental Mathematics, **1**, pp. 141-165, 2012.

Investigation of plasma resistance of the HSQ electronic resist for prototyping of nanoelectronic devices

A. Miakonkikh[1], A. Shishlyannikov[2], A. Tatarintsev[1], V. Kuzmenko[1], K. Rudenko[1], E. Gornev[2]
1. Valiev Physics and Technology Institute, Russian Academy of Sciences, Moscow, 117218 Russia
2. JSC Molecular Electronics Research Institute, Moscow, 124460 Russia
e-mail: ashishlyannikov@niime.ru

A silicon-inorganic negative electronic resist based on hydrogen silsesquioxane (HSQ) is one of the most widespread electronic resists, characterized by ultrahigh resolution up to several nanometers, while masks made of it have fairly good resistance in chemically active plasma. It was previously demonstrated [1] that selectivity (S) of a given resist in the processes of anisotropic reactive ion etching, with respect to the underlying layer, depends on the radiation dose; however, at doses of ~1000 μC/cm^2, the selectivity value ($S = R_{layer}/R_{HSQ}$) reaches a constant value.

However, in the general case, the plasma resistance of a resist and, accordingly, the selectivity of the reactive ion etching process is not a constant, but depends both on the properties of the resist, and on the plasma chemistry, as well as the modes of reactive ion etching of structures. Therefore, the aim of this study is to comprehensively study the capabilities of an HSQ resist when transferring a topological pattern to layers of functional materials (monocrystalline silicon, metallic Ta layers, dielectric SiO_2 layers, Al_2O_3, HfO_2, Si_3N_4, and low-k porous dielectric based on organosilicate glass (OSG) on silicon substrates), taking into account the limited thickness of the mask, which is typical of electronically sensitive resistors. We used the recipes for the anisotropic reactive ion etching of nanostructures under the HSQ mask, typical for creating prototypes of nanoscale transistors of integrated circuits.

It is established that HSQ resist masks can be used to manufacture prototypes of micro- and nanoelectronic devices with topological dimensions up to 10 nanometers using a wide range of materials, including creating structures with relatively high aspect ratios with an absolute thickness of the layers of functional materials of tens of nanometers.

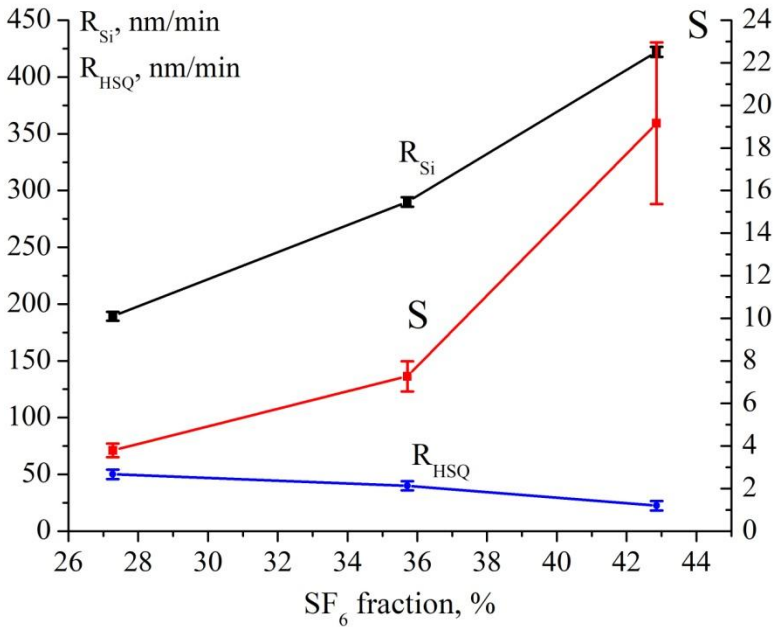

Fig. 1. Etching rates of silicon and HSQ resist versus SF_6/C_4F_8 plasma composition.

1. A. Miakonkikh, N. Orlikovskiy, A. Rogozhin, A. Tatarintsev, K. Rudenko. «Dependence of the resistance of the negative e-beam resist HSQ versus the dose in the RIE and wet etching processes». Russian Microelectronics, **47** (3), pp. 157-164, 2018.

Electron beam lithography on the surface with 3D relief

A. Miakonkikh, A. Tatarintsev, K. Rudenko
Valiev Institute of Physics and Technology, Russian Academy of Sciences, Moscow, 117218 Russia
e-mail: tatarintsev@ftian.ru

Direct electron beam lithography (EBL) is widely used research tool allowing the design and prototyping of device structures for nanoelectronics, nanophotonics, nanoelectromechanics up to sub-10 nm critical topology dimensions. Unlike photolithography, electron-beam lithography has a greater depth of field of the exposure, and therefore, can be used for complex three-dimensional relief patterning.

Three-dimensional device nanostructures in some aspects can be more efficient and profitable than planar technologies because of the more advantageous geometric, electrical and physical properties. Typical example is the transition to three-dimensional architecture carried out by INTEL Corp. with the development to 22 nm technology by invention of FinFET transistors [1].

In this work, we investigated the possibility of EBL along a three-dimensional surface profile without preliminary planarization of surface. To assess the possibilities of using lithography for complex relief, a negative e-beam resist HSQ was used, which has a high selectivity in the processes of anisotropic plasma etching [2]. This negative resist also has a high planarizing ability demonstrated in [3]. We have shown that according our technique of exposure it is possible to form lithographic pattern on strongly non-planar surface covered by fin-structures with 50 nm wide and 90 nm high while critical dimensions of litho-pattern was achieved up to 10 nm (Fig 1).

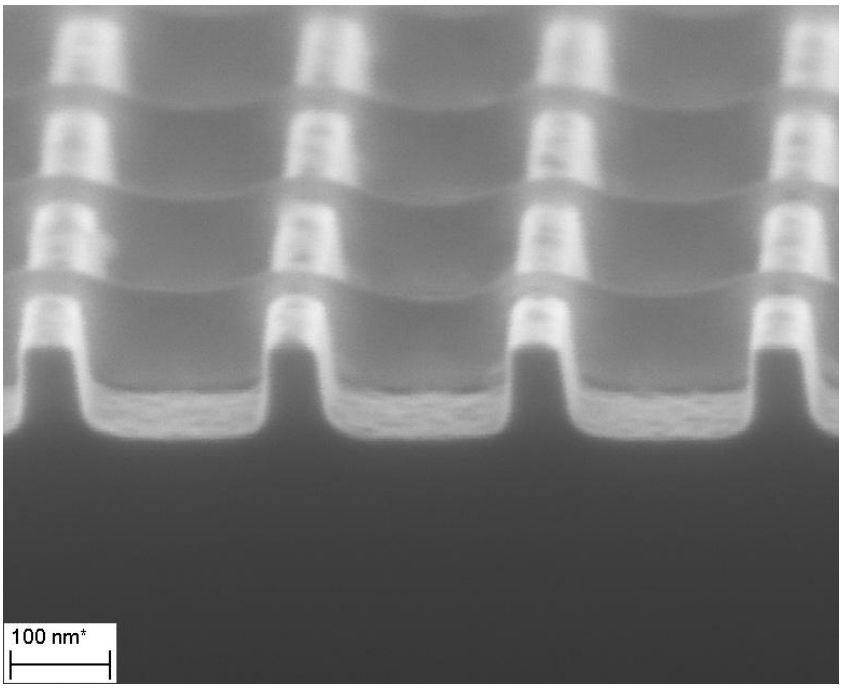

Fig. 1. An example of high-resolution lithography on a surface with complex three-dimensional relief.

1. M. Bohr. “The evolution of scaling from the homogeneous era to the heterogeneous era”. IEEE Int. Electron Devices Meeting (IEDM), 2011, pp. 1.1.1–1.1.6.
2. A.V. Miakonkikh, A.V. Shishlyannikov, A.A. Tatarintsev et al. “A Study of the Plasma Resistance of a High-Resolution HSQ Electronic Resist for Prototyping Nanoelectronic Devices.” Russ. Microelectronics, **50**, pp. 297–302, 2021.
3. Y. Guerfi, J.B. Doucet, G. Larrieu. “Thin-dielectric-layer engineering for 3D nanostructure investigation using an innovative planarization approach”. Nanotechnology, **26**, p. 425302, 2015.

Stochastic effects in memristors: Theory and applications

Y.V. Pershin
Department of Physics and Astronomy, University of South Carolina, Columbia, South Carolina 29208, USA
E-mail address: pershin@physics.sc.edu

The cycle-to-cycle variability is a common feature of memristive devices, such as electrochemical metallization (ECM) cells and valence change memory (VCM) cells. The analysis of electronic circuits with stochastic memristors requires novel approaches as the stochasticity is not captured by the standard Kirchhoff's laws. Generally, the description of these circuits should be based on probabilities or probability distribution functions and involve the calculation of circuit variables "on average".

The evolution of certain circuits with binary or multi-state memristors (in particular, ECM cells) can be imagined in terms of transitions between discrete states of the circuit (for the transition scheme example, see Fig. 1). To describe these transitions mathematically, we pioneered the use of master equation [1]

$$\frac{dp_\Theta(t)}{dt} = \sum_{i=1}^{N}\left(\gamma^m_{\Theta_m} p_{\Theta_m}(t) - \gamma^m_\Theta p_\Theta(t)\right) , \qquad (1)$$

where Θ denotes a circuit state, $p_\Theta(t)$ is the probability to find the circuit in the state Θ at time t, Θ^m is the state different from Θ by the state of m-th memristor, and $\gamma^m_{\Theta_{(m)}}$ is the transition rate. The master equation approach is suitable for circuits combining linear and/or non-linear resistors, binary and/or multi-state memristors, current and/or voltage sources.

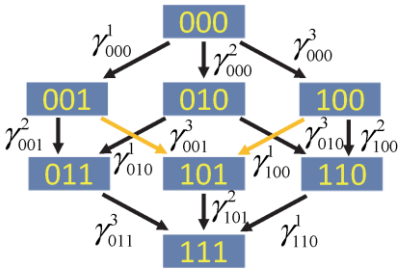

Fig. 1. Transition scheme for a circuit of three memristors experiencing the off-to-on switching. Here, 0(1) represents the OFF (ON) resistance state. From [1].

Compared to stochastic/Monte Carlo simulations, the use of master equation offers two major advantages. First, the master equation can be solved analytically at least in some cases (two examples can be found in [1]). Second, a lot of information on circuit dynamics can be obtained from a single calculation without the need for averaging. Importantly, in the case of symmetries, a single degree of freedom (variable) can be used to describe equivalent circuit configurations. Therefore, the complexity of master equation can be reduced substantially in some cases.

The master equation can be easily implemented in SPICE, a general-purpose circuit simulation program. In Ref. [2], we used a collection of 1 Farad capacitors combined with voltage-controlled current sources to simulate Eq. (1). In this approach, the occupation probabilities are represented by capacitor voltages, while the transitions are implemented with the help of voltage-controlled current sources. Examples of LTspice codes can be found in Ref. [2].

In my talk, I will also discuss a generalization of the master equation approach to the circuits involving reactive components (capacitors and/or inductors) [3]. The mathematical description of such circuits is more involved as it relies on occupation probability functions of reactive variables satisfying the Chapman-Kolmogorov equation. Emerging applications for stochastic memristors will be discussed including the simulation of fundamental physics models.

1. V. J. Dowling, V. A. Slipko and Y. V. Pershin. "Probabilistic Memristive Networks: Application of a Master Equation to Networks of Binary ReRAM cells". Chaos, Solitons & Fractals, **142**, p. 110385, 2021.
2. V. J. Dowling, V. A. Slipko and Y. V. Pershin. "Modeling networks of probabilistic memristors in SPICE". Radioengineering, **30**, pp. 157-163, 2021.
3. V. A. Slipko and Y. V. Pershin. "Theory of heterogeneous circuits with stochastic memristive devices". IEEE Trans. Circuits Syst. II (Early Access), 2021.

Light sensitive memristors based on $GeSi_xO_y$ films with Ge nanoclusters

V.A. Volodin[1,2], G.N. Kamaev[1,2], I.D. Yushkov[1,2], G.K. Krivyakin[1,2], S.G. Cherkova[1], M. Vergnat[3]
1. Rzhanov Institute of Semiconductor Physics, Russian Academy of Sciences, Novosibirsk, Russia, E-mail volodin@isp.nsc.ru. 2. Novosibirsk State University, Pirogova Str. 2, Novosibirsk 630090, Russia. 3. Université de Lorraine, CNRS, IJL, F-54000 Nancy, France.

For the development of information technology, more and more memory arrays are needed. Recently, memristors have been the most promising candidates for the creation of modern universal memory. Lately, prospects for the use of memristors in optoelectronics have emerged [1]. The possibility of optically stimulated switching of memristors is promising for creating optical computers, technical vision and neuron networks.

The memristor effect is based on controlled switching of dielectrics to high and low resistance states (HRS and LRS, correspondingly) and is observed in a wide class of materials. The most promising materials for practical use in memristors are oxides and suboxides of metals and semiconductors.

The advantage of germanosilicate glasses ($Si_xGe_yO_z$ solid alloys) is that the technology of its deposition is simple, not expensive and fully compatible with silicon technology. The peculiarities of these solid alloys are the two possibilities of nanoscale fluctuations of the potential (parameters of the energy bands). The widths of the band gaps in SiO_2 (8-9 eV) and GeO_2 (4-5 eV) differ significantly. It allows modulating the parameters of the traps of the following type - the inclusion of germanium oxides in silicon oxide. Another possibility is the controlled formation of precipitates with excess of germanium atoms (or oxygen deficit regions), which are also charge traps, as well as amorphous nanoclusters and/or germanium nanocrystals.

The studied $Si_xGe_yO_z$ solid alloys films (~50 nm) were obtained by simultaneous evaporation of GeO_2 and SiO_2 (or SiO) powders in high vacuum (10^{-8} Torr) and deposition onto n-type, p-type Si(001), and on $Al/SiO_2/Si(001)$ heated up to 100 °C. The films of different stoichiometry were deposited: by evaporation of GeO_2 and SiO_2 sources, with accordance to chemical composition we will mark it as $GeO_x[SiO_2]_{(1-x)}$; and by evaporation of GeO_2 and SiO sources, with accordance to chemical composition it is $GeO_x[SiO]_{(1-x)}$ film. The transparent ITO contacts were used as top electrode. The stoichiometry and structure of the samples was determined using electron microscopy, X-ray photoelectron spectroscopy, transmittance and reflectance and Fourier transform infrared (FTIR) absorption spectroscopy. The presence of Ge-clusters in the films was detected from analysis of the Raman spectra. Dark and light-illuminated current-voltage (I-V) characteristics were measured using ammeter and voltmeter setup at room temperature in air atmosphere.

It was found, that as-deposited $GeO_x[SiO]_{(1-x)}$ films contain amorphous Ge nanoclusters. The furnace annealings at temperature 500 ^oC lead to further forming of a-Ge clusters in both types of the films.

In $ITO/Si_xGe_yO_z/Al/SiO_2/Si(001)$ structures (MIM-structures) no memristor effects were found. Reversible (up to several thousand cycles) resistive switchings from HRS to LRS (memristor effect) were observed for the semiconductor-dielectric-metal structures, namely p-Si (or n-Si)/ $GeO[SiO_2]$ (or GeO[SiO]) /ITO structures (MIS structures) in air atmosphere. Both negative and positive photoconductivity were observed in the annealed MIS structure when both negative/positive voltage biases were applied to the top ITO electrode. This is possibly due to light-stimulated recharging of holes originating from Ge-nanoclusters, which act as traps [2]. The effects of light illumination on I-V characteristics of the MIS structures and on resistive switching of these structures were studied and discussed. This may possibly open a pathway towards memristors that can be switched by light pulses. Another promising direction could be the creation of optoelectronic devices combining the properties of a memristor and a light-emitting diode, as, for example, using MIS with silicon nanocrystals.

The study was supported by Russian Foundation for Basic Research (project No. 19-07-00367).

1. Z. Zhou, Y. Pei, J. Zhao, G. Fu, and X. Yana. “Visible light responsive optoelectronic memristor device based on CeO_x/ZnO structure for artificial vision system”. Appl. Phys. Lett., **118**, p. 191103, 2021.

2. V.A. Volodin, G.N. Kamaev, M. Vergnat. “Negative and Positive Photoconductivity and Memristor Effect in Alloyed GeO[SiO] Films Containing Ge Nanoclusters”. Physica Status Solidi (RRL) Rapid Research Letters, **14**, p. 2000165, 2020.

Investigation of conductive filament growth and rupture in ReRAM structures based on hafnium oxide

E. Ganykina[1,2], A. Rezvanov[1], Ye. Gornev[1]
1. JSC Molecular Electronics Research Institute. Zelenograd, Moscow, Russia, eganykina@niime.ru
2. Moscow Institute of Physics and Technology, Dolgoprudny, Russia

Currently, ReRAM memory is one of the most promising types of memory due to its non-volatility, compatibility with CMOS technology, and high speed of operation, which in turn allows it to be effectively used for neuromorphic calculations [1]. For a clear understanding of ReRAM operation, a thorough study of oxygen ions transport mechanism inside the resistive oxide layer is necessary.

In this paper Au/Ti/HfO_2/Au/Si memristor is studied. When a positive voltage is applied to the upper electrode, the formation of a conductive filament begins, which leads the device to the SET state. When the polarity is changed, the filament ruptures and the device state changes from SET to RESET [2]. Such type of switching is caused by the migration of oxygen vacancies inside the conducting layer, which largely depends on the temperature and the electric field.

Three partial differential equations are self-consistently solved for calculating oxygen vacancies concentration n_V, the electric potential V and the temperature T: the oxygen vacancies diffusion equation (1), the current continuity equation for electrical conduction (2) and Fourier equation for Joule heating (3).

$$\frac{dnv}{dt} = \nabla \cdot (-u_V n_V + D_V \nabla n_V + S_V D_V n_V \nabla T) \quad (1)$$

$$\nabla \cdot (\sigma \nabla V + \varepsilon \frac{d}{dt} \nabla V) = 0 \quad (2)$$

$$\rho C_p \frac{dT}{dt} - \nabla \cdot (k \nabla T) = \sigma (\nabla V)^2 \quad (3)$$

Due to the combination of several physical effects: drift (driving force is the electric field), diffusion (driving force is the concentration gradient) and thermal diffusion (driving force is the temperature gradient), oxygen vacancies form a conducting layer inside the dielectric [3]. The electrons injected from the electrode jump over positively charged vacancies, converting hafnium oxide into a conducting state [4]. It is assumed that the electrical conductivity and the coefficient of thermal conductivity depend on n_V.

This model quantitatively explains the dynamic process of resistive switching: the SET process involves the formation of a conductive filament under the influence of temperature and an electric field with its subsequent expansion; the RESET process involves the thermal rupture of the filament with the formation of an insulating region.

Overall the paper presents a theoretical model of a memristor based on hafnium oxide, which was used to obtain the distributions of the concentration of oxygen vacancies, electric potential and temperature in the SET and RESET processes.

1. G.Ya. Krasnikov and Ye.S. Gornev "Semiconductor electronics development at JSC "MIRE and Micron". Hystory of the Domestic Electronics, **1**, pp. 510-538, 2012 (in Russian).
2. Goux L. OxRAM technology development and performances //Advances in Non-volatile Memory and Storage Technology, pp. 3-33, 2019.
3. Larentis S. et al. Resistive switching by voltage-driven ion migration in bipolar RRAM—Part II: Modeling. IEEE Transactions on Electron Devices, **59** (9), pp. 2468-2475, 2012.
4. A. Kalantarian HfO_2-Based Resistance Switching Non-Volatile Random Access Memory: Low Power Operation and Reduced Variability. Stanford University, 2015.

Repetitive nonlinear behaviour during the RESET process in bipolar resistive switching of $Al_2O_3/HfO_2/TaO_xN_y$ stack

O. Permiakova, A. Rogozhin, E. Smirnova, K. Rudenko
Valiev IPT RAS, Moscow, Russia, o.permyakova@phystech.edu

The extremely high density of memristors in planar design was achieved via crossbar architecture. The main drawback of crossbar architecture is the sneak path issue because of which crossbar can only operate correctly with a built-in selector. For this purpose a field-effect transistor can be connected in series with memristor, nevertheless the usage of the transistor increases the effective cell size and is unsuitable with 3D integration of crossbar. Other selector devices are diode in series with memristor and self-selective memristor which are suitable for 3D integration. In this work, we consider the properties of the self-selective Pt/Al_2O_3 (0.5nm)/HfO_2 (1.5nm)/TaO_XN_Y (4nm)/TiN device.

Active media of device was fabricated via plasma enhanced atomic layer deposition and electrodes were fabricated via magnetron sputtering. TMA, TEMAH, TBTDET, H_2O and nitrogen plasma were used as precursors for Al, Hf, Ta, O and N, respectively. I-V characteristics were measured with Keithley-4200 SCS during DC sweeps from -1.5 V to 1.5 V with current compliance 1 mA. Electroforming was accomplished under constant bias voltage -3 V.

Figure 1a shows typical I-V characteristics of $Al_2O_3/HfO_2/TaO_XN_Y$ device as well as HfO_2/TaO_XN_Y device, adding an ultrathin layer of Al_2O_3 increases the resistance in the low-resistance state (LRS) and also adds nonlinearity (step-like current increase) during LRS at positive voltage. This nonlinearity makes the device self-selective in the write schemes V/2 and V/3. According to these schemes, half the voltage (V/2) or a third of the voltage (V/3) is applied to all unselected word and bits lines of the crossbar array to suppress parasitic leakage current flow. The coefficient of nonlinearity is defined as the ratio of current at the reading voltage and current on a one-half (V/2) or one-third (V/3) of reading voltage. Choosing the read voltage before step as 0.6 V (Figure 1a) or the read voltage on the peak of step as 0.675 V, we can obtain the following characteristics using the median I - V characteristic. Non-linearity of the device at V_{read}=0.6 V ($R_{HRS}/_{RLRS}$=9) for V/2 method was 4.91 and for V/3 method 9.99, at V_{read}=0.675 V (R_{HRS}/R_{LRS}=24) for V/2 method was 11.9 and for V/3 method 27.1.

Some possible reasons for the appearance of nonlinearity of resistive switching characteristics re proposed. Nonlinearity can be associated with adjacent layers that differ greatly in dielectric constant [1] or occur because of to change in conductivity from direct tunnelling to Fowler-Nordheim tunnelling when the potential barrier from Al_2O_3 decreases due to increased value of electric field inside the device [2].

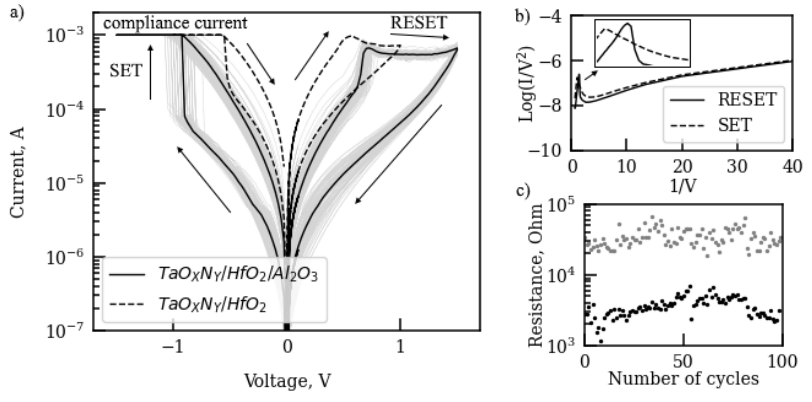

Figure 1. a) Measured I-V characteristics of devices. Solid gray lines - I-V characteristics during 100 DC sweeps and solid black lines - median I-V characteristic of $Al_2O_3/HfO_2/TaO_XN_Y$ device, dotted black lines - median I-V characteristic of HfO_2/TaO_XN_Y device; b) Tunneling curve fitting of the $Al_2O_3/HfO_2/TaO_XN_Y$ device in LRS; c) Resistance change depending on DC sweep number at 0.6 V for HfO_2/TaO_XN_Y device.

1. Y. Chen, S. Hu, Z. Lin, B. W. Fowler, H. Huang, C. Lin, S. Kim, Y. Chang and J. C. Lee. "Graphite-based Selectorless RRAM: Improvable Intrinsic Nonlinearity for Array Applications". Nanoscale, **10**, pp. 15608-15614, 2018.
2. U. Chand, K. Huang, C. Huang and T. Tseng, "Mechanism of Nonlinear Switching in HfO_2-Based Crossbar RRAM With Inserting Large Bandgap Tunneling Barrier Layer". IEEE Trans. Electron Devices, **62**, pp. 3665-3670, 2015.

Investigation of the defect distribution in multilayer dielectric stacks for ReRAM application using C-AFM technique

A. Isaev[2], A. Rogozhin[1], E. Smirnova[1], K. Rudenko[1]
1. Valiev Institute of Physics and Technology of RAS, Moscow, Russia, rogozhin@ftian.ru
2. Moscow Institute of Physics and Technology, Dolgoprudnij, Russia

Resistive memory devices (memristors) based on transition metal oxides (HfO_x, TiO_x, TaO_x, ZrO_x, etc.) are one of the most promising and rapidly developing devices for the next generation of nonvolatile memory [1] due to the possibility of high density of elements, scalability, low power consumption and low switching time [2, 3]. In addition, memristor technology is compatible with standard CMOS fabrication. In such devices, conductivity switching occurred due to the reversible formation of conductive filaments (bridges) from defects, usually from oxygen vacancies. For the correct formation of conductive filaments, the electroforming operation is required. For the mass production of devices, the electroforming stage is not suitable.

Research results show that the electroforming voltage is determined by the presence of defects in oxide layers [4]. This is especially true for highly advanced oxide layers obtained by atomic layer deposition. Apparently, by creating additional defects, for example, conducting annealing [5] or processing the structure with the ion beam [6], it is possible to significantly reduce the forming voltage or even switch the structure to a low-resistance state without electroforming. One of the possible techniques for the defect distribution analysis is based on C-AFM.

In this work defect distribution and parameters of the three types of dielectric stacks were investigated. The structures HfO_2 (2 nm)/HfO_x (4 nm)/TiN, HfO_2 (2 nm)/TaO_x (4 nm)/TiN and Al_2O_3 (0.5 nm)/HfO_2 (1.5 nm)/TaO_x (4 nm)/TiN were formed by atomic layer deposition. Conductive AFM with Pt-coated tips was used for investigation of the distributions and parameters of the defects in the dielectric stacks. It was shown that the density of the filaments at the same forming voltage in the Al_2O_3/HfO_2/TaO_x/TiN is about 60 μm^{-2} (fig. 1) that is the highest among three types. Also filaments for the structure is the smallest (median filament diameter is about 14 nm).

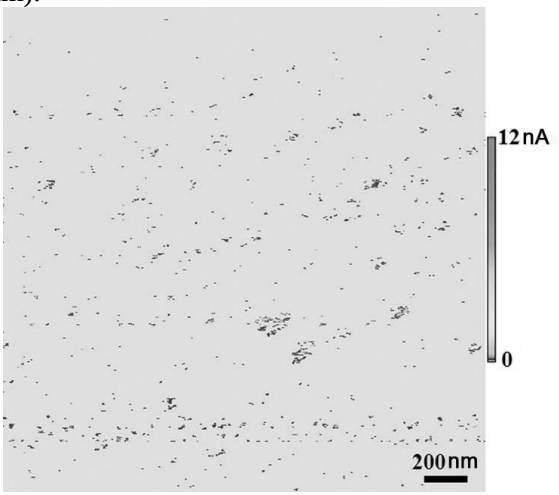

Fig. 1. Current distribution obtained by C-AFM for the structure Al_2O_3 (0.5 nm)/HfO_2 (1.5 nm)/TaO_x (4 nm)/TiN.

1. J. Meena et al. Nanoscale Research **9**, 526 (2014).
2. Chua L. IEEE Trans Circuit Theory 1971, **18** (5):507–519.
3. Kim S: MINATEC 2012; June 21-24 2012. Grenoble: MINATEC; 2012:4.
4. D. Ielmini, R. Waser, Wiley-VCH Book, ISBN: 978-3-527-33417-9. Wiley-VCH, Weinheim, Germany 2016.
5. M. Lanza, G. Bersuker, M. Porti et al., Appl. Phys. Lett., 2012, 101, 193502.
6. J.L. Pacheco, D.L. Perry, D.R. Hughart, M. Marinella, and E. Bielejec, arXiv:1710.09491 [physics.app-ph], 2017.

Materials for on-chip interconnects: challenges and solutions

M.R. Baklanov
North China University of Technology, Beijing 100144
MIREA – Russian Technological University, Moscow 119454
e-mail: baklanovmr@gmail.com

The modern ULSI device incorporate up to several billions transistors and other electronic components that must be interconnected to provide the proper functionality. The width of the conducting wires and the actual dielectric in between them fell below 100 nm in 2008, and is now on the order of tens of nm. As a result, the total resistance (R) of the wires together with a capacitance (C) between them increases the signal propagation time (RC delay). To solve this problem, low resistivity metal (Cu instead of Al) and materials with low dielectric constant (low-k) were introduced. The transition from Al to Cu was one of the most significant changes in semiconductor manufacturing, and the damascene process became the industry standard instead of Al etching because Cu cannot be patterned by plasma etching. In the damascene technology the porous low-k dielectric is deposited and patterned before the metal deposition. The patterned dielectric is then covered with a thin diffusion barrier and filled using a superfilling technique, where a higher deposition rates must be achieved at the bottom, resulting in a void-free and seamless filling of trenches and vias with high aspect ratios.

However, the integration of new materials that started at end on 1990th was extremely challenging. The issue of (porous) low-k materials is that they are generally soft, mechanically weak, and do not adhere well to silicon or metal wires. Furthermore, porous low-k materials do not withstand conventional interconnect processing. Cu has high diffusivity into silica and organosilicate glasses (OSG) that have been selected as low-k candidates. Therefore, Cu is isolated from low-k material by conductive and dielectric barriers. These barriers have higher resistivity than Cu (metal barriers) or much higher k-value (dielectric barrier) than the isolating low-k. Therefore, they need to be as thin as possible to realize advantages of Cu and low-k, and presently their thickness is approaching to the physical limit. In addition, Cu undergo to electromigration that limits the lifetime of ULSI circuits.

These challenges requested search of new interconnect materials that can allow to avoid the observed phenomena. New metals like Co, Ru, Mo, Ir, Rh … have been analyzed and introduced because of higher resistance to electromigration and, probably, they have also less strict requirements to the diffusion barriers. New low-k materials with a carbon bridge between Si atoms in silica-like matrix have been developed. They have improved mechanical properties because of higher bending rigidity of Si–C–Si bonds than that of Si–O–Si. Other candidates based on SiCN and BCN have also been considered. They have higher intrinsic dielectric constant than OSG materials but have much better mechanical properties, better plasma resistance and better compatibility with diffusion barriers. The absence of plasma damage and the thinning of the diffusion barrier make it possible to obtain the integrated dielectric constant better than that of OSG of materials.

New integration approaches based on temporary pore stuffing by polymers and cryogenic etching allowed to reduce plasma etch related degradation of low-k materials. Some new conductors, such as Mo and Ru, can be patterned by plasma, and therefore, they offer the opportunity to return from damascene to subtractive technology (metal etch first, then the gap filling by flowable dielectric). Complete subtractive approach is demonstrated as the low-k replacement approach. However, so-called semi-damascene technology (partially subtractive) is becoming more popular. The major advantage of subtractive technology is possibility to avoid plasma exposure of low-k dielectrics and therefore may also allow to use new types of dielectric layers based on metal-organic frameworks (MOF). Another advantage is the barrier deposition onto the dense metal surface, which makes it easier to scale the barrier thickness.

New materials for pore sealing (like self-assembling monolayers) have been introduced and allowed to reduce the thickness of diffusion barriers. To overcome limitations of optical lithography, extreme UV lithography and selective deposition are under exploration.

All these challenges, new materials and their problems and advantages, new integration approaches will be discussed during the presentation.

The work was supported by RFBR grant 18-29-27022.

Evolution of low-*k* films properties near critical curing temperature

A.S. Vishnevskiy[1], D.S. Seregin[1], G.A. Orlov[1], V.A. Storonkin[1],
I.S. Ovchinnikov[1], K.A. Vorotilov[1], M.R. Baklanov[1,2]
1. MIREA – Russian Technological Univ. (RTU MIREA), Moscow, Russia, vishnevskiy@mirea.ru
2. North China University of Technology (NCUT), Beijing, P. R. China, baklanovmr@gmail.com

This paper presents the temperature dependence of the properties of the sol-gel periodic mesoporous organosilica (PMO) low-*k* films modified with various organic bridging groups connecting silicon atoms. Film-forming solutions were prepared in an aqueous acidic solvent medium using hydrolysis and co-condensation reactions of MTMS (55 mol%) and one of the alkylene alkoxysilanes, the monomers of which contain a methylene (BTESM), ethylene (BTMSE) or phenylidene (BTESB) bridging group (see Fig. 1). The nonionic surfactant Brij® L4 (40 wt%) was used as a porogen. The PMO films were spin-coated on silicon wafers using these film-forming solutions, followed by soft baking at 200 °C and the non-cumulative annealing in air at temperatures from 200 to 700 °C and separately at 1000 °C for 30 min/each.

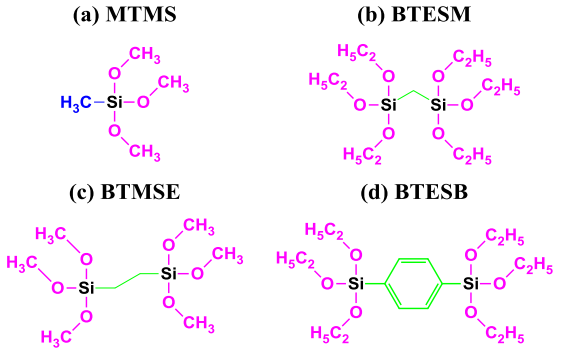

Fig. 1. Examples of the most popular and used in this work precursors, where MTMS is methyltrimethoxysilane (a) commonly used to obtain organosilicate glasses; BTESM is bis (triethoxysilyl) methane (a), BTMSE is 1,2-bis (trimethoxysilyl) ethane (b) and BTESB is 1,4-bis (triethoxysilyl) benzene (c), all are used to prepare PMO.

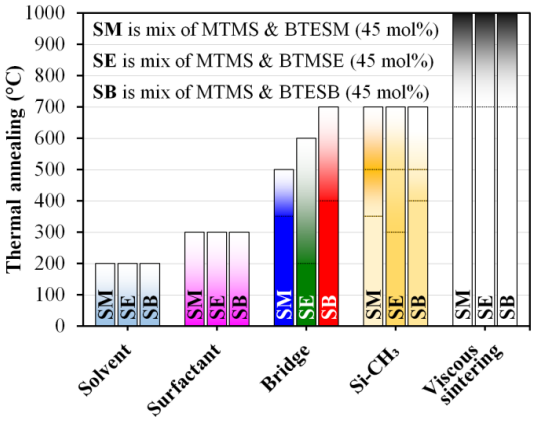

Fig. 2. Temperature diagram of evaporation of the solvent residues, destruction of the surfactant and the corresponding bridge, intensifition/destruction of the methyl group and occurrence of viscous synthesis.

It was shown that phenylidene bridging groups in the MTMS-BTESB samples have the best temperature stability (~400 °C, see Fig. 2) upon annealing in air. These samples have the highest Young's modulus and minimum pore size in the entire range of heat treatment. However, these films are characterized by weak hydrophobicity, higher values of shrinkage, refractive index (RI), dielectric constant *k*, dielectric loss tangent tgδ, and lower open porosity compared to the copolymer films MTMS-BTESM and MTMS-BTMSE. This is due not only to the higher optical density of these films, but also to the steric factor of the BTESB molecules and their π-stacking, which leads to the appearance of a large number of silanol groups. The MTMS-BTESM films are significantly inferior in mechanical properties and pore size, but differ in the highest hydrophobicity and porosity, have the lowest values of shrinkage, RI, *k* and tgδ. However, in their structure, carbon bridging groups (Si–CH_2–Si) are transformed into siloxane ones (Si–O–Si) during heat treatment in air [1]. As a result, terminal methyl groups are formed and Si–OH bonds are suppressed. Thus, the hydrophobicity of the films increases, but the presence of terminal methyl groups negatively affects the Young's modulus due to the less network linkages. The MTMS-BTMSE samples are only slightly inferior in shrinkage, RI, and hydrophobicity, but have very similar of the *k* and tgδ values, Young's modulus and pore size (≤400 °C). At the same time, films with ethylene bridges are characterized by the lowest thermal stability; this is indicated by a monotonic decrease in the number of C–C bonds during heat treatment in air.

This work was supported by the RFBR (grants 18-29-27022 and 18-29-27024) and the Ministry of Science and Higher Education of the Russian Federation (project 0706-2020-0022).

1. T. Asefa, M.J. MacLachlan, H. Grondey, N. Coombs and G.A. Ozin. "Metamorphic Channels in Periodic Mesoporous Methylenesilica". Angew. Chem. Int. Ed., **39** (10), pp. 1808–1811, 2000.

Post-processing hydrophobization of microporous low-*k* films

D.A. Vorotyntsev, A.S. Vishnevskiy, D.S. Seregin, K.A. Vorotilov
MIREA – Russian Technological University (RTU MIREA), Moscow, Russia, techcenter@mirea.ru

The study analyses the surface modification of microporous organosilicate film with hexamethyldisilazane (HMDS) vapour for hydrophobization with methyl groups [1]. Film-forming solutions were prepared in an aqueous acidic solvent medium using hydrolysis and condensation reactions of 1,4-bis (triethoxysilyl) benzene (BTESB, Fig. 1 a). The surfactant Brij® L4 (30 wt%) was used as a porogen. The phenylene-bridged film was formed by spin-on deposition. Thereafter, it was subjected to heat treatment on a hot plate in air at a temperature T_a = 120 °C, 30 min and then at T_a = 200 °C, 30 min. After, two pieces were split from a Si wafer with a film: "w/o" – without HMDS processing and "with" – with HMDS one (Fig. 1 b). Both samples were placed in a N_2-purged chamber of the hot plate, on which a gradual (10 °C/min) heating from ~20 °C to T_a = 390 °C was performed with a holding time of 30 min. Subsequently, the films were cooled to T_a = 100 °C (~5 °C/min). Then, the "w/o" sample was removed from the chamber, and the "with" sample was processed in HMDS vapour at a flow of 50 NL/h for 5 min. Temperature stability was checked by cumulative heat treatment in air at T_a = 250; 300; 350; 400; 430 °C, 30 min/each (+60 min at T_a = 350 °C).

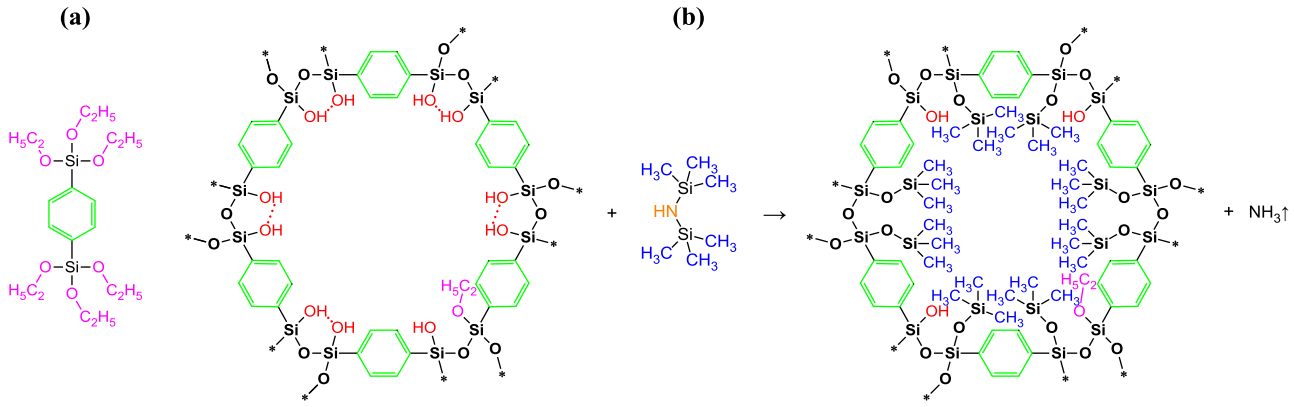

Fig. 1. Structure of BTESB monomer molecule (a) and 2-dimensional illustration of the process of hydrophobization with HMDS as the example of a pore (formed by six BTESB molecules) and four HMDS molecules (b).

It was shown that after surface modification of the test film sample prepared from single BTESB, the number of silanol groups and the water molecules adsorbed on them tend to decrease, whereas the number of methyl groups tends to increase. It leads to a decrease in the hydrophilicity of the film surface, such as an increase in the value of the water contact angle, a decrease in the *k* value, and the dielectric loss tangent. Thus, relatively large HMDS molecules (0.775 nm [2]) can penetrate into the open microporous structure of the material under study, the average pore diameter of which is 0.66 nm, and can react with a part of its surface silanols. Silylation of the microporous film with HMDS reduces open porosity with no change of the pore size distribution. However, analysis of the FTIR spectra showed limited (less than 350 °C in air) temperature stability of methyl groups introduced by heat treatment with HMDS vapour, which is also time dependent. Herein, ellipsometric measurements and FTIR spectroscopy indicated the pore walls strengthening of the hydrophobized films during heat treatment. It results in less porosity reduction, decrease in the shrinkage, and increase in the Young's modulus. Furthermore, it was shown that the annealing of the porous 1,4-phenylene-bridged film in N_2 at 390 °C leads to the destruction of some of the bridging groups with the formation of terminal methyl groups Si–CH_3. This effect is enhanced upon further heat treatment in air.

This work was supported by the RFBR (grant numbers 18-29-27022 and 18-29-27024) and the Ministry of Science and Higher Education of the Russian Federation (project 0706-2020-0022).

1. T.-Y. Li, C.-H. Yu, H.-Y. Lu, B.-Z. Wan. "Effect of Hydrophobic Tail Length of Polysorbate Surfactants on Properties of Porous Silica Ultra-Low-k Film". ECS J. Solid State Sci. Technol., **2** (3), pp. 61–68, 2012.
2. O. Böhm, R. Leitsmann, P. Plänitz, T. Oszinda, M. Schaller, M. Schreiber. "Novel k-restoring scheme for damaged ultra-low-k materials". Microelectron. Eng., **112**, pp. 63–66, 2013.

Effect of precursors hydrolysis conditions on structure and properties of benzene bridged organosilica glass films

G.A. Orlov, A.S. Vishnevskiy, D.S. Seregin, K.A. Vorotilov
MIREA – Russian Technological University (RTU MIREA), Moscow, Russia, georgiiorlov@mail.ru

The research and development of low-*k* dielectrics with superior properties for VLSI metallization systems is an urgent task. However, to meet industrial requirements low-*k* material should have several contradictory properties: high porosity, small pore size and high Young's modulus value. At present periodic mesoporous organosilicas (PMOs) containing ≡Si–O–Si≡ bonds, bridging organic groups between silicon atoms and terminal methyl groups are promising materials for application in interconnects. Modification of the silicate structure with benzene bridging groups provides smaller pore size and higher Young's modulus in comparison with methylene and ethylene containing films. However, high hydrolysis rate of 1,4-bis (triethoxysilyl) benzene (BTESB) along with a steric effect at network formation, cause difficulties in formation of optimal copolymer structure. The hydrolysis of BTESB plays the key role to obtain films with desired structure and properties.

In this work we have studied an effect of water content in film-forming solutions on formation of the porous structure and properties of the BTESB based PMO low-*k* films.

Film-forming solutions were prepared with different BTESB content from 25 to 100 mol% relative to methyltrimethoxysilane (MTMS). Polyethylene glycol dodecyl ether (Brij® L4) was used as a porogen in an amount of 30 wt%. After spin-coating, the films were dried at 200 °C, 30 min on a hot plate and annealed at 430 C, 30 min in a diffusion oven.

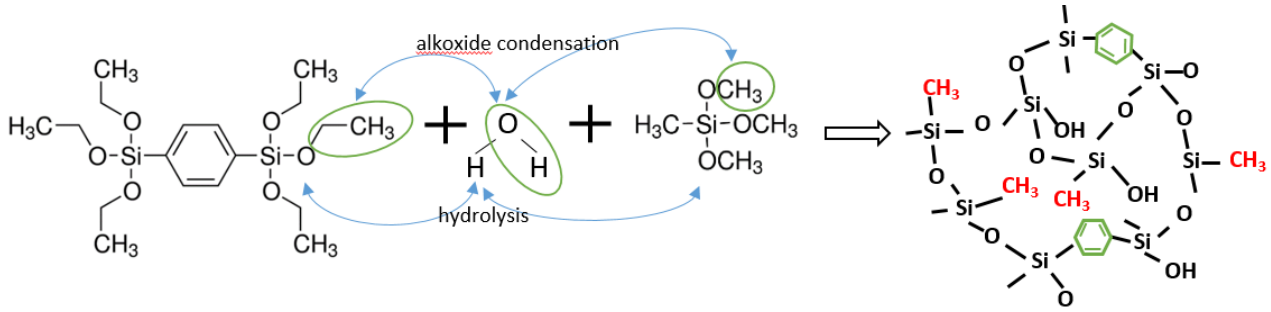

Fig. 1. Co-hydrolysis and co-condensation of alkoxides precursors with formation of cross-linked organosilica copolymer with benzene bridges.

It was found that uniform films are formed at H_2O/EtO = 0.4 and MTMS/BTESB = 75/25, 55/45, and 40/60. Increase of the benzene group content up to 100 mol% leads to a striations formation. At H_2O/EtO = 0.6 homogeneous films were formed only at MTMS/BTESB = 75/25 and 55/45. A further benzene content increase leads to films evaporation from the substrate after annealing due to incomplete condensation as a result of low flexibility of the 1,4-benzene unit with Si in a para-configuration [1].

The films obtained at H_2O/EtO = 0.4 demonstrate small pores (about 1 nm in diameter) and open porosity V_{open} 29% (except the sample with MTMS/BTESB = 75/25 with V_{open} = 21%). The pore size and open porosity increase up to ~2.5 nm and ~35%, dielectric constant *k*~ 2.3. The lower water content in the film-forming solution leads to incomplete alkoxides hydrolysis, as a result lower amount of silanols are available to interact with surfactant molecules. This results in a highly crosslinking structure and almost a two-fold increase in the Young's modulus, but the dielectric constant in this case increases k~2.7–2.9.

This work was supported by the RFBR 18-29-27024 and the Ministry of Science and Higher Education of the Russian Federation (project 0706-2020-0022).

1. A.S. Vishnevskiy, S. Naumov, D.S. Seregin, et al. “Effects of Methyl Terminal and Carbon Bridging Groups Ratio on Critical Properties of Porous Organosilicate Glass Films”. Materials, **13** (20), pp. 4484(1–21), 2020.

Spin-on deposition of low-*k* films: Effect of solvent

M.V. Selivanov, A.S. Vishnevskiy, D.S. Seregin, K.A. Vorotilov
MIREA – Russian Technological University (RTU MIREA), Moscow, Russia, selivanov-99@inbox.ru

Semiconductor manufacturing requires high purity defect-free materials. Spin-on deposition might be attributable to specific defects due to some peculiarities of deposition via a liquid phase, see fig.1 [1]. Deposition of low-*k* films includes preparation of initial sol through hydrolysis and polycondensation of silicon alkoxides in an organic solvent. The solvent effects not only on initial sol properties, but as well on spin-on process. The solvent evaporation promotes the condensation of oxoalkoxide species, accompanied by metal–oxygen network formation and an increase in the liquid's viscosity causing gradual cessation of convective liquid outflow. For this reason, the vapor pressure of the solvent (boiling point) determines the film thickness. Moreover, the solvent affects the formation of radial stripes and poor wetting of the substrate surface. Radial runways are wave-like defects that create a non-uniform film thickness profile due to Marangoni convections (fig.1). In the present work, porous low-*k* films are deposited from initial sols with different solvents and structure-directing agents via the spin-on coating technique.

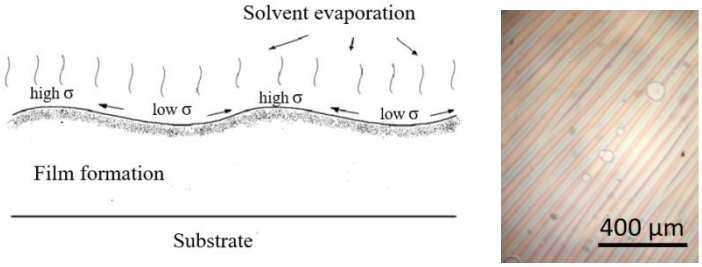

(a) (b)

Fig. 1. Schematic illustration of the striation formation (a) and optical micrograph of the striations in the sol-gel film (b) (σ-surface tension)

Several types of polar and aprotic solvents were used, including monoatomic alcohols: ethanol, isopropanol, butanol, hexanol; diatomic alcohols: ethylene glycol and diethylene glycol; cyclic ether: tetrahydrofuran, methyl isobutyl ketone (ketone class) and 2-methoxyethanol (glycol ether). Nonionic surfactants with different molecular weights were used as structure-directing agents: Brij®L4, Brij®52, Brij®76 and the ionic surfactant - cetyltrimethylammonium bromide CTAB. These surfactants were selected as they might be used in evaporation induced self-assembly to create ordered porous structure with a small pore size (less than 3.5 nm).

It was found that uniform and defect-free porous low-*k* films provide tetrahydrofuran and butanol-based solutions. Butanol can be used with both nonionic and ionic surfactants. Uniform films were formed using the nonionic surfactants Brij®L4 and Brij®76 with tetrahydrofuran in the initial solution, while in the case of Brij®52 granulated defect coating was formed. CTAB does not dissolve in the film-forming solution in this case. When isopropanol is used then striations are observed in the films, regardless of the surfactant used.

Type and molecular weight of a surfactant influence on the refractive index of the films regardless of the solvent. The lowest refractive index value (1.218 - 1.223) was observed in samples, which porous structure was formed using CTAB surfactant. Despite the lower refractive index, samples from CTAB-containing solutions did not show lowest dielectric constant due to their hydrophilicity. Films deposited from Brij®76-containing solutions demonstrates the lowest dielectric constant $k = 2.08 \pm 0.05$.

This work was supported by the RFBR 18-29-27024 and the Ministry of Science and Higher Education of the Russian Federation (project 0706-2020-0022).

1. H. Kozuka. *Radiative Striations in Spin-Coating Films*. In: Klein L., Aparicio M., Jitianu A. (eds) Handbook of Sol-Gel Science and Technology. Springer, Cham, 2018.

Modeling the characteristics of memristors based on low-dimensional materials

F. Meshchaninov[1,2], D. Zhevnenko[1,2], V. Kozhevnikov[1,2], E. Shamin[1,2], E. Gornev[1,2]
1. Moscow Institute of Physics and Technology (State University), Dolgoprudny, Russia.
2. JCS Molecular Electronics Research Institute, Zelenograd, Russia

The development of the microelectronics areas related to the construction of artificial intelligence systems requires constant improvement of the corresponding component base. One of the most promising solutions in this area is associated with the memristor [1, 2].

Depending on the material of the functional layer and the design features of the memristor, the main disadvantages vary from structure to structure, however, most of them are somehow determined by the random nature of the processes occurring inside the device [3-5]. One of the important directions in the development of new generation memristors is the use of promising low-dimensional materials to increase the stability of characteristics [6].

In this work, we carried out a meta-analysis of the features (fig. 1) of memristors with the inclusion of two-dimensional structures, examined the relationship of these features with elements of various models, including our model of mobility modification [5]. Based on the results obtained, the requirements for the study for comparing the models with each other were described. In the course of the analysis, both the previously obtained experimental results with a memristor based on hafnium oxide [7] and synthetic samples were used.

This research was funded by Ministry of Science and Higher Education of the Russian Federation (grant number 075-15-2020-791)

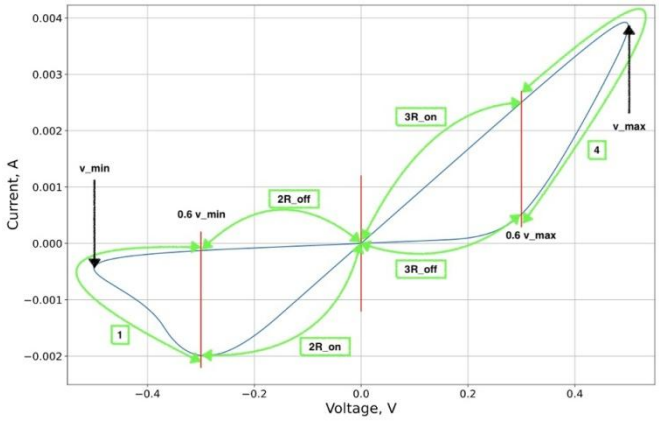

Fig. 1. Example of I-V curve slicing for feature evaluation.

1. L. Chua. «Memristor-the missing circuit element». IEEE Transactions on Circuit Theory, **18**, pp. 507-519, 1971.
2. D. B. Strukov et al. «The missing memristor found». Nature, **453**, pp. 80-83, 2008.
3. W. Sun et al. “Understanding memristive switching via in situ characterization and device modeling”. Nature communications, **10**, pp.1-3, 2019.
4. D. V. Guseinov et al. “Capacitive effects can make memristors chaotic”. Chaos, Solitons & Fractals, **144**, p. 110699, 2021.
5. D. Zhevnenko et al. “Simulation of memristor switching time series in response to spike-like signal”. Chaos, Solitons & Fractals, **142**, p. 110382, 2021.
6. J. Liu et al. “A robust nonvolatile resistive memory device based on a freestanding ultrathin 2D imine polymer film”. Advanced Materials, **31**, p. 1902264, 2019.
7. O. O. Kapitanova et al. “Resistive switching in graphene/graphene oxide/ZnO heterostructures”. Journal of the Korean Physical Society, **64**, pp. 1399-1402, 2014.

Impact of built-in fields dynamics and switching kinetics of polarization on the retention loss in FRAM based on thin $Hf_{0.5}Zr_{0.5}O_2$ films

E.V. Kondratyuk, V.V. Mikheev, D.V. Negrov, A.A. Chouprik
Moscow Institute of Physics and Technology, Dolgoprudny, Moscow Region, Russia,
E-mail address: ekaterina.v.kondratyuk@phystech.edu

Hafnium oxide ferroelectric films have emerged as viable candidates for nonvolatile ferroelectric memories because of their full compatibility with the modern Si microelectronics technology [1]. Currently, ferroelectric random access memory (FRAM) is one of the most promising concepts of non-volatile memory since it advantages other memory devices available on the modern market in terms of operation parameters: writing speed, power consumption and endurance. In ferroelectric memory capacitor, the information is stored in the orientation of polarization. The reading of the stored information occurs through the probing of the electrical current during a unipolar readout voltage pulse applied to the ferroelectric capacitor – either the flowing charge of the polarization reversal or its absence indicates the stored FE capacitor state and thus defines the stored bit value. The readout charge stored in a FE capacitor can eventually decrease, thus resulting in the retention loss. This phenomenon is caused by the change of coercive voltage with time due to the built-up of internal electric filed and following appearance of an imprint of P-V hysteresis (i.e., a shift along V-axis) for the monodomain FE capacitor. Such dependence of ferroelectric properties on time is called the aging of ferroelectric layer [2]). In a result of the aging, the amplitude of the predefined readout voltage can turn out close to the coercive voltage of the aged capacitor, which causes the decrease of the switched ferroelectric domains fraction and thus the possible readout failure. Another important issue affected by built-in internal bias field is the kinetics of polarization switching, which determines the speed of read and write operations. Built-up fields suppress the applied electric field across ferroelectric layer thus causing the decrease of switching speed.

The built-in internal bias field and their dynamics during the aging may be associated with: (i) the dead layer at the interface and the change of its thickness, (ii) the charge accumulation/depletion of the oxygen vacancies due to their migration or trapping/detrapping of carriers by the traps in HfO_2, (iii) (mis)alignment of the dipole defects. In this work, to resolve the origin of the retention loss we have correlated the device performance with the results of capacitance transient spectroscopy and in situ piezoresponse force microscopy [3]. Ferroelectric capacitors W (10 nm)/$Hf_{0.5}Z_{0.5}O_2$ (10 nm)/TiN (20 nm) with a high rate of retention loss were fabricated for this purpose and studied. We have shown the current models of the kinetics of polarization switching require improvement to be applied to the $Hf_{0.5}Zr_{0.5}O_2$ capacitors due to built-up of internal electric fields. Switching kinetics can be characterized by the average characteristic switching time and average activation energy for switching domains, which were found to be equal to $1.5 \cdot 10^{-9}$ s и 9.6 MV/cm respectively. Further, we have demonstrated that the built-in field is associated with the accumulation of the positive charge at the interfaces with electrodes due to short-term trapping/detrapping effect and long-term charge diffusion. The redistribution of charges during the aging of the FE memory cell is fully defined by the domain structure. At the polydomain state of ferroelectric $Hf_{0.5}Zr_{0.5}O_2$-based memory cell, the retention loss is faster compared to monodomain state. In contrast, the polydomain state demonstrates an improved endurance compared to monodomain state. Therefore, such important performance of FE HfO_2-based memory as the retention and endurance are related oppositely, and the precise balance between them should be found before the memory devices can be implemented by the electronics industry.

This work was performed using equipment of MIPT Shared Facilities Center. Studies of aging effect and supported by the Russian Science Foundation (Project 20-19-00370). Device fabrication was supported by the Ministry of Science and Higher Education of the Russian Federation (agreement No. 075-00337-20-03, project FSMG-2020-0001).

1. T. S. Böscke, J. Müller, D. Brauhaus, U. Schröder, U. Böttger.. Appl. Phys. Lett., 99, p. 102903, 2011.
2. Yu.A. Genenko, Ju. Glaum, M.J. Hoffmann, K. Albe. Mater. Science and Eng. B, 192, pp. 52-58, 2015.
3. A. Chouprik, E. Kondratyuk, V. Mikheev, Y. Matveyev, et al. Acta Materialia, 204, 11651, 2021.

Development of a biocompatible flexible ferroelectric field effect transistor based on thin hafnium oxide films

V.V. Mikheev, A.A. Chouprik, E.V. Kondratyuk, E.V. Korostylev, E.A. Guberna, G. Margolin, D.V. Negrov

Moscow Institute of Physics and Technology, 9 Institutskiy per., Dolgoprudny, Moscow Region, Russia, mikheev.vv@phystech.edu.

Neuroprostheses based on functional electrical stimulation are a means for compensation of lost motor sensory or cognitive modality that might have been damaged as a result of an injury or a disease. Progress in neuroprosthetic technology has led to advances in the therapy of neurological diseases. In particular, deep brain stimulation helps patients suffering from Parkinson's disease and is an option for treating severe mental illnesses, such as depression and obsessive-compulsive disorder, epilepsy and other psychiatric disorders.

A further stage in the development of bioimplants requires the fabrication of flexible logical elements and, potentially, microcontrollers, including transistors and non-volatile memory storage. Non-volatile memory elements should provide high integration density, low power consumption, high performance, sufficient endurance and uniformity of operating parameters. One of the most promising candidates for such memory is ferroelectric field-effect transistors (FeFET). Compared to the commonly devices used the flash memory FeFET exhibits small read and write time and provides potentially unlimited endurance and high scalability.

Until recently, only ferroelectric polymers and organic crystals were considered as functional materials in flexible ferroelectric memory devices because of their inherent flexibility. However, application of these materials in electronics is substantially limited by the low switching speed of ferroelectric polarization and high coercive voltages. In contrast, classical ferroelectric materials exhibit high switching rates and residual polarization. However, due to the high leakage currents such materials require sufficiently large film thicknesses of hundreds of nanometers and thus undergo internal mechanical stress when bent. That is why discovery of ferroelectricity in ultrathin (5-30 nm) films of doped hafnium oxide paves the way towards flexible biocompatible ferroelectric memory [1]. Flexible ferroelectric capacitors coupled with flexible transistor based on C_{60} channel (1T-1C structure) has been already demonstrated in 2017 [2]. However, fullerenes used as a channel in field effect transistors require complicated growth, low integration density and low production yield of transistors. Thus, implementation of such memory cells in neuroprostheses is quite limited.

In this work, we develop flexible ferroelectric field effect transistor with ferroelectric hafnium oxide as a functional layer and graphene as a channel. Polyimide films are used as a substrate due to its high mechanical strength, flexibility, excellent insulation properties and inertness to chemical reactions. To date, we have developed low temperature technological process for fabrication of flexible ferroelectric capacitors based on ferroelectric hafnium oxide and demonstrated electroresistance switching effect in graphene channel caused by polarization reversal in ferroelectric layer of ferroelectric field-effect transistor.

This work was performed using equipment of MIPT Shared Facilities Center and supported by the Russian Science Foundation (Project 20-19-00370).

1. T.S. Boscke, J. Muller, D. Brauhaus, U. Schröder, U. Böttger, Appl. Phys. Lett. **99**, 102903 (2011).
2. H. Yu, C.-C. Chung, N. Shewmon, Sz. Ho, J. H. Carpenter, R. Larrabee, T. Sun, J. L. Jones, H. Ade, B. T. O'Connor, F. So., Adv. Funct. Mater. **27**, 1700461 (2017).

Impact of Temperature on Single Event Upset in SRAM Cells with Technology Node Scaling

D. Popov, D. Silkin, A. Sultanov, A. Mukhametdinova, B. Gallyamov
National Research University Higher School of Economics (Moscow Institute of Electronics and Mathematics), Moscow, Russia, da.popov@hse.ru

Electronic devices in space environment are exposed to different types of radiation. High fault-tolerance of SRAM cells to the single event upset after heavy ion exposure is an important condition for the reliable operation of aerospace and other special-purpose equipment [1]. Modern technology computer-aided design makes it possible to evaluate the radiation hardness of a semiconductor device at the early stages of design, which can significantly reduce economic losses. However, reliable simulation result can be obtained only after calibration based on experimental data.

In this work, the physical TCAD model was developed to account for the heavy ion strike into 6T SRAM cell for different technology nodes taking into account temperature effects.

As soon as the single event upset depends not only on the MOSFET structure under the strike but also on the whole SRAM cell circuit behavior, the most correct SEU simulation can be achieved by coupling the TCAD (structure) simulator with the SPICE (circuit) simulator.

6T SRAM cells (see Fig. 1) based on 130nm MOSFET, 90nm MOSFET, and 30nm FinFET devices are considering. The struck of the Oxygen ion was simulated at drain pn-junction n-left transistor (red area in Fig. 1) at temperatures of 300 K, 423 K, and 573 K.

The TCAD model was validated based on experimental data for collected charge. In Figure 2 shows the dependence of the collected charge after the heavy ion impact on temperature for three technology nodes. Points in the Figure 2 indicate experimental data from [2]-[3] for 300 K. The temperature dependence is consistent with the data from [4]. The simulation RMS error for all the devices is not more than 15%.

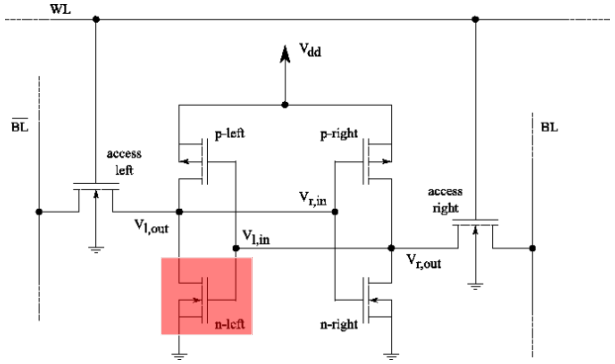

Fig. 1. 6T SRAM circuit diagram with the indication of the ion hit location.

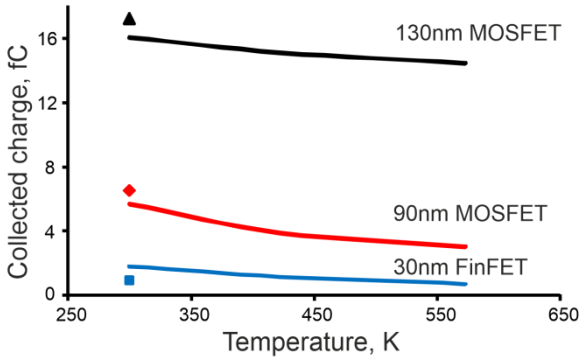

Fig. 2. Collected charge dependence on temperature for different channel lengths.

The physical TCAD model of the heavy ion impact on semiconductor structures was developed based on experimental data. The model was used to determine the values of the critical collected charges leading to the switching of 6T SRAM cells based on 130nm, 90nm MOSFETs, and 30nm FinFET in the temperature range from 300 K to 573 K.

1. R.L. Patterson, et al. “Electronic Components for Use in Extreme Temperature Aerospace Applications”, 12th International Components for Military and Space Electronics Conference (CMSE 08), San Diego, 2008.
2. D. Kobayashi. “Scaling Trends of Digital Single-Event Effects: A Survey of SEU and SET Parameters and Comparison With Transistor Performance”, IEEE Trans. on Nucl. Sci., **68** (2), pp. 124-148, 2021.
3. G. Li, et. al. “Influence of Fin Width on Single-Event-Upset Characteristics of FinFET SRAM”, Semiconductor Science and Technology, **35** (3), pp. 1-5, 2020.
4. D. Truyen, et al. “Temperature Effect on Heavy-Ion Induced Parasitic Current on SRAM by Device Simulation: Effect on SEU Sensitivity”, IEEE Trans. on Nucl. Sci., **54** (4), pp. 1025-1029, 2007.

Raman scattering of structural modifications in $Ge_2Sb_2Te_5$ thin films during thermal crystallization: in-situ Raman scattering study

V. Glukhenkaya, A. Romashkin, A. Yakubov, P.I. Lazarenko, M. Fedyanina, A.A. Sherchenkov
National Research University of Electronic Technology, Moscow, Russia.
E-mail: *kapakycek2009@yandex.ru*

The thin films of $Ge_2Sb_2Te_5$ (GST) have been successfully used as an active functional layer in the elements of nonvolatile optical phase change memory, in particular, devices of nanophotonic and integrated optic. It is possible due to the high-rate phase transformations (<50 ns) from amorphous to crystalline states accompanied by the large optical contrast between states [1]. However, the lack of detailed understanding of the structural transformation mechanisms in GST thin films prevents further optimization and development of the multilevel PCM technology. So, the aim of this work is an "in-situ" investigation of the local structural rearrangements in GST thin films during thermal crystallization based on the simultaneous measurement of the temperature dependences of Raman scattering spectra and resistivity.

The amorphous $Ge_2Sb_2Te_5$ thin films (30 nm thickness) were deposited by the magnetron sputtering on the Si and SiO_2 substrates with planar electrodes of TiN/W/TiN/Al (30/50/15/600 nm). The optical properties in the range from 300 to 2100 nm were measured by ellipsometry. The temperature dependences of the Raman spectra and resistivity for the GST thin films were obtained through simultaneous measurements in the temperature range from 30 to 350 °C in an Ar atmosphere. The seven peaks in the obtained Raman spectra were decomposed by the Gaussian fitting. The results of the investigation of GeTe and Sb_2Te_3 bulk materials were used for the association of the peaks with structural unit vibrations. The structure analysis was performed by the X-ray diffraction method before and after thermal exposure.

Analysis of the Raman spectra temperature dependences showed that heating leads to changes in the peak parameters: intensities, peak areas, FWHMs and shifts peak position (fig.1). These changes occur in the temperature ranges of 145-160 °C and 265-290 °C (and can correspond to the transitions from an amorphous state to fcc, and further from fcc to hcp phases. It should be noted that the sharp changes of the refractive index were also observed in the identified temperature ranges of phase transition. All of these property modifications in total indicate the ongoing structural rearrangements.

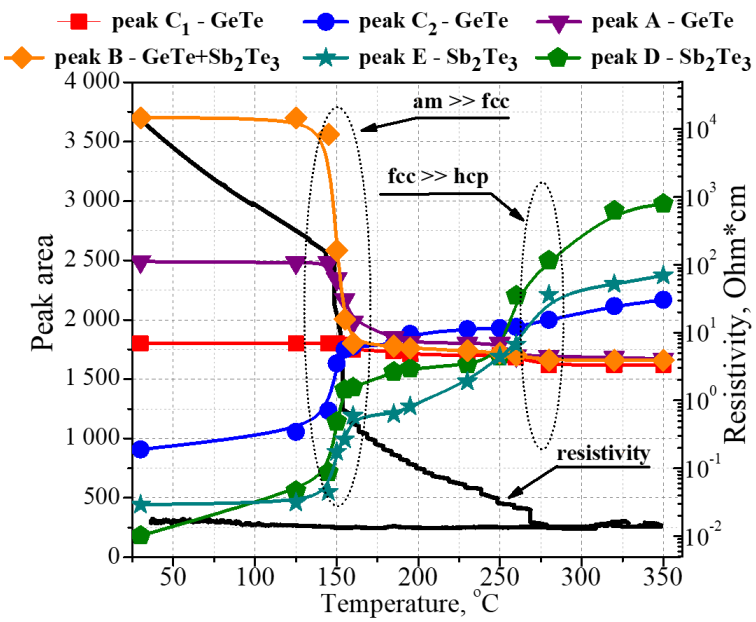

Fig. 1. Temperature dependences of peak areas of $Ge_2Sb_2Te_5$ thin film.

A quantitative and qualitative analysis of the temperature dependences of the Raman spectra showed that the crystallization of GST from the amorphous state to the metastable fcc state takes place through the rearrangement of Ge/Sb atoms from tetrahedral and pyramidal configurations into defective octahedral one for GeTe and Sb_2Te_3 compounds, respectively, whereas the fcc→hcp transition takes place primarily due to the local rearrangements of Sb atoms caused by the elongation of the covalent bonds.

This work was supported by Russian Science Foundation (project No. 20-79-10322).

1. M. Wuttig, H. Bhaskaran. "Phase-change materials for non-volatile photonic applications, Nat. Photonics, **11**, pp. 465-476, 2017.

Methylated porous low-k materials: critical properties and plasma resistance

A.A Rezvanov[1,2], A.V. Miakonkikh[3], A.S. Vishnevskiy[4], D.S. Seregin[4], K.A. Vorotilov[4], K.V. Rudenko[4], M.R. Baklanov[3,5]

1. Moscow Institute of Physics and Technology, Dolgoprudny, Russian Federation
2. Molecular Electronics Research Institute, Zelenograd, Moscow, Russian Federation
3. Valiev Institute of Physics and Technology RAS, Moscow, Russian Federation
4. Research and Education Center "Technological Center", Moscow, RTU MIREA – Russian Technological University, Russian Federation
5. Department of Microelectronics, North China University of Technology, Beijing, People's Republic of China
arezvanov@niime.ru

Nowadays there is an increasing demand for high-speed devices in all areas of industry and services. In this regard, the reported research is related to optimization of chemical composition during the development of new low dielectric constant (low-k) materials for the back end of line (BEOL) technology [1]. The presently selected by semiconductor industry porous organosilicate glass (p-OSG) based low-k dielectrics have been implemented in the modern process flows to reduce the negative impact of RC-delays [2, 3]. The OSG low-k dielectrics have silica-like matrix, where terminal methyl (CH_3) groups replace the part of bridging oxygen atoms. In the present work, we targeted a systematic study of methyl group concentration on the most important critical properties of OSG low-k materials, such as porosity and pore size, k-value, mechanical properties and resistance to plasma damage reduction.

Series of low-k samples with different methyl group concentration were prepared. The film-forming solutions were prepared by hydrolysis and condensation of tetraethoxysilane (TEOS, 99.999%) and methyltriethoxysilane (MTEOS, 99.9%) in a solvent mixture. The low-k characteristics and their evolution after exposure in plasma were evaluated by using several experimental techniques: FTIR (Fourier Transform Infrared Spectroscopy), SE (Spectroscopic Ellipsometry), EP (Ellipsometric Porosimetry), XPS (X-ray Photoelectron Spectroscopy), Nanoindentation and Hg probe based capacitance-voltage (CV) measurements. For the etch tests a semi-commercial ICP (Inductively Coupled Plasma) reactor was used.

Increase of the methyl group concentration by changing TEOS/MTEOS ratio decreases the open porosity, k-value and Young's modulus and increases the mean pore radius although the template concentration was kept constant. The etch rate change in SF_6 or Ar/SF_6 plasmas have non-monotonic character. The increase of the etch rate well correlates with the number of fluorine atoms penetrated into pores. Plasma damage by fluorine radicals was significantly reduced in the samples with high methyl group concentration. When the carbon concentration in low-k is below of certain critical level in respect to fluorine atoms concentration, the low-k can almost completely loose carbon containing groups even before the etch process starts. On the other hand, at high carbon concentration the front of demethylated low-k can move with the same speed as the etch front. In this case one can achieve the lowest plasma damage. However, an important drawback of carbon rich OSG low-k is reduced mechanical properties. Therefore, the carbon concentration must be optimized and in this particular case it was achieved by selection of TEOS/MTEOS ration 40/60 that corresponds to the bulk carbon concentration about 10 atomic % (XPS). Higher concentration of fluorine radicals will request higher concentration of carbon containing groups [4].

1. K. Maex, M.R. Baklanov, D. Shamiryan, F. Iacopi, S.H. Brongersma, and Z.S. Yanovitskaya, J. Appl. Phys. **93**, 8793, 2003.
2. M.R. Baklanov, P.S. Ho, E. Zschech, Advanced Interconnects for ULSI Technology (Wiley & Sons, 2012).
3. A.S. Valeev, G.Ya. Krasnikov, V.A. Gvozdev, and P.I. Kuznetsov, RU patent No. 2548523 (17 December 2013).
4. A.A Rezvanov, A.V. Miakonkikh, A.S. Vishnevskiy, D.S. Seregin, K.A. Vorotilov, K.V. Rudenko, M.R. Baklanov, J. Vac. Sci. Technol. A **38**, 033005, 2020.

Study of electrodynamic parameters of the low-k thin films in the THz-IR ranges

A. Gavdush, G. Komandin
Prokhorov General Physics Institute of the Russian Academy of Sciences, Moscow, Russia,
arsenii.a.gavdush@mail.ru, gakomandin@mail.ru.

The electrodynamic parameters of thin dielectric films differ from the parameters of bulk materials with equivalent composition due to the size effects and morphological features [1]. Both the applied and fundamental importance of studying the formation of thin films and correct modelling of their broadband dielectric response function is determined by the high demand of such objects in various branches of science and technology, including microelectronics, biophotonics, and astrophysics. An absorption spectrum is the most often obtained result in the broadband measurements by means of optical methods. This result reveals the energy spectrum of electronic transitions and resonance vibrations of ions. With this approach, the most important parameter that is the contribution of electrodipole oscillations to the total low-frequency dielectric constant remains out of consideration.

In order to solve the posed problem, we use experimental data obtained by various methods, including coherent submillimeter spectroscopy, terahertz time-domain pulsed spectroscopy and infrared Fourier transform spectroscopy. The combination of these methods allows a detailed analysis of elementary electrodipole absorption processes in the dielectric response, caused by both intrinsic and extrinsic mechanisms [2]. The addition of the ow-frequency impedance measurements data possesses self-calibration that further improves the reliability of the results.

The impact of substrates to the result of broadband dielectric response measurements of multilayer samples is an extremely important aspect in analyzing experimental data and further decomposition of a broadband spectrum into elementary excitations. Analysis of the experimental data within the framework of the matrix approach [3] makes it possible to separate the dielectric contributions from the absorption bands of thin films in a multilayer sample, while taking into account the dispersion of absorption lines according to the Drude-Lorentz dielectric model. The contribution to the dielectric permittivity of the vibrational absorption bands of O–Si–O, CH_3, Si-CH_3 as well as trapped water was determined. When considering the dielectric response of thin films of organosilicate glasses in the THz range, a significant contribution due to the Boson peak was shown. The impact of morphology (and in particular, of porosity) to the dielectric permittivity, both to the whole spectrum and to each of the absorption peaks, was analyzed. Thus, the main mechanisms to the formation of the low-frequency dielectric permittivity of thin films of organosilicate glasses on various substrates have been established.

The research was supported by the Grant RFBR № 18-29-27010 MK.

1. G.A. Komandin, V.S. Nozdrin, A.A. Pronin, O.E. Porodinkov, V.B. Anzin, I.E. Spektor. "Dielectric loss of thin-films SiO_2 samples on Al in THz-IR range." Phys. Solid State, **62**, pp. 267-272, 2020.
2. G.A. Komandin, V.S. Nozdrin, I.E. Spektor, O.E. Porodinkov, D.S. Seregin, A.S. Vishnevskiy, K.A. Vorotilov, A.S. Sigov. "Dielectric contribution of the IR absorption bands of porous organosilicate glass thin films on a platinum sublayer." J. Phys.D.: Appl. Phys., **54**, 215304, 2021.
3. P. Grosse, B. Harbecke, B. Heinz, R. Meyer and M. Offenberg. "Infrared spectroscopy of oxide layers on technical Si wafers." Appl. Phys. A, **39**, pp. 257-268, 1986.

Development and characterization of processes for atomic layer deposition of ruthenium films

E. Smirnova, V. Kuzmenko, A. Miakonkikh, A. Rogozhin
Valiev Institute of Physics and Technology of RAS, Moscow, Russia, smirnova@ftian.ru

For the controlled growth of films using the plasma-enhanced ALD method, it is very important to gain a deep understanding of the physical and chemical mechanisms underlying the growth process. For this purpose, combination of *in situ* methods of plasma diagnostics can be used, such as optical emission spectroscopy (OES) [1] and the Langmuir probe method [2], which can also serve as tools for monitoring the process. Plasma radiation provides information about the components present in the plasma and makes it possible to identify the particles of reagents delivered by the plasma to the surface.

The deposition process of ruthenium films (Fig. 1) was carried out on a commercial FlexAl tool (OIPT, UK) in a plasma-enhanced mode using an ICP remote plasma source. The light emitted during the plasma step of ALD cycle was captured by a quartz optical fiber connected to an Ocean Optics HR4PRO spectrometer (Ocean Insight, Florida, USA). This spectrometer works in a wavelength range of 200-900 nm and has a resolution of approximately 0.5 nm. To obtain the electron temperature and the concentration of plasma ions in the reactor the double Langmuir probe current–voltage (I–V) curve was analyzed. The probe is made of a tungsten wire with a diameter of 0.5 mm, and length 33 mm. Probe was positioned near the wafer.

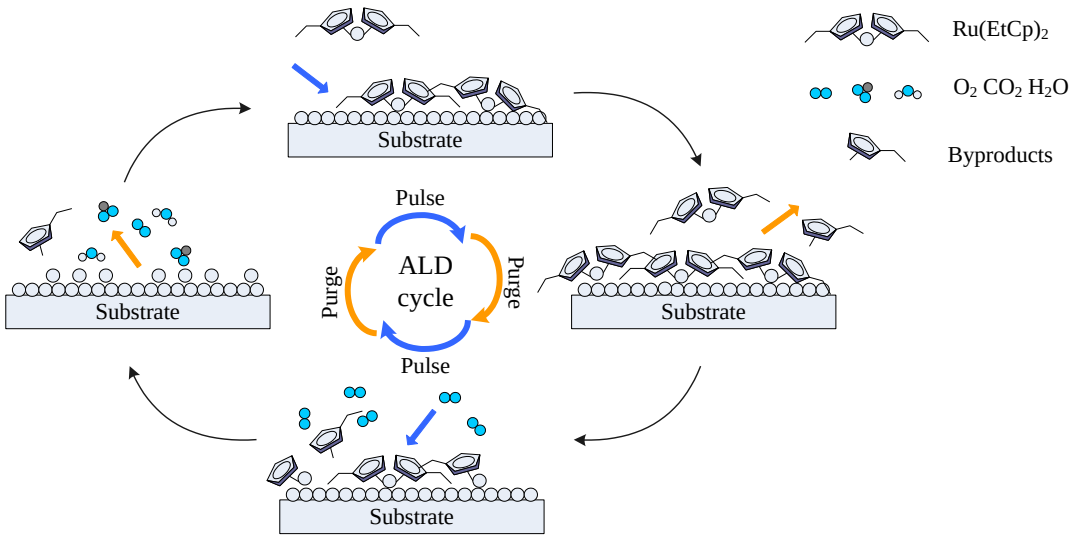

Figure 1. Schematic model of Ru ALD using the sequences $Ru(EtCp)_2$–O_2.

The radiation in the applied Ru ALD recipe (O_2 plasma, 75 W, 65 mTorr) is weak, so the initial search for lines characterizing surface reactions was carried out at higher powers. The emission spectrum of the O_2 plasma recorded after the precursor dosage in the basic recipe was compared with the emission spectrum of the stationary oxygen plasma at the same parameters. An increase in the plasma power has little effect on the conductivity of the film, but increases the roughness.

Observation of plasma during the ALD process makes it possible to monitor the the oxidation reaction of the precursor on the surface, for example, in our case, the OH (308-311 nm), CH (314 nm), CO (519 nm) bands of decreasing intensity are observed. Measurements by double Langmuir probe were carried out in a stationary (Ar, O_2) plasma without a precursor and showed an anomaly in the dependence of the plasma density on the input power. We propose that the remote discharge density in it is affected not only by plasma parameters in the source, but also the transport through the reactor volume.

The study by Program no. 0066-2019-0004 for Valiev IPT RAS by RFBR (project № 18-29-27029).

1. A. J. M. Mackus et al "Optical emission spectroscopy as a tool for studying, optimizing, and monitoring plasma-assisted atomic layer deposition processes". J. Vac. Sci. Technol. A **28**, pp. 77-87, 2010.
2. Y.P. Raizer. *Gas Discharge Physics.* Springer-Verlag Berlin Heidelberg, 1991.

Cobalt for advanced interconnects

A. Rogozhin[1], A. Miakonkikh[1], E. Severov[2], K. Rudenko[1]
1. Valiev Institute of Physics and Technology of RAS, Moscow, Russia, rogozhin@ftian.ru
2. Moscow Institute of Physics and Technology, Dolgoprudnij, Russia

Modern integrated circuits (IC) contain billions of electronic components and all of them should be electrically connected. The metallization system provides interconnections inside ICs. The system is extremely complex. Modern IC process (for example, Intel 10nm) consists of a 13-layer metallization stack [1]. Critical dimensions are 30-40 nm at the M0-M2 metal layers. At the 180 nm process (in 1998) IBM replaced the aluminum interconnect with copper for its significantly lower resistivity, higher scalability, and higher current density capabilities [2]. At the moment the possibilities of the Cu interconnect are almost exhausted. There are two main alternatives to copper now: cobalt and ruthenium [3-5]. Both of them have higher resistivity but could be used without barriers or with an ultrathin barrier. Both materials are greatly stable to electromigration. Electron mean free paths in Co and Ru are comparable with line width at M0-M2 metallization layers. In this work plasma etching processes for cobalt and thermostability of cobal/low-k contact are investigated.

For plasma etching experiments cobalt layers were magnetron sputtered on SiO_2/Si, TaN/Si and TaN/SiO_2/Si structures. Then e-beam lithography was used for mask formation. HSQ resist was used on this step. For some samples the resist was hardened using annealing, UV radiation or O_2 plasma exposure. After that, different recipes were used for cobalt plasma etching. In our case Co etching in the plasma of CO/NH_3 mixtures was found to be extremely inefficient. At low temperature the etching rate was too low. At higher temperature (60 °C) Co film was broken into flakes. Etching in the plasma of CF_3Br appeared to be inefficient too. The most effective process was found to be etching in the plasma of BCl_3/Ar. In this case hardiness of the resist mask played a great role.

To investigate thermostability of Co/low-k contact cobalt layers were magnetron sputtered on porous organosilicate glass (low-k) films. In some cases, TiN or Ru barrier layers were used. All the cobalt layers were capped with 3-nm thick TiN layer. The samples were annealed for 45 min at 400, 500 and 600 °C. It was shown that the main problems during annealing are cobalt oxidation, redistribution and adhesion to low-k film.

The reported study was funded by RFBR according to the research project № 18-37-20076.

1. C. Auth et al., IEDM (2017); doi: 10.1109/IEDM.2017.8268472
2. M. R. Baklanov, C. Adelmann, L. Zhao, S. De Gendt, ECS J. Solid State Science and Technology, 4 (1) Y1-Y4 (2015); doi: 10.1149/2.0271501jss.
3. O. V. Pedreira, K. Croes, A. Leśniewska, C. Wu, M. H. van der Veen,et al. Proc. IEEE Int. Rel. Phys. Symp. (IRPS), Apr. 2017, pp. 6B-2.1–6B-2.8, doi: 10.1109/IRPS.2017.7936340.
4. A. Pyzyna, H. Tsai, M. Lofaro, L. Gignac, H. Miyazoe, IEEE Int. Intercon. Tech. Conf. (IITC) (2017); doi: 10.1109/IITC-AMC.2017.7968982.
5. Marleen H. van der Veen, # N. Heylen, O. Varela Pedreira, I. Ciofi, IEEE Int. Intercon. Tech. Conf. (IITC) p. 172-174 (2018); doi: 10.1109/IITC.2018.8430407.

Towards the problem of IC reliability: instability of the shape of the boundary of adjoining conductive films under the action of electric current and mechanical stresses

T. Makhviladze, M. Sarychev
Valiev Institute of Physics and Technology (RAS), Moscow, Russia, tarielmakh@mail.ru .

A theory has been developed that describes the effect of electromigration of ions that occurs at the interface of layers of conductive joined materials under the action of an electric current on the stability of the initially flat shape of that interface when the action of mechanical stresses generated by the substrate (residual stresses) is taken into account. The presented new results are based on our previous works on the theory of electromigration processes and its application to nano- and microelectronic technology [1-7].

A system of equations describing the relationship between changes in the interface profile and the mechanical stresses that arise in the interface due to ion fluxes initiated by a small spatial-periodic perturbation of the interface is formulated and solved. The criteria for the perturbation amplitude growth with time, i.e. the criteria for interface shape instability depending on the external conditions, were found.

For a more detailed analysis and estimations two particular practically significant cases are considered when the interface is formed by the junction of the same materials and when the junction materials essentially differ so that the diffusive mobility of ions can be neglected in one of them. In these cases, the dependences of the boundaries of the perturbation wavelength regions at which interface instability takes place on external conditions (temperature, current density and residual mechanical stresses generated by the substrate) have been analytically obtained and investigated. The expressions for the characteristic times of exponential growth of the perturbation amplitude have also been obtained.

The estimates that have been carried out show that the appearance of electromigration instability of the interface is possible under conditions those are quite common for accelerated experiments. For example, at $T \sim (100 \div 500)\ ^{o}\mathrm{C}$, $|j| \sim (10^{10} \div 10^{12})\ \mathrm{A/m^2}$ the wavelengths of perturbations (e.g. of vibrational nature) initiating instability are in the range of $\lambda \sim (10 \div 10^{3})$ μm. These results may be of interest for investigation of the problem of increasing the reliability of micro- and nanoelectronic structures.

This work was carried out within the framework of the State Assignment of Valiev Institute of Physics and Technology of the Russian Academy of Sciences, Ministry of Science and Technology of the Russian Federation, subject No. 0066-2019-0004.

1. T.M. Makhviladze, M.E. Sarychev, K.A. Valiev, “Modeling of ion electromigration process in microelectronic structure”, *Proceeding of the 6th Int. Conference on the Numerical Analysis of Semiconductor Devices and Integrated Circuits (NACECODE)*, pp. 521-525, Boole Press, Dublin, Ireland. 1989.
2. K. Valiev, T. Makhviladze, M. Sarychev *et al.* “Nano- and micrometer-scale thin-film-interconnection failure theory and simulation and metallization lifetime prediction. Part 1: A general theory of vacancy transport, mechanical-stress generation, and void nucleation under electromigration in relation to multilevel-metallization degeneration and failure”. Russian Microelectronics, **38**, pp.364-384, 2009.
3. K. Valiev, T. Makhviladze, M. Sarychev *et al.* “Nano- and micrometer-scale thin-film-interconnection failure theory and simulation and metallization lifetime prediction. Part 2: Polycrystalline-line degradation and bulk failure”. Russian Microelectronics, **39,** pp.145-157, 2010.
4. R.V. Goldstein, T.M. Makhviladze, M.E. Sarychev. “Instability of the conducting film surface under mechanical and electrical loads”. Letters on materials, **4,** pp.171-174, 2014.
5. R.V. Goldstein, T.M. Makhviladze, and M.E. Sarychev. “Influence of electrical current on the stability of a conducting film surface”. J. Surf. Investigation, **9,** pp.67-74, 2015.
6. R.V. Goldstein, T.M. Makhviladze, and M.E. Sarychev.” Electromigration-induced instability of the interface between solid conductors”. Phys. Mesomechanics, **21**, pp.275-283, 2018.
7. T.M. Makhviladze and M.E. Sarychev. “Influence of point defects on the initiation of electromigration in an impurity conductor”. Russian Microelectronics, **50,** pp.376-383, 2021.

Symmetries and Entanglement in Quantum Networks

P. Vojta, D. Solenov
Department of Physics, St. Louis University, St. Louis, Missouri 63103, USA

Symmetry is a key to many physics phenomena. It occurs in arrangements of atoms forming symmetric lattices or in electron systems resulting in various types of ordering. It also plays an important role in classical information processing. We will show how symmetry emerges in quantum network description of driven multi-state quantum systems, particularly those used to implement quantum gates in gate-based quantum information processing. While typically not explicitly acknowledged, it is intimately related to the ability to manipulate entanglement and process quantum information. For instance, just like in many other phenomena, change of symmetry can be related to dramatic change in accessible qubits' evolution patterns - to their ability to alter and propagated quantum entanglement. We will show what types of symmetries are available in systems of several qubits and how they govern accessible entanglement manipulation.

In standard gate-based quantum computing, information is stored in qubits and manipulated by gates applied to those qubits, as well as measurements. When a gate is applied, a subset of targeted qubits forms a coherently driven multi-state quantum system. In most cases auxiliary states residing in each physical qubit are utilized to perform various gates. When no physical interaction between qubits is introduced (single-qubit gates), these states can naturally be labeled 0, 1, 2, etc., where states 0 and 1 encode the qubit. In case of an entangling gate, interaction between qubits is introduced, mixing states that belong to different qubits and interaction media (e.g., photons). Often there is an adiabatic route that connects non-interacting multi-qubit states such as 00, 01, etc. with complex states formed as the result of the interaction. Thus, one can still use non-interacting labels for states and the interaction shifts into the relation between theses states – edges of the resulting quantum network in Hilbert space (see the figure, as an example). In this description [1], physical interaction between qubits enters via symmetry (or lack thereof) of edges in quantum network, with each edge representing possible (accessible) transition in the system.

Quantum network description of quantum gates naturally allows for clear concurrent (i.e., fast) entanglement manipulation on many qubits that is difficult to construct as a concurrent combination of traditional smaller gates, such as control-NOTs due to spectral crowding and other issues. The key property that controls such ability is symmetry of edges. For example, in a system of 3 qubits with the network of states shown in the figure, all sets of connections parallel to a given face of the cube must be identical if qubits are isolated (non-interacting) – in this case only single qubit manipulations are possible. When the symmetry of the network is lower (due to interactions), entanglement manipulations become accessible. As the result, there is a relation between symmetry and entanglement – some symmetries must be broken in order to manipulate entanglement.

The symmetries of quantum networks are not identical to traditional crystal point group symmetries. They also affect phases associated with each edge (transition). As the result regular point group symmetry manipulations (flips, rotations, etc.) must be corrected to account for proper phase handling. In some cases the operations are not correctable, corresponding to changes in the overall group structure.

1. D. Solenov, “Quantum Walks as Mathematical Foundation for Quantum Gates”, Quantum Information and Computation, **20**, p. 0230, 2020.

Quantum computing with single neutral atoms in optical microtraps

S.S. Straupe, I.B. Bobrov, E.V. Kovlakov, D. Shchepanovich, S.P. Kulik
Quantum Technology Centre, M. V. Lomonosov Moscow State University, 119991 Moscow, Russia.
straupe@physics.msu.ru

We will discuss the advantages and limitations of a quantum computing architecture based on single rubidium atoms in arrays of optical tweezers. Both fundamental limitations inherent to this model and current status of research in this field will be discussed. We will particularly focus on experimental works in this direction in QTC MSU.

Descriptional Complexity of Unitary Transformations in Quantum Computing

A. Kaltchenko
Wilfrid Laurier University, Waterloo, Canada, E-mail address: akaltchenko@wlu.ca

Introduction and notation

Motivated by the results of [1], we introduce $K(U_n)$ - the Kolmogorov complexity of finite-dimensional unitary transformation, which can been seen as a computable approximation of the (generally incomputable or infinite) exact descriptional complexity of a unitary transformation acting on n qubits.

Kolmogorov complexity [2] of a (classical) string or, more generally, of a classical finite object, was defined as the shortest effective binary description of that string or object. In computer science, Kolmogorov complexity is commonly presented as the shortest binary program p, which runs on a Turing machine.

Let H be a 2-dimensional complex vector space (Hilbert space). One qubit is described by a unit vector in $\mathcal{H}$. Then, for any integer n, the state of n qubits corresponds to a unit vector in n-folded space $H\otimes^n$. Let U_n be a unitary transformation on $H\otimes^n$, represented by a *n* x *n* unitary matrix.

We note that any unitary transformation U_n can be implemented as a quantum computation on Quantum Turing Machine (QTM) as well as using quantum logic circuits. For a comprehensive introduction to- and reference on- quantum computing, see, for example, [3].

Main result

We obtain an upper bound: $K(U_n) \leq 4n + O(1)$.

Loosely speaking, $K(U_n)$ is the number of (classical) bits, which is required to compute (in other words, to describe) unitary transformation U_n.

Conclusion

We point out that the exact classical description with of an arbitrary unitary transformation U_n is generally incomputable or infinite. So, in a most general case, our $K(U_n)$ is the length of the binary program which *approximates* U_n. Nevertheless, it fits quite nicely with *discrete* classical and quantum Turing machines as well as with quantum circuits and quantum algorithms with a *discrete* set of quantum gates. Thus, $K(U_n)$ reflects the (classical) computational complexity of a quantum circuit in the Kolmogorov [2] sense and provides a tool and theoretical framework for the analysis of quantum circuit complexity.

1. P.M.B. Vitanyi, "Quantum Kolmogorov Complexity Based on Classical Descriptions", IEEE Transactions on Information Theory, **47** (6), 2001, arXiv:quant-ph/0102108.
2. A.N. Kolmogorov, "Three approaches to the quantitative definition of information", Problems Inform. Transmission, 1:1, 1965.
3. M. A. Nielsen, I. L. *Chuang, Quantum Computation and Quantum Information*, Cambridge, University Press, 2000.

Probing non-Markovian quantum dynamics with data-driven analysis

I.A. Luchnikov[1,2,3], E.O. Kiktenko[1,3,4], M.A. Gavreev[1,3],
H. Ouerdane[2], S.N. Filippov[3,4,5], and A.K. Fedorov[1,3]

1. Russian Quantum Center, Skolkovo, Moscow 143025, Russia
2. Skolkovo Institute of Science and Technology, Moscow 121205, Russia
3. Moscow Institute of Physics and Technology, Moscow Region 141700, Russia
4. Steklov Mathematical Institute of Russian Academy of Sciences, Moscow 119991, Russia
5. Valiev Institute of Physics and Technology of Russian Academy of Sciences, Moscow 117218, Russia

A precise understanding of the influence of an environment on quantum dynamics, which is at the heart of the theory of open quantum systems, is crucial for further progress in the development of controllable large-scale quantum systems. However, existing approaches to account for complex system environment interaction in the presence of memory effects are either based on heuristic and oversimplified principles or give rise to computational difficulties. In practice, one can take advantage of available experimental data and replace the first-principles simulation with a data-driven analysis that is often much simpler. Inspired by recent advances in data analysis and machine learning, we suggest a data-driven approach to the analysis of the non-Markovian dynamics of open quantum systems. Our method allows capturing the most important properties of open quantum systems, such as the effective dimension of the environment, eigenfrequencies of the joint system-environment quantum dynamics, as well as reconstructing the minimal Markovian embedding, predicting dynamics, and denoising of measured quantum trajectories. We demonstrate the performance of the suggested approach on various models of open quantum systems, including a qubit coupled with a finite environment, a spin-boson model, and the damped Jaynes-Cummings model.

The development of the data processing scheme, analysis of the spin-boson model, and analysis of the damped Jaynes-Cummings model are supported by the Russian Science Foundation (19-71-10092) and by the Leading Research Center on Quantum Computing (Agreement no. 014/20; analysis of non-Markovian processes for NISQ devices). The analysis of the finite-environment-induced non-Markovian quantum dynamics is supported by the Foundation for the Advancement of Theoretical Physics and Mathematics “BASIS” for support under Project No. 19-1-2-66-1. The authors thank Alexander Ryzhov and Georgiy Semin for fruitful discussions.

1. I.A. Luchnikov, E.O. Kiktenko, M.A. Gavreev, H. Ouerdane, S.N. Filippov, and A.K. Fedorov. "Probing non-Markovian quantum dynamics with data-driven analysis: Beyond “black-box” machine learning models". arXiv:2103.14490.

Elements of satellite quantum network

V.L. Kurochkin[1,3,4], A.V. Khmelev[1,2,3], V.F. Mayboroda[3,4], R.M. Bakhshaliev[3,4], A.V. Duplinsky[3], Y.V. Kurochkin[1,2,3,4,]

1. Russian Quantum Center, Skolkovo, Russia E-mail: v.kurochkin@rqc.ru
2. Moscow Institute of Physics and Technology (National Research University), Dolgoprudny, Russia
3. QRate, Moscow, Russia
4. NTI Center for Quantum Communications, National University of Science and Technology MISiS, Moscow, Russia

Quantum key distribution (QKD) is a promising technique to secure key exchange using individual light quanta. Currently, commercial companies and governments of the leading countries are challenged to elaborate a vast network of quantum communication for the long distances, so known as Quantum Internet of Things, to provide reliable security of distributed information. However, quantum channels based on an optical fiber have limitations of the distance due to photon losses and it causes exponential decrease in secure key rate.

Free-space quantum communication allows for the creation of long-distance and global quantum networks by employing satellites as trustworthy nodes for receivers on Earth [1-3]. The satellite launched to low Earth orbit (400-600 km) with a QKD payload can establish a quantum communication link between any two parties on the globe. So, it is possible due to less attenuation of a laser beam in the atmosphere than in an optical fiber. Even though a portion of the signal is lost due to laser beam diffusion in the atmosphere, diffraction losses associated with the laser beam's limited aperture, and the telescope's limited diameter at the ground receiver, the overall attenuation is significantly less than that of ground-based fiber-optic transmission. Hence, it makes the distribution of the quantum key using satellites a promising solution for solving the problem of building large-scale networks.

Satellite quantum cryptography, like many advanced scientific fields, is at the intersection of several scientific and technical tasks, such as the study of quantum security, time synchronization of a satellite and ground station, calculations of spacecraft trajectories, precise positioning into space, and the development of pointing and tracking systems for both ground and satellite systems.

In this article, we focus on the principles of designing ground stations for satellite-based quantum networks. We present the results of studies on the tracking and registration of weak reflected sunlight from satellites performed at two observatories. The experiments have been carried out at a 1.2 m telescope in Kourovka and a 0.6 m telescope in Zvenigorod, both of which are located more than 1500 kilometers apart. As a result, we have shown the requisite light tracking and stabilization precision in the optical component for coupling photons into optical fibers, as well as the ability to register them by a single-photon detector.

Finally, we have developed a full-operation optical ground station system for real quantum key distribution with satellite. Hence, we report the first steps towards the creation of the long-distance quantum communication networks in Russia and suppose that combining a satellite quantum network with urban fiber-optic quantum networks via a ground station expands the scope of quantum communication in the future.

This work was supported by The Russian Science Foundation (Grant No. 17-71-20146)

1. Y.A. Chen, Q. Zhang, T.Y. Chen et al., "An integrated space-to-ground quantum communication network over 4,600 kilometres", Nature, **589**, pp. 214–219, 2021.
2. V.L. Kurochkin, A.V. Miller, V.E. Rodimin, S.S. Vorobey, M.Y. Balanov, Y.V. Kurochkin, "Quantum key distribution for ultra-long distances based on microsatellites", *XVI International Conference on Luminescence and Laser Physics Devoted to the 100th Anniversary of Irkutsk State University*, E.F. Martynovich, K.V. Grigorichev and F.A. Stepanov, 2069, p. 03003, AIP Conference Proceedings, Arshan, Russia, 2018.
3. J. Yin, Y.H. Li, S-K. Liao et al., "Entanglement-based secure quantum cryptography over 1,120 kilometres", Nature, **582**, pp. 501–505, 2020.

Estimating performance of quantum processor individual components based on an available data

Ya. Zolotarev[1,2], I. Luchnikov[1,2], J. López-Saldívar[1,2], A. Fedorov[1,2], and E. Kiktenko[1,2,3]
1. Russian Quantum Center, Skolkovo, Moscow 143025, Russia.
2. Moscow Institute of Physics and Technology, Moscow Region 141700, Russia.
3. Department of Mathematical Methods for Quantum Technologies, Steklov Mathematical Institute of Russian Academy of Sciences, Moscow 119991, Russia.

An accurate characterization of basic quantum computation processing components, such as quantum register initialization, implementation of native gates, and realization of read-measurement, is of critical importance for the effective quantum computing. A standard toolkit for such tasks consists of various quantum state/process tomography methods (see e.g. [1]) and special (randomized) benchmarking procedures [2]. However, both of these approaches require stopping the processor from handling external request. This is particularly important from the viewpoint of cloud-based quantum computing, where running of quantum circuits is performed by remote users.

In our work we develop a continuous monitoring system which allows one to obtain estimates on (i) initial state of the quantum register, (ii) quantum channels of native gates, and (iii) positive operator-valued measures (POVMs) of read-out measurements, without borrowing any quantum computational time of the quantum processor.

As input for our system, we use a set of circuits executed on the current processor and the corresponding read-out results. After each subsequent circuit run, we update the current estimate on quantum processor components based on accumulated data. It is important to note that the input circuits are assumed to be out of any control (e.g., they can be designed by remote users).

In our monitoring system we employ the automatic differentiation technique, available in contemporary machine learning libraries [3], Riemannian optimization, realized in QGOpt library [4], and our self-developed noisy quantum circuits emulator based on tensor networks. We demonstrate the performance of the developed monitoring system using an emulator from Qiskit as a source of information about some unknown quantum processor.

The research is supported by the Russian Science Foundation (Grant No. 19-71-10091) and Russian Roadmap for Quantum Computing.

1. P. Cerfontaine, R. Otten, and H. Bluhm. "Self-Consistent Calibration of Quantum Gate Sets". Phys. Rev. Appl. **13**, 044071, 2020.
2. E. Magesan, J. M. Gambetta, and J. Emerson. "Robust randomized benchmarking of quantum processes". Phys. Rev. Lett. **106**, 180504, 2011.
3. Tensorflow library https://www.tensorflow.org
4. I. A. Luchnikov, A. Ryzhov, S. N. Filippov, and H. Ouerdane. "QGOpt: Riemannian optimization for quantum technologies". SciPost Phys. **10**, 079, 2021.
5. Qiskit library https://qiskit.org

Quantum circuits simulation with Multi-scale Entanglement Renormalization Ansatz

I.A. Luchnikov[1,2], A.V. Berezutskii[1,3], and A.K. Fedorov[1,2]
1. Russian Quantum Center, Skolkovo, Moscow 143025, Russia
2. Moscow Institute of Physics and Technology, Moscow Region 141700, Russia
3. Institut quantique & Département de physique, Université de Sherbrooke, Québec J1K 2R1, Canada

Understanding the limits of classical simulation of interacting many-body quantum systems is crucial for the field of quantum technologies. Specifically, an important problem is to simulate quantum circuits using classical resources. There are a number of techniques allowing approximate simulation of quantum circuits based on tensor networks and neural networks architectures [1-3]. However, all of them suffer from inaccuracies caused by dimensionality reduction, whereas real quantum hardware suffers from errors induced by interaction with the environment. Systematic comparison of errors in classical simulation schemes with errors emerging in quantum hardware defines actual limitations of classical simulation. Both quantum hardware and classical simulation methods are being improved constantly and the question about limits of classical simulation remains unanswered. We make our contribution in this race by introducing a new method of classical simulation of quantum circuits based on Multi-scale Entanglement Renormalization Ansatz. Multi-scale Entanglement Renormalization Ansatz has more expressive power than Matrix Product State ansatz and allows exact quantum fidelity evaluation in contrast with neural networks. We benchmark the new method against existing classical simulation methods and existing quantum hardware.

The development of the new classical simulation technique of quantum circuits is supported by the Russian Science Foundation (19-71-10092) and by Russian Roadmap for Quantum Computing.

1. J. Bjarni, B. Bauer, and G. Carleo. "Neural-network states for the classical simulation of quantum computing." arXiv:1808.05232, 2018.
2. P. Feng, and P. Zhang. "Simulating the Sycamore quantum supremacy circuits." arXiv:2103.03074, 2021.
3. Y. Zhou, E. Miles Stoudenmire, X. Waintal. "What limits the simulation of quantum computers?." Phys. Rev. X, **10**, 041038, 2020.

Quantum tomography of multi-level quantum systems

B.I. Bantysh, Yu.I. Bogdanov
Valiev Institute of Physics and Technology of Russian Academy of Sciences, Moscow, Russia
bbantysh60000@gmail.com

Multi-level quantum systems (or qudits) are of wide interest for quantum computing. Moving from qubits to qudits improves some of the well-known quantum algorithms. By using qubits, the implementation of the Toffoli gate and its generalizations can be significantly simplified in comparison with the qubit implementation.

The practical use of multi-level quantum systems, however, implies the development of methods for their characterization and debugging. The most complete information in this sense is provided by the quantum tomography (QT) procedure. To implement QT it is required to carry out an informationally complete set of measurements with the subsequent reconstruction of the initial quantum state of the qudit.

Several classes of high-symmetry measurement protocols are known. These protocols are able to reconstruct an arbitrary quantum state with a high precision. The practical implementation of such protocols, however, depends on the specific method of encoding the information in a particular physical quantum system. Thus, a qudit state encoded in spatial modes of light can be projected onto an arbitrary qudit state using a single spatial light modulator and a photodetector. When storing information in the energy states of an atom, the measurement basis change may require a sequential implementation of a number of two-level transitions. The readout of the atom levels populations is also performed sequentially.

The described features can significantly affect the efficiency of the QT procedure. In the study, we compare the capabilities of various measurement protocols, both in the ideal case and in the presence of instrumental errors. It is shown that two-level tomography protocols, although less efficient, allow one to estimate a quantum state more accurately.

This work was supported the Program of activities of the leading research center "Development of an experimental prototype of a hardware and software complex for the technology of quantum computing based on ions" (Agreement No. 014/20), and by the Foundation for the Advancement of Theoretical Physics and Mathematics BASIS (project no. 20-1-1-34-1)

Quantum measurements, complete information matrix and high-precision control of quantum states

Yu.I. Bogdanov
Valiev Institute of Physics and Technology of Russian Academy of Sciences, Moscow, Russia
bogdanov_yurii@inbox.ru

The report presents a general approach for estimating quantum information technologies by means of measurements. The developed methods are used for precision reconstruction of quantum states under conditions of significant influence of decoherence and quantum noise. Monitoring of the amount of information about quantum states and parameters of quantum states, including the loss of information caused by the effect of quantum noise, is considered. Various types of decoherence and quantum noise are discussed, including bit-flip and phase-flip, amplitude and phase relaxation, readout errors, etc. The results of the analysis of the characteristics of the accuracy of statistical reconstruction for a wide range of quantum tomography protocols are presented.

The results of this research are of practical value for the tasks of provision of quality and effectiveness of quantum information technologies.

This work was supported by the Ministry of Science and Higher Education of the Russian Federation (program no. 0066-2019-0005 for the Valiev Institute of Physics and Technology, Russian Academy of Sciences), and by the Foundation for the Advancement of Theoretical Physics and Mathematics BASIS (project no. 20-1-1-34-1)

Quantum memory on multi atom-resonator system

S.A. Moiseev[1 *], A.M. Zheltikov[1,2,3,4 **]

*1. Kazan Quantum Center, Kazan National Research Technical University n.a. A.N.Tupolev-KAI, 10 K. Marx, Kazan 420111, Russia. * qm.kzn@yandex.ru*

2. M.V. Lomonosov Moscow State University, Moscow 119991, Russia

3. Texas A&M University, College Station, Texas, USA

*4. Russian Quantum Center, Skolkovo, Moscow Region 143025, Russia ** zheltikov@physics.msu.ru*

The creation of quantum memory (QM) initiated the development of two basic approaches. The first uses a single atom in a QED cavity, the second exploits atomic ensembles, which can be located in the resonator or in free space. The approaches have their advantages and disadvantages. Among the disadvantages of QM on a atom in QED cavity, we note the need for strong temporary synchronization of the time mode of the signal photon wave packet, which makes it extremely difficult to store a photon with an arbitrary time mode. On the other hand, the use of QM on atomic ensembles allows storage of pulses with arbitrary temporal form and is critical to time synchronization but it is difficult to realize perfect dynamical control of these atomic ensembles. In this work, we propose a QM scheme based on a system of resonators, where each contains one atom, and show that such a scheme allows storage single-photon wave packets of arbitrary time form.

The scheme contains a common resonator coupled with waveguide and with a number (N=4,5,…) of microresonators where each contains single three-level atom with Λ scheme of quantum transition. We assume that the microresonators constitute a periodic structure of resonant lines with a period of Δ covering the spectral range $\Delta_{in}=(N-1)\Delta$, while the frequency of the common resonator coincides with the center of the frequency comb of the microresonators and carrier frequency ω_s of a signal photon similar to the work [1]. Initially we assume that all the atoms are prepared on the ground states $|1\rangle$ and a single photon wave packet is launched from the waveguide to the common resonator and interacts there with each atom on transition $|1\rangle - |3\rangle$. The photon is stored in the presence of additional control laser fields acting on an adjacent atomic transition $|2\rangle - |3\rangle$ in each microresonator. Together with control laser field, a photon field provides resonant Raman transition of atoms $|1\rangle \rightarrow |2\rangle$ at the condition of sufficiently large frequency detuning $\Delta_0 = \omega_{31} - \omega_s >> \delta\omega_s$ on the optical transition $|1\rangle - |3\rangle$ ($\delta\omega_s$- spectral width of photon wave packet, $\delta\omega_s < \Delta_{in}$).

The solution of the equation for the wave function of atoms and a photon in the multi-resonator scheme under found optimal interaction parameters indicates that a photon can be completely absorbed by the this quantum system and its quantum state transfers into the microresonators at $t>\delta\omega_s^{-1}$. This happens without reflecting the photon into the waveguide, and when the common resonator is completely emptied for a certain time. During this time period, energy oscillation occurs in each microcavity between the resonator mode and the atomic transition $|2\rangle - |3\rangle$. By choosing the equal Rabi frequency amplitudes of the controlling laser fields, it is possible to synchronize these oscillations and to achieve simultaneous emptying of the microresonator modes at a certain moment of time $t_s<1/\Delta$ before rephasing of microresonator field modes at $\tau = 1/\Delta$. Switching off all the controlling laser control fields at this moment of time, we finish the storage process of a single-photon wave packet by transferring its quantum state to long-lived states $|2\rangle$ of N atoms, where dephasing of these modes is transferred to the long-lived atomic coherence on the transition $|2\rangle - |3\rangle$.

Retrieval of the stored photon is realized via time reversible quantum dynamics by launching the control laser fields at t=T which lead to the excitation of the microresonator field modes. The time reversal scenario shows irradiation of a photon in the echo pulse at $t_{echo} = T+\tau$ from the common resonator to the waveguide with efficiency close to unity, since the presence of atoms does not affect the frequency of the resonator comb at equal Rabi frequencies in different microresonators.

The considered QM scheme operates for arbitrary temporal shape of a photon wave packet, which simplifies operation of such QM by using coherent control of only N (4,5,6…) single atoms. In particular, the scheme can be implemented in a planar photonic system of microresonators situated in a common large resonator where signal photon and control laser fields propagate orthogonally to each other.

The research was supported by Government of Russian 745 Federation (project no. 14.Z50.31.0040, Feb. 17, 2017).

1. S. A. Moiseev, et al. "Broadband multiresonator quantum memory-interface." Scien. Reps. **8**, 3982 (2018).

Emerging 2D Ferromagnetism in Silicene, Germanene and Graphene Compounds at the Monolayer Limit and beyond

Dmitry V. Averyanov, Andrey M. Tokmachev, Oleg E. Parfenov, Igor A. Karateev, Ivan S. Sokolov, Alexander N. Taldenkov, and Vyacheslav G. Storchak
National Research Center "Kurchatov Institute", Kurchatov Sq. 1, Moscow 123182, Russia
E-mail:vgstorchak9@gmail.com

Traditional 2D materials are intrinsically non-magnetic. However, current trends in condensed matter and materials research evidence that magnetism, a fundamental force of nature, is conquering the 2D realm. Recent discovery of intrinsic 2D ferromagnetism in Cr-based layers initiated the search for novel 2D magnets with tunable properties. We discovered a class of 2D ferromagnets based on 2D-Xenes, elemental analogues of graphene – layered structures of silicene [1] or germanene [2] functionalized by rare-earth atoms. We track the evolution from the antiferromagnetism of the bulk to intrinsic 2D ferromagnetism of a few monolayers of MSi_2 [1, 3, 4] and MGe_2 [2, 3, 4]. The magnets are compatible with the mature Si and Ge technological platforms, which is instrumental for engineering new spintronic devices.

A similar approach can be applied to graphene: By analogy with 2D magnets based on silicene and germanene, we synthesized a monolayer of EuC_6.The system demonstrates the anomalous Hall effect and negative magnetoresistance [5]. EuC_6 monolayer exhibits strong magnetic response: its magnetic transition temperature is controlled by low magnetic fields – a fingerprint of 2D ferromagnetism [5]. Remarkably, the imprinted ferromagnetism does not destroy the advantageous transport properties of graphene: the system supports low mass carriers [5, 6]. Similar to its silicene and germanene analogues, EuC_6 monolayer demonstrates competing magnetic states [6].

Up to date, intrinsic 2D magnetism has been demonstrated in various materials scaled down to a single monolayer. However, the question is whether 2D magnetism extends beyond the monolayer limit. Our recent findings demonstrate that submonolayer superstructures of Eu atoms self-assembled on the silicon surface exhibit 2D ferromagnetism [7].

This work is supported by NRC "Kurchatov Institute" (No. 1055) and the Russian Science Foundation (grants 20-79-10028 and 19-19-00009).

1. A.M. Tokmachev, D.V. Averyanov, O.E. Parfenov, A.N. Taldenkov, I.A. Karateev, I.S. Sokolov, O.A. Kondratev, and V.G. Storchak, "Emerging two-dimensional ferromagnetism in silicene materials", Nature Communications **9**, p. 1672(9), 2018.
2. A.M. Tokmachev, D.V. Averyanov, A.N. Taldenkov, O.E. Parfenov, I.A. Karateev, I.S. Sokolov, and V.G. Storchak "Lanthanide f^7 metalloxenes – a class of intrinsic 2D ferromagnets", Materials Horizons **6**, pp. 1488-1496, 2019.
3. D.V. Averyanov, I.S. Sokolov, M.S. Platunov, F. Wilhelm, A. Rogalev, P. Gargiani, M. Valvidares, N. Jaouen, O.E. Parfenov, A.N. Taldenkov, I.A. Karateev, A.M. Tokmachev, and V.G. Storchak, "Competing magnetic states in silicene and germanene 2D ferromagnets", Nano Research **13**, pp. 3396-3402, 2020.
4. O.E. Parfenov, A.M. Tokmachev, D.V. Averyanov, I.A. Karateev, I.S. Sokolov, A.N. Taldenkov, and V.G. Storchak, "Layer-controlled laws of electron transport in two-dimensional ferromagnets", Materials Today **29**, pp. 20-25, 2019.
5. I.S. Sokolov, D.V. Averyanov, O.E. Parfenov, I.A. Karateev, Taldenkov, A.M. Tokmachev, and V.G. Storchak, "2D ferromagnetism in europium/graphene bilayers", Materials Horizons **7**, pp. 1372-1378, 2020.
6. I.S. Sokolov, D.V. Averyanov, F. Wilhelm, A.Rogalev, O.E. Parfenov, A.N. Taldenkov, I.A. Karateev, A.M. Tokmachev and V.G. Storchak, "Emerging 2D magnetic states in a graphene-based monolayer of EuC_6", Nano Research, in press, 2021. https://doi.org/10.1007/s12274-021-3494-9.
7. A.M. Tokmachev, D.V. Averyanov, A.N. Taldenkov, I.S. Sokolov, I.A. Karateev, O.E. Parfenov, and V.G. Storchak, "Two-dimensional magnets beyond the monolayer limit", ACS Nano, in press, 2021.

Multilayer semiconductor-dielectric nanostructures as the base for neuromorphic, photonic, and RF ICs

V.P. Popov[1], M.S. Tarkov[1], I.E. Tyschenko[1], K.V. Rudenko[2], A.V. Miakonkikh[2]
1. Rzhanov Institute of Semiconductor Physics, Novosibirsk, Russia, E-mail: popov.isp.nsc.ru
2. Valiev Institute of Physics and Technology, Moscow, Russia, E-mai: Rudenko@ftian.ru

Physical limits of the scaling of field-effect devices which are proposed more than 90 years ago [1], and the requirements of highly reliable electronic components lead to an expansion of the functionality and types of integrated devices based on semiconductor-insulator heterostructures. Downsizing the transistor make it active area comparable to the size of a few dozens of atoms, increasing the contribution of quantum effects to its properties. With a decrease in the size of elements and an increase in their frequency operation the heat losses significantly enhance due to intrinsic heat release and limited thermal and electrical conductivity of copper interconnects, that requires of integration with heat sink as single-crystal layers of metals or diamond. One of the ways to solve these problems is the development of hybrid integrated circuits (ICs) with parallel CMOS, microwave and optical information processing based on neuromorphic systems. Despite the more than sixty-year history, the fabrication of thin (~ 10 nm) epitaxial layers similar in structural and transport properties to a bulk semiconductor (S) or a dielectric (D) in the semiconductor-insulator structures with metal (M) (MDM, MDS, SDS) remains an technologically challenging task due to differences in lattice structures and thermal expansion coefficients. The development of the direct bonding (DB) method for obtaining multilayer silicon-on-insulator (SOI) heterostructures makes it possible, along with atomic-layer deposition (ALD) / etching (ALE), to form MDM, MDS, and SDS structures suitable for creating neural network, photonic, microwave and spintronic ICs, including those with quantum information processing (QIP). Under application of this DB method the devices could integrate the low- and high-k dielectrics, ferroelectrics, quantum wells and points of A^3B^5 and A^2B^6 semiconductors, photonic crystals and waveguides.

Rzhanov and Valiev Institutes have accumulated extensive experience in the fabrication of SOI structures by the method of direct bonding, ion synthesis and hydrogen transfer, as well as experience in the creation of new semiconductor-on-dielectric heterostructures with specified functional characteristics, for example, on diamond or sapphire (Fig. 1), and the devices on their basis: Radiation-Hardened Logic CMOS ICs and MEMS for extreme and highly reliable electronics, FET-sensors of physical, chemical and biological objects, Neural Network ICs, power supply ICs, photodetector matrices, emitters and multiplexers [2, 3].

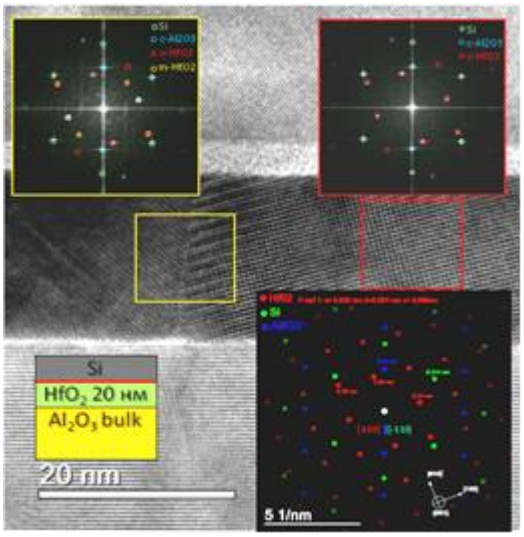

Fig1.Cross-section HRTEM and FFT images of lattices of Si, HfO_2 and sapphire in SOS structure.

Presented talk also considers the possibilities of application of SOI ICs with low-k and high-k dielectrics, as microwave IC transceivers, or mobile neural network ICs based on FeFETs with effective learning algorithms, respectively. The latter devices are being developed and can have performance and energy efficiency that are not inferior to the human brain [4].

Their development is supported by RFBR Project #19-29-03031 and by the Program #0066-2019-0004 of the Ministry of Science and Higher Education of Russia.

1. J. E. Lilienfeld, Method and apparatus for controlling electric currents, 1930.
2. I.E. Tyschenko, V.P. Popov. In: Advances in semiconductor nanostructures. Elsevier, (2017).
3. V. Popov, et al., Solid-State Electronics, **159**, 63 (2019).
4. K. Ni, X. Yin, A.F. Laguna, et al. Nature Electron. **2**, 521 (2019).

Efficient computation of EM scattering from a dielectric cylinder covered with graphene strips

B. Guizal[1], Y. Jeyar[1], M. Antezza[1,2]
1. Laboratoire Charles Coulomb (L2C), UMR 5221 CNRS-Université de Montpellier, F-34095 Montpellier, France
2. Institut Universitaire de France, 1 rue Descartes, Paris Cedex 05 F-75231, France

We present a numerical approach for the solution of EM scattering from a dielectric cylinder partially covered with graphene. It is based on a classical Fourier-Bessel expansion of the fields inside and outside the cylinder to which we apply the ad-hoc boundary conditions in the presence of graphene. Due to the singular nature of the electric field at the ends of the graphene sheet, we introduce auxiliary boundary conditions to better take this reality into account. The result is a very simple and very efficient method allowing the study of diffraction from such structures.

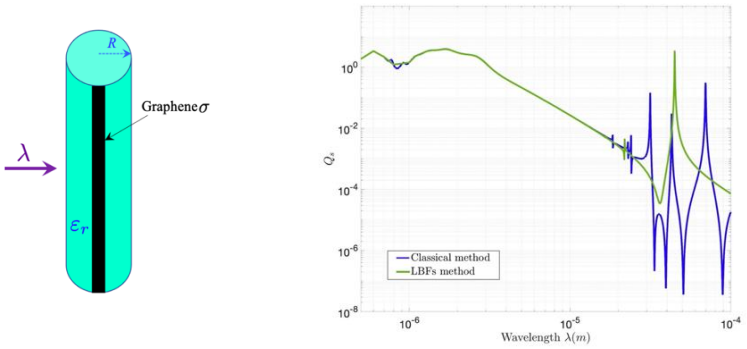

Figure 1 : (left) Sketch of the diffraction problem, (right) Scattering efficiency spectrum for a cylinder of radius R = 0.5μm and permittivity ε_r = 3.9 immersed in air, with a graphene sheet of chemical potential μ = 0.5 eV at T = 300 K.

Diffraction of electromagnetic waves from circular cylinders is rather a simple and classical problem [1]. In this situation, the incoming and outgoing fields can be represented in terms of circular waves expressed under Fourier-Bessel expansions. All the channels are independent because of the circular symmetry and homogeneity of the cylinder. However when this cylinder is partially covered with a graphene sheet, this breaks the symmetry and homogeneity at the level of the surface and then all the channels can be mixed thus leading to interesting physical phenomena. Under this situation, the boundary conditions lead to an algebraic system linking the outgoing amplitudes of the fields to the incoming ones. This system may be singular in the case of transverse magnetic polarization (TM: the magnetic field is parallel to the direction of invariance of the cylinder). This is due to the singularities of the tangential component of the electric field at the ends of the graphene sheet. One way of solving this issue is to use a supplementary expression of this field right at the level of the circumference of the cylinder in terms of Local Basis Functions (LBFs) able to reproduce the singularities [2].

Figure 1 shows an example where a plane wave is impinging on a circular cylinder (radius R and dielectric permittivity ε_r) partially covered by a graphene (conductivity σ). This diffraction problem can be solved through the expansion of the fields in terms of Fourier-Bessel modes (called the “classical method” hereafter). Because of the singularities of the electric field under TM polarization the convergence (versus the number of Fourier-Bessel modes) is slow. This problem is fixed handled through the introduction of Local Basis Functions (LBFs). Figure 1 shows the scattering efficiency versus the wavelength, obtained with the classical method and with the LBFs method. It can be clearly seen that the LBFs method is very stable as compared to the classical one which shows many spurious peaks. For the LBFs method the number of modes necessary to achieve convergence (stabilization of the fourth digit for example) is very low: about 40 modes contrary to the classical method where even more than 150 modes do not give the same results.

1. J. A. Kong, *Electromagnetic Wave Theory*. Wiley, 1986.
2. R. B. Hwang, "Highly improved convergence approach incorporating edge conditions for scattering analysis of graphene grating", Scientific Reports **10**, N°:12855, 2020.

Wafer-scale deposition of Graphene and 2D Materials for the Optoelectronic Industry: (PE) CVD, (PE) ALD & ALE

T. Miller, F. Reale, D. Stanton, H. Knoops, R.S. Sundaram, O. Thomas
Oxford Instruments Plasma Technology, Yatton, UK, thomas.miller@oxinst.com

Graphene and hybrid nanomaterials such as Transition Metal Dichalcogenides (TMDs) have revealed unforeseen electrical, optical, and mechanical properties which make them unique candidates for next-generation nanotechnology devices, ranging from large scale consumer devices to quantum electronics.

Traditional vapour-phase synthesis methods of bulk semiconductors have recently undergone a resurgence of research interest for the growth of low-dimensional materials and heterostructures [1-3]. In particular, Chemical Vapour Deposition (CVD) has been extensively investigated to achieve materials with atomic planes of Van der Waals solids [4, 5]. Of special interest are heterostructures created by stacking atomic layers of different materials with complementary characteristics to achieve novel functionality [6].

Oxford Instruments Plasma Technology is at the forefront of successful scaled-up wafer-sized deposition of these materials. I will give an overview of our nanomaterial processing capabilities including CVD and Plasma Enhanced CVD (PECVD) deposition of graphene on 150 mm wafers, TMDs such as WS_2 and 2D heterostructures such as graphene and MoS_2 with applications in optoelectronics. Finally, I will introduce our developments in technology for the fabrication processes of 2D materials-based devices. These include Atomic Layer Etching (ALE) for damage free layer thickness control and Atomic Layer Deposition (ALD) for the deposition on Molybdenum and Tungsten based 2D materials and high-quality dielectric deposition.

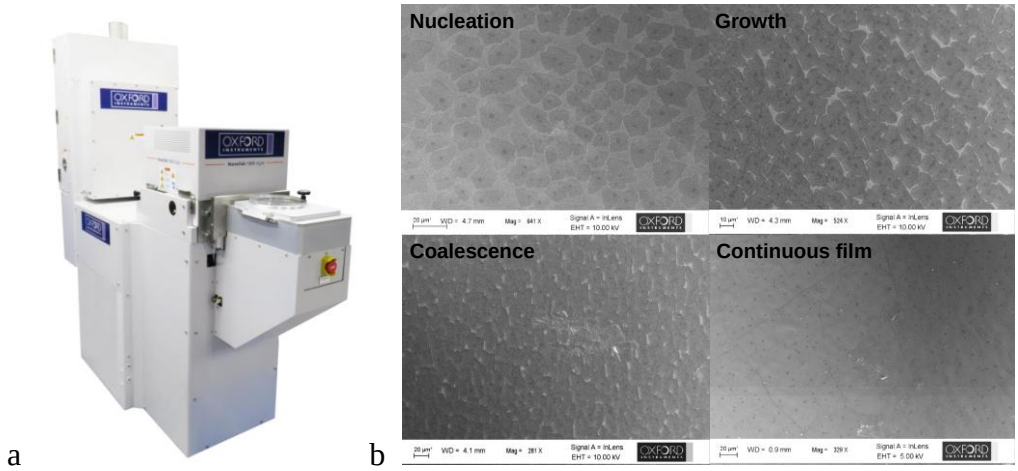

Figure 1: (a) Oxford Instruments Nanofab system for the growth of 1D/2D nanomaterials and heterostructures. (b) SEM images showing the growth stages of graphene on Cu foil.

1. X. Li et al. “Large-area synthesis of high-quality and uniform graphene films on copper foils”. Science, **324**, pp. 1312-1314, 2009.
2. S. Bae et al. “Roll-to-roll production of 30-inch graphene films for transparent electrodes”. Nat Nanotech., **5**, pp. 574-578, 2010.
3. K. Kang et al. “High-mobility three-atom-thick semiconducting films with wafer-scale homogeneity”. Nature, **520**, pp. 656-660, 2015.
4. F. Reale et al. "From bulk crystals to atomically thin layers of group VI-transition metal dichalcogenides vapour phase synthesis". Applied Materials Today, **3**, pp. 11-22, 2016.
5. Mercado et al. “A Raman metrology approach to quality control of 2D MoS_2 film fabrication”. J Phys D Appl Phys., **50**, 184005, 2017.
6. L. Yuan, “Van der Waals heterostructures and devices”. Nature Reviews Materials, **1**, 16042, 2016.

Controlling the PT symmetry of graphene Dirac plasmons and its application to terahertz laser transistors

Taiichi Otsuji[1*], Akira Satou[1], Victor Ryzhii[1], Hirokazu Fukidome[1], Maxim Ryzhii[2], and Koichi Narahara[3]

1. Research Inst. of Electrical Comm., Tohoku University, Sendai. Japan,
{otsuji, a-satou, v-ryzhii, fukidome}@riec.tohoku.ac.jp
2. Dept. Computer Science and Technol., University of Aizu, Aizu-Wakamatsu, Japan
m-ryzhii@u-aizu.ac.jp
3. Dept. of Electrical and Electronic Eng., Kanagawa Institute of Technology, Atsugi, Japan,
narahara@ele.kanagawa-it.ac.jp

Graphene has a linearly dispersive and gapless unique electronic band structure. This allows both electrons and holes to behave as relativistic charged particles of massless Dirac fermions. The quantum of plasma oscillation of graphene Dirac fermions is called the graphene Dirac plasmon (GDP), which can dramatically enhance the interaction of terahertz (THz) waves with graphene. We have proposed an original current-injection graphene THz laser transistor, demonstrating single-mode THz lasing at low temperatures[1-3)], and discovered the THz giant gain enhancement effect by GDPs even at room temperature[4,5)]. However, in order to realize room temperature intense THz lasing and ultrafast modulation operation, which are necessary for the next generation 6G and 7G wireless communications, further breakthroughs are needed. In this talk we present our novel idea and strategy to introduce completely new physics and principles to simultaneously break through the limits of quantum efficiency and modulation speed.

In quantum mechanical equations, Hermitianity (i.e., the complex transpose matrices of the Hamiltonian operators are equal to each other) has been commonly assumed as the Hamiltonian for finding realistic solutions. However, it was discovered that even non-Hermitian Hamiltonians with parity and time-reversal ($\mathcal{PT}$) symmetries can provide realistic solutions[6)]. Non-Hermitianity implies that the Hamiltonian is complex, i.e., physically there is an energy flow in and out of the system under consideration. Therefore, $\mathcal{PT}$ symmetry can be given by a basic element of a pair of complementary gain and loss mediums; $\mathcal{PT}$ symmetry leads to a perfect transmission property (unidirectional), and $\mathcal{PT}$ symmetry breaking prevents this. This means that $\mathcal{PT}$ symmetry can be differentiated only for singularities identified on the frequency axis.

The concept and strategy of this study are as follows. Apart from the laser gain seed due to the population inversion of the graphene carrier, the gain enhancement effect of the GDP is implemented into the laser cavity, and a mean to control/manipulate the $\mathcal{PT}$ symmetry of the GDPs is introduced. The device is realized in the authors' original dual-grating-gate graphene channel field effect transistor (ADGG-GFET) structure, and by actively controlling the $\mathcal{PT}$ symmetry of the GDP metasurface under electrical bias applications. Practical device design and numerically simulated performance projections will be presented.

This work was supported by JSPS KAKENHI #21H04546, #20K20349, and #21H04546, Japan.

1. V. Ryzhii, M. Ryzhii, and T. Otsuji, "Negative dynamic conductivity of graphene with optical pumping," J. Appl. Phys., **101**, 083114, 2007.
2. T. Otsuji, S. Boubanga Tombet, A. Satou, M. Ryzhii, and V. Ryzhii, "Terahertz-wave generation using graphene: toward new types of terahertz lasers," IEEE J. Sel. Top. Quantum Electron., **19**, 8400209, 2013.
3. D. Yadav, G. Tamamushi, T. Watanabe, J. Mitsushio, Y. Tobah, K. Sugawara, A.A. Dubinov, A. Satou, M. Ryzhii, V. Ryzhii, and T. Otsuji, "Terahertz light-emitting graphene-channel transistor toward single-mode lasing," Nanophoton., **7**, 741-752, 2018.
4. T. Watanabe, T. Fukushima, Y. Yabe, S.A. Boubanga Tombet, A. Satou, A.A. Dubinov, V. Ya Aleshkin, V. Mitin, V. Ryzhii, and T. Otsuji, "The gain enhancement effect of surface plasmon polaritons on terahertz stimulated emission in optically pumped monolayer graphene," New J. Phys., **15**, 075003, 2013.
5. S. Boubanga-Tombet, W. Knap, D. Yadav, A. Satou, D.B. But, V.V. Popov, I.V. Gorbenko, V. Kachorovskii, and T. Otsuji, "Room temperature amplification of terahertz radiation by grating-gate graphene structures," Phys. Rev. X, **10**, 031004, 2020.
6. M.-A. Miri, and A. Alu, "Exceptional points in optics and photonics," Science, **363**, eaar7709, 2019.

UTC-PD-Integrated HEMT Double-Mixer for Optical to MMW/THz Carrier Frequency Down-Conversion

A. Satou[1,3], D. Nakajima[1,3], K. Nishimura[1,3], T. Hosotani[1,3],
T. Suemitsu[2,3], K. Iwatsuki[3], and T. Otsuji[1,3]

1. Research Institute of Electrical Communication, Tohoku University, Sendai, Japan, a-satou@riec.tohoku.ac.jp
2. Center for Innovative Integrated Electronic Systems, Tohoku University, Sendai, Japan
3. Research Organization of Electrical Communication, Tohoku University, Sendai, Japan

To realize future ultra-broadband ubiquitous, resilient 6G/7G communication networks, the seamless, transparent linkage between optical and wireless networks is required [1]. We have studied the so-called photonic double-mixing functionality of transistors as a candidate of an efficient carrier frequency down-converter [2]. It down-conversion process consists of photomixing of an optical carrier and subcarrier signals, generating the difference-frequency beat-note of the MMW/THz data signal, and RF mixing of the beat-note MMW/THz data and LO signals, generating an IF data signal. Recently, we have developed a MMW/THz double-mixer based on an InGaAs-channel high-electron-mobility transistor (HEMT) with the uni-traveling-carrier photodiode (UTC-PD) structure (UTC-PD-integrated HEMT) [3], demonstrating the significant enhancement of its double-mixing conversion gain by over 43 dB from that of a standard HEMT double-mixer. In this paper, we review recent progress on development of the UTC-PD-integrated HEMT and address prospects for further enhancement of its conversion gain and operation frequency.

The UTC-PD-integrated HEMT embeds a UTC-PD into the source side a HEMT (Figs. 1(a) and (b)). The UTC-PD enables high absorption of the optical signals as well as fast extraction of photoholes to the source contact and injection of only photoelectrons into the channel, which lead to the double-mixing conversion gain much higher than a normal HEMT. Furthermore, we revealed that the reduction of the UTC-PD mesa size down to optical diffraction limit monotonicaly ehnances the conversion gain (Fig. 1(c)), due to the suppression of very long in-plane diffusion of photoelectrons in the large mesa that severely limits the cutoff frequency of the UTC-PD. Although the drop of the DC photocurrent, i.e., the degradation of photoabsorption efficiency, becomes an issue for the small mesa size with usual planar source contact, we showed that it can be avoided by introducing a grating-type source contact (Figs. 1(b) and (c)).

For further enhancement of the conversion gain is possible by optimization of the UTC-PD and HEMT parts and by introducing a very high intensity subcarrier LO signal with help of a certain phase-locking technique [4]. Also, for further enhancement of the operation frequency, utilization of the 3D rectification effect observed recently in a plasmonic THz detector [5] is promising.

This work was supported by the Commissioned Research of NICT, Japan.

1. Iwatsuki and K. Tsukamoto, Proc. SPIE **9387**, pp. 93870J-1-8, 2015.
2. K. Sugawara *et al.*, J. Lightwave Technol. **34**, pp. 2011-2019, 2016.
3. A. Satou *et al.*, J. Lightwave Technol. **39**, pp. 3341-3349, 2021.
4. K. Kasai *et al.*, 46th European Conference on Optical Communication (ECOC 2020), Th1G-7, 2020.
5. A. Satou *et al.*, Conference on Lasers and Electro-Optics 2021 (CLEO 2021), STh2C.1, 2021.

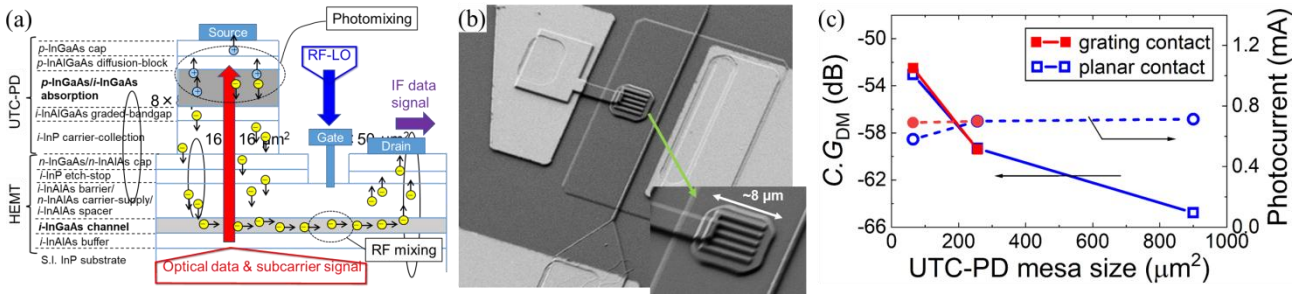

Fig. 1 (a) A cross-sectional schematic view of a UTC-PD-integrated HEMT, (b) an SEM image of the fabricated device, and (c) the double-mixing conversion gain and DC photocurrent vs UTC-PD mesa size.

Novel designs and materials in THz quantum cascade lasers

D. Ushakov[1], A. Afonenko[1], O.Yu. Volkov[2], I.N. Dyuzhikov[2], V.V. Pavlovskiy[2], A. Dolgov[3], R. Galiev[3], S. Pushkarev[3], D. Ponomarev[3], R. Khabibullin[3]

1. Belarusian State University, Minsk, Belarus

2. Institute of Radio-Engineering and Electronics of RAS, Moscow, Russia

3. V.G. Mokerov Institute of Ultra-High Frequency Semiconductor Electronics of the Russian Academy of Sciences, Russia, khabibullin@isvch.ru

Over the past two decades, the operation temperature of terahertz quantum cascade lasers (THz QCLs) has continuously increased from cryogenic level to the current record value of 250 K (about -23 ºC) [1]. Here we review the state-of-the-art and future prospects of THz QCL designs with two-quantum wells in active module based on conventional heterojunction GaAs/AlGaAs and alternative material system HgCdTe [2]. We have analyzed the temperature dependence of the peak gain and predicted the maximum operation temperatures of the given designs.

THz QCL is one of the spectrally brightest solid-state sources at THz frequencies with a potentially wide range of practical applications in high-resolution spectroscopy [3, 4] and imaging systems [5]. The main barrier to the use of THz QCL “outside the laboratory” is their low operating temperatures. The limiting factors for increasing the operation temperatures of THz QCLs are associated with strong optical phonon scattering, the presence of parasitic current channels and the formation of electric field domains as was shown in [6, 7]. Recently, the mode loss spectra for THz QCLs with double metal waveguide (DMW) were demonstrated in [8]. It was shown the high level of propagation loss of THz radiation in DMW, which exceeds 30 cm^{-1} for room temperature. Thus, to improve the high-temperature performance of THz QCLs it is needed to develop new concepts of active region designs and to reduce losses in DMW.

Acknowledgments

This work was supported by the Russian Science Foundation Grant No. 21-72-30020.

1. Khalatpour A. et al. 2020 *Nat. Photonics* **15** 16.
2. Ushakov D.V., Afonenko A.A. et al. 2020 *Opt. Express* **28** 25371.
3. Hubers H.-W, H. Richter et al 2019 *J. Appl. Phys.* **125** 151401.
4. Volkov O., Pavlovskiy V. et al 2021 *IEEE Trans. Terahertz Sci. Technol.* **11** 330.
5. Sterczewski L.A., Westberg J. et al 2019 *Optica* **6** 766.
6. Khabibullin R.A., Shchavruk N.V. et al *Opto-Electronics Review* **27** 329.
7. Ushakov D.V., Afonenko A.A. et al. 2019 *Quantum Electronics* **49** 913.
8. Ushakov D.V., Afonenko A.A. et al. 2018 *Quantum Electronics* **48** 1005.

Strain-induced THz detectors for spectroscopic and imaging applications

D. Lavrukhin[1], A. Yachmenev[1], Yu. Goncharov[2], K. Zaytsev[2], R. Khabibullin[1], D. Ponomarev[1,2]
1. V.G. Mokerov Institute of Ultra-High Frequency Semiconductor Electronics of the Russian Academy of Sciences, Russia, ponomarev_dmitr@mail.ru
2. Prokhorov General Physics Institute of the Russian Academy of Sciences, Russia

Photoconductive antenna (PCA)-coupled THz detectors are widely used in modern spectroscopic applications for the needs of various branches of science and technology [1-2]. We report for the very first time on a PCA-detector which was developed using an artificially strained InGaAs/InAlAs superlattice (SL) heterostructure.

Recently we showed [3] that strain-induced InGaAs-based heterostructures could be efficiently used for the PCA-detectors since they allow sub-picosecond photocarrier lifetimes with moderate mobility without using any compensating p-type dopants. The developed THz detector demonstrates advancement over the conventional PCA-detector based on a lattice-matched (LM) InGaAs/InAlAs SL when operating with an optical probe power above 6 mW [4]. The detectors have a 3.5 THz detection bandwidth and a signal-to-noise (S/N) ratio above 70 dB. The strain-induced detector shows a quadratic dependence of its S/N ratio on optical probe power while the S/N ratio for LM InGaAs/InAlAs-based PCA-detector starts saturating at 5 mW. Moreover, the noise floor in the strained detector is almost independent of probe power compared to the LM InGaAs/InAlAs-based detector which demonstrates a rapid growth of the noise floor with an increase of probe power.

Therefore, we believe that strain-induced PCA-detectors coupled to fiber telecom lasers could open a pathway toward the development of cost-effective THz photoconductive devices.

1. A. Yachmenev, S. Pushkarev, R. Reznik, R. Khabibullin, and D. Ponomarev. “Arsenides-and related III-V materials-based multilayered structures for terahertz applications: Various designs and growth technology”. Progress in Crystal Growth and Characterization of Materials **66**(2), p.100485, 2020.

2. A. Yachmenev, D. Lavrukhin, I. Glinskiy, N. Zenchenko, Y. Goncharov, I. Spektor, R. Khabibullin, T. Otsuji, and D. Ponomarev. “Metallic and dielectric metasurfaces in photoconductive terahertz devices: a review”. Opt. Eng., **59**(6), p. 061608, 2020.

3. D. Ponomarev, A. Gorodetsky, A. Yachmenev, S. Pushkarev, R. Khabibullin, M. Grekhov, K. Zaytsev, D. Khusyainov, A. Buryakov, and E. Mishina. “Enhanced terahertz emission from strain-induced InGaAs/InAlAs superlattices”. J. Appl. Phys., **125**(15), p. 151605, 2019.

4. D. Lavrukhin, A. Yachmenev, Yu. Goncharov, K. Zaytsev, R. Khabibullin, A. Buryakov, E. Mishina, and D.S. Ponomarev. ”Strain-induced InGaAs-based photoconductive terahertz antenna detector”. IEEE Trans. THz. Sci. Technol., **11**(4), pp. 417-424, 2021.

Novel III-V semiconductor heterostructures for functionally integrated devices

T.A. Bagaev[1], M.A. Ladugin[1], A.A. Padalitsa[1], A.A. Marmalyuk[1], Yu.V. Kurnyavko[1], A.V. Lobintsov[1], A.I. Danilov[1], S.M. Sapozhnikov[1], V.V. Krichevskii[1], V.P. Konyaev[1], V.A. Simakov[1], S.O. Slipchenko[2], A.A. Podoskin[2], N.A. Pikhtin[2]

1. Stel'makh Research and Development Institute "Polyus", Moscow, Russia, bagaevta@niipolyus.ru.

2. Ioffe Institute, Russian Academy of Sciences, St. Petersburg, Russia, SergHPL@mail.ioffe.ru

High-power pulsed semiconductor laser oscillators 0.9 μm wavelength in distance and velocity measurement systems, in devices for detecting and transmitting optical signals, as well as in spectroscopy and scientific research are used. The increase in power of such devices can be done in various ways. One of them is the creation of multielement laser oscillators (laser diode bars and arrays). This approach allows one to increase the output power, but the size of the emitting aperture increases significantly. An increase in power can also be achieved by monolithic integration, when heterostructures with several emitting regions connected by tunnel junctions are created in a single epitaxial process (Fig. 1 (a)). This approach makes it possible to increase the differential quantum efficiency of laser diodes in proportion to the number of emitting regions, provide radiation beams parallelism, significantly reduce the distance between emitting regions, and reduce devices series resistance.

Epitaxial integration paves the way for combining several functionally different components within a single chip. To control light pulses an electronic key (dinistor, thyristor, transistor) must be introduced into the emitter. To miniaturize and improve the reliability of operation, as well as the convenience of controlling the output characteristics of powerful emitters, it is possible to integrate two sequentially formed structures in a single growth process: a laser and a thyristor. Such thyristor lasers with a switch-on voltage of 15-25 V demonstrated output power of 50-60 W in a pulse mode of operation (Fig. 1 (b)). Further steps at epitaxial integration with an electronic switch (thyristor) of several laser emitting regions within one heterostructure were aimed. Semiconductor emitters based on them reached a record power in a pulsed mode of operation: 90 W for devices with two and 120 W for devices with three laser sections (Fig.1 (b)).

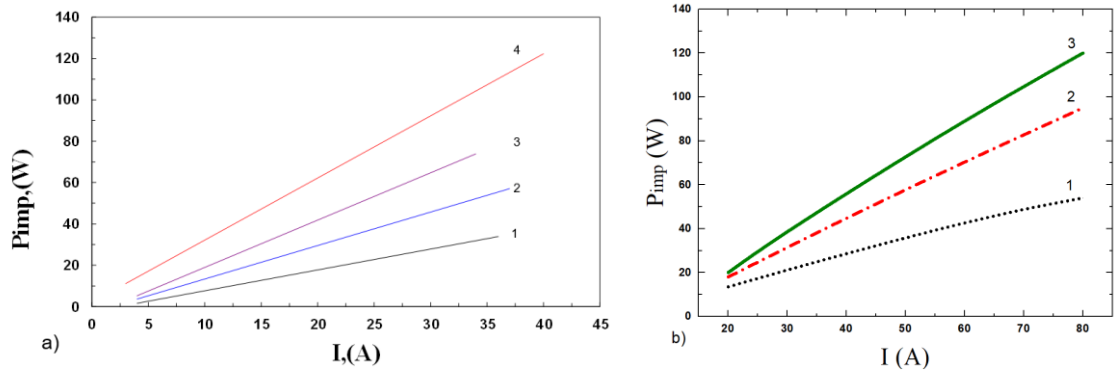

Fig. 1. Light-current characteristics: a) single (1), double (2), triple (3) and (4) quadruple epitaxially integrated laser diodes; b) single (1), double (2) and triple (3) laser -thyristor (wavelength 900 nm, pulse duration - 100 ns, repetition rate - 10 kHz).

Picosecond infrared laser crystallization of Ge layers in Ge/Si multi-nanolayers for optoelectronic applications

V.A. Volodin[1,2], G.K. Krivyakin[1,2], A.V. Bulgakov[3,4], Y. Levy[3], J. Beránek[3], S. Nagisetty[3], N.M. Bulgakova[3], P.V. Geydt[2], A.A. Popov[5]

1. Rzhanov Institute of Semiconductor Physics, Novosibirsk, Russia, volodin@isp.nsc.ru.
2. Novosibirsk State University, Pirogova street, 2, Novosibirsk, Russia.
3. HiLASE Centre, Institute of Physics AS CR, Za Radnicí 828, 25241 Dolní Břežany, Czech Republic.
4. Kutateladze Institute of Thermophysics SB RAS, Ac. Lavrentiev Ave. 1, Novosibirsk 630090, Russia.
5. Institute of Physics and Technology, Yaroslavl Branch, Russian Academy of Sciences, Yaroslavl, 150007 Russia.

Ultrashort laser annealing (ULA) with femto- and picosecond pulses is used for crystallization and nano-structuring of amorphous semiconductor films [1]. The ULA technique allows to selectively crystallize regions that absorb radiation in order to create *p-i-n* structures with narrow-gap semiconductor nanocrystals in *i*-layer. Such structures can be used in optoelectronics, for example as *p-i-n* photodiodes [2] or solar cells.

In this work, a-Si:H/a-Ge:H multilayer structures (MLS) consisted of 4 silicon (40 nm) and 3 germanium (15 nm) alternating amorphous layers were produced by plasma enhanced chemical vapor deposition on glass and Si(100) substrates. The MLS samples were annealed by a picosecond laser (HiLASE PERLA-B, λ=1030 nm, pulse duration 1.4 ps) with the pulse energy density (laser fluence) in the range from 17 to 175 mJ/cm^2. The structural analysis was performed by Raman spectroscopy using a T64000 spectrometer with micro-Raman setup and an Ar laser (514.5 nm) as an excitation source. The Raman spectrum of the as-deposited MLSs contains broad bands at ~480 cm^{-1} and ~275 cm^{-1} that are related to maximum density of vibrational states of amorphous silicon (a-Si) and germanium (a-Ge), respectively. The vibration frequencies of Ge–Si bonds, which are present at the Ge/Si heteroboundaries, are ~400 cm^{-1} but the spectrum of as-deposited MLS reveals almost no features at this frequency indicating that the concentration of these bonds is low.

Depending on laser fluence, we have distinguished several regimes of ULA. After treatment with fluences below app. 50 mJ/cm^2, the structure of MLS remained practically unchanged. Only for the sample on Si substrate, a barely noticeable peak corresponding to nanocrystalline germanium appeared at 46 mJ/cm^2. In the fluence range 50-70 mJ/cm^2, selective crystallization of Ge is observed in MLS on glass while the Si layers remain amorphous. Therewith ULA with a fluence of 60 mJ/cm^2 results in partial crystallization of Ge layers without Ge-Si intermixing while, at a fluence of 70 mJ/cm^2, the Ge layers are almost fully crystallized but some Ge-Si intermixing occurs (the Ge–Si peak at ~400 cm^{-1} appears). For MLS on the Si substrate, similar ULA-induced selective crystallization is observed at higher fluences, in the range 100–120 mJ/cm^2. With further increase in fluence up to 145 mJ/cm^2 and higher, almost complete intermixing of the Ge and Si layers occurs in the MLS on both substrates and at fluences above app. 160 mJ/cm^2, a completely crystalline Ge-Si solid alloy is formed. At a fluence of 175 mJ/cm^2, the Raman signal becomes lower that can be explained by partial ablation of the film under these ULA conditions. The surface morphology of the MLS after ULA was investigated. The roles of linear and nonlinear processes of laser energy absorption in MLS annealing are discussed for pico- and femtosecond pulse durations.

In conclusion, the main achievement is that ULA regimes are found when the Ge layers are partially crystallized while the Si layers remain amorphous without noticeable intermixing of Ge and Si.

Acknowledgements: This work was supported by the Ministry of Education and Science of the Russian Federation, grant FSUS-2020-0029.

1. D.V. Amasev, M.V. Khenkin, R. Drevinskas, P. Kazansky, and A.G. Kazanskii. “Anisotropy of optical, electrical, and photoelectrical properties of amorphous hydrogenated silicon films modified by femtosecond laser irradiation”. Tech. Phys., **62**, pp. 925–929, 2017.
2. Z. Remes, J. Stuchlik, The-ha Stuchlikova, J. Kupcik, V. Mortet, A. Taylor, P. Ashcheulov, and V.A. Volodin. “Electroluminescence of thin film p-i-n diodes based on a-SiC:H with integrated Ge nanoparticles”. Eur. Phys. J. Appl. Phys., **88**, p. 30302, 2019.

Aluminum doped thermomigrated silicon channels for high voltage solar cell: structure and electrical properties

A. Lomov[1], B. Seredin[2], S. Martyushov[3], I. Gavrus[2]

1. Valiev Institute of Physics and Technology of Russian Academy of Sciences, Russia, Moscow lomov@ftian.ru

2. Platov South-Russian State Polytechnic University, Russia, Novocherkassk, seredinboris@gmail.com

3. Technological Institute for Superhard and Novel Carbon Materials, Russia, Troitsk, mart@tisnum.ru

Development of new photovoltaic converters (solar cells, photovoltaic cells) has been receiving increasing attention in recent years. A wide range of materials are used for their production: from traditional silicon to organic. Since the usual photovoltaic cell is a planar structure, the output voltage U from one element is limited under ~ 1 V by the parameters of its p-n junction. Therefore, to increase it, it is necessary to additionally assemble the cells into batteries. The way to work around this problem and create monolithic high-voltage solar cells is by forming a series of through vertical multijunctions (VMJ) in the silicon wafer. Such a structure can be obtained by the thermomigration (ThM) based process, usually called temperature gradient zone melting (TGZM) [1, 2]. Despite the obvious time-related attractiveness (~ 1 hour) of the ThM process, the formation of a VMJ structure in a silicon wafer requires precision and high-tech operations, which hinders the use of this technology. For example, structural distortions arising from the rupture of the solvent zone in at least one of the vertical p-n junctions, can lead to low efficiency of the High-Voltage Solar Cell (HVSC) or its complete damage. The work was carried out on a conventional substrate Si(111) (P, 4×10^{14} cm^{-3}; ρ = 10 Ω·cm, 60 mm diameter, 400 μm thickness, a density of microdefects ≤ 10^2 cm^{-2}. The process of Al solvent- melt thermomigration was conducted in a vacuum in the 1100-1200°C temperature range. The aluminum content in the Si(Al) thermomigration channels is $(0.95–1.05)\times10^{19}$ cm^{-3} according to SIMS [3]. A 15-cell HVSC module based on an array of VMJ aluminum thermomigrated doped silicon channels was fabricated. This paper presents the results of a study of the electro- and photovoltaic characteristics of both the cells and the HVSC module (Fig.1). X-ray projection topography and high-resolution diffractometry were applied to characterize structural distortions in the VMJ array.

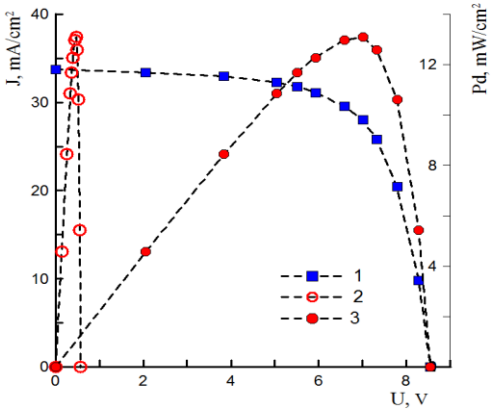

Fig.1 Experimental solar characteristic of HVSC module on the generated voltage U: load current density J (1) and the power density Pd of photoconversion for single (2) and fifteen (3) cells (Solar radiation simulator "Technoexan" (T = 25°C, illumination AM1.5D, illumination power 1000 W/m2). HVSC area of 15 cells is 10.5 $см^2$.

It is shown that the electrical parameters of the cells of the studied HVSC module (with the efficiency of 13%) based on the VMJ array have comparable values with the main electrical parameters of the planar analogues, despite the design features of the channels and the presence of structural distortions near the boundaries of the substrate matrix. However, multichannel HVSC modules can be used to manufacture high-voltage solar modules with output voltage that is proportional to the number of the cells.

The investigation was supported by: Program no. #0066-2019-0004 of the Ministry of Science and Higher Education of Russia for Valiev Institute of Physics and Technology of RAS; RFBR grant no. 19-07-00306; Platov South-Russian State Polytechnic University (NPI).

1. V. N. Lozovskii and V. P. Popov. “On the stability of the growth front during crystallization by the moving solvent method”. Sov.Phys.-Crystallogr., **15**, pp. 116-122, 1970.

2. T. R. Anthony, H. E. Cline. "Lamellar devices processed by thermomigration". J. Appl. Phys., **48**, pp. 3943-3949, 1977.

3. A. Lomov, A.Yu. Belov, B. Seredin, A. Tatarintsev, S. Simakin. “Determination of Al content in Al/Si thermomigration fabricated structures by X-ray diffraction”. Proceedings of the ICMNE – 2018. p. 139. Moscow-Zvenigorod, Russia, 2018.

Prospects for the use of composite materials in optoelectronic devices

R. Galutin, P. Razzchivalov
Institute of Nano – MicroSystem Technology, National University of Electronic Technology (MIET), Zelenograd, Moscow, Russian Federation
E-mail address: r-g-work@yandex.ru, razzhivalovpavel@gmail.com

This article discusses the prospects for the use of composite materials for the equipment of space systems for remote sensing of the Earth. One of the development problems in the design of special-purpose equipment is disclosed. This problem is observed when using traditional materials in the design of special-purpose equipment. Its solution is the use of new composite materials that can provide the required characteristics with a margin of safety [1]. The most widely considered composite material is "SKELETON". Its strength and thermal characteristics were given [2]. On the example of an optoelectronic converter, a simulation of tests using this material was carried out. Based on the results of 3D modeling of strength tests and heat sink, a conclusion was made about the possible use of this material. Other composite materials were also given as an alternative.

1. The official website of Roscosmos [Electronic resource]: website. - Access mode: //www.roscosmos.ru.
2. S. Kataev, V. Sidorov, S. Gordeev. Diamond-Carbide Composite Material "SKELETON" for Heat Sinks in Electronic Equipment Products. New technologies, No. 3, pp. 60-64, 2011. (in Rissian)

Improving the convergence of numerical methods for solving Maxwell's equations by processing edge singularities of the electromagnetic field

I.A. Semenikhin
Valiev Institute of Physics and Technology of the Russian Academy of Sciences, Moscow, Russia, isemenihin@gmail.com

When the real parts of the dielectric constants of two contacting materials have opposite signs, in instance, in the case of a metal and a dielectric, surface plasmons may appear at the interface [1]. Surface plasmons have recently been intensively studied with the aim of using in nano-photonic devices for guiding and confining light. If the interface is not a smooth surface and geometric edges are present, then in this case strong singularities of the field can appear near them, which complicates the numerical simulation of such systems. In some cases, similar to those given in [2,3], the calculation of the field even in the simplest systems, such as diffraction gratings, is not possible by conventional methods. The singularities primarily occur in the components of the electromagnetic field lying in a plane perpendicular to the edge. In particular, for TM polarization the components of the electric field near the edge asymptotically change proportionally to $\rho^{\tau-1}$, where ρ is the distance to the edge and the parameter τ characterizing the singularity depends on the geometric characteristics and dielectric constants of the contacting media. In number of simple cases the value of τ can be obtained analytically [2,3], in the rest it is necessary to solve the transcendental equation numerically. In general, τ is a complex value and $\rho^{\tau-1} = \rho^{\mathrm{Re}(\tau)-1}\exp[i\,\mathrm{Im}(\tau)\ln\rho]$. For $0 < \mathrm{Re}(\tau) < 1$ and a finite imaginary part of τ the oscillations of electric components with decreasing ρ tend to infinity both in amplitude and frequency. The closer $\mathrm{Re}(\tau)$ is to zero, the slower the numerical methods converge, moreover, at $\mathrm{Re}(\tau) = +0$ the conventional calculation methods cease to work [2, 3].

The behavior of the field near the edge singularity has been studied for a long time [4, 5, 6], since understanding the law of the field variation, we can take it into account in the numerical calculation. So, if we can get a solution in the region near the singularity, then using the expansion in smooth functions outside this region, and joining these two solutions on the boundary, we can achieve very fast convergence. Based on the results obtained earlier by other authors, we somewhat reformulate the method of calculating the field near the singularity for more convenient integration with solution methods used in the rest part of the domain [7]. We implement the transition from the static case, where the problem reduces to solving the eigenvalue problem similar to that arising in modal methods, to the case of finite wavelength. As examples of practical application the solution near the edges is added to several well-known methods, resulting in exponentially fast convergence. Additionally, we performed calculations of the electromagnetic field in the cases $\mathrm{Re}(\tau) = +0$ analyzed in [2, 3], for which it was not possible to obtain the result by conventional methods.

This work was supported by the Ministry of Science and Higher Education of the Russian Federation (program no. 0066-2019-0005 for the Valiev Institute of Physics and Technology, Russian Academy of Sciences)

1. S.A. Maier, *Plasmonics: Fundamentals and Applications*, Springer, 2007.
2. L. Li and G. Granet, “Field singularities at lossless metal-dielectric right-angle edges and their ramifications to the numerical modeling of gratings”, J. Opt. Soc. Am. A, **28**, pp. 738-746, 2011.
3. L. Li and G. Granet, “Field singularities at lossless metal–dielectric arbitrary-angle edges and their ramifications to the numerical modeling of gratings”, J. Opt. Soc. Am. A, **29**, pp. 593-604, 2012.
4. J. Meixner, “The behavior of electromagnetic fields at edges”, IEEE Trans. Antennas Propag., **20**, pp. 442-446, 1972.
5. G. I. Makarov and A. V. Osipov, “Structure of Meixner's series”, Radiophysics and Quantum Electronics, **29**, pp. 544–549, 1986.
6. J. G. Van Bladel, *Singular Electromagnetic Fields and Sources*, 1st ed. Wiley-IEEE Press, 1996.
7. I. Semenikhin, “Improving accuracy of the numerical solution of Maxwell's equations by processing edge singularities of the electromagnetic field”, J. of Comp. Phys., **441**, 110440, 2021.

Design of a distributed compensation of a narrow gap capacitance for a THz transit-time generator

N. Simonov, V. Vyurkov, K. Rudenko, V. Lukichev

Valiev Institute of Physics and Technology, Russian Academy of Sciences, Moscow, Russia, E-mail nsimonov@ftian.ru

In the range of terahertz frequencies, there is a sharp decrease in the generation power of both optical and electronic devices [1]. Thus, the development of efficient sources and detectors of the THz range, operating at room temperature, is a complex and urgent problem.

In this work, we continue to consider low-dimensional solid-state transient structures based on thin silicon layers (2D) and an array of silicon nanowires (1D) for the generation and detection of terahertz radiation [2, 3]. The advantage of such active structures is that they can be fabricated using modern planar silicon technology. Their promise lies in the ability to provide a radiation power of 1-10 mW, which is required for practical applications.

The most important property of the structure for generation is the presence of negative conductivity (negative real part of the admittance) in the linear regime. In this case, the system releases electromagnetic energy, obtaining it from the energy of the dc voltage. Note that for transit structures, the presence of negative differential conductivity on the static characteristics is not necessary, as in the case of tunneling and resonant tunneling diodes. Negative conductivity in transit structures occurs at frequencies reciprocal to the transit-time and its multiples [3].

The cell consists of two metal electrodes lying on the heavily-doped silicon separated by an undoped silicon gap 100 nm wide and 100 μm long through which a current flows. Despite the relatively low capacitance of the gap (~ 0.04 pF), at terahertz, it significantly changes the admittance of the generating device, which impairs its matching with the antenna or waveguide. Worth noting, that the influence of the parasitic capacitance of electrodes is a general problem in the terahertz range for all solid-state structures including plasmon ones.

The difficulty of the gap capacitance compensation originates in the fact that it behaves like a slot line. For example, at a frequency of 1 THz, this slot line length of 100 μm is equal to one-third of the wavelength. As a result of electromagnetic modeling, it was found that this circumstance prevents the design of an effective outer compensation circuit. However, this paper proposes a method of "distributed compensation" of the slot's capacitance for solid-state generating elements. According to the method, the length of the slot is divided into small sections with practically lumped capacitances, which makes it possible to compensate their capacitances independently using additional inductivities. Such compensation ensures that the solid-state device could be matched to the antenna, which is necessary for the start of generation at terahertz frequencies.

1. S.S. Dhillon, M.S. Vitiello, E.H. Linfield et al. "The 2017 terahertz science and technology Roadmap (Topical Review) ". J. Phys. D: Appl. Phys., **50**, pp. 043001, 2017.
2. V. Vyurkov, A. Miakonkikh, A. Rogozhin, M. Rudenko, K. Rudenko, and V. Lukichev. "Barrier-injection transit-time diodes and transistors for terahertz generation and detection". Proc. SPIE, **11022**, pp. 1102202, 2019.
3. V. Vyurkov, I. Semenikhin, K. Rudenko, and V. Lukichev. "Transit-time diodes and transistors with variable injection for generation and detection of THz radiation". ITM Web of Conferences, EDP Sciences, **30**, pp. 08001, 2019.

Ultra-sensitive terahertz detection with tunnel field-effect transistors

D. Svintsov[1], D. Bandurin[2], I. Gayduchenko[3], G. Alymov[1], A. Geim[2], G. Fedorov[1]
1. Moscow Institute of Physics and Technology, Dolgoprudny 1414700, Russia
2. School of Physics, University of Manchester, Manchester M13 9PL, UK.
3. Moscow Pedagogical State University, Moscow 119435, Russia

Tunnel field-effect transistors (TFETs) are considered as main candidates for future low-power electronic circuits. The origin of low-power switching is the steep dependence of source-drain interband tunneling current on the overlap between conduction and valence bands [1]. The normalized steepness of gate-current characteristic $d\ln I_{sd}/dV_g$ is not limited by e/kT, where e is the elementary charge and kT is the thermal energy. Such sub-thermal switching was demonstrated experimentally (for review see [2]).

Despite numerous applications of TFETs in logic circuits, it was not realized that strong (nonlinear) sensitivity of tunnel current to gate and drain voltages also implies efficient rectification of high-frequency signals by such transistors. Here, we study the operation of tunnel field-effect transistors with gate-induced tunnel junctions as detectors of sub-THz (0.13 THz) radiation [3]. We show high responsivity (~4 kV/W) and low noise equivalent power (~0.2 pW/Hz$^{1/2}$) at T = 10 K, which are competing to those of superconducting and semiconducting hot-electron bolometers.

Our devices were made of bilayer graphene encapsulated in hexagonal boron nitride. Induction of finite band gap and excess carrier density was achieved by simultaneous action of back and top gates. Short sections of graphene bilayer (~300 nm) close to the source and drain contacts were not covered by the top gate, and were controlled by the bottom one only. Thus, by application of gate voltages of opposite polarity to the gates, it was possible to induce a p-n junction between single-gated and double-gated regions. Further enhancement of gate voltages could result in overlap between conduction and valence bands at the two sides of the junction, thus pushing it to tunneling regime. The radiation is fed to TFET from THz antenna coupled between source and gate, the photovoltage was read out between source and drain.

We have found that dependence of photoresponse on top gate voltage differs drastically in the gapless and gapped regimes of transport. In the gapless regime, the voltage responsivity is quite low (max ~0.1 kV/W) and symmetric with respect to charge neutrality point. In the gapped regime (i.e. at finite back gate voltage), the responsivity reaches 4 kV/W, is highly non-linear in intensity, and is strongly asymmetric with respect to charge neutrality. The strongest responsivity is achieved at opposite doping of channel and contacts. We have verified that both current and voltage responsivities grow in the tunneling regime, compared to the regime of intraband ohmic transport.

The observed dependences are in a good agreement with the theory of rectification at gate-controlled junctions near the contacts. The responsivity of the device can be calculated known the quasi-static non-linearities of TFET conductance $G(V_g,V_d)$-characteristics, dG/dV_g and dG/dV_d. The latter were calculated under assumption of quantum ballistic transport at the contacts and drift-diffusive transport in the long channel. Being in a good agreement with current measurements, our theory shows that even higher responsivity can be achieved in TFETs with junction at the middle of the channel, as well as in TFETs with extra ‘doping gates’ [4].

1. A.M. Ionescu, H. Riel. Nature **479**, 329–337 (2011).
2. H. Lu, A. Seabaugh. IEEE J. Electron. Dev. Soc. **2**, 44–49 (2014).
3. I. Gayduchenko, S.G. Xu, G. Alymov, M. Moskotin, I. Tretyakov, T. Taniguchi, K. Watanabe, G. Goltsman, A.K. Geim, G. Fedorov, D. Svintsov, D.A. Bandurin. Nat. Commun. **12**, 543 (2021).
4. G. Alymov, V. Vyurkov, V.Ryzhii, D. Svintsov. Sci. Rep. **6**, p. 24654 (2016).

Power enhancement of THz generation based on transit-time diodes with varying injection

I. Semenikhin[1], N. Simonov[1], A. Borzdov[2], V. Borzdov[2], V. Vyurkov[1], K. Rudenko[1], V. Lukichev[1]
1. Valiev Institute of Physics and Technology RAS, Moscow, Russia, vvyurkov@gmail.com
2. Belarusian State University, Minsk, Belarus

In the range of terahertz frequencies, an abrupt drop in generation power of both optical and electronic devices occurs [1]. Therefore, the efficient THz sources and detectors predominantly operating at room temperature are challenging. Here we continue the consideration of solid-state transit-time structures for generation and detection of terahertz radiation [2–3]. The advantage of such structures is that they can be fabricated using modern planar silicon technology.

The most important property of the structure for generation is the presence of negative conductivity (negative real part of the admittance) in the linear (low signal) regime at the desired frequency. In the case the system releases energy obtained from the applied *dc* voltage.

The cell consists of two metal electrodes lying on the heavily-doped silicon separated by a short undoped silicon span (approximately 100 nm) through which a current flows. To some extent the cell reminds an ancient electron lamp. However, for the latter a ballistic transport (without scattering) is crucial for generation. Meanwhile, the ballistic regime is hardly achievable in solid-state structures at room temperature. Luckily, the varying injection guarantees negative conductivity even for strong scattering. In our structure the potential barrier between contacts changes its height and thus the thermal injection rate with respect to the potential drop.

The analytical dependences of real and imaginary parts of admittance (conductivity) on the frequency ω and the transit-time t_0 are depicted in Fig. 1. The regime of saturated drift velocity ($v_d = 10^7$ cm/s for silicon) was taken into consideration. The thermal fluctuations with the frequencies in the negative conductivity range could be gained and result in generation if only the outer circuit feedback is properly organized. Worth mentioning, both the real and imaginary parts of admittance along with the substantial contact capacitance must be accounted for matching with antenna. The fair matching is vital for the generation at all to arise.

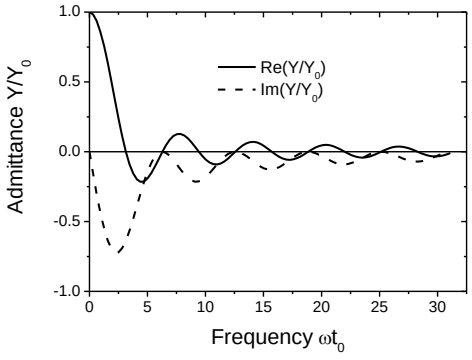

Fig. 1.

The structure under consideration could be audibly multiplied, that is several transit spans might be placed in series. Two benefits are to be derived from the proposal. Firstly, the output serial capacitance is diminished inversely proportional to number of spans. This drastically facilitates matching with outer circuit (antenna or waveguide). Secondly, the generation power is to be augmented proportionally to the number of spans.

1. S.S. Dhillon, M.S. Vitiello, E.H. Linfield et al. “The 2017 terahertz science and technology Roadmap (Topical Review)“. J. Phys. D: Appl. Phys., **50**, p. 043001, 2017.

2. V. Vyurkov, A. Miakonkikh, A. Rogozhin, M. Rudenko, K. Rudenko, and V. Lukichev. “Barrier-injection transit-time diodes and transistors for terahertz generation and detection”. Proc. SPIE, **11022**, p. 1102202, 2019.

3. V. Vyurkov, I. Semenikhin, K. Rudenko, and V. Lukichev. “Transit-time diodes and transistors with variable injection for generation and detection of THz radiation”. ITM Web of Conferences, EDP Sciences, **30**, p. 08001, 2019.

Effects of the peak current and valley current of the current-voltage curve in self-excitation and amplification processes in GaAs/AlAs THz resonant tunneling nanostructures

A.A. Aleksanyan, A.L. Karuzskii, Yu.A. Mityagin, A.V. Perestoronin, N.A. Volchkov, A.P. Chernyaev[1]

P. N. Lebedev Physical Institute of Russian Academy of Sciences, Moscow, Russia, karuz@sci.lebedev.ru
1. Institute of Physics and Technology (State University) Moscow District, Dolgoprudny, Russia

Mechanisms for detecting the THz radiation in resonant tunneling diode (RTD) nanostructures are of interest for solid-state electronics. The terahertz range makes it possible to implement a quantum amplification mode in an RTD that is effective in this range [1]. The competition between the processes of self-excitation (including in the quantum mode) and amplification is discovered by the changes in the *I–V* characteristic near the resonance peak (-1.280 V in Fig. 1) depending on the power. The more intense, without external power, feature of self-excitation (-1.307 V) with the participation of the LO-polaritons decreases with increasing power, and the feature of the classical regime [1] of self-excitation or amplification (-1.280 ÷ -1.269 V) grows. In the NDC region, the amplified power P_{am} becomes a variable parameter, and the detection is characterized by the sensitivity $(\partial^2 I/\partial U^2)/(\partial I/\partial U)$ A/W [2]. The independent P_{am} and rectified current $I(u(t))$ in the form $(\partial^2 I/\partial U^2)P_{am}=(\partial I/\partial U)I(u(t))$ correspond to zero or infinite derivatives. Near the resonant peak current they manifest themselves as smoothed "steps" of the *I–V* curve and "discontinuities" on the derivatives. Weak currents in the *I–V* characteristic valley (-1.7 V), due to a decrease in the effective width of the resonance level [1] at low conductivity, lead to the predominance of the quantum self-excitation and amplification regime at all powers, the absence of "smoothing" current steps and "discontinuities" of the *I-V* characteristic (-1.72÷ -1.69 V), corresponding to zero or infinite derivatives in the expression $(\partial^2 I/\partial U^2)P_{am}=(\partial I/\partial U)I(u(t))$. At low conductivity, switching between stable current states corresponds to the charge build-up during the creation-annihilation of LO-polaritons [2]. The quantum mode significantly increases the detecting efficiency of RTDs even at minimum microwave powers.

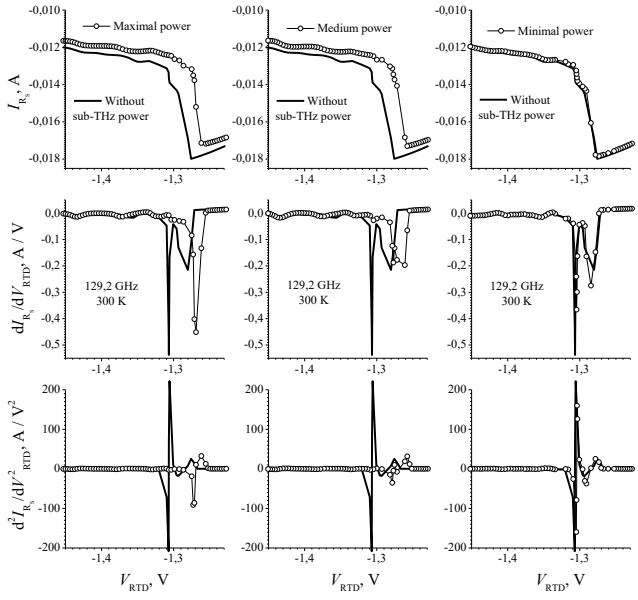

Fig. 1. The first (center) and second (bottom) derivatives of *I-V* curves (top) for a double-barrier RTD with and without incident sub-THz power. *T*=300 K, active layers of AlAs/GaAs barriers/well 23/45/20 Å.

1. V.F. Elesin, "Theory of coherent oscillations in a resonant tunneling diode". JETPh, **89**(2) pp. 377-383, 1999.
2. A.A. Aleksanyan et al. "Electrically stimulated high-frequency replicas of a resonant current in GaAs/ AlAs resonant-tunneling double-barrier THz nanostructures". Proc. SPIE, **10224**, 102240O pp. 1-7, 2016.

Investigations of the transmission and reflection spectra of THz radiation of magnetic metallic nanowires

L.A. Fomin[1], V.G. Krishtop[1], E.N. Zhukova[2,5], D.L. Zagorsky[3], I.M. Doludenko[3], S.G. Chigarev[4], E.A. Vilkov[4]

1. Institute of Microelectronic Technology RAS, Chernogolovka, Russia
2. Moscow Institute of Physics and Technology, Dolgoprudny, Russia
3. Federal Research Center "Crystallography and Photonics" RAS, Moscow, Russia
4. Fryazino Branch of the Kotelnikov Institute of Radio Engineering and Electronics RAS, Fryazino, Russia
5. Institute of General Physics, RAS, Moscow, Russia, fomin@iptm.ru

In the process of developing and investigating of THz radiation sources in spintronics based on anisotropic magnetic micro- and nanostructural transitions on magnetic metals, it is proposed to observe the recently predicted fundamental physical effects occurring in micro- and nanostructures containing ferromagnetic, antiferromagnetic metals, heavy metals and insulating tunnel layers [1, 2]. Theoretical works [3, 4] predicted the possibility of creating a laser operating in the frequency range from 3 to 40 THz in structures with transitions between magnetic metals, when currents from 10^5 to 10^7 A/cm^2 flow through them. The effect of electric current rectification (diode effect) was also predicted in media with noncollinear and noncoplanar magnetic structures [5] in the resonance frequency range for spin-flip transitions lying in the THz range, which opens the way for creating THz radiation detectors. In this regard, it is of interest to study the spectral characteristics of heterogeneous metallic nanowires in this frequency range. Metallic nanowires (NWs) obtained by matrix synthesis are of particular interest among nanomaterials. The advantage of the method is its variability, the ability to obtain various types of NW in the pores of the matrix. The first works were devoted to the deposition of NWs from one metal, then multicomponent NWs were obtained both homogeneous (so-called alloys) and heterogeneous (so-called layered) [6]. In this work, we studied the emission and transmission spectra of arrays of heterogeneous nanowires from two ferromagnetic materials, Ni/Co, FeNi/Co, and Ni/Fe on an IR Fourier spectrometer Bruker "Vertex80v" on air in the range from 15 to 250 THz. It was found that in the 15-20 THz range, there is a palisade of peaks associated with nanowires in the reflection spectra and a low signal intensity in the transmission spectra; with an increase in frequency of 20-35 THz, the transmission spectra for nanowires from different materials are close and similar to the membrane spectrum, and the reflection spectra have large peaks. In the range 55–150 THz, the transmittance of the membrane in which the NW array is located is about 90%, and in the presence of NWs it decreases (for example, to 20% for Ni/Co wires). Additional peaks appear at 56 and 60 THz for Ni/Co NWs, 73 and 113 THz for FeNi/Co NWs, and 57, 72, and 114 THz for Ni/Fe NWs. At frequencies 20-35 THz, the influence of the atmosphere is so strong that the signal from the wires cannot be distinguished. Thus, heterogeneous nanowires strongly respond to radiation in the 15–20 THz range, which gives grounds for future attempts to make a THz radiation detector based on them. In the future, it is planned to investigate the frequency range 1-15 THz, as well as partially bleed off the membrane and carry out spectral measurements in vacuum in order to exclude absorption of THz radiation by the polymer and the atmosphere.

1. T.H. Dang, J. Hawecker, E. Rongione, et al. "Ultrafast spin-currents and charge conversion at 3d-5d interfaces probed by time-domain terahertz spectroscopy". Appl. Phys. Rev. **7**, p. 041409, 2020.
2. Ke Huang, Liang Wu, Maoyu Wang, et al. "Tailoring magnetic order via atomically stacking 3d/5d electrons to achieve high-performance spintronic devices" Appl. Phys. Rev. **7**, p. 011401, 2020.
3. A.M. Kadigrobov, R.I. Shekhter, M. Jonson. "Photon generation in ferromagnetic point contacts". Low Temperature Physics **38**, p. 1133, 2012.
4. Yu.V. Gulyaev, P.E. Zilberman, I.V. Malikov, et al. "Spin-injection terahertz radiation in magnetic junctions" JETP Lett. **93**, p. 259, 2011.
5. A.A. Fraerman, O.G. Udalov " Diode effect in a medium with helical magnetic structure" Phys. Rev. B. **77** p. 094401, 2008.
6. D.A. Cherkasov, D.L. Zagorskii, R. I. Khaibullin, et al. "Structure and Magnetic Properties of Layered Nanowires of 3d-Metals, Fabricated by the Matrix Synthesis Method". Physics of the Solid State **62**, p. 1695, 2020.

Competing mechanisms of strain relaxation in Ge/Si(001) heteroepitaxy

O.S. Trushin
Valiev Institute of Physics and Technology of RAS, Yaroslavl Branch, Yaroslavl, Russia, otrushin@gmail.com

Heteroepitaxial system Ge/Si(001) plays an important role in modern semiconductor technology and optoelctronics. Well known problem for such systems is defect formation during growth and successive thermal treatments. Improving quality of heteroepitaxial structures requires fundamental knowledge about atomic mechanisms of defects nucleation in such systems. While modern experiment does not allow to study dynamics of defect generation at atomic level, computer modeling might be useful tool. Standard view on the nature of defect formation in Ge/Si structure assumes relaxation of misfit strain in that system through nucleation of 90° dislocation as the result of reaction of two 60° dislocations in mirror planes [1]. However modern experimental studies using HRTEM provided disputed information on the existence of defects with more complex core structure [2, 3]. It was main goal of this work to clarify this issue using atomistic computer simulations. By combining the modified DRAG and NEB methods [4] it was possible to perform systematic comparison of Minimal Energy Paths for nucleation of dislocations with different core structures in Ge/Si(001) system. Model system for the fcc(100) geometry consisted of 31 atomic layers of substrate and 17 film layers with lateral sizes of 50*3 atomic rows. Thus, maximal number of atoms in the model was up to 75000. As an initial state of the system we used heteroepitaxial structure with coherent interface (atoms of the film adopt lattice of the substrate). Possible final states were configurations containing different types of defects.

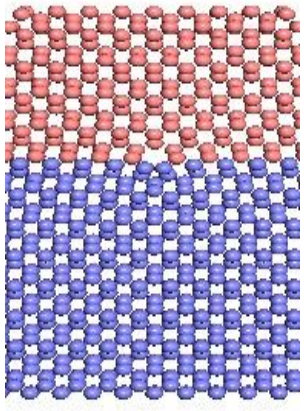

Fig. 1 Standard 90°-dislocation.

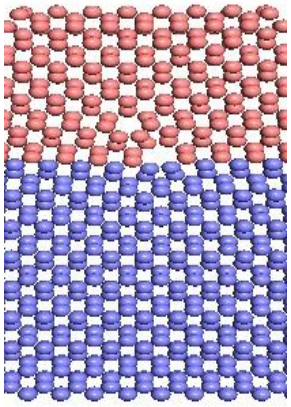

Fig. 2 Complex defect: 60°+60°.

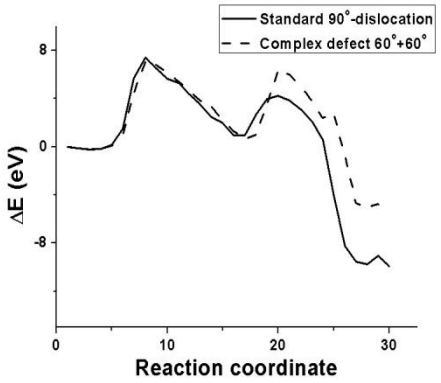

Fig. 3 Energy profiles for standard and complex defects.

Energy profiles for two alternative transition paths which differ by final state configurations (Fig. 1, Fig. 2) are shown in Fig. 3. Analysis of these curves shows that both types of defects are indeed local minima, but standard 90°-dislocation is more energetically favorable than complex defect 60°+60°. Thus both defects might be present in experimental samples, however with different probability.

The reported study was carried out under State Programs #0066-2019-0003 of the Ministry of Science and Higher Education of Russia.

1. R. Hull “Misfit strain and Accomodation in SiGe heterostructures” in *Germanium Silicon: Physics and Materials.*, **56**, Academic Press: San Diego, 1999.
2. Y.B. Bolkhovityanov, O.P. Pchelyakov, and S.I. Chikichev, “Silicon-germanium epilayers: physical fundamentals of growing strained and fully relaxed heterostructures”, Phys.-Usp., **44**, pp. 655-680, 2001.
3. A. Marzegalli et al, "Onset of plastic relaxation in the growth of Ge on Si(001) at low temperatures: Atomic-scale microscopy and dislocation modeling". Phys. Rev. B., **88**, p. 165418, 2013.
4. O. Trushin, et al. “Minimum energy path for the nucleation of misfit dislocations in Ge/Si(001) heteroepitaxy”, Modeling Simul. Mater. Sci. Eng., **24**, p. 035007, 2016.

Re-orientation of graphoepitaxial fluorite films towards small-index crystallographic planes

P.B. Mozhaev[1], I.K. Bdikin[2], J. Bindslev Hansen[3], C.S. Jacobsen[3]

1. Valiev Institute of Physics and Technology of Russian Academy of Sciences, Moscow, Russia, pbmozh@nm.ru

2. TEMA-NRD, Mechanical Engineering Department and Aveiro Institute of Nanotechnology (AIN), University of Aveiro, Aveiro, Portugal, bdikin@ua.pt

3. Department of Physics, Quantum Physics and Information Technology, Technical University of Denmark, Kongens Lyngby, Denmark, jbh@fysik.dtu.dk

Re-orientation of epitaxial thin films during growth with alignment of the small-index crystallographic planes (SICPs) along the surface of the film was often observed for different materials. This effect was usually limited to very small re-orientation angles (<1º) and the *h*, *k*, *l* indexes of the SICPs were usually 1 or 0. We report on re-orientation of graphoepitaxial fluorite thin films towards SICPs (012), (013), with re-orientation angles up to 5º. Three conditions should be fulfilled for such a re-orientation: (i) the initial orientation of the film must be in vicinity of the orientation of the SICP, (ii) the film structure should show certain plasticity to allow re-orientation due to formation of defects, and (iii) the deposition conditions should promote formation of these defects.

The CeO_2 films on $NdGaO_3$ tilted-axes substrates (TAS) showed re-orientation towards (012) plane in the intermediate range of deposition rate and oxygen partial pressure. For lower deposition rate or higher oxygen pressure the film grows graphoepitaxially, completely oxygenated and relaxed. For higher deposition rate (lower oxygen partial pressure) the oxygen deficiency results in stronger bonds between the substrate and the film and formation of completely strained CeO_2 lattice and corresponding graphoepitaxial tilting of the film axes. In the intermediate range the plasticity of the film is high enough for defects formation, but the bonds with the substrate are insufficient to impose strict epitaxial relations, providing possibility of re-orientation of the film.

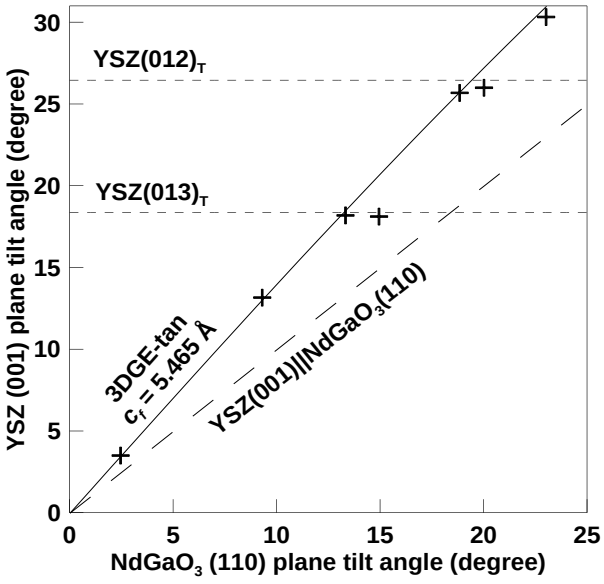

Fig. 1 Graphoepitaxial growth of YSZ films on $NdGaO_3$ TAS, oxygen-depleted surfaces. In vicinity of (012), (013) SICPs the film re-orients towards the SICP.

The $Y:ZrO_2$ films on $NdGaO_3$ TAS at standard deposition conditions always followed the graphoepitaxial growth mode. Suppressing of the epitaxial bonding between the film and the substrate by intentional depletion of substrate surface with oxygen provided necessary conditions for re-orientation of the $Y:ZrO_2$ film towards SICPs. The effect was observed both for (012) and (013) planes (see Fig. 1).

When the film experiences additional tilting towards the substrate plane, the observed re-orientation angles can be as high as 3-5º. The re-orientation from the substrate plane is also possible, but the observed inclination angle is limited to 0.2-0.5º, and some of such films are re-oriented partially.

The re-oriented films show a lower spread of orientations of domains, revealed as a decrease of the width of the rocking curve. The reason is the orienting effect of the film surface during growth, opposite to the mis-orienting effect of dislocations generation for ordinary graphoepitaxial films. The lattice of the film experiences distortion due to surface tension, contractive for CeO_2 surfaces and tensile for $Y:ZrO_2$ surfaces. This effect is observed as a deviation of the lattice constant normal to the surface plane from the standard value. This tetragonal distortion increases with thickness of the film, as revealed by an increased lattice constant variation of the re-oriented films.

The research was supported by Program no. 0066-2019-0004 of the Ministry of Science and Higher Education of Russia for Valiev Institute of Physics and Technology of RAS.

Magnetron deposition of MoS_2 ultrathin films

A.I. Belikov, A.I. Syomochkin, K.Z. Phyo, V.N. Kalinin
Bauman Moscow State Technical University (BMSTU), Moscow, Russia, Asyomochkin@bk.ru

Over the past decade, layered materials have caused a paradigm shift in understanding of two-dimensional nanomaterials fundamental properties and have provided new opportunities for creating promising nano-electronic and photonic setups. Extensive studies of graphene's electron-optical properties and isolated molecular layers of transition metal dichalcogenides (TMDs), obtained by crystal layers' mechanical separation, caused a series of discoveries that contributed to the prototype's creation of electronic devices. Among the TMDs, molybdenum disulfide (MoS_2) is the most studied and promising new semiconductor. The MoS_2 monolayer has a relatively high optical absorption coefficient, high value of charge carrier mobility which are an important characteristic for the designed new nano-sized systems [1].

MoS_2 ultrathin films during their growth can have both crystalline and amorphous structures. Therefore, it is assumed that the use of the magnetron sputtering method will make it possible to realize orientational effects in the process of film deposition by using an external magnetic field. Molecules under the action of magnetic field will orient themselves and integrate into the structure with a certain grain orientation, forming the texture of the film and its polycrystallinity.

In the present work magnetron sputtering method with the external magnetic field applying to deposit MoS_2 thin films was used. Molybdenum disulfide target with a purity of 99.7% and a diameter of 75 mm was used. Sputtering process was stabilized on direct current equal to 0.05 A, and the voltage was 420 V. Argon (99.9995% purity) was used as the working gas. The distance from the target to the substrate (Si(111)) was formed as a result of many experiments and was taken as 110 mm. The gas consumption was 550 ml per hour, which corresponds to a pressure of 6.7×10^{-1} Pa. External magnetic field forming system was based on two magnets and the induction at the substrate surface was varied from 40 to 600 mT by increasing the gap between the magnets (from 10 to 30 mm). The magnetic field induction was measured over the region of the substrate; the Hall transducer plane was normal to the direction of the magnetic induction vector of the studied magnetic field. The slope of the substrate holder was varied (0, 30, 60, 90 degrees) to study the effect of the deposition angle on the properties of MoS_2 thin films, and the location of the north (N) and south (S) pole of the magnet were varied as well (N/S is the magnetic field lines are parallel to the substrate surface, N/N is the magnetic field lines are perpendicular to the substrate surface), to study the influence of magnetic field lines orientation on thin film structure formation. And the deposition time (20-30 sec) was the next variable parameter. Atomic force microscopy (AFM "NT-MDT Solver-Next") was used to measure the thickness (scanning of the "film-substrate" section), roughness and the average grain size of thin films. The optical band gap was determined due to the Kubelka-Munk-Gurevich equation and Tauc relation. The reflectance spectrum was obtained with an "Epsilon" spectrophotometer in wavelength range 380-1100 nm.

Table 1. Investigation of MoS_2 ultrathin films.

Sample №	1	2	3	4	5	6
Deposition parameters: 1. magnets poles 2. magnets gap 3. deposition time 4. substrate orientation angle	 1. N/N 2. 10 mm 3. 20 sec 4. 0°	 1. - 2. - 3. 20 sec 4. 0°	 1. N/S 2. 20 mm 3. 20 sec 4. 0°	 1. N/N 2. 20 mm 3. 20 sec 4. 0°	 1. N/S 2. 30 mm 3. 30 sec 4. 30°	 1. N/S 2. 30 mm 3. 30 sec 4. 0°
Film thickness, nm	7	12	14	21	15	29
Film roughness *Ra*, nm	1,14	1,847	1,27	0,52	1,671	1,359
Average grain size, nm	175,2	291,3	190,2	50,1	257,3	101,5
Energy band gap, eV	1,62	1,54	1,58	1,56	1,35	1,51

The minimum film roughness is achieved with a single-pole arrangement of the magnets. The film thickness increases without a magnetic field. The maximum value of the band gap energy was found on MoS_2 films deposited with a single-pole arrangement of magnets, with a 10 mm magnets gap, without tilting the substrate.

1. Wang Q.H. et al. *"Electronics and optoelectronics of two-dimensional transition metal dichalcogenides"*. Nat. Nanotechnol., **7**, pp. 699–712, 2012.

AFM study of the MoS_2 thin films growth initial stage

A.I. Belikov, K.Z. Phyo, M.M. Guk
Bauman Moscow State Technical University (BMSTU), Moscow, Russia, belikov@bmstu.ru

Extensive studies of 2D materials electronic-optical properties demonstrate the possibilities of their nanoelectronics application as a part of spintronic devices, field-effect transistors on flexible substrates, plasmonics devices and others. Those devices use ultra-thin (up to a monolayer) films of transition metal dichalcogenides, including MoS_2. For such films requirements analysis shows that continuous ultra-thin (less than 10 nm thick) MoS_2 films are needed, and the restrictions imposed on the production technology are low (up to 300 °C) process temperatures. The set of possible methods that provide reproducible formation of films on large-sized substrates for the implementation of group technology is very limited. One of these methods is magnetron deposition using sputter stoichiometric targets. The MoS_2 crystal has a distinct anisotropic layered structure. That determines the film structure features formation during sputtered radical fluxes condensation on substrates in magnetron deposition processes. In this regard, it is necessary to know the MoS_2 films growth mechanisms at the growth initial stages and on various types of substrates.

In a MoS_2 films magnetron deposition process, there may be a stoichiometric ratio violation and a sulfur shortage in the film. Therefore, the effect of sputtering modes of stoichiometric targets on the chemical composition of the films was previously evaluated. As a result, the modes providing the Mo and S required stoichiometric ratio in the films were determined. MoS_2 films were formed at the different deposition times (10, 20, 30 seconds). The deposition was carried out simultaneously on the silicon (111) and sapphire (0001) substrates. The stoichiometric MoS_2 target with a purity of 99.9% and diameter of 75 mm sputtering at the direct current mode and at 10 W power on the magnetron and 0.5 Pa argon pressure was used. The temperature of the substrates was 200°C. The growth rate of the films was approximately of 0.3 nm/s.

The morphology of the obtained samples was studied on some selected surface areas by AFM methods. The films thickness was measured along the "film-substrate" boundary, in 10 cross sections, the results were averaged. Small values of the thickness standard deviation along the length of the stage (Table 1) indicate a high uniformity and continuity of the obtained films. The film samples optical band gap energy values were determined by using spectrophotometry and the reflection spectra, basing on the dependences of the reduced absorption coefficients on the photon energy, in accordance with the Kubelka-Munch and Tauc approaches.

Table 1. MoS_2 films characteristics and deposition modes

Substrate	Deposition time, s	Deposition velocity, nm/s	ThF thickness, nm		Roughness *Ra*, nm	Average grain size, nm	Band gap energy, eV
			Average value	Standard deviation			
Si (111)	10	0,35	3,51	0,04	0,26	141	1,73
	20	0,25	5,09	0,06	0,56	125	1,71
	30	0,38	11,52	0,07	0,61	134	1,69
Sapphire (0001)	10	0,35	3,51	0,03	0,43	53	1,73
	20	0,25	5,00	0,05	0,62	54	1,71
	30	0,34	10,20	0,06	0,75	46	1,70

The AFM analysis indicates different mechanisms of the MoS_2 films growth on the silicon and sapphire. So, on the sapphire, at the second stage (20 s), as can be seen from Fig. 1, islands with a pronounced layered structure are formed on the surface, oriented unidirectionally, the layers are located perpendicular to the surface. The films on the silicon surface have a low roughness and flat islands are detected, the thickness of which multiples correlates with MoS_2 one molecular layer thickness. Such growth features can be explained with the surface energy different values: specific surface energy MoS_2 (~1.72 J/m^2), Si (~1.9 J/m^2), sapphire (~1.525 J/m^2).

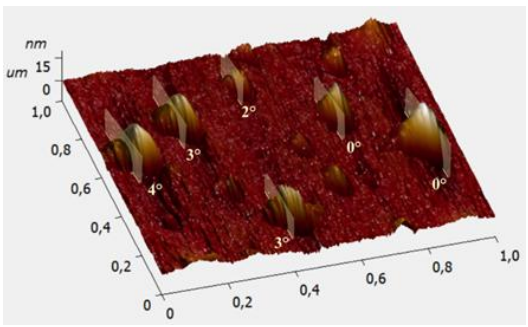

Figure 1. AFM 3D-image (1x1μm^2): MoS_2 film after 20 s deposition on the sapphire substrate.

Atomic layer deposition of thin films of hafnium oxide using Izofaz TM 200-01 system

S. Zyuzin[1,2], Ya. Zasseev[3], A. Rezvanov[1], V. Panin[3], V. Gvozdev[1], Ye. Gornev[1]
1. JSC Molecular Electronics Research Institute. Zelenograd, Moscow, Russia, szyuzin@niime.ru
2. Moscow Institute of Physics and Technology, Dolgoprudny, Russia
3. JSC Research Institute of Precision Machine Manufacturing, Zelenograd, Moscow, Russia

Atomic layer deposition (ALD) is a modern nanotechnological process that is being researched and improved in leading laboratories and institutions all over the world [1, 2]. ALD is used for thin films deposition of various structures, e.g. widely used high-k dielectrics [3]. This paper presents results achieved in thin films deposition of hafnium oxide by using novel ALD system "Izofaz TM 200-01" developed by Research Institute of Precision Machine Manufacturing [4]. Fig. 1 shows the general view of this system.

Hafnium oxide HfO_2 was deposited on 200 mm silicon wafers. Metalloorganic precursor TEMAH (tetrakis(ethylmethylamino)hafnium(IV)) is used alongside with argon as carrier gas. Second precursor (oxidant) is atomic oxygen O decomposed from molecular oxygen O_2 in remote plasma source at 250 W. The temperature is 300 °C.

Thin films of hafnium oxide with various thicknesses (100-300 Å) were obtained. Thickness non-uniformity of $\sigma \leq 2\%$ was achieved while depositing films both on flat surfaces and surfaces with high-aspect trenches ($AR \geq 10$). The measured GPC was around 1 Å/cycle. Refractive index lies within tabular values for HfO_2 (1.9-2.07, observed 2.01-2.07). Typical data derived from the wafer with 100 ALD cycles is shown in Fig. 2.

Obtained data shows that the process genuinely is an atomic layer deposition, and this ALD system is eligible to deposit thin hafnium oxide films of high quality.

Fig. 1. General view of "Izofaz TM 200-01" ALD system [4].

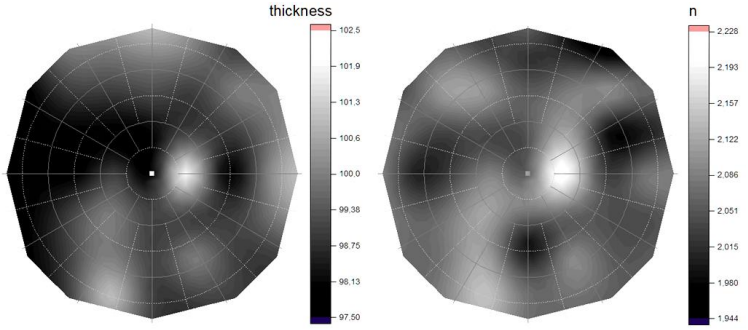

Fig. 2. Visualization of data on refractive index (on the left) and thickness (on the right) of HfO_2 film.

1. G.Ya. Krasnikov and Ye.S. Gornev, "Semiconductor electronics development JSC MERI and Mikron" History of domestic electronics, **1**, pp. 510-538, 2012 (in Russian).
2. S.M. George "Atomic layer deposition: an overview" Chemical Reviews, **110**, pp. 111-131, 2009.
3. R. Arghavani et.al. "High-k/Metal Gates for High-Volume Manufacturing" Nanochip Technology Journal, **5**, pp. 2-7, 2007.
4. V.V. Odinokov et.al. "Izofaz TM 200-01 system for thermal and plasma-enhanced atomic layer deposition of Al_2O_3" Electronics and microelectronics UHF, **1**, pp. 10-14, 2019 (in Russian).

Optimal linear-optical generation of entangled two-qubit states

M.Yu. Saygin, S.A. Fldzhyan, S.P. Kulik
Quantum Technology Centre, M. V. Lomonosov Moscow State University, 119991 Moscow, Russia.
saygin@physics.msu.ru

The capability of linear optics to generate entangled states is widely exploited in photonic quantum information processing. However, it is challenging to obtain entangled logical qubit states, which is usually required by many quantum algorithms. Among the states of interest, the two-qubit ones are the most applicable. In our talk we report on the most compact and efficient linear-optical generation of two-qubit states that does not imply feed-forward operations. The schemes have been obtained by computer optimization algorithms, thus, our findings highlight the importance of computer methods in designing quantum optical setups. We envision that such methods will be playing a more integral role in the development of practical quantum devices in the future.

Collective qubits on double quantum dots with Coulomb interaction

A. Levin[2], L. Fedichkin[1,2], V. Vyurkov[1,2]
1. Valiev Institute of Physics and Technology RAS, Moscow, Russia, vvyurkov@gmail.com
2. Moscow Institute of Physics and Technology (State University), Dolgoprudny, Russia

The implementation of a solid-state quantum register based on space states in field-defined double quantum dots (DQD possesses one electron in two adjacent tunnel bound dots) in an ultrathin silicon bar was proposed [1, 2]. To some extent, the structure reminds that of the field-effect transistor with multiple separate gates [2]. Therefore, the construction follows a natural way of nanoelectronics. Scalability is audible and it opens up a possibility of large-scale quantum computer.

An individual qubit consists of two DQDs. Then the quantum information can be encoded and processed without charge transfer between dots (the probability to find electron in a dot permanently equals 1/2). Quantum algorithms could be effectuated via manipulation with gate potentials. The read-out is performed when a transmission of current through the channel in a regime of Coulomb blockade is organized [3]. Worth noting, during quantum computation the current is switched off and thus has no influence on a qubit evolution.

Here we propose visibly the same structure but where the states of DQDs evolve only due tunneling and Coulomb interaction. As the exchange interaction is eliminated, the spin polarization of electrons in a strong magnetic field is no more necessary. The structure could be obviously developed into an ensemble quantum computer where instead of single silicon bar a number of them are placed under controlling electrodes (gates). In the construction, the decoherence rate retains the same and the final error of quantum calculations is diminished by a simple averaging the results of individual registers operating in parallel.

However, the situation dramatically changes when one introduces fairly strong Coulomb interaction between DQDs constituting a collective qubit. It turned out that in the case when DQDs hold on each other they resist much better against decoherence. To prove the sentence we simulated the evolution of two identical DQDs as a fragment of collective qubit (Fig. 1).

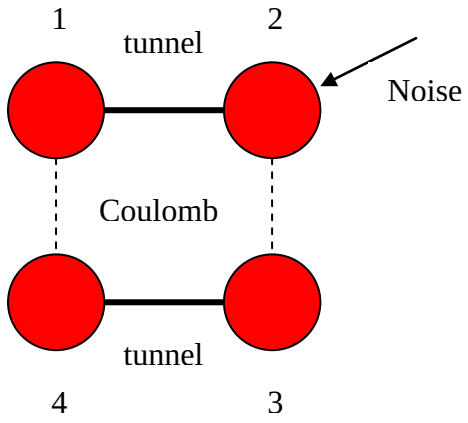

Fig. 1.

Here the upper dot 2 is subject to external noise (alternating potential). The most detrimental noise at the frequency exciting the resonant transitions between symmetric and antisymmetric states in DQD (Rabi oscillations) was involved into the model. Two-particle non-stationary Schrödinger equation was solved for switched off and switched on Coulomb interaction between DQDs. The error was calculated via projection into initial ideal state. In the second case the Rabi oscillations of the upper qubit are substantially suppressed. Feasibly, the effect will be much stronger for a great number of DQDs incorporated into a collective qubit.

1. V. Vyurkov, S. Filippov, and L. Gorelik, Quantum computing based on space states without charge transfer. Physics Letters A **374** (2010) 3285-3291.
2. S. Filippov, V. Vyurkov, and A. Orlikovsky. Quantum computing on silicon-on-insulator structure. VII Workshop of the European Network on Silicon on Insulator technologies (EUROSOI-2011), January 17-19 2011, Granada, Spain, Conference Proceedings, pp. 101-102.
3. M. Rudenko, V. Vyurkov, S. Filippov, A. Orlikovsky. Quantum register in a field-effect transistor channel. Int. Conf. “Micro- and Nanoelectronics '2014”, Moscow, Russia, 2014, Book of Abstracts, q1-05.

Super resolution of two point sources by means of spatial mode transformation and photon statistics analysis

K.G. Katamadze[1,2], B.I. Bantysh[2], D.O. Akatiev[3], N.A. Borshchevskaya[1], E.V. Kovlakov[1], Yu.I. Bogdanov[2], S.P. Kulik[1]

1. Quantum Technology Centre, M. V. Lomonosov Moscow State University, 119991 Moscow, Russia.
2. Institute of Physics and Technology, Russian Academy of Sciences, 117218 Moscow, Russia.
3. Federal State Budgetary Institution of Science Federal Research Center Kazan Scientific Center of Russian Academy of Sciences, Kazan, Russia
kak@quantum.msu.ru

The standard theory of diffraction shows that the resolution of an image obtained by a linear optical scheme is restricted by the diffraction limit. The image is a convolution of the source with a point spread function (PSF), the size of which is limited by the numerical aperture of the objective, and by the wavelength. There are many methods for overcoming the diffraction limit [1], but most of them are based on nonlinear interaction of radiation with a sample, complex excitation and luminescence suppression, and have a very restricted field of application.

On the other hand, recently, methods of statistical image processing have begun to actively develop, which make it possible to restore image details on scales lying within the diffraction limit. These methods are based on the same principles as in the quantum state. A certain image model is developed, a set of measurements is selected that allows obtaining maximum information about the model parameters, and then, based on a set of mutually complementary measurements, a statistical assessment of these parameters is made.

Another approach is based on the use of information on radiation statistics to reconstruct the source image. For example, in work [2] it was shown that mapping of correlation functions of the N-th order allows improving the image resolution by $\sqrt{N}$ times. In particular, in [3–5], this was demonstrated by the example of single-photon sources.

In the present work, we investigate the prospects of combining these two approaches. We consider the problem of resolving two point sources with different statistics of photons based on spatial modes filtering and measuring photon statistics with subsequent statistical reconstruction of the sources parameters. In contrast to most works in which the problem of two equal intensity sources resolution is considered, we consider the general case of two sources of different intensities, which is much more common in a real experiment.

This work was supported by the Ministry of Science and Higher Education of the Russian Federation (program no. 0066-2019-0005 for the Valiev Institute of Physics and Technology, Russian Academy of Sciences), by the Foundation for the Advancement of Theoretical Physics and Mathematics BASIS (projects no. 20-1-1-34-1 and 21-1-3-40-1), and Russian Foundation for Basic Research (projects no. 19-31-27001 and 20-32-70153).

1. P. R. Hemmer and T. Zapata, “The universal scaling laws that determine the achievable resolution in different schemes for super-resolution imaging”. Journal of Optics, **14** (8), p. 083002, 2012.
2. T. Dertinger, R. Colyer, G. Iyer, S. Weiss, and J. Enderlein, “Fast, Background-Free, 3D Super-Resolution Optical Fluctuation Imaging (SOFI)”, Proc. Natl. Acad. Sci. **106**, p. 22287, 2009.
3. O. Schwartz and D. Oron, “Improved Resolution in Fluorescence Microscopy Using Quantum Correlations”, Phys. Rev. A, **85**, p. 33812, 2012.
4. O. Schwartz, J. M. Levitt, R. Tenne, S. Itzhakov, Z. Deutsch, and D. Oron, “Superresolution Microscopy with Quantum Emitters”, Nano Lett. **13**, p. 5832, 2013.
5. D. Gatto Monticone, K. Katamadze, P. Traina, E. Moreva, J. Forneris, I. Ruo-Berchera, P. Olivero, I. P. Degiovanni, G. Brida, and M. Genovese, “Beating the Abbe Diffraction Limit in Confocal Microscopy via Nonclassical Photon Statistics”, Phys. Rev. Lett. **113**, p. 143602, 2014.

Variational simulation of Schwinger's Hamiltonian with polarization qubits

O.V. Borzenkova[1], G.I. Struchalin[2], A.S. Kardashin[1], V.V. Krasnikov[2], N.N. Skryabin[2], S.S. Straupe[2], S.P. Kulik[2], and J.D. Biamonte[1]

1. Skolkovo Institute of Science and Technology, 3 Nobel Street, Moscow 121205, Russia.

2. Quantum Technology Centre and Faculty of Physics, M. V. Lomonosov Moscow State University, 1 Leninskie Gory Street, Moscow 119991, Russia.

Variational quantum eigensolver (VQE) is the class of hybrid quantum-classical algorithms for finding eigenvalues of a given Hamiltonian. First, the quantum apparatus prepares a probe state using some quantum scheme – the so-called ansatz. Then, the prepared state is measured, and the mean Hamiltonian value is calculated using the obtained results. During VQE, the mean value is minimized by varying ansatz parameters, and the attained minimum corresponds to the ground energy of the Hamiltonian. The probe state preparation followed by measurements is a quantum part of VQE, while calculation of the mean Hamiltonian value and optimization is carried out by classical computers.

Simulation of quantum chemistry and quantum physics problems on classical computers involves operations with quantum states that often require exponentially large storage capacity with the increasing system size. The simulation can be accelerated by transferring classically intractable subtask to the quantum apparatus and reformulating the problem as a variational model.

In the present work, we study the effect of noise on VQE performance. We apply VQE to the Schwinger model that has a quantum phase transition. The experimental testbed is a free-space optics setup, where an arbitrary polarization two-qubit state can be prepared. The photon source is based on spontaneous parametric down-conversion in PPKTP crystal installed in the Sagnac interferometer. The probe state undergoes artificial noise and decoherence employing liquid-crystal waveplates with time-dependent retardance.

We specifically exploit the possibility to engineer noise to explore the limits of variational algorithms in identifying and quantifying quantum phase transitions with noisy qubits. We find that despite the presence of noise, one can detect the phase transition of the Schwinger Hamiltonian even for a two-qubit system using variational quantum algorithms.

The results are published in work [1].

1. O. V. Borzenkova, G. I. Struchalin, A. S. Kardashin, V. V. Krasnikov, N. N. Skryabin, S. S. Straupe, S. P. Kulik, and J. D. Biamonte. "Variational Simulation of Schwinger's Hamiltonian with Polarisation Qubits". Applied Physics Letters, **118**, p. 144002, 2021.

Education setup for quantum optics and quantum information tasks

N. Borshchevskaia[1], K. Katamadze[1,2], E. Mareev[1], F. Potemkin[1], B. Bantysh[1,2], G. Avosopiants[1,2], Yu. Vladimirova[1], S. Kulik[1]

1. Quantum Technology Centre, M. V. Lomonosov Moscow State University, 119991 Moscow, Russia.
2. Valiev Institute of Physics and Technology, Russian Academy of Sciences, 117218 Moscow, Russia
bornad@quantum.msu.ru

We present an educational complex for practical work in quantum optics and quantum informatics. It allows one to explore basic principles of quantum optics: nonclassical light states, entanglement and probabilistic nature of measurement results.

The first part of the lab includes classical tasks for better understanding of how the standard polarizing elements work. Other tasks are implemented in the universal setup based on nonclassical light states, which are generated during spontaneous parametric down conversion.

It is designed to carry out tomography of quantum states and processes and one or two-photon interference. It also allows one to investigate correlational properties of basic light states of quantum optics.

In addition, the universal setup demonstrates a quantum random number generator and some well-known quantum key generation protocols.

The theoretical description includes Stockes, Johnes, Mueller, and Poincare methods for understanding the principles of manipulating with pure and mixed states of light.

This work was supported by the Ministry of Science and Higher Education of the Russian Federation (program no. 0066-2019-0005 for the Valiev Institute of Physics and Technology, Russian Academy of Sciences), by the Foundation for the Advancement of Theoretical Physics and Mathematics BASIS (projects no. 20-1-1-34-1 and 21-1-3-40-1).

Some properties of maximal trace measure of quantum computer error rate

A.A. Kurkin[2], L.E. Fedichkin[1]
1. Valiev Institute of Physics and Technology, Russian Academy of Sciences, Moscow, Russia, leonid@phystech.edu
2. Moscow Institute of Physics and Technology, Dolgoprudny, Russia

The important factor hindering nowadays quantum computers from demonstration of practically useful large-scale computations is still high error rate in quantum registers during computation. To evaluate error rates and to optimize qubits parameters for error reduction purposes one needs some realistic measure suitable for error estimation for given quantum register density matrix distortion [1, 2].

In our work we analyze new measure of decoherence based on maximal trace measure. It is defined as maximal trace norm of deviation matrix which is the difference of density matrices of quantum computer for ideal and noisy evolutions respectively. We obtain some useful estimates of its value for single qubit evolutions. Then we get its relations with operator norm based on maximal eigenvalue measure. For multiqubit quantum registers we do numerical simulation for two nonunitary evolution channels: relaxation and dephasing.

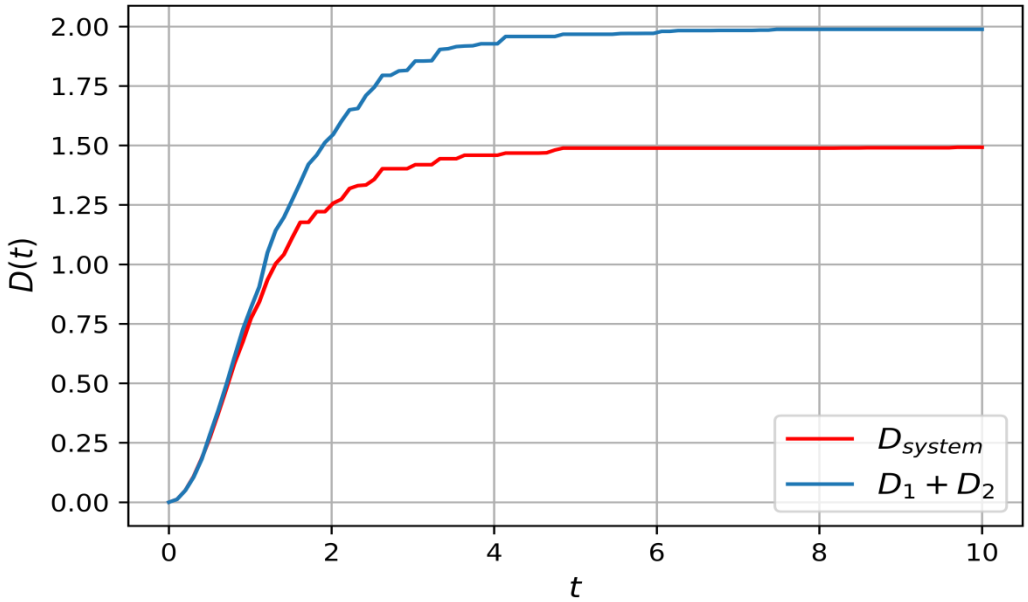

Figure 1. Trace decoherence measure of two-qubit system and sum of two trace decoherence measures of individual qubits under same dephasing interaction with environment.

Our results show that it has some useful properties and, in particular, in these cases maximal trace measure is additive for low error rates as shown in Fig. 1.

1. L. Fedichkin, V. Privman. “Quantitative Treatment of Decoherence”. Topics in Applied Physics, **115**. pp. 141-167, 2009.
2. A. Fedorov, L. Fedichkin, V. Privman. “Evaluation of Decoherence for Quantum Control and Computing”. Journal of Computational and Theoretical Nanoscience, **1**, pp. 132-143, 2004.

On the way to a scalable Yb ion quantum computer

I. Semerikov[1], I. Zalivako[1], A. Borisenko[1], M. Aksenov[1], A. Korolkov[1,2], N. Kolachevsky[1,2], K. Khabarova[1,2]

1. Lebedev Physical Institute of RAS, Moscow, Russia
2. Russian Quantum Center, Moscow, Russia

Quantum computations are one of the major topics in modern physics. Several impressive results were demonstrated recently in this field [1, 2]. Ultracold trapped ions are one of the leading physical platforms for a quantum computer implementation. The highest quantum volume has been demonstrated with ions [3]. In Russia a project aimed at quantum computations with ions was started in 2020 under the LRC grant. Following leaders in the field $^{171}Yb^{+}$ ions were chosen for quantum information processing. Several ways for quantum information encoding are being investigated: optical qubit on the 435 nm quadrupole transition and hyperfine qubit in an electronic ground state with Raman excitation at 435 nm or 355 nm. Each of these approaches has its own advantages and disadvantages that will be discussed in the talk. Also, the current status of the project will be presented. A system for universal quantum computations with 5 qubits was built; single-qubit operations on optical qubit have been demonstrated.

1. Arute, Frank, et al. "Quantum supremacy using a programmable superconducting processor." Nature **574** (7779), pp. 505-510, 2019.
2. Pino, Juan M., et al. "Demonstration of the trapped-ion quantum CCD computer architecture." Nature **592** (7853), pp. 209-213 (2021).
3. https://www.honeywell.com/us/en/news/2021/03/quantum-milestone-how-we-quadrupled-performance

Quantum error reduction with deep neural network applied at the post-processing stage

A.A. Zhukov[1], W.V. Pogosow[1,2]
1. Dukhov Research Institute of Automatics (VNIIA), 127055 Moscow, Russia.
2. Institute for Theoretical and Applied Electrodynamics, Russian Academy of Sciences, 125412 Moscow, Russia,
zugazoid@gmail.com

In this report, we have proposed a method for the application of classical neural networks for the improvement of the outcomes of noisy quantum devices at the post-processing stage [1, 2]. In contrast to other suggestions, using our approach, it is possible to get data for training a neural network without relying on a classical simulator or any other source of ideal data. The approach is most suitable to the very important problem of digital simulation of quantum dynamics, for which limitations in accessible Trotter steps numbers are currently crucial. The limitation is associated with the error accumulation due to the hardware imperfections.

Our method is based on artificial noise enhancement on the training stage that can be done by incorporation of fictitious Trotter blocks formally equivalent to identity gates into the circuit. Their role is to increase noise level due to the hardware imperfections while preserving the circuit's general structure and its relevant features. The network is trained to transform data obtained with such fictitious steps towards data obtained without them, that is, for rather shallow circuits, for which hardware errors are not critical. This idea seems to be more prospective for near-term generations of quantum computers with reduced gate errors, for which circuits at the training stage can already support large entanglement.

After being trained, the network can be applied to new data with the same Trotter step number, i.e., increased in the same way as at the training stage, but without fictitious Trotter steps. The amount of noise in this case is similar to that at the training stage. This trick allows for the effective increase of the Trotter number due to the post-processing, in the sense that errors become suppressed and results of simulations, which must have error rates below a given level, start to include data with larger Trotter step number. As a result, an initial time interval for which quantum simulation produces acceptable results compared to the ideal results for the solution of the Schrodinger equation has been extended.

We have demonstrated the basic ingredients of our approach using a particular example: digital quantum simulations of the dynamics of the transverse-field Ising chain. A deep neural network with simple architecture was used at the post-processing stage. The proof-of-principle results obtained on a real 5-qubit IBM Athens quantum processor show that our method allows us to double or triple the number of Trotter steps while maintaining the same level of errors. Thus, significant error reduction is the main result of our method.

We believe that the proposed approach can be useful in the context of error mitigation in noisy quantum devices (especially of next generations with hardware errors decreased and qubit number increased). Particularly, it can be used in the case of periodic quantum circuits and in combination with other error reduction tools, such as postelection partial error correction.

1. J. Biamonte, P. Wittek, N. Pancotti, P. Rebentrost, N. Wiebe, and S. Lloyd, "Quantum machine learning", Nature **549**, 195, 2017.
2. M. Schuld, I. Sinayskiy, and F. Petruccione. "An introduction to quantum machine learning", Contemporary Physics **56**, 172, 2015.

A quantum algorithm for calculation of π on non-ideal quantum computers

G.A. Bochkin, S.I. Doronin, E.B. Fel'dman, A.I. Zenchuk
Institute of Problems of Chemical Physics of Russian Academy of Sciences, 142432, Chernogolovka, Moscow Region, Russian Federation. E-mail address: bochkin.g@yandex.ru

An algorithm for calculating π on a noisy quantum computer is suggested. The idea is as follows: we consider a single qubit initially in the state $|0\rangle$, then applying unitary transformation corresponding to rotation of the Bloch sphere around the *y*-axis by φ radians. Then it is measured in the computational basis ($|0\rangle, |1\rangle$). The probability of observing the state $|1\rangle$ is then, in the ideal case,

$$p(\varphi) = \sin^2(\varphi/2) = (1-\cos\varphi)/2. \quad (1)$$

Thus, successive roots of the equation $p(\varphi)=1/2$ differ by π, providing a way to estimate it. Of course, in practice, rotating by a given angle φ requires choosing some other physical parameter, such as the duration of a control pulse *t* (this is the case for transmon or NMR qubits, for example). We assume that $\varphi = ct + \varphi_0$. The constants *c* and φ_0 must be estimated at the time of the quantum computer calibration. Since the most natural method of estimating *c* involves determining period of *p* as a function of *t* (thus estimating $2\pi/t_{period}$), the above method covertly uses a known value of π unless an independent method of estimating *c* is used. To estimate *c*, we note that the area below the curve $y=f(t)$ (where *f* is such that $p(\varphi)=f(t)$) but above the line $y=1/2$ is equal to $1/c$. Formally, the area *I* is

$$I = \int_{t_1}^{t_2}\left(f(t) - \frac{1}{2}\right)dt = \frac{1}{c}, \quad (2)$$

where $f(t_1)=f(t_2)=0.5$, and $f(t)>0.5$ for *t* such that $t_1<t<t_2$.

Thus, by running this algorithm many times for each of several different values of *t*, we can empirically measure $f(t)$ for them, estimate t_1, t_2 and *I*, and estimate π as $(t_2-t_1)/I$.

In practice, however, the measurement on a quantum computer is non-ideal: the probability of obtaining $|1\rangle$ after measurement cannot reach 0 or 1, no matter what unitary transformation is performed. We assume that the experimental probability is a linear function of the ideal one, that is, the actual probability $P(t)$ is

$$P(t) = \alpha\frac{1-\cos(ct+\varphi_0)}{2} + \beta \quad (3)$$

where α, β are parameters describing measurement errors, and φ_0 is the systematic angle error (ideally $\alpha=1$, $\beta=0$, $\varphi_0=0$). If we can estimate the measurement errors and correct them so that probability can reach 0 and 1, the above algorithm can be used with slight adjustments. See [1] for the details.

Our algorithm can run on quantum computers with high level of measurement errors, and does not use any two-qubit operations which are highly noisy on current quantum computers.

We ran this algorithm on a five-qubit IBM quantum computer for 64 different values of *t*, 8192 time for each *t*, and obtained the result $\pi = 3.157 \pm 0.017$ [1]. The obtained accuracy is not high (classical algorithms can do much better), but we view our algorithm as a way to check the accuracy of a contemporary quantum computer on a simple task it can do given the current level of errors. Our result is consistent with the hypothesis of those errors being random.. It is worth noting that another suggested algorithm for calculating π with a much more complicated quantum part [2] does not offer substantially better accuracy.

We acknowledge funding from the Ministry of Science and Higher Education of the Russian Federation (Grant No. 075-15-2020-779).

1. G.A. Bochkin, et al. "Calculation of π on the IBM quantum computer and the accuracy of one-qubit operations". Quantum Information Processing, **19**, art. no. 257, 2020.
2. T.Noto. "Quantum circuit to estimate pi using quantum amplitude estimation". arXiv:2008.02623.

Sequences of selective rotation operators for three group clustering on qutrits by means quantum annealing

V. Zobov, I. Pichkovskiy
Kirensky Institute of Physics Federal Research Center KSC SB RAS, Krasnoyarsk, Russia, rsa@iph.krasn.ru

Quantum computers in compare with classical ones will allow achieve higher performance when solving artificial intelligent problems such as clustering [1] and associative memory [2]. Clustering is partitioning a set data points into subset in according to proximity of their properties (in our case according to distances between two points on Cartesian plate). This problem has already been solved on two-level quantum elements (qubits) in work [1] with quantum annealing technique. As we showed earlier [3] the transformation to three-level elements (qutrits, the spins $S=1$) will allow solving same problem on less amount of quantum elements. In this report we used sequences of selective rotation operators for realization this algorithm. In the case of clustering by the quantum annealing technique, at initial moment of time system is prepared in the ground state of the initial Hamiltonian including interaction with a transverse magnetic field. Then the Hamiltonian adiabatically changed in time to the final Hamiltonian, in the ground state of which we encode the solution of problems. We take the final Hamiltonian for clustering into three groups in the following form [3]:

$$H_f = \sum_{i,j} H_{ij} \qquad H_{\mathrm{ij}} = R_{ij}\left(2\left[|1,1\rangle\langle 1,1|_{i,j} + |0,0\rangle\langle 0,0|_{i,j} + |-1,-1\rangle\langle -1,-1|_{i,j}\right] - 1\right) \qquad (1)$$

where R_{ij} is distance between data points i and j. The Hamiltonian (1) has written with projectors on calculation basis of eigenvectors of projections operators S_i^z on axis Z with projections 1, 0, -1. If we express projectors in Hamiltonian (1) with spins operators [2], then it takes form:

$$H_{ij} = R_{ij}\left(S_i^z S_j^z + 3S_i^z S_i^z S_j^z S_j^z - 2S_i^z S_i^z - 2S_j^z S_j^z + 1\right) \qquad (2)$$

For realization algorithms on real physical system the interaction in the Hamiltonian (2) should be expressed with dipole-dipole and Zeyman interactions. For this purpose, we divide the complete evolution operator into a product of individual operators, to each of which we apply the following transformations of the evolution operator using selective operators of rotations around the axes Y and Z [4]:

$$\exp\left[-3iJ_{ij}S_i^z S_j^z S_j^z\right] = \exp\left[-2iJ_{ij}S_i^z\right]\left\{-\pi\right\}_{y,j}^{2\leftrightarrow 3}\exp\left[-iJ_{ij}S_i^z S_j^z\right]\left\{-\pi\right\}_{y,j}^{1\leftrightarrow 2}\exp\left[-iJ_{ij}S_i^z S_j^z\right]\left\{\pi\right\}_{y,j}^{1\leftrightarrow 2}\left\{\pi\right\}_{y,j}^{2\leftrightarrow 3}$$

$$\exp\left[-i\theta S_i^z\right] = \left\{2\theta\right\}_{z,i}^{2\leftrightarrow 3}\left\{2\theta\right\}_{z,i}^{1\leftrightarrow 2} \qquad \exp\left[-i3\varphi S_i^z S_i^z\right] = \left\{2\varphi\right\}_{z,i}^{1\leftrightarrow 2}\left\{2\varphi\right\}_{z,i}^{2\leftrightarrow 3}\exp\left[-2i\varphi I\right]$$

All unnecessary interactions in each evolution operator will be “turned off” using the inversion operators. Thus, we have obtained the desired sequence of selective rotation operators and evolution operators with the dipole-dipole interactions. After applying the found sequence to the fife qutrit system, the set of six points is grouped into three clusters according to the proximity of their coordinates.

This work was supported by a grant from the Fund for the Development of Theoretical Physics and Mathematics "Basis" # 20-1-5-41-1.

1. V. Kumar, G. Bass, C. Tomlin, and Dulny, J. “Quantum annealing for combinatorial clustering”. J. QINP., **2**, 2, pp 1-14, 2018.
2. V. Zobov and I. Pichkovskiy. “Associative memory on qutrits by means of quantum annealing”. QINP, **19**, pp. 1-12, 2020.
3. V. E. Zobov, I. S. Pichkovskiy. “Clustering by quantum annealing on three-level quantum elements qutrits” arXiv preprint arXiv:2102.09205, 2021.
4. V. E. Zobov, I. S. Pichkovskiy. “Sequences of Selective Rotation Operators to Engineer Interactions for Quantum Annealing on Three Qutrits”. SPIE, **11022**, p. 11022-2V, 2018.

Study of inert gas pressure influence on electroforming and resistive switching of TiN-TiO_2-SiO_2-W memristors

E.S. Gorlachev, V.M. Mordvintsev, S.E. Kudryavtsev
Yaroslavl Branch of the Valiev Institute of Physics and Technology of Russian Academy of Sciences, Yaroslavl, Russia, egorlachev@yandex.ru

Memristors based on metal-insulator-metal sandwich structures are very prospective not only as non-volatile memory elements alternative to flash memory, but, even more importantly, as a base device for new-generation neuromorphic computing. We have manufactured and studied memristors with SiO_2 insulator layers, which are cheap, scalable and fully in the framework of the traditional Si-based technology. Furthermore, our approach is to use sandwich structures with an open SiO_2 layer sidewall, and therefore the study of a gas medium composition and pressure influence on the memristor functioning is very important. In our recent publications [1, 2], we have discussed the role of oxygen and we have showed the existence of a threshold value of O_2 pressure at which the resistive switching stops and its dependence on the value of the limitation current during electroforming and switching. In this work, we will report the results of the studies of inert gas influence on the memristor electroforming and resistive switching. We have studied TiN-TiO_2-SiO_2-W sandwich structures with a 23 nm thickness of the SiO_2 insulator layer. During this experimental work, we have used our custom-made experimental setup [1], which allowed us to perform electroforming and switching of memory elements in a controlled gas medium with a pressure from 10^{-4} Torr to 1 atm. We have used inert nitrogen and argon gases. The resistivity bistability effects were activated by performing a procedure of electroforming by applying a quasi-static electric pulse starting at 10 V and then with a 2 V increase up to 20 V with three attempts for each voltage. The resistive switching was performed by pulses of 5 V, 30 ms for the "ON" switching and 5–8 V, 100 ns for the "OFF" switching. For the reported experiments, the limitation current during electroforming and resistive switching was 60 mA. Firstly, we have established that the functioning ("ON"/ "OFF" resistive switching) in inert gases (both for nitrogen and argon) of the memory elements, which were subjected to electroforming in vacuum (~10^{-4} Torr), reliably takes place in the entire gas pressure range including the maximum experimental value of 1 atm. However, this requires a full removal of any sorbed oxidizing components (oxygen, water) from the setup by performing its flushing with inert gas before the experiments. Secondly, we have discovered that the electroforming, when carried out in an inert gas atmosphere, takes place at a maximum inert gas pressure of 100 Torr (fig. 1). However, after such electroforming, the memory elements became sensitive to the inert gas pressure and only reliably functioned for its values lower than 100 Torr.

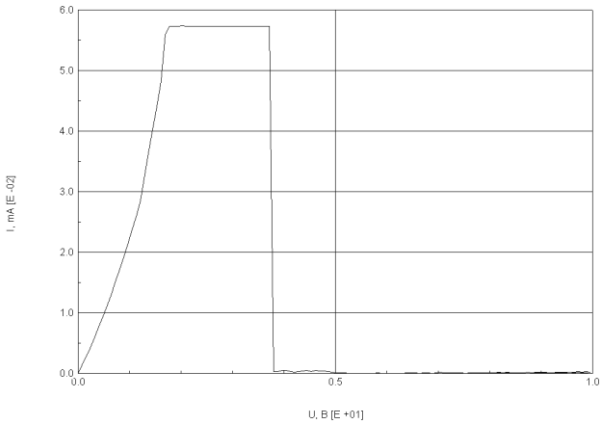

Fig. 1. Current-voltage curve for the electroforming process of a memristor under a 100 Torr argon pressure.

1. E.S. Gorlachev, V.M. Mordvintsev, S.E. Kudryavtsev. "Investigations of the resistive switching of the TiN-TiO_2-SiO_2-W memristors in the oxygen atmosphere with varying pressure." Proc. SPIE, **11022**, pp. 110220D-1-6, 2019.
2. V.M. Mordvintsev, E.S. Gorlachev, S.E. Kudryavtsev, V.L. Levin. "Influence of oxygen pressure on switching in memoristors based on electromoformed open sandwich structures." Russ. Microelectron., **49**, pp. 269-277, 2020.

Effect of electrodes material on the I-V-curve and switching of memristors on the base of electroformed open metal-SiO_2-metal sandwich structure

S.E. Kudryavtsev, V.M. Mordvintsev, V.V. Naumov, E.S. Gorlachev
Yaroslavl Branch of the Valiev Institute of Physics and Technology, Russian Academy of Sciences, Yaroslavl, Russia, E-mail: galinagenevskaya@yandex.ru

Memory on electroformed open "sandwich" metal-insulator-metal (MIM) structures is one of the varieties of memristor memory, which has been actively studied in recent years. Open "sandwich"-MIM-structures are obtained from conventional "sandwich"-MIM-structures by local etching of two upper layers, which leads to the appearance of a free butt-end of the dielectric film, opened to the gas phase and performing the function of an insulating slit between two metal electrodes. Electroforming is carry out by a supply of voltage to the metal electrodes according to a certain algorithm, after which the structure acquires the properties of a non-volatile electrically reprogrammed memory element.

Previously, the most promising was the open "sandwich" structure TiN-SiO_2-W, while the lower TiN electrode was electrically connected with an emitter of a bipolar n-p-n transistor, which provided electrical decoupling of the elements in the memory matrix. The SiO_2 layer thickness was about 20 nm. The presence of a "natural" TiO_2 layer formed on the TiN surface and controlled in thickness in the range 1-3 nm was played fundamental role [1]. Actually we should talk about the structure of TiN-TiO_2-SiO_2-W. Manufactured prototypes, which represent a low-dimensional (3×3) matrix, were able to function as a non-volatile electrically reprogrammed memory several years ago. The main limitations hindering the practical implementation of the technology are the complexity, duration, and insufficient reliability of the electroforming process.

The used design of the memory cell allowed its operation only in one polarity ("minus" on the upper W electrode). Experiments for both voltage polarities were possible to perform by manufacturing memory elements without a transistor structure. Electroforming process with a "plus" on W happens more stable in this case [2]. Besides, the electroformed structures demonstrate the possibility of multiple writing of N-type current-voltage (I-V) characteristics at a slowly varying voltage (about 1 V/s) without breakdowns and uncontrolled shutdowns what earlier (at "minus" on W) was not observed. It could be due to the material of the electrodes and the shape of the insulating gap, apart from the polarity of the voltage. Some samples were prepared to study the influence of these factors on the nature of electroforming and I–V characteristics. The samples were made without a transistor and with various open "sandwich" structures: ordinary TiN-TiO_2-SiO_2-W, W-SiO_2-TiN, W-SiO_2-TiO_2-TiN, W -SiO_2-W, TiN-SiO_2-TiN, TiN-SiO_2-TiO_2-TiN. Manufacturing technologies for various structures were similar, but had more or less basic details.

The study of electroforming processes in various structures and I–V characteristics at both voltage polarities made it possible to unambiguously identify the main factor responsible for the presence of stable electroforming and the absence of breakdowns when prescribing quasistationary I–V-curves. The production of an anode of a structure from tungsten at any (upper or lower) position of this electrode became this factor.

The use of tungsten as the upper electrode was caused by some general considerations about the operation of the structure, but it might not be optimal. The samples with the TiN-TiO_2-SiO_2-Mo structure were prepared in order to search the best material for the anode. The electroforming of such structures requires significantly lower voltages (4.5-6.5 V), which will make the process more reliable.

The results obtained experimentally will optimize the design of the memory element.

1. V.M. Mordvintsev, S.E. Kudryavtsev. "Effect of constructional features of the insulating gap of open TiN–SiO_2–W and Si–SiO_2–W "sandwich" structures on the process of their electroforming" Russ. Microelectron., **46**, pp. 243-251, 2017.
2. V.M. Mordvintsev, E.S. Gorlachev, S.E. Kudryavtsev. "Effect of the electroformation conditions on the switching stability of memristors based on open "sandwich" structures in an oxygen medium." Russ. Microelectron., **50**, pp. 146-154, 2021.

Memristor Effect in Electrolyte–Insulator–SemiconductorStructure

A.E. Berdnikov, A.A. Popov
Valiev Institute of Physics and Technology of Russian Academy of Sciences, Yaroslavl Branch, Yaroslavl, 150007, Russia, imiraslab4@yandex.ru; aapopov@mail.ru

To expand the possibilities of creating neural networks and programmable logic matrices based on the memristor effect, it was research in the structure of electrolyte-dielectric-semiconductor. This structure provides the following capabilities. It is possible to form a structure in which a matrix of open electrodes is formed on a lattice of a thick dielectric, located on the surface of a thin dielectric having a memristor effect. Switching to the open state of this structure is possible with the simultaneous presence of liquid (electrolyte) and electric voltage. The application of the liquid is possible, for example, by inkjet printing, or by some kind imprinting of biochemical process on the surface of the chip.

When voltage is applied, the structure switches into an open state. If there is no liquid or if there is a not enough of it, the corresponding cell will remain off. This switch on process can be called the formation phase. In this case, metal is galvanically deposited from the electrolyte at the place where the current-conducting filament appears, and a current-conducting rail is formed to the nearest open metal electrode. When the surface of the chip is drained after formation phase, this structure remains in conductive state. If a reverse voltage is applied in the end of formation phase, then the not fully formed conductive paths will be dissolved in the electrolyte. This can be called the offset process. Furthermore it is possible for several conduction channels to form around one electrode during the formation process. Since the distance from the electrode to the filaments is different, the number of finally formed paths can depend on the amount of liquid and the concentration of the electrolyte. In turn, the resistance of a particular cell in the open state depends on the number of formed tracks. Further behavior of the formed cells is the same as for a conventional memristor.

Experiment. Single-crystal p-type silicon wafers were used as a substrate. The reverse side of the substrates was additionally doped with boron at a level of the order of 10^{19} cm^{-3} to ensure ohmic contact, and was covered by a metal film. The front (working) side of the substrates was doped with boron to a level of the order of 10^{15}-10^{19} cm^{-3}. For MIS structures, silicon oxide enriched by silicon with a thickness of 30-40 nm, obtained by plasma-chemical deposition in a low-frequency discharge, was used. When on a similar structure the metal electrode is formed, the memristor effect was observed. A water solution of copper sulfate was used as an electrolyte.

It was found that the sample has a conductivity switching effect. It was found that copper hemispheres appear on the surface of the dielectric. The volume of these hemispheres corresponds to the time integrals of the current passed through the sample. Rails on chip surface are not observed because contacted electrode was immersed in electrolyte and not contacted with chip surface.

Electrolyte using also allowed define filament location for further its investigation.

Influence of the kind of metal on memristor effect in MIS structures

O.M. Orlov[1], A.A. Popov[2], A.A. Stepanov[1], P.S. Sattarov[1]
1. JSC Molecular Electronics Research Institute, Zelenograd, Russia.
2. Valiev Institute of Physics and Technology of Russian Academy of Sciences, Yaroslavl Branch, Yaroslavl, Russia.

Investigations were carried out of the influence of the kind of metal in the MIS structure on the conductivity switching effect. Metals are characterized by two parameters that can influence on mersistor effect, the work function of an electron and the binding energy of the atom. Most metals have a work function less than p-type silicon. When they come into direct contact, a Schottky diode can occur. This is not the case with platinum; there must be an ohmic contact. Whether this feature affects on the memristor effect is one of the objectives of this study. Some hypotheses pf the mechanism of the memristor effect suggest the formation of a metal filament in dielectric. Its formation may depend on the binding energy of the metal atoms. Checking for the presence of such dependence is the second task of the study. The third task is to check the technological compatibility of different metals and methods of their deposition.

Single-crystal p-type silicon wafers were used as a substrate. For MIS structures, two types of dielectric were used: silicon nitride with a thickness of 4-5 nm and silicon oxide with a thickness of 30-40 nm. Silicon nitride was obtained by LP CVD at 700 °C from gas mixture of dichlorosilane and ammonia [1]. Silicon oxide obtained by plasma-chemical deposition in a low-frequency (55 kHz) discharge at 380 °C from gas mixture of monosilane and nitrogen monoxide [2].

For nitrides, Cu, Al, Ni, Co obtained by electron beam evaporation, and W, Ti obtained by magnetron sputtering were tested. For the oxides, V, Al, Ni, Co obtained by electron beam evaporation, Pt, Cu, Ti and the W-Ti alloy (10% Ti), obtained by magnetron sputtering, and In deposited in the liquid phase were tested.

It was found that for silicon nitride the memristor effect was observed for all types of metals. The structures have typical reproducible bipolar resistive switching. Switching voltages are close for different samples. Memory window is 4-5 orders.

For MIS with silicon oxide, the effect was observed also for all metals. The only exception is MIS structures with a copper electrode. In this case, abnormally high currents are observed both in the closed state and in the conducting state, the memory window was 2 orders of magnitude, which is 2-4 orders of magnitude less than with other metals. Subsequently, a short circuit was observed between the semiconductor and the metall. Perhaps it is associated with the abnormally high diffusion mobility of copper in silicon oxide and silicon.

The results obtained show that the energy parameters of metals have practically does not affect on the memristor effect. More important are the manufacturability of metal deposition and its compatibility with the materials used.

The work was carried out at the RFBR grant 19-29-0318 and the program of fundamental investigation №0066-2019-0003 Ministry of Science and Higher Education of RF.

1. O. M. Orlov, A. A. Gismatulin, et al Russian Microelectronics, **49**, pp. 372–377, 2020.
2. A.E. Berdnikov, V.N. Gusev, et al. Semiconductors, **47**, p. 641, 2013.

Analysis and comparison of methods for extracting parameters of compact memristor models

D. Zhevnenko[1,2], F. Meshchaninov[1,2], V. Kozhevnikov[1,2], E. Shamin[1,2], E. Gornev[1,2]
1. Moscow Institute of Physics and Technology (State University), Dolgoprudny, Russia.
2. JCS Molecular Electronics Research Institute, Zelenograd, Russia

One of the most promising solutions in the field of energy efficient memory desing is associated with the memristor [1, 2] - a nonlinear element of electrical circuits, the resistance of which can reversibly change due to the flow of electric charge through it and remain constant after limiting the flow of charge.

The key disadvantage of such devices at the moment is the low stability of characteristics, associated with the random nature of the processes occurring within the micro- and nanometer region of the functional layer [3]. The accuracy of most models significantly depends on the method and quality of extraction of its parameters.

We review modern approaches to solving the inverse problem of extracting model parameters from an experiment, and also demonstrate the application of these parameter extraction methods to the developed compact model of mobility modification [4] from an experiment [5].

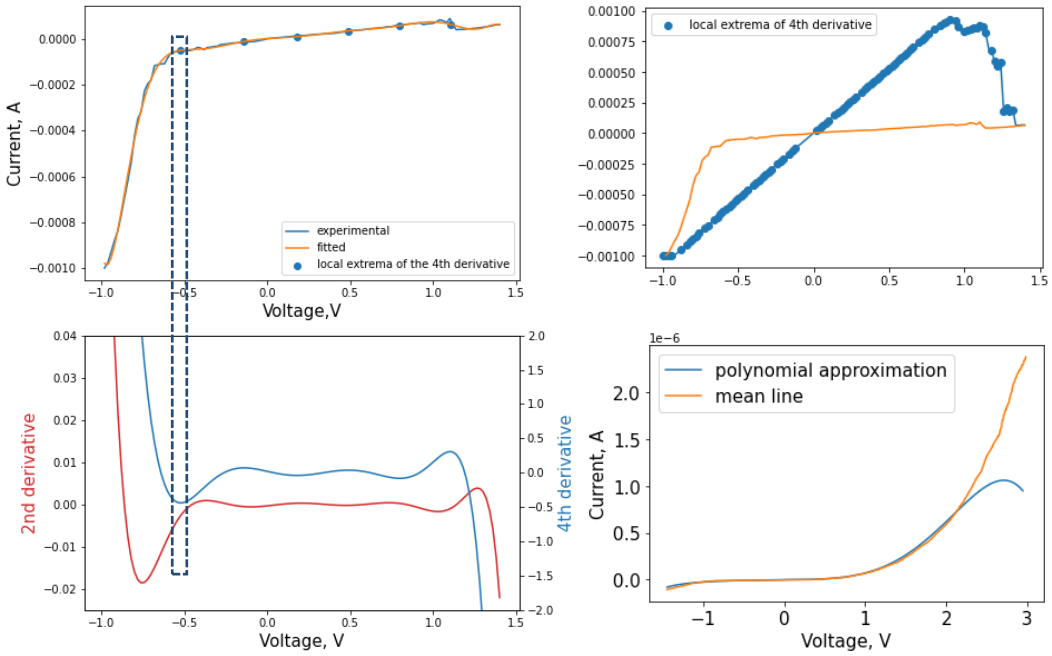

Fig. 1. Evaluation of the switching point, examples of local extrema highlights, and example I-V curve midline approximation by a polynomial.

This research was funded by Ministry of Science and Higher Education of the Russian Federation (grant number 075-15-2020-791)

1. L. Chua. «Memristor-the missing circuit element». IEEE Transactions on circuit theory, **18**, pp. 507-519, 1971.
2. D. B. Strukov et al. «The missing memristor found». Nature, **453**, pp. 80-83, 2008.
3. W. Sun et al. “Understanding memristive switching via in situ characterization and device modeling”. Nature communications, **10**, pp.1-3, 2019.
4. D. Zhevnenko et al. “Simulation of memristor switching time series in response to spike-like signal”. Chaos, Solitons & Fractals, **142**, pp. 110382, 2021.
5. Zajcev, S. A., et al. “Effekt rezistivnogo pereklyucheniya v strukturah TiN/$Hf_xAl_{1-x}O_y$/HfO_2/TiN i TiN/HfO_2/Ti/TiN”, *Mikroelektronika* 43.5 (2014): 337-337 (in Russian).

On memristive properties of vanadium oxide

D. Khakhulin[1], Z. Vakulov[2], R. Tominov[3], V. Smirnov[3], O. Ageev[4]
1. Research Laboratory of Functional Nanomaterials Technology, Southern Federal University, Taganrog, Russia, dhahulin@sfedu.ru
2. Federal Research Centre The Southern Scientific Centre of the Russian Academy of Sciences, Rostov-on-Don, Russia, vakulov@ssc-ras.ru
3. Institute of Nanotechnologies, Southern Federal University, Taganrog, Russia, vasmirnov@sfedu.ru
4. Research and Education Centre 'Nanotechnologies', Southern Federal University, Taganrog, Russia, ageev@sfedu.ru

Transition metal oxides attract a lot of research interest as materials for neuromorphic devices due to their promising memristive properties [1-5]. We have investigated the memristive properties of vanadium oxide, since this material allows to combine the effects of resistance switching associated both with the formation of a conductive filament and with a metal-insulator transition. Figure 1 shows the endurance test (a) and the cumulative distribution function of this dataset (b).

a) b)

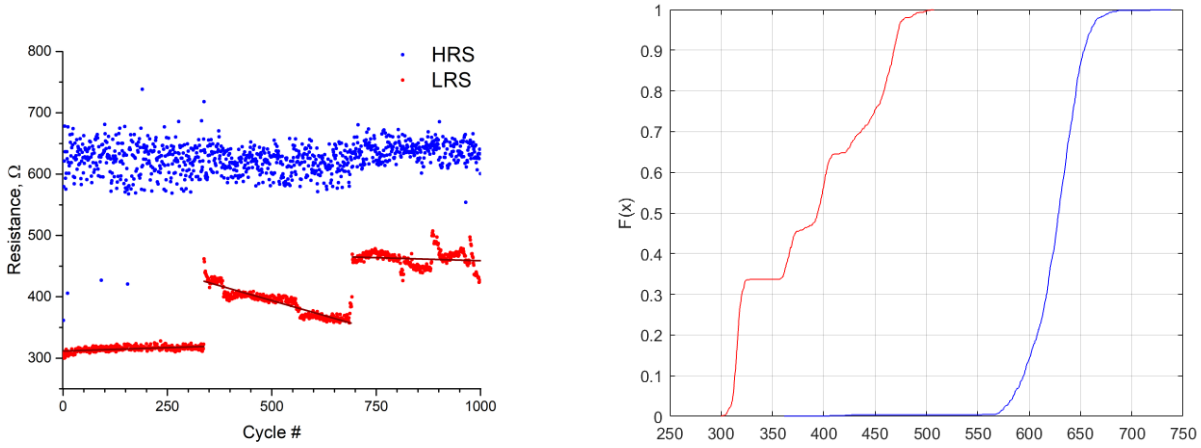

Figure1. Endurance measurement (a) and cumulative distribution function (b) of the vanadium oxide test structure.

The thickness of the vanadium oxide films didn't exceed 100 nm. Electrical measurements have shown that test structures can achieve stable switching for up to 10 thousand cycles. In this case, the U_{on} and U_{off} voltages do not exceed 1.2 V in absolute value, and the U_{read} voltage is less than 0.1 V. At the same time, the samples demonstrate several low resistance states. This makes it possible to use vanadium oxide in neuromorphic architectures for the implementation of multi-state elements. The study was conducted on the equipment of the Research and Education Centre "Nanotechnology", Southern Federal University. The reported study was funded by the Russian Foundation for Basic Research, project number 19-29-03041 mk, and partially supported by Grant of the President of the Russian Federation MK-6252.2021.4.

1. O.A. Ageev and B.G. Konoplev (Eds.). *Nanotechnology in Microlectronics.* Nauka, Moscow, 2019.
2. K. Moon et al. "RRAM-based synapse devices for neuromorphic systems". Faraday Discussions, **213**, pp. 421-451, 2019.
3. J.G. Yoon. "A New Approach to the Fabrication of Memristive Neuromorphic Devices: Compositionally Graded Films". Materials, **13**(17), 3680, 2020.
4. M. Darwish Mahmoud. "Memristive behaviour in vanadium dioxide elements: simulation and modelling". Tavaszi Szél–Spring Wind, **22**.
5. C. Sung, H. Hwang and I. K. Yoo. "Perspective: A review on memristive hardware for neuromorphic computation". J. Applied. Phys., **124**(15), 151903, 2018.

On uniformity of PLD-grown films

D. Khakhulin[1], Z. Vakulov[2], O. Ageev[3]

1. Research Laboratory of Functional Nanomaterials Technology, Southern Federal University, Taganrog, Russia, dhahulin@sfedu.ru

2. Federal Research Centre The Southern Scientific Centre of the Russian Academy of Sciences, Rostov-on-Don, Russia, vakulov@ssc-ras.ru

3. Research and Education Centre 'Nanotechnologies', Southern Federal University, Taganrog, Russia, ageev@sfedu.ru

To guarantee stability and reproducibility of parameters of a ReRAM device, it is necessary to ensure the uniformity of electrical and physical properties of the active layer material [1-3]. When depositing memristive films by the PLD method, there is an issue of intensive depletion of the target material (Fig. 1 (a)) due to the uneven distribution of pulses over the target surface (Fig. 1 (b)). This leads to so-called "flip-over effect" and high non-uniformity of the film thickness. Our model allows us to estimate the density of pulses on the target surface for the Neocera Pioneer 180 PLD module (Neocera LCC, USA) of NANOFAB NTK-9 nanotechnological complex (NT-MDT, Russia) depending on various technological parameters. This, in turn, allows us to propose a target-scanning algorithm, which provides higher uniformity evaporation of the target material (Fig. 1 (c)) and, at the same time, ensures the thickness uniformity of the resulting film (Fig. 1 (d)). The study was conducted on the equipment of the Research and Education Centre "Nanotechnology", Southern Federal University. The reported study was funded by the Russian Foundation for Basic Research project number 19-38-60052.

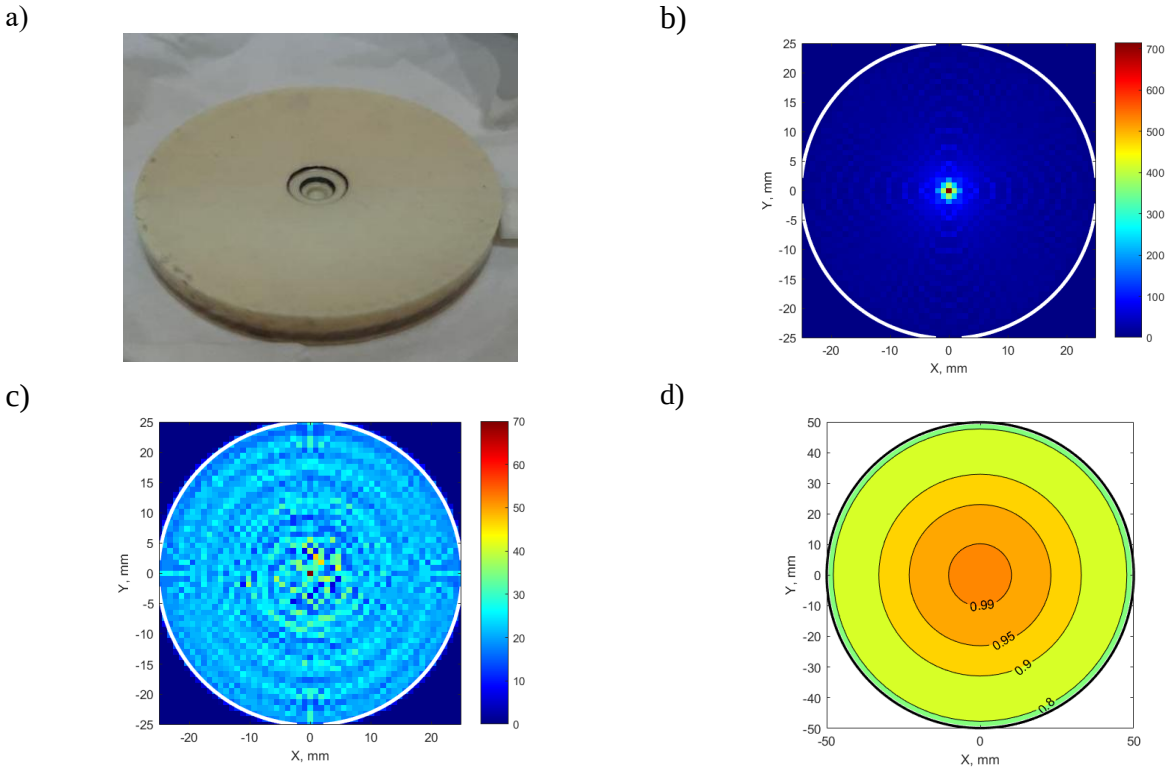

Figure 1. Target depletion (a), laser pulses density -standard case (b), optimized pulses (c), resulting relative thickness (d).

1. O.A. Ageev and B.G. Konoplev (Eds.). *Nanotechnology in Microlectronics.* Nauka, Moscow, 2019.

2. M. A. Zidan, J. P. Strachan and W. D. Lu. "The future of electronics based on memristive systems". Nature Electronics, **1**(1), pp. 22–29, 2018.

3. C. Sung, H. Hwang and I. K. Yoo. "Perspective: A review on memristive hardware for neuromorphic computation". J. Appl. Phys., **124**(15), 151903, 2018.

Formation of nanocrystalline $BaTiO_3$ thin films by pulsed laser deposition

Z. Vakulov[1], K. Korzun[2], R. Tominov[3], V.A. Smirnov[3], O.A. Ageev[3]
1. Federal Research Centre The Southern Scientific Centre of the Russian Academy of Sciences (SSC RAS), Russia, vakulov@ssc-ras.ru
2. Eindhoven University of Technology, Eindhoven, Netherlands, k.korzun@tue.nl
3. Research and Education Center "Nanotechnology" of Southern Federal University, Russia, ageev@sfedu.ru

Barium titanate ($BaTiO_3$) is one of the most promising materials for the manufacture of nanoelectronic devices, such as non-volatile memory elements [1], thin-film MEMS [2], and energy harvesters [3]. These devices require high-quality films with a smooth surface. Various technological techniques can be used to form nanocrystalline $BaTiO_3$ thin films: molecular beam epitaxy, rf sputtering, MOCVD, sol-gel, and pulsed laser deposition (PLD). The PLD method is widely used for multicomponent oxides thin films fabrication since it allows the formation of complex stoichiometric oxides thin films in a reactive atmosphere. However, since $BaTiO_3$ is a multicomponent oxide, the parameters of the films (crystallographic orientation, resistance, concentration and mobility of charge carriers, optical and piezoelectric properties, and surface roughness) depend on the composition and structure of the film, which in turn depends on the synthesis conditions [4-6]. Thus, the purpose of the work is to study the effect of the substrate temperature under PLD on the nanocrystalline $BaTiO_3$ thin films parameters. Nanocrystalline $BaTiO_3$ thin films were formed by PLD using a Pioneer 180 module (Neocera Co., USA) of the NANOFAB NTK-9 cluster nanotechnological platform (NT-MDT, Russia). The number of pulses was constant and amounted to 50 000 at a laser pulse repetition rate of 10 Hz. Films were obtained at a temperature of 300 °C÷600 °C on Si substrates. It was established that with an increase in the substrate temperature from 300 °C to 600 °C, the thickness of the nanocrystalline $BaTiO_3$ thin films decreasing from 101.4±8.1 nm to 78.1±5.9 nm, which may be directly linked to the re-deposition process and reactive diffusion in the films. At the same time, the surface roughness and average grain diameter of the films decreased from 6.1±0.5 nm to 1.2±0.1 nm and from 212.3±13.2 nm to 39.1±2.2 nm, respectively. This effect can be associated with an increase in the energy of condensed particles on the substrate surface [7]. In addition, an increase in the substrate temperature from 300 °C to 600 °C leads to an increase in the concentration of charge carriers in the $BaTiO_3$ films by a factor of 1.5 (from 1.9×10^{13} cm^{-3} to 2.8×10^{13} cm^{-3}) and a change in charge carrier mobility from 7.2 $cm^2/(V\cdot s)$ to 10.1 $cm^2/(V\cdot s)$. Obtained results make it possible to fabricate nanocrystalline $BaTiO_3$ films with controlled parameters, which can be used for promising lead-free energy harvesters of "green" energy devices. The reported study was funded by the Russian Foundation for Basic Research, projects numbers 19-38-60052, 18-29-11019 mk, and 19-29-03041 mk, and partially supported by Grant of the President of the Russian Federation MK-6252.2021.4. The work was done on the equipment of the Research and Education Centre "Nanotechnology", Southern Federal University.

1. V.A. Smirnov, R.V. Tominov, V.I. Avilov, N.I. Alyabieva, Z.E. Vakulov, E.G. Zamburg, D.A. Khakhulin, and O.A. Ageev. "Investigation into the Memristor Effect in Nanocrystalline ZnO Films". Semiconductors, **53**, pp. 72-77, 2019.
2. T. Harigai, Y. Tanaka, H. Adachi, and E. Fujii. "Piezoelectric properties of lead-free (Na, Bi)TiO_3–$BaTiO_3$ (001) epitaxial thin films around the morphotropic phase boundary". Appl. Phys. Express, **3**, pp. 111501.
3. G. Suo, Y. Yu, Z. Zhang, S. Wang, P. Zhao, J. Li, and X. Wang. "Piezoelectric and triboelectric dual effects in mechanical-energy harvesting using $BaTiO_3$/polydimethylsiloxane composite film". ACS Appl. Mater. Interfaces, **3**, pp. 34335-34341, 2016.
4. O.A. Ageev and B.G. Konoplev (Eds.). *Nanotechnology in Microlectronics*. Nauka, Moscow, 2019.
5. J. Gonzalo, R.G. San Román, J. Perriere, C.N. Afonso, and R.P. Casero. "Pressure effects during pulsed-laser deposition of barium titanate thin films". Appl. Phys. A, **66**, pp. 487-491, 1998.
6. A.Y. Fasasi, M. Maaza, E.G. Rohwer, D. Knoessen, C. Theron, A. Leitch, and U. Buttner. "Effect of Zn-doping on the structural and optical properties of $BaTiO_3$ thin films grown by pulsed laser deposition". Thin Solid Films, **516**, pp. 6226-6232, 2008.
7. M. Liu, X.Q. Wei, Z.G. Zhang, G. Sun, C.S. Chen, C.S. Xue, H.Z. Zhuang, and B.Y. Man. "Effect of temperature on pulsed laser deposition of ZnO films". Appl. Surf. Sci., **252**, pp. 4321-4326, 2006.

Reasons for the weak manifestation of the field effect in metal-$Ba_{1-x}Sr_xTiO_3$-Si structures

D.A. Belorusov, E.I. Goldman, G.V. Chucheva
Fryazino Branch of the Kotelnikov Institute of Radioengineering and Electronics of Russian Academy of Science, Fryazino, Russia. E-mail: gvc@ms.ire.mssi.ru

Solid solutions of barium-strontium titanate ($Ba_{1-x}Sr_xTiO_3$ or BST) have ferroelectric properties above the room temperature, and their dielectric constant remains sufficiently high in the paraelectric phase. Despite lengthy (several decades) studies, there are still no reports of operating conducting surface channels of minority charge carriers in Si in structures based on these ferroelectrics. In this work, on the basis of a developed one-dimensional model of the high-frequency (HF) impedance of Ni-BST-Si objects with an insulator in the paraelectric phase, the reason for the weak manifestation of the field effect is revealed and ways of its elimination are discussed. Let $C_{SE}(V_{SE})$ be the RF capacitance voltage characteristic of the metal-BST-metal structure with exactly the same ferroelectric layer as in Ni-BST-Si. Then from the RF impedance model follows the inequality:

$$\left\{\left[1-\frac{\left(C+\frac{\sigma^2}{\omega^2 C}\right)}{C_s}\right]\left[\frac{\left(C+\frac{\sigma^2}{\omega^2 C}\right)}{C_{SE}}+\frac{\left(C+\frac{\sigma^2}{\omega^2 C}\right)}{C_s}-1\right]\right\}^{1/2} < \frac{\sigma}{\omega C}, \qquad (1)$$

where C and σ are the high-frequency capacitance and the conductivity of the Ni-BST-Si sample, is ω the cyclic frequency of the high-frequency signal, C_s is the capacity of the charged layer in Si. In Figures 1 and 2 show characteristics, respectively, of the structures Ni-$Ba_{0.8}Sr_{0.2}TiO_3$-Si and Ni-$Ba_{0.8}Sr_{0.2}TiO_3$-Pt with an insulator thickness of 350 nm, measured at 1 MHz and 121°C.

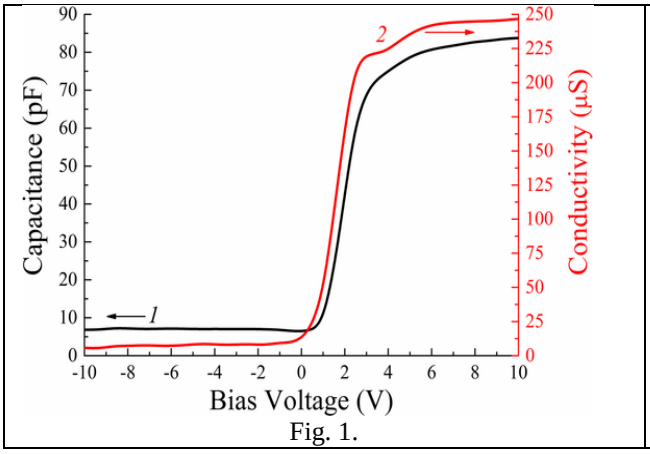

Fig. 1.

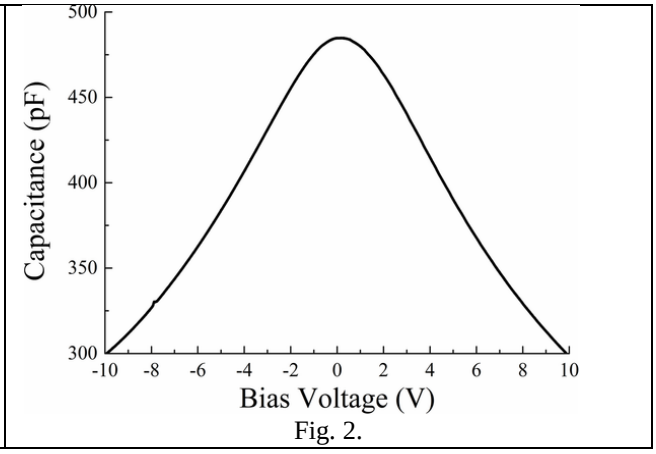

Fig. 2.

Under experimental conditions $C_{SE} >> C$ and $\sigma/\omega C << 1$, therefore, inequality (1) follows $C \approx C_S$. The capacity of a semiconductor in the flat band state is C_{sfb} = 9.17 pF; therefore, the band bending in Si is significantly limited: less than 0.033 V at depletion and 0.165 V at enrichment. Thus, the overwhelming part of the external voltage drops across the insulator; almost complete screening of the polarization of the ferroelectric gap in the metal-BST-Si structure occurs due to the recharging of surface electron traps in the interphase layer between BST and Si. Based on the range of changes in external voltage, their concentration should be at least 10^{14} cm^{-2}. To eliminate the activity of traps in the interfacial layer, it is natural to use the experience gained in planar silicon technology on the passivation of surface localized electronic states. The termination of the recharging of centers in the interfacial layer will make it possible to create transistors based on metal-BST-Si with a working surface channel of minority charge carriers and will ensure the construction of high-quality cells of non-volatile memory FeRAM.

The work was carried out within the framework of the state task and partially supported by the Russian Foundation for Basic Research (projects No. 18-29-11029, No. 19-29-03042).

The temperature dependence of the local piezoresponse and the surface potential in the $Ba_{1-x}Sr_xTiO_3$ ferroelectric thin film

D.A. Kiselev[1,2], M.S. Afanasiev[1], G.V. Chucheva[1]

1. Fryazino branch of the Kotel'nikov Institute of Radioengineering and Electronics of Russian Academy of Sciences, Vvedensky Square 1, Moscow region, 141190 Fryazino, Russia

2. National University of Science and Technology "MISiS", Leninskiy pr. 4, 119049 Moscow, Russia

(dm.kiselev@gmail.com)

Barium strontium titanate (BST), with Sr stoichiometry lower than 0.3, is a lead-free ferroelectric material which dielectric permittivity can be significantly tuned via an applied dc electric field. Recent results show that BST heterostructures display high dielectric tenability with minimal temperature dependence from −10 to 90 °C [1]. For the development of the nanotechnology, the knowledge of local electrical properties becomes essential. To get such information, nondestructive scanning probe microscopy is a quite powerful technique to use because it does not require external electrical contacts and lithographic steps. Here we report measurements of temperature dependence of piezoresponse (or polarization) and surface potential at nanoscale of BST film across the phase transition. The $Ba_{0.8}Sr_{0.2}TiO_3$ film of 100 nm thickness was grow on (111)Pt/Ti/SiO_2/Si substrate using by high-frequency sputtering of the polycrystalline target in an oxygen atmosphere using an installation Plasma-50SE (Russia). Nanoscale studies were carried out on an Asylum Research MFP-3D atomic force microscope with the integrated temperature control. A heater is used to heat the sample from 25 ºC to 250 ºC with accuracy of 0.1 ºC. We use a range of scanning probe techniques, namely, the piezoresponse force microscopy (PFM) and the Kelvin probe force microscopy (KPFM). PFM hysteresis loops were collected in the DART (dual a.c. resonance tracking) mode with triangle pulse waveforms applied to the tip. The local surface potential is mapped using KPFM. The resulting surface potential distribution was characterized by KPFM in air, wherein the surface potential corresponds to the contact potential difference (CPD) between the tip and the film. The temperature dependence of the PFM amplitude and the surface potential are shown in the Figure 1.

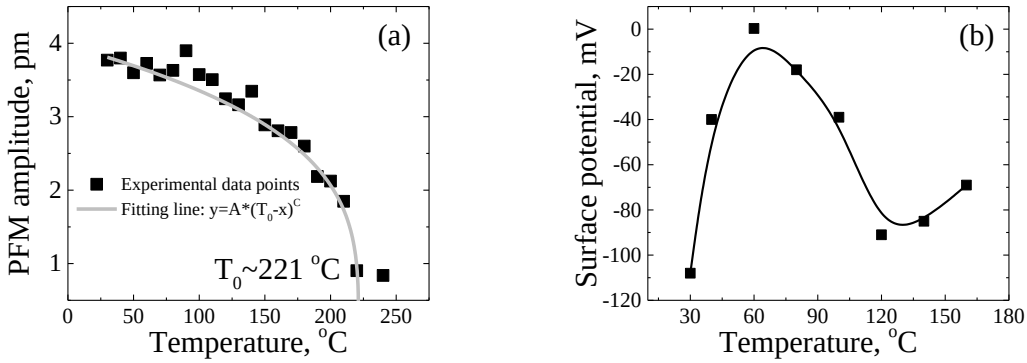

Figure 1. The temperature dependence of the PFM amplitude obtained from PFM hysteresis loops (a) and the surface potential signal (b).

It can be seen, that the PFM amplitude decreases monotonically with increasing temperature and has a minimum value at 221 ºC. In contrast, the surface potential signal takes a minimum values at ~60 ºC, and we associate it with the phase transition temperature, which is typical for the $Ba_{0.8}Sr_{0.2}TiO_3$ composition [2]. The paper discusses the possible mechanisms of different behavior of PFM signal and surface potential depending on temperature.

This work was carried out as part of a state assignment and was partially supported by the Russian Foundation for Basic Research (projects 18-29-11029 and 19-29-03042).

1. S. Zhong, S.P. Alpay, M.W. Cole, E. Ngo, S. Hirsch and J. D. Demaree "Highly tunable and temperature insensitive multilayer barium strontium titanate films" Appl. Phys. Lett., **90**, p. 092901, 2007.

2. S.A. Gridnev and I.I. Popov "Kinetics of phase transformation at the Curie point of ferroelectric ceramic $Ba_{0.8}Sr_{0.2}TiO_3$" Ferroelectrics, **561**, pp. 127-134, 2020.

Chemical solution deposition of $BiFeO_3$ films with layer-by-layer control of the coverage and composition

V. Safina[1], A. Abramov[1], A. Sobol[2], V. Slabov[3], L. Trusov[2],
A. Vasiliev[2], V. Shur[1], A. Kholkin[1,3], D. Alikin[1]

1. School of Natural Sciences and Mathematics, Ural Federal University, Ekaterinburg, Russia, 620000.
2. Faculty of Chemistry, Moscow State University, Moscow, Russia, 119991.
3. Department of Physics & CICECO—Aveiro Institute of Materials, University of Aveiro, Aveiro, Portugal.

$BiFeO_3$ is a unique multiferroic material with high spontaneous polarization and anti-ferromagnetic properties at room temperature [1, 2]. The coexistence of these properties allows to consider it in the applications to the different ferroelectric memory devices with combined electric-magnetic writing/readout and in the sensors and actuators compatible to the micro- and nanoelectronics. The most expensive part of the technological processing of the $BiFeO_3$ films is epitaxial growth demanding specific equipment and challenging to scale properties uniformly.

The chemical solution deposition makes it possible to cover large-scale wafers with thickness from a few to few hundred nanometers. To achieve the films with thicknesses larger than 100 nm, the layer-by-layer deposition method is usually used. It makes possible to increase the thickness of the film and keep the stoichiometry of the initial solution, which excludes aggregation of reagents in the initial solution. Nevertheless, the surface coverage and microstructure of the films are often imperfect. As a result, the pores and micro-breaks can act as leakage channels in the material.

In our work, we study the role of the deposition and gelation steps of the sol-gel process to the quality of the films' microstructure and leakage current in the material. The local approach based on the piezoresponse force and conductive atomic force microscopies combination was used to evaluate the functional properties of $BiFeO_3$ thin films obtained by layer-by-layer deposition. The morphology, distribution of local piezoelectric properties, and leakage current were analyzed depending on the number of deposited film layers. It was found that the final properties of the obtained thin films are determined not only by the heat-treatment conditions at the crystallization stage but also by the morphology of the film formed at the gelation stage. The film coverage quality was demonstrated to strongly affect further crystallization kinetics, the final morphology of the films, and their electromechanical properties.

The investigations were made possible by the Russian Science Foundation (grant 19-72-10076). The equipment of the Ural Center for Shared Use "Modern nanotechnology" UrFU was used.

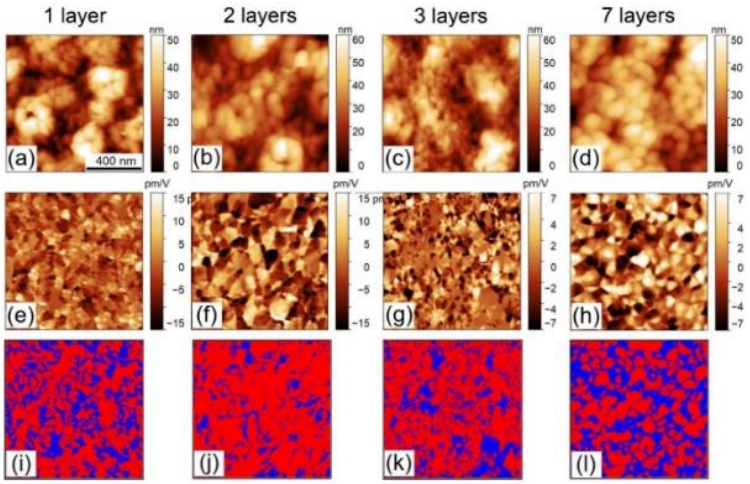

Figure 1 – (a)-(d) Topography, (e)-(h) piezoelectric response and (i)-(l) distribution of the polar (red)/non-polar (blue) phase in polycrystalline $BiFeO_3$ films obtained by the sol-gel method with the various number of the layers.

1. G. Catalan, J.F. Scott. "Physics and Applications of Bismuth Ferrite". Advanced Materials, **21**, pp. 2463-2485, 2009.
2. S. Fujino, M. Murakami, V. Anbusathaiah. "Combinatorial discovery of a lead-free morphotropic phase boundary in a thin-film piezoelectric perovskite". Applied Physics Letters, **92**, pp. 202904, 2008.

Specific of magneto-optical response of nanostructures with various shapes and sizes for magnetic memory elaboration

A.V. Prokaznikov[1], V.A. Paporkov[2], V.A. Chirikov[2]
1. Yaroslavl Branch of the Institute of Physics and Technology, RAS, Universitetskaya, 21 Yaroslavl, 150007, Russia
2. Yaroslavl Demidov State University, Sovetskaya, 14 Yaroslavl, 150000, Russia
E-mail: prokaznikov@mail.ru

In the present time a great interest is paid to the magnetic memory elaboration, which is based on topological specific of magnetic structures. It makes possible to decrease sufficiently the size of magnetic objects that possess an elementary bit of information as well as to increase a speed of operations writing/reading. All these facts testify to a prospect of further investigations and elaborations in the region of creation, transition, storage and transformation of the structures on the base of non-trivial compact magnetic configurations.

In the present investigations the results of studying of regularities of magneto-optical response are presented from the structures with different forms and sizes. These investigations are based on experimental data and computer simulations. The results of investigations have demonstrated that some peculiarities take place in behavior of magneto-optical hysteresis loops by the presence of magnetic vortices (Fig. 1) as well as in the form of hysteresis by magnetization reversal. It was discovered that the form of magnetic hysteresis corresponds to the energy minimization for a system by magnetization reversal.

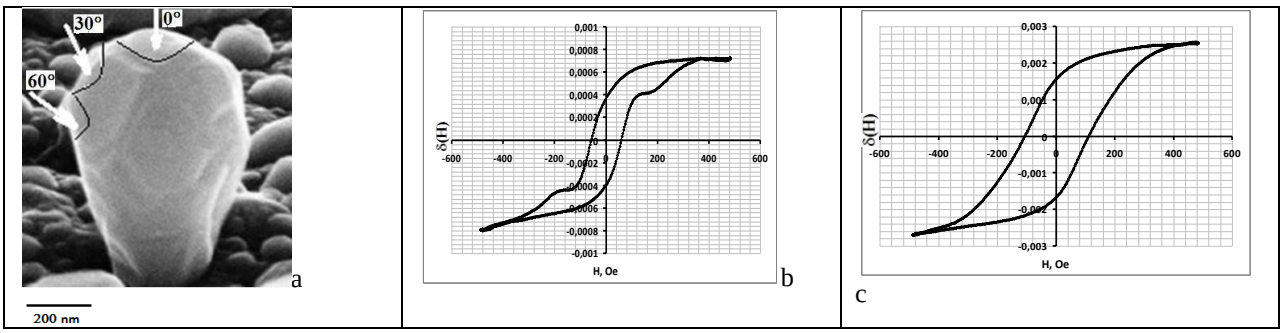

Figure 1. Typical PbSe structure with 30 nm thick cobalt film. The white arrows show the angles 0°, 30°, 60°, the arcs, conventionally, depict the available areas with different curvatures for the electromagnetic radiation incident at an appropriate angle with a wavelength of 633 nm. – (a). Magneto-optical hysteresis loops in TMOKE configuration, measured at angles: 52.5° – (b), 65° – (c) for Co film thickness – 10 nm.

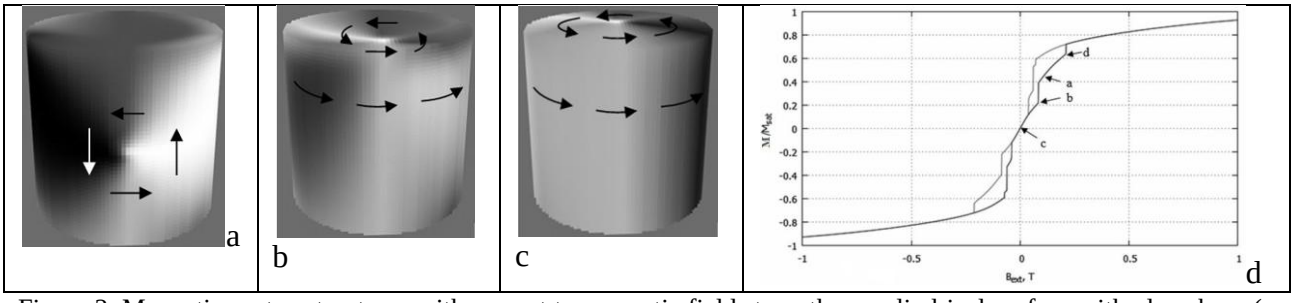

Figure 2. Magnetic vortex structures with respect to magnetic field strength on cylindrical surface with plane base (a-c) without magnetic anisotropy; corresponding hysteresis loop (d).

It was demonstrated by means of computer simulations that magnetic vortex position on a cylindrical metallic surface is controlled by magnetic field strength (Fig. 2). The position of a vortex depends on parameters of a system that are determined by technological features of manufacturing of the nanostructure. The facts mentioned above allow to formulate requirements to technology of manufacturing of the structures for realization of compact memory on magnetic vortices.

Nanoscale field sensor with adjustable operating temperature for biosensor applications

A.A. Skorik[1,2], I.V. Bozhev[1,2], I.I. Tsiniaikin[1,2], G.V. Presnova[3], M.Yu. Rubtsova[3], V.A. Krupenin[1,2], D.E. Presnov[1,2,4]

1. Faculty of Physics, Moscow State University, 119991 Moscow, Russia, skorik.aa17@physics.msu.ru
2. MSU Quantum Technology Centre, Moscow, 119991, Russia, bozhjev.ivan@physics.msu.ru
3. Faculty of Chemistry, Moscow State University, 119991 Moscow, Russia, gpresnova@gmail.com.
4. Nuclear Physics Institute, Moscow State University, 119991 Moscow, Russia, denis.presnov@physics.msu.ru

One of the most promising devices for various diseases diagnosing is a biosensor based on field-effect transistors with a nanowire (NW) channel. The advantage of such device is their high sensitivity due to the high ratio of the NW surface area to its volume. Sensors based on field-effect transistors do not need the additional labels for registration, allow quick and real-time measurements. Also the state of the art allows easily integrate such sensors in complex diagnostic devices [1, 2]. Some applications require a specific temperature regime to achieve optimal biosensor performance. In the case of a DNA sensor, rising up the operating temperature of the system to the value at which DNA hybridization starts, will increase the specificity and avoid false positive results, as well as shorten the analysis time dramatically. An accurate temperature control technique which allow set up sensor at 85-90 °C will allow the complete removal of the analyte from its surface and use it many times.

For the fabrication of the experimental structures, we use a silicon-on-insulator (SOI) material with a top Si layer of 110 nm thick. Sensing element (Si NW channel of 110 nm wide and 4 μm long), was formed using “top-down” approach. It is based on reactive ion etching of the upper SOI layer through a mask formed by electron beam lithography [2]. For precise control of analyte temperature, a thermometers based on thermoresistive metallic strips (10 μm wide and 100 μm long) were located very close to the sensitive element of the sensor system. The heating elements were formed near the edge of the chip. Both thermometers and heaters were covered by a dielectric layer to isolate them from contact with a testing liquid. The fabrication of thermostatic elements was performed simultaneously with the titanium contact pads of the sensor [2], and did require additional technological steps.

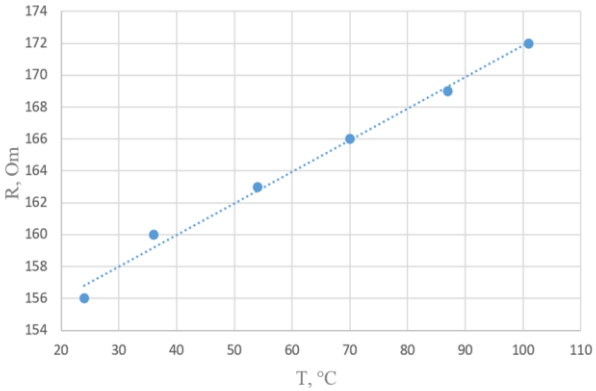

The calibration of the thermoresistive sensors was done using external calibrated heating oven and shows linear dependence of the resistance on temperature (0.2 Ohm per 1 °C). Linear temperature dependences on the power applied to the heaters located on the chip was also demonstrated (the accuracy of setting the temperature – 2 °C). We also developed the second method of heating using commercially available heating element located on the back of the chip holder. The power required to reach a biosystem temperature of 100 °C has been determined. For on-chip heaters P_1 = 0.19 W, for an external heater P_2 = 0.22 W. The developed method allows accurate setting the temperature of the biosensor system in the range of 20-120 °C.

This research was performed according to the Development program of the Interdisciplinary Scientific and Educational School of Lomonosov Moscow State University «Photonic and quantum technologies. Digital medicine».

1. G.V. Presnova, I.I. Tcinyaykin, I.V. Bozhev., M.Yu. Rubtsova, V.V. Shorokhov, A.S. Trifonov, M.M. Ulyashova, V.A. Krupenin, D.E. Presnov, "Thyroglobulin detection by biosensor based on two independent Si NW FETs". Proceedings of SPIE, **11022**, p. 110220Z, 2019.
2. I.I. Tsiniaikin, G.V. Presnova, I.V. Bozhev, A.A. Skorik, M.Yu. Rubtsova, A.A. Kamalov, S.T. Matskeplishvili, O.V. Snigirev, V.A. Krupenin, D.E. Presnov, "A Sensor System Based on a Field-Effect Transistor with a Nanowire Channel for the Quantitative Determination of Thyroid-Stimulating Hormone", Moscow University Physics Bulletin, **75**(6), pp. 645–656, 2020.

Features of the formation of highly sensitive nanoscale films SnO_2 doped with platinum for sensing applications

K.A. Tsarik, V.A. Petukhov, N.S. Struchkov
National Research University of Electronic Technology, Moscow, Russia, tsarik_kostya@mail.ru

Chemical gas sensors based on tin oxide attract the attention of researchers due to the possibility of detecting flammable and explosive [1], toxic and harmful gases in the air, as well as volatile organic compounds emitted by humans [2]. This is due to the fact that reversible chemisorption of active gases on their surface is accompanied by reversible changes in conductivity [3]. An important problem that complicates the use of semiconductor oxide sensors is low selectivity in the analysis of gas mixtures and insufficient stability during operation under real conditions. The processes occurring on the surface of tin oxide under the action of active gases remain unclear, and the relationship between the surface structure and the sensitivity of sensors has not been established. Therefore, studies of methods for increasing the sensitivity of a nanostructure by doping and changing the stoichiometry in the oxide structure and their relationship with electrical and gas-sensitive properties are relevant.

In this work, a technique was developed for the formation of a highly sensitive Pt:SnO_2 layer with a thickness of 100 nm. A silicon chip with Pt contacts on a thick SiO_2 film was created by photolithography. The chip had 40 contact pads with extended microstripes. Between a pair of them there was an area for applying a sensitive layer of 50x40000 μm^2, for subsequent measurement of its electrophysical characteristics. To create the film, magnetron sputtering was used from an Sn target with a purity of 99.999% with a high purity Pt insert. The amount of platinum was chosen for doping the SnO2 film by 3%. The dependence of the rate of deposition of Pt:SnO_x on the surface of silicon oxide on the ratio of the mixture argon: oxygen (Ar: O_2) was investigated. The deposition was carried out through a lithographic mask at a pressure of 0.5 Pa and a speed of 1.3 nm/min.

The resulting films were investigated by atomic force microscopy (AFM) and X-ray diffraction (XRD). The electrical characteristics were studied using a Keithley 2450 source-meter. The obtained measurement results showed the need for additional oxidation of the resulting film. Annealing of samples with oxide films was carried out in dry air at a temperature of 600 °C for 4 hours. After the performed annealing, the films were again investigated by the above methods. The film has a granular surface with crystallite sizes less than 100 nm. Taking into account the influence of adsorption processes on the electrophysical properties of the obtained structures, all measurements were carried out in a dry air atmosphere using a blown-through measuring cell with the possibility of heating up to 350 °C.

The temperature dependences of the conductivity of the films between the contacts are obtained. The electrical properties of the films are investigated when gas, small doses of ammonia, ethanol and acetone were fed into the measuring volume. As a result, at fluxes of 20 ppm, the ratio of the detection resistance to the resistance in clean air R_{sens}/R_{air} for the detection of ammonia is about 0.6, for ethanol is about 0.5, and for acetone is about 0.6. The results show a high sensitivity of the sensor structure. Due to the thin film thickness, the recovery time was extremely short after detecting the presence of gases in the air.

This work was carried out with the financial assistance of the Ministry of Education and Science in the framework of state task FSMR-2020-0017.

1. Yin, X. T., Zhou, et al. “A highly sensitivity and selectivity Pt-SnO_2 nanoparticles for sensing applications at extremely low level hydrogen gas detection”, Journal of alloys and compounds, **805**, pp. 229-236, 2019.
2. Khatoon, Zeenat, et al. "Doped SnO_2 nanomaterials for e-nose based electrochemical sensing of biomarkers of lung cancer", ACS omega, **5** (42), pp. 27645-27654, 2020.
3. Al-Hashem, M., Akbar, S., & Morris, P. “Role of oxygen vacancies in nanostructured metal-oxide gas sensors: a review”. Sensors and Actuators B: Chemical, **301**, p. 126845, 2019.

Nanochannels based on graphene formed by ion etching to develop array-based gas sensors

A.V. Lashkov, N.V. Yakunina, A.V. Romashkin, K.A. Tsarik
National Research University of Electronic Technology, Moscow, Russia; lav.lab-sm.sstu@rambler.ru

Recently, it has been possible to form highly sensitive gas sensors based on modified graphene. One of the types of modifications is the formation of nanoscale channels [1]. One of the ways to implement them is ion beam etching [2]. Channel width <10 nm is critical to provide high sensitivity [3]. In this work, the necessary doses of Ga^+ FIB (30 pA, 30 kV) were found to etch graphene located in gaps (L_G 50 μm) between pairs of metal contacts (in the amount of 39). Graphene was etched off faster than silicon oxide, in contrast to CNTs [4]. Three types of structures were formed: a) short-ribbons (L_S 1 μm); b) long-ribbons (L_L 15 μm); c) graphene electrodes with nanogap ~50 nm, coated by polyaniline (PANi). With increasing the length of the ribbons (struct. B), despite of their width (about 30-40 nm by AFM (Fig. 1a)), an increase in resistance by two orders of magnitude is observed (in comparison with struct. A (Fig. 1b)), which cannot be explained without considering the features of etching and the concentration of initial and formed defects (the formation of which also occurs during etching), as well as the emergence of field control of the channel, which can be explained by the defects occurring with a long tape length and forming a significant part of the channel length with altered properties and effective width. Another factor influencing this effect is the defocusing of the beam during etching of a large array of lines, which can be used to form sensitive structures (width <10nm, according to Raman spectra, Fig. 1d [1]) without using high-cost high-resolution lithography or He^+ FIB etching. Also high conductivity (six orders higher of macroscopic values for non-doped PANi [5]) for structures of nanogap with PANi were found, which can be used as selective gas sensing structures.

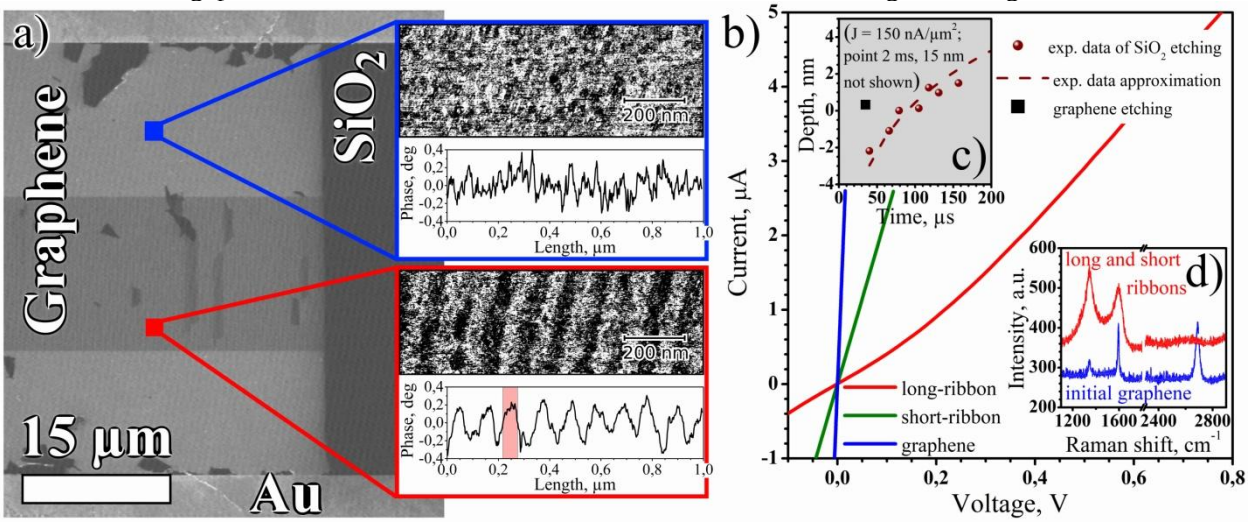

Figure 1. Dimensions of structure B (a). I -V characteristic (b). Depth versus etching time (c). Raman data (d)

The reported study was funded by RFBR, project number 19-38-60034.

1. M. Mehdi Pour, A. Lashkov, A. Radocea et al. "Laterally extended atomically precise graphene nanoribbons with improved electrical conductivity for efficient gas sensing". Nat. Commun., **8**, 820, 2017.
3. X. Li, X. Wang, L. Zhang et al. "Chemically derived, ultrasmooth graphene nanoribbon semiconductors". Science, **319**, pp. 1229-1232, 2008.
2. A. N. Abbas et al. "Patterning, characterization, and chemical sensing applications of graphene nanoribbon arrays down to 5 nm using helium ion beam lithography". ACS Nano, **8** (2), pp. 1538-1546, 2014.
4. A. V. Emelianov, A. V. Romashkin, K. A. Tsarik et al. "On the high charge-carrier mobility in polyaniline molecular channels in nanogaps between carbon nanotubes". Semiconductors, **51**, pp. 488–491, 2017.
5. A. V. Romashkin, A. V. Emelianov, K. A. Tsarik, I. I. Bobrinetskiy. "Deposition of polymers on structures with nano-gaps fabricated between carbon nanotubes by focused ion beam etching". Proceedings SPIE, International Conference on Micro- and Nano-Electronics, 10224, 102241R, Zvenigorod, 2016.

Spray-coated carbon nanotube network onto metal microwires to form selective gas-sensitive structures with fast response to ammonia

A.V. Romashkin, D.D. Levin, E.V. Alexandrov, V.K. Nevolin
National Research University of Electronic Technology, Moscow, Russia; romaleval@gmail.com

Recently, ppb-level sensitivity of structures based on functionalized carbon nanotubes (CNTs) to ammonia was achieved; however, despite the high sensitivity, the problem of the selectivity of sensor response, even with respect to humidity, remains [1]. It was possible to achieve some difference in the response due to the use of metal clusters together with low density CNT network [2]. The use of metallic microwires, in contrast to clusters, makes it possible to more controllable form structures with CNT-Me contacts and to study the share of changes in contact resistance during the sorption of various gases to overall sensor response. In the present work Pt/Cr microwires were used (thickness 30 nm, width ~ 2 μm, gap 18 μm, 100 microwires in channel), obtained by a laser maskless lift-off lithography and oriented perpendicular to the current direction, on top of which CNTs were spray deposited by own-design equipment. Structures with many contacts of individual CNTs with metal (structure A) were formed and, as in the previous results [3], even in spite of the small Me thickness, an uneven CNT distribution over the surface was observed: a decrease in the CNT network density near Me (Fig. 1a), that increase resistance of sample (Rs ~ 67.5 MOhm/□ compared with Rs~16.3 MOhm/□ for reference structure B without Me microwires, obtained in one process with the same average CNT network density). Also structure C with higher CNT network density without Me microwires (Rs ~0.3 MOhm/□) was used as reference sample in sensor response measurements. Sensor responses to water and NH_3 vapors were measured, which showed a higher rate of NH_3 and water desorption in the case of the CNT-Me structure (in 60 s after the gas supply off 8.8 %/min for CNT-Me, and 2.2 %/min for a pure CNTs of str. C, Fig. 1b), as well as some improvement in the response of the of CNT-Me Schottky contacts (relative to CNT-CNT contacts, the CNTs themselves) to NH_3 relative to H_2O (ratio of response on NH_3 (200 ppm) to response on humidity 80 % for str. A is 0.84, but for str. B is only 0.6). This effect is very interesting since the share of CNT network near Me microwire (distance from Me ~0.5 μm) is not more than 5 % of total CNT network, but increasing response (relatively to pure CNT) is 155 %, which indicates that the share of the changes in CNT-Me contacts to the overall sensor response is quite large. Higher desorption rate (>4 times) at the initial stage and the same rate as for pure CNT in the final stage also is due to small share of near-Me regions of str. A and also probably is due to lower CNT network density of str. A relative to str. C.

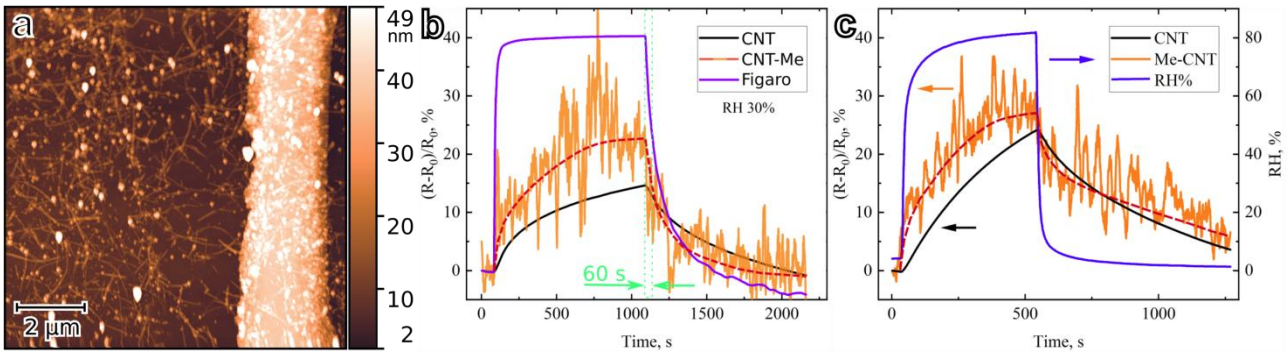

Fig. 1. AFM image of CNT network near Me microwire (a), sensor response on 200 ppm NH_3 (b) and on humidity (c).

This work was carried out with the financial assistance of the Ministry of Education and Science in the framework of state task FSMR-2020-0017.

1. F. Rigoni, S. Freddi, S. Pagliara, et al. "Humidity-enhanced sub-ppm sensitivity to ammonia of covalently functionalized single-wall carbon nanotube bundle layers". Nanotechnology, **28** (25), p. 255502, 2017.
2. A. Abdelhalim, et al. "Highly sensitive and selective carbon nanotube-based gas sensor arrays functionalized with different metallic nanoparticles" Sens. Actuator B-Chem. **220**, pp. 1288-1296, 2015
3. Y. A. Polikarpov, A. V. Romashkin, N. S. Struchkov, et al. "High uniform carbon nanotube thin films spray deposition on substrates with patterned structures having height difference" 2019 IEEE Conference of Russian Young Researchers in Electrical and Electronic Engineering (EIConRus). pp. 1980-1985, 2019.

Gate-controlled sensing of ammonia by single-layer MoS_2 field effect transistor

N.S. Struchkov[1], N.P. Nekrasov[1], A.V. Emelianov[1], I.I. Bobrinetskii[1,2]
1. National Research University of Electronic Technology, Moscow, Russia, struchkov.nikolaj@gmail.com.
2. University of Novi Sad, Novi Sad, Serbia, bobrinet@mail.ru

Recent advances in electronic technologies and computer science give rise to the development of a new class of gas analyzing devices called e-nose. The e-nose is designed to analyze multi-component gas mixtures, which is highly promising in the field of personal medicine, ecology, and industry. However, fundamentally new sensitive materials are required to unleash e-nose potential. 2D-materials are promising candidates as they provide a unique set of characteristics including room temperature operations, high sensitivity, low dimensions and allow to design arrays of sensors integrated on a single substrate with altered selectivity. MoS_2 field-effect transistors (MoS_2-FETs) demonstrate adjustable sensitivity to toxic gases by gate voltage variation, which expands selective detection techniques and requires deep study.

We fabricated back-gated MoS_2-FETs with standard photolithography technique on Si substrate with 300 nm SiO_2 dielectric layer and CVD-grown single-layer MoS_2 flakes. FET comprises thermally spattered 60 um long parallel Au/Ti electrodes with 150/20 nm thicknesses. The channel width was determined by the size of the flakes beneath electrodes, while channel length was 1.5 μm. AFM cross-section confirmed MoS_2 to be 0,7 nm thick, which are single-layer flakes. Raman spectroscopy also confirmed the single-layer nature of MoS_2 by A_{1g} and E^1_{2g} modes positioning at 403 cm^{-1} and 383 cm^{-1}, respectively. Electrical measurements validated n-type conductivity of single-layer MoS_2-FET, though the mobility in the absence of passivation was about 10^{-1} cm^2 $V^{-1}s^{-1}$ that is inferior to top literature results [1]. Transfer characteristics are affected by humidity due to trapping states induced by water molecules on the surface. Compared to a dry condition, water adsorbate decreases I_{on}/I_{off} ratio both for gate voltage switching and after transition process by order of magnitude. We revealed asymmetry of output current-voltage characteristics presumably induced by difference in Schottky barriers at electrode/MoS_2 junction resulting in photocurrent generation. The potential barrier presumably decreases electron mobility.

MoS_2-FET exhibits room-temperature NH_3 high sensing response by decreasing the current after exposure following the interaction model of electron-donating NH_3 with an n-type semiconductor. Sensitivity was about 50% at 200 ppm NH_3 exposure with a signal-to-noise ratio of about 8 and response/recovery time of about 100 s. When we applied a negative gate voltage, the sensitivity increases up to 4 times presumably by reducing the initial number of charge carriers in MoS_2 [2]. Therefore, rapid and high responsive MoS_2-FETs were developed via traditional photolithographic technique for NH_3 molecules detection in dry and humid atmosphere.

This work is supported by Russian Science Foundation under grant No. 19-19-00401.

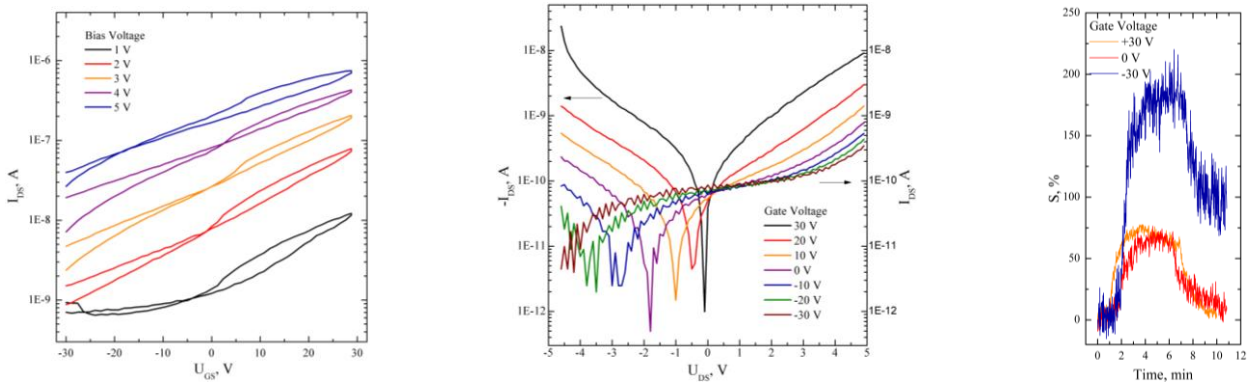

Fig.1 (a) MoS_2-FET transfer characteristic, (b) drain characteristics, (c) current response to 200 ppm of NH_3.

1. N. Huo et al. "High carrier mobility in monolayer CVD-grown MoS_2 through phonon suppression" Nanoscale, **10**, pp. 15071-15077, 2018.
2. D. J. Late et al. "Sensing behavior of atomically thin-layered MoS_2 transistors" ACS nano, **7**, pp. 4879-4891, 2013.

Nonlinear distortions in planar electrochemical transducer

D. A. Zhevnenko[1,2,3], E. S. Gornev[2,3], P. V. Dudkin[1,2], T. V. Krishtop[1], V. G. Krishtop[1,4]
1. Seismotronics LLC, Moscow, Russia
2. Moscow Institute of Physics and Technology (State University), Dolgoprudny, Russia.
3. JCS Molecular Electronics Research Institute, Zelenograd, Russia
4. Institute of Microelectronics Technology and High Purity Materials RAS, Chernogolovka, Russia.

Planar electrochemical microsystems (Fig.1.) have high perspective to design and development of motion parameters sensors. They have several main advantages over MEMS included high device lifetime and sensitivity in the low-frequency regions due to the electrochemical principle of registration [1, 2]. Nowadays, fabrication technology of planar electrochemical sensors is actively developing [3-5].

The study of nonlinear distortions is extremely important in the development and design of devices [6, 7], since the level of nonlinearities is directly related to the dynamic range of the device.

The research includes the study of key system parameters that contribute to the nonlinear distortion of the device response. The contribution was evaluated for each significant process, including electromigration, convection and temperature effects. The dependence of THD on the amplitude and height of the microchannels by electrodes is plotted. Based on that, the rate of THD change was estimated at different signal amplitudes, which allows choosing the most appropriate sensor configuration for each task and increasing its efficiency.

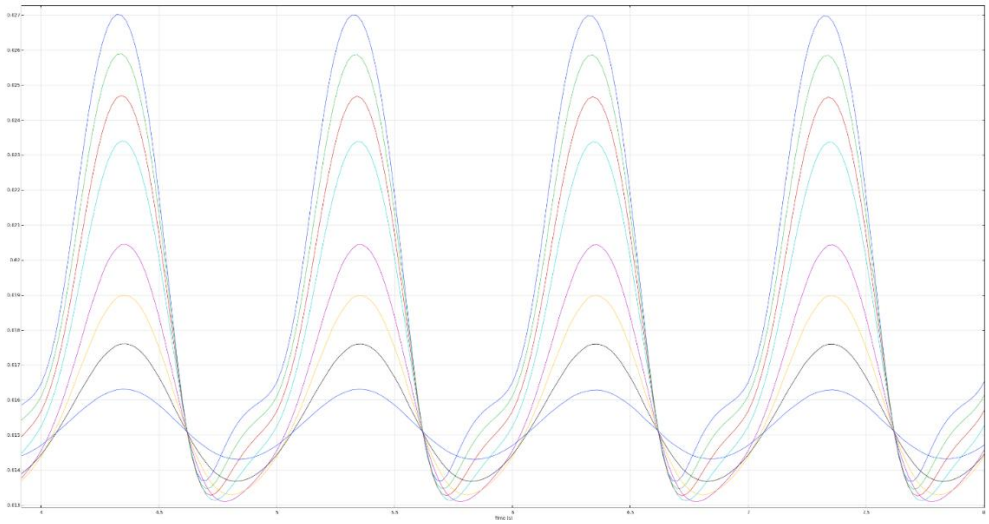

Figure 1. Nonlinear device responses to sinusoidal signals with different amplitudes.

1. A.S. Shabalina et al. "Modern measuring instruments based on molecular electronic transducers". Achievements of Modern Radioelectronics, **9**, pp. 33-42, 2014.
2. A.S. Bugaev et al, "Molecular electronic transducers for measuring instruments". Journal of Communications Technology and Electronics (Radiotekhnika i Elektronika), **11**, 2018.
3. D.A. Zhevnenko et al. «Mass and charge transfer modeling in planar electrochemical transducers». Electronic Engineering. Series 3. Microelectronics, **164**, №4, pp.31-37, 2016 (in Russian).
4. A.V. Novikov et al. «The planar silicon-based microelectronic technology for electrochemical transducers». Proc. SPIE **10224**, ICMNE-2016, 102241J, 2016.
5. D.A. Zhevnenko, S.S. Vergeles, T.V. Krishtop, D.V. Tereshonok, E.S. Gornev, V.G. Krishtop. «The simulation model of planar electrochemical transducer». Proc. SPIE **10224**, ICMNE-2016, 102241I, 2016.
6. V.M. Agafonov, A.S. Bugaev, A.A. Oryol. "Nonlinear Effects in Molecular-Electronic Cell of a Planar Type". Nano- and Microsystems Technology, **5**, p.32, 2009.
7. V.M. Agafonov, A.N. Antonov, D.L. Zaitsev. "Intrinsic noise and nonlinearity of diminutive angular molecular-electronics transducers". Sensors & Systems, **1**. pp. 7-12, 2010.

MEMS Devices based on Self-Organizing Semiconductors Structures

M. Denisenko, A. Isaeva, I. Lysenko
Southern Federal University, Taganrog, Russia, dema@sfedu.ru

In this paper, we consider a method for constructing MEMS structures using a self-assembly operation based on controlled self-organization of mechanically stressed semiconductor layers.

An important area of modern microsystem technology is the development of highly sensitive linear acceleration sensors. One of the most sensitive to the displacement of the inertial mass (IM) accelerometers are constructions that use tunneling current to record changes in the distance between the electrodes [1]. Such accelerometers have important advantages: hypersensitivity (the ratio between the tunneling current and the interelectrode distance is exponential); reduction of characteristic dimensions (small sensitive area because of tunnel contact, there is no need for big IM due to small displacements). Another promising direction is nanoelectromechanical (NEM) switches. These devices have a number of advantages over CMOS electronic switches, such as low leakage current, energy efficiency, stability, good dynamic characteristics, and can be used in ultra-low-power electronics. In the designing process of NEM-switches, an important point is to solve the problem of "sticking" of contacts, which leads to an increase in operating voltages and even to the failure of the device. The solution can be the use of tunnel contacts, which are devoid of this disadvantage [2]. The presence of a tunnel gap will avoid direct contact of the electrodes during the switching process. The NEM-switch design variant is schematically shown in fig. 1.

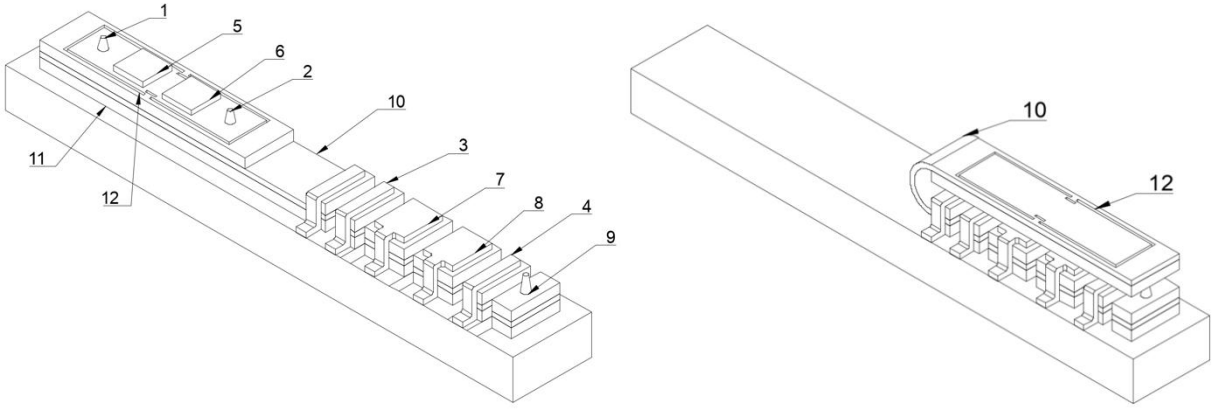

a b

Fig. 1. Unfolded (a) and final folded (b) structure on NEM-switch.

The U-shaped elastic suspension 10 in it is formed of two semiconductor layers as follows: the outer layer is made of InAs, the inner one is made of GaAs (these layers are shown in white in the figure). Mechanical stresses in the heterofilm [3] (due to the difference in the values of the lattice constants) twist it with controlled local release from the substrate by etching the sacrificial layer 11. Other parts of structures are: 1-4 – tunneling contacts; 5-8 – electrostatic actuators; 9 – beam support tip; 12 – flat elastic suspension.

The simulation results [3] suggest that such structures of sensor elements are promising. It should be noted that prior to selective etching of the sacrificial layer, the unfolded state of the structure makes it possible to envisage additional technological operations for modifying the structure, for example, using a focused ion beam.

This work was financially supported by the grant of President of Russian Federation (project number MK-2130.2020.8).

1. Niu, W.M., Fang, L.Q., Xu, L., Li, X., Huo, R.K., Guo, D.Q., Qi, Z.Y. “Summary of Research Status and Application of MEMS Accelerometers” Journal of Computer and Communications, **6**, P. 215–221, 2018.
2. Niroui F. et al. "Nanoelectromechanical tunneling switches based on self-assembled molecular layers" IEEE 27th International Conference on Micro Electro Mechanical Systems (MEMS), P. 1103–1106, 2014.
3. Lysenko I.E., Denisenko M.A., Isaeva A.S., Popov V.D. “Three-Axis Tunneling Micro accelerometer Based on Self-Organizing Structures” International Journal of Engineering Trends and Technology **68.11** P. 92-96, 2020.

Designing thermal MEMS on a system level

S. Evstafyev, V. Samoylikov, S. Timoshenkov
National Research University "MIET", Zelenograd, Russia, madcatse@gmail.com

In recent years, micromechanical sensors and actuators have shown steady growth. In its majority, microelectromechanical systems (MEMS) and devices based of them find application in consumer electronics, automotive, mechanical engineering and other fields of technology [1]. In this regard, there is an important task to improve methods of development of devices based on microelectromechanical elements with predetermined characteristics. Although computer-aided design tools can accurately calculate the behavior of a particular designed device, this usually requires a large amount of processor time, and each iteration in design will result in the need for re-simulation. In contrast to computer simulation, analytical calculations do not predict the end result with a high degree of accuracy, but they allow for quick estimation and determination of the necessary ways of device design development.

In this paper, a systematic method for designing a basic design of a thermal MEMS is discussed using the example of a thermal micromechanical mirror developed by MIET. The mirror is made with microelectronic technology and consists of two movable bimorph structures made of aluminum and silicon dioxide. A reflective element with an aluminum coated surface is attached to the movable beams. The movable beams are fixed to a silicon substrate and are controlled by applying voltage to electrical heating elements formed inside the movable beams. Heating causes uneven expansion of the materials that make up the beams, which in turn causes the structure to move.

Based on the previous studies [2], [3], a sequence of steps was developed to determine the performance characteristics of the selected design for the micromechanical mirror element. The first step is an analysis of the desired specifications for the required actuator edge movement, maximum geometric dimensions, maximum power consumption, speed parameters and mass-size characteristics of the device. Next, a set of materials and manufacturing process are selected, and the values of the radius of curvature and displacement are calculated. The basic design of the element is developed, the dependence of mirror edge movement on overheating is determined. Based on the selected geometry, displacement, superheat and the energy to be applied to the mirror are determined. Based on the energy value obtained, the required power value is calculated and the time required for heating is determined, in turn limited by the required speed. When all the parameters of the initial specifications are fulfilled, it is possible to proceed to the analysis by means of finite element methods.

The developed algorithm is planned to be subsequently implemented in the form of an application program or a computer-aided design system, which will make it possible to quickly design the thermal micromechanical elements with predetermined performance characteristics.

1. M.K. Mishra, V.Dubey, P.M. Mishra, I.Khan. "MEMS Technology: A Review". Journal of Engineering Research and Reports, **4**, pp. 1-24, 2019.
2. S.S. Evstafyev, V.K. Samoylikov, "Research and analysis of heat exchange processes of a micromechanical mirror based on a thermal microactuator", Proc. SPIE 11022, *International Conference on Micro- and Nano-Electronics 2018*, pp. 110220U, SPIE, Zvenigorod, 2019.
3. S.S. Evstafyev, V.K. Samoylikov, V.V. Kalugin, "Analysis of dynamic characteristics of the thermal micromechanical actuator". *Proceedings of the International Scientific and Practical Conference "Intelligent Systems and Microsystems Engineering 2018"*, pp. 22-28, Elbrus, 2018.

Investigation of the Gas-Phase Deposition of Material Layers in Plasma-Vacuum Systems for MEMS production processes

V. Samoylikov, S.Timoshenkov, S. Evstafyev, P. Gornostaev
National Research University "MIET", Zelenograd, Russia, madcatse@gmail.com

One of the fundamental processes in the technology for the production of microelectromechanical systems (MEMS) for various purposes is the gas-phase deposition of thin layers of materials. This paper categorizes the gas-phase deposition processes and methods for their study.

Mathematical modeling of gas-phase deposition processes is carried out on the basis of idealized schemes or assumptions in most cases, which may differ from the actual physical picture inherent in one or another design of the reaction chamber. Therefore, it becomes necessary to search for more rational methods and techniques for studying the processes of gas-phase deposition of material layers. The correct choice of the method of study can be facilitated by visualizing the results of interaction of the gas stream with the deposition surface [1]. To this end, visualization techniques based on the deposition of Si_3N_4 and SiNH layers and the effect of auto doping have been proposed and developed.

It is established that high homogeneity of the electrophysical parameters of the structures can be obtained in the reaction volume with high-intensity metabolic processes. These requirements are met by reactors that have jet injections of the gas-vapor mixture into the deposition zone, which leads to a complex hydrodynamic flow that hinders mathematical modeling. Therefore, to obtain (quantitative) regularities of gas-phase deposition processes of material layers used in MEMS, it is suggested to use methods of physical modeling and modeling by analogy. Physical modeling of the deposition process was carried out on the basis of the sublimation process and analog modeling - on the process of heat exchange. The visualization of vapor-gas local jet stream interaction with wafers was carried out in the industrial unit for gaseous-phase deposition of silicon epitaxial layers (SEL). It was shown that the SEL deposition rate is determined by the intensity of two oppositely directed flows: forward (at the moment of a wafers being above the nozzle) and backward (at the moment of a wafers being between the nozzles). The use of the auto alloying effect has shown that the distribution of the dopant impurity from the local source in the deposition zone is inhomogeneous and a significant part of the impurity is transferred in the direction of the jet motion.

Analog modeling technique was developed and experimental studies were verified both on the model and in the real SEL deposition process. The discrepancy between the results does not exceed ±10...12%, which indicates the adequacy of the processes being compared. There is a significant difference in the value of temperature gradients in the active zone and the passive zone of deposition. The value of this difference reaches 15 to 20 times. This difference becomes especially significant at the beginning of the active zone and at the end of the passive circulation zone. Based on the developed methodology, a study of the SEL deposition process was carried out. The results were processed in a generalized form, which are represented by the following criterion relationships:

$$\phi_x = 3.0\,\mathrm{Re}_d^{-1.0}\,Sc^{-0.35}(x/d)^{1.4},\ \text{if}\ 8\cdot10^2 < \mathrm{Re}_d < 2.2\cdot10^3,$$

$$\phi_x = 0.83\,\mathrm{Re}_d^{-0.25}\,Sc^{-0.35}(x/d_c)^{2.5},\ \text{if}\ 2.2\cdot10^3 < \mathrm{Re}_d < 4.1\cdot10^3. \qquad (1)$$

The discrepancy between the simulation results and the real process does not exceed ± 10%. On the basis of the research the area of the technological process with the highest possible homogeneity of SEL deposition parameters was determined. The process of plasma chemical deposition (PCD) of SiH_xN_y layers has been studied. As a defining parameter of the PCD process, the number Re_L, characterizing the gas dynamics of the process was chosen. Studies were performed at reaction chamber pressures of 100, 50 and 10 Pa, which corresponds to values Re_L =1.2, 0.8 and 0.4. It is shown that greater uniformity of the deposited layer occurs at higher pressures.

The paper provides the rationale for these techniques, a description of the toolkit, and gives recommendations for processing the results of the study.

1. N.Haoyin, L.Shijie, C.Caixia. *Modeling and simulation of silicon epitaxial growth in Siemens CVD reactor*. Journal of Crystal Growth, **404**, pp. 89-99, 2014.

FEM simulation of AlN-based MEMS energy harvester

P.S. Shlepakov, I.V. Uvarov
Valiev Institute of Physics and Technology of Russian Academy of Sciences, Yaroslavl Branch, Russia,
E-mail p.shlepakov@bk.ru, i.v.uvarov@bk.ru

MEMS sensors of various types were developed in the recent decades. These devices have low power consumption and are typically powered by a battery. However, recharging or replacement of the battery is sometimes impossible, e.g. in GPS trackers or strain gauges in buildings. Instead of the battery, the energy of environmental sources like wind or sunlight can be used. A widely available source is mechanical vibrations. Oscillations of building structures, household appliances or human body can be converted to electricity by a harvester. Among several harvesting principles, the piezoelectric transduction has the simplest design compatible with microtechology and demonstrates the highest efficiency [1]. To all appearance, the future belongs to the lead-free piezoelectric materials like AlN and ZnO. In recent decades, a lot of research is focused at the AlN-based transducers. These devices have a footprint of about 1 cm^2 and provide output power up to 64 μW. Their disadvantage is the narrow bandwidth, which limits the application of the harvester by a specific vibrating item. The bandwidth can be expanded by combining several resonators at a single chip, but the price is the significant increase of the harvester size. In this work, we propose a compact piezoelectric transducer of about 1 mm in size. Performance of the device is estimated by the finite element method (FEM).

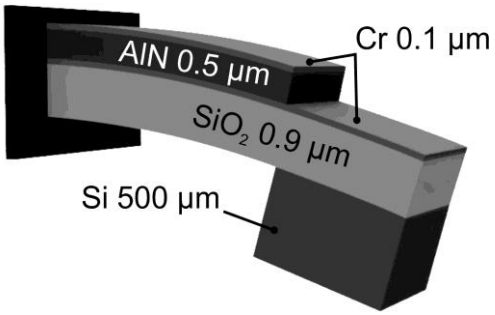

Figure 1. Design of the harvester.

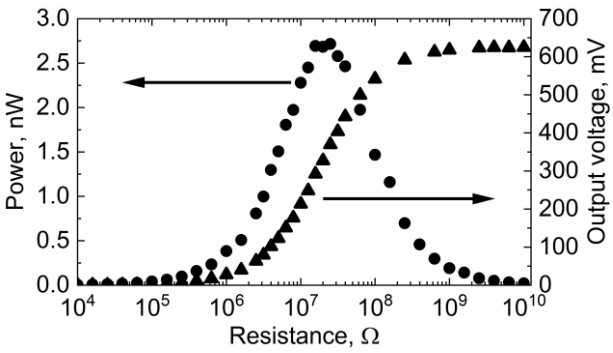

Figure 2. Output power and voltage as a function of the load resistance.

The harvester is designed as a multilayer cantilever shown in figure 1. The piezoelectric layer has a thickness of 0.5 μm and is sandwiched between two 0.1 μm thick chromium electrodes. These films are deposited on the 0.9 μm thick basic layer of SiO_2. The length and width of the cantilever are in the range of 500-1000 μm and 200-1000 μm, respectively. The cantilever is equipped by an inertial mass (IM) made of silicon. The harvester is attached to the vibrating item. When the item moves with acceleration, the cantilever deflects from its initial position. Mechanical stress polarizes AlN, which results in the potential difference between the electrodes and the current in the external circuit. The wider the beam, the more charge is accumulated at the electrodes and the higher output current can be generated. This makes wider cantilevers preferable. The device without IM can't generate enough charge to accumulate electricity due to small deflection of the cantilever ~0.1 μm. Addition of IM increases the deflection by three orders of magnitude. A natural frequency f_0 can be adjusted in the range of 45-160 Hz by varying the IM size. For the minimal amplitude of acceleration of household devises 0.2 m/s^2 the harvester generates maximal power of 2.7 nW and provides the output voltage of 0.35 V. The optimal load resistance is 25 MΩ, see figure 2. The figure of merit equals to 66 $\mu W/(g^2 \cdot cm^3)$, which is ten times higher than that for conventional piezoelectric harvesters. The enhancement is achieved due to the small size and high quality factor.

This work is supported by Program no. 0066-2019-0002 of the Ministry of Science and Higher Education of Russia for Valiev Institute of Physics and Technology of RAS.

1. S. Roundy and P.K. Wright. "A piezoelectric vibration based generator for wireless electronics". Smart Mater. Struct., **13**, pp. 1131-1142, 2004.

Nanomechanical resonator based on a silicon nitride nanowire

P.O. Mikhailov[1,2], A.A. Dorofeev[1,2], A.A. Popov[1], S.G. Kafanov[3], Yu.A. Pashkin[3], A.S. Trifonov[1,2], S.A. Pankratov[1,2], D.E. Presnov[1,2,4], V.A. Krupenin[1,2]

1. Faculty of Physics, Moscow State University, 119991 Moscow, Russia, aa.dorofeev@physics.msu.ru
2. MSU Quantum Technology Centre, Moscow, 119991, Russia, krupenin@phys.msu.ru
3. Department of Physics, Lancaster University, Lancaster, LA1 4YB, United Kingdom, y.pashkin@lancaster.ac.uk
4. Nuclear Physics Institute, Moscow State University, 119991 Moscow, Russia, denis.presnov@physics.msu.ru

At present, due to the remarkable progress in nanotechnologies, nanoelectromechanical systems (NEMS) become intensively studied objects of research in fundamental and applied physics [1]. NEMS applications cover many areas such as ultrasensitive mass, force, pressure and displacement measurements. The study of superfluids with NEMS is of particular interest [2].

In this work, we have developed an original fabrication technique of nanomechanical resonators based on silicon nitride and studied their vibrational properties. The fabrication process includes the stages that are standard for the CMOS technology: electron beam lithography, thin-film deposition, and reactive-ion etching. The distinctive features of the developed technology are the simplicity and a small number of fabrication steps: we use the same patterned aluminum film as a protective mask for etching of silicon nitride and as conductive leads of the device.

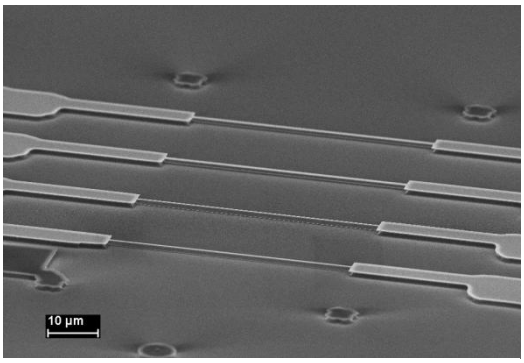

Fig. 1. Scanning electron micrograph of four nanowires.

The NEMS structure is based on a suspended nanowire (beam) clamped at both ends (see Fig. 1) Nanowires with a cross section of 200×100 nm^2 and length of 50-100 μm, coated with a 30 nm thick aluminum layer, were fabricated from silicon wafers covered with a 200 nm thick low-stress silicon nitride layer. Mechanical vibrations in the system are excited and detected by the magnetomotive method: the sample is placed in a magnetic field $\boldsymbol{B} = 5$ T and an alternating current passes through the conducting film. As a result, the nanowire vibrates due to the Lorentz force and produces a characteristic response curve when the drive frequency is close to the resonance frequency. The resonance frequency of such a nanowire is extremely sensitive to external factors. Characterisation of a 70-μm-long nanowire in vacuum at $T = 10$ mK gave a resonance frequency of 2.116 MHz and a quality factor $Q \sim 2.8\times10^3$. The theoretical estimate of the resonance frequency is ~ 2.8 MHz. The discrepancy between the theoretical and measured values can be attributed to the built-in stress of the silicon nitride film, which was not taken into account.

Next, the resonator was placed in a specially designed cell connected to the source of ^{4}He gas through the narrow capillary lines and mounted on the mixing chamber plate of a dilution refrigerator, to study the phenomenon of turbulence in superfluids, namely, interaction of the resonator with quantum vortices in superfluid ^{4}He. Turbulence in the superfluid helium was generated by a quartz tuning fork located at a distance of 2 mm from the resonator. By monitoring the resonance frequency of the resonator over a period of time, changes in the resonance frequency due to the interaction of individual quantum vortices with the nanowire were observed with a millisecond resolution. The time dependence of the resonance frequency revealed the vortex dynamics, including the various stages of interaction of a single quantum vortex with the nanowire: the moment of capture of a vortex by the nanowire, their interaction and vortex release [3]. This experiment proves that NEMS are viable tools in studies of superfluids.

This research was supported by the Interdisciplinary Scientific and Educational School of Moscow State University «Photonic and Quantum Technologies. Digital Medicine».

1. W-M. Zhang et al. “Tunable micro- and nanomechanical resonators”. *Sensors* **15**, 26478–26566 (2015).
2. D.I. Bradley et al., “Operating nanobeams in a quantum fluid”. *Scientific Reports* **7**, 4876 (2017).
3. A. Guthrie, S. Kafanov, M.T. Noble, Yu.A. Pashkin, G.R. Pickett, V. Tsepelin, A.A. Dorofeev, V.A. Krupenin, D.E. Presnov, “Nanoscale real-time detection of quantum vortices at millikelvin temperatures”. *Nature Communications* **12**, 1-6 (2021).

Research of resonance frequencies of silicon membranes for hydrophone applications

S. Malokhatko[1,2], E. Gusev[1], O. Ageev[1,2], T. Efimov[3], E. Rassolov[3], R. Romashko[3]

1. Southern Federal University, Institute of Nanotechnologies, Electronics and Equipment Engineering, Taganrog, Russia, malohatko@sfedu.ru

2. Research and Education Center "Nanotechnologies" of Southern Federal University, Taganrog, Russia, ageev@sfedu.ru

3. Optoelectronics Department, Institute of Automation and Control Processes Far Eastern Branch of the Russian Academy of Sciences (IACP FEB RAS), Vladivostok, Russia, efimov@iacp.dvo.ru

In this paper, square-shaped silicon membranes were designed and manufactured for use in a fiber-optic acoustic hydrophone. The values of the edge length (6-9 mm) and thickness (30-50 μm) of the membranes are calculated taking into account the registered pressures (0.1-14 Pa), frequencies (2-60 kHz) and the dynamic range of the adaptive interferometer, which allows measuring the deflection of the membrane from 2 to130 nm [1]. It is determined that are satisfied the requirements by square-shaped silicon membranes of 8×8 mm^2 and thickness of 40 to 50 μm, the frequency values in this case are in the range of 9.2 kHz to 42.3 kHz. A membrane with a thickness of 50 μm was formed by anisotropic etching of silicon. The amplitude-frequency response of the membranes was experimentally measured using an adaptive holographic interferometer in an air environment (fig. membrane 1). Since this membrane had a large number of defects [1], the amplitude-frequency response of the membrane is characterized by the absence of pronounced resonant frequencies. In addition, the membrane had a low sensitivity. Therefore, additional studies of the conditions of anisotropic etching of silicon were carried out, aimed at reducing the concentration of surface defects. Based on the obtained results, a membrane was formed with a resonant frequency of 10.1 kHz (fig. membrane 2), corresponding to the results of numerical modeling. Improving the technique of anisotropic etching of silicon has significantly reduced the effect of defects on the resonant characteristics of silicon membranes, which makes them promising for use in fiber-optic acoustic receivers.

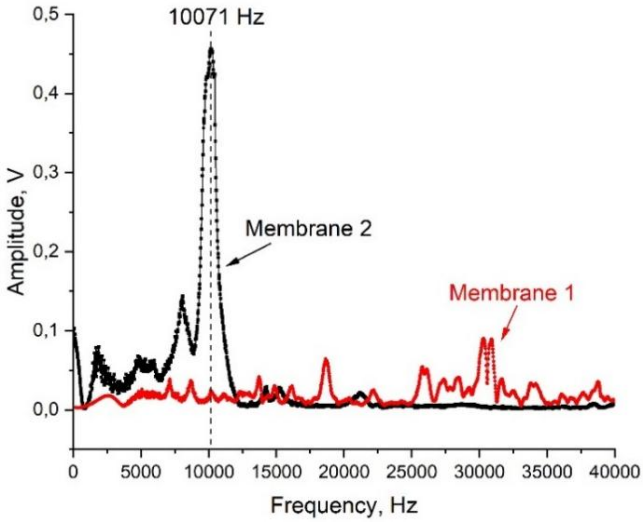

Figure. Amplitude-frequency characteristics of silicon membranes with dimensions of 8×8×0.05 mm^3 (membrane 1) and 8×8×0.044 mm^3 (membrane 2).

The reported study was funded by RFBR, project number 20-37-90087. The study of resonance properties of the membrane supported by the Russian Science Foundation under Grant No. 19-12-00323. The fabrication of the membranes was done on the equipment of the Research and Education Centre "Nanotechnology" of Southern Federal University.

1. S.V. Malokhatko, E.Yu. Gusev, E.A. Rassolov, A.M. Khannanov and O.A. Ageev. "Research of the mechanical parameters of silicon membranes for acoustic sensors". Journal of Physics: Conf. Ser, **1695,** 2020.

High-Performance $A^{III}B^{V}$ Photodetector for On-Chip Optical Interconnects

I.V. Pisarenko[1], E.A. Ryndin[1], B.G. Konoplev[2]
1. Saint Petersburg Electrotechnical University "LETI", Russia, ivan123tgn@yandex.ru, rynenator@gmail.com
2. Southern Federal University, Taganrog, Russia, kbg@sfedu.ru

An optoelectronic approach implies the replacement of metal inter-element and -component connections in integrated circuits by high-performance on-chip optical links. It allows to overcome the limitations of traditional interconnecting techniques and to improve the performance of next-generation chips significantly. Within the approach being considered, various advanced designs of ultrafast optoelectronic devices were developed. An injection laser with a double $A^{III}B^{V}$ nanoheterostructure and a functionally integrated optical modulator [1] is an advanced device that provides the generation of optical signals with terahertz modulation frequency in $A^{III}B^{V}$-on-Si optical interconnections. However, an efficient detection of laser pulses with subpicosecond edges generated by the laser-modulator requires a high-speed and technologically compatible photodetector. Nowadays, multiple promising designs of optical sensors are proposed [2], [3], but they have essential disadvantages and do not meet the specified requirements to the full.

In this paper, we demonstrates that it is possible to improve the response time characteristics of traditional $A^{III}B^{V}$ *p-i-n* photodiode through the formation of a transverse control heterostructure, whose electric field relocates photogenerated charge carriers from an absorbing region to special recombination layers with short lifetime and low carrier mobility during the back edge of an optical pulse. To research transients in the photodetector with controlled relocation, we propose two time-domain numerical models and applied Octave software for their implementation. The first model is based on the Schrodinger-Poisson equation system and describes essential quantum-mechanical aspects of electron and hole transport in the device. The second model applies the well-known drift-diffusion approximation to take into account semiclassical effects emerging during the photodetector operation.

The analysis of the numerical simulation results enabled to draw the following important conclusions. The mechanism of carrier mobility and lifetime modulation due to their controlled transverse relocation between thin semiconductor layers grown by molecular beam epitaxy at different temperatures ensures the decrease in photodetector response time to 0.1–0.5 ps when maintaining sufficiently high pulse sensitivity comparable to *p-i-n* photodiode with similar parameters. The fastest photoresponse of the sensor with controlled relocation is provided at certain optimal ratio between charge carrier mobilities in the absorbing and low-temperature-grown (LTG) regions. If mobility ratio is higher than the described one, the redistribution of charge carriers in the LTG regions is more durable, and response time gradually elongates. In contrast, if the ratio is lower, the mobility modulation is less efficient. The redistribution of electrostatic potential in the photodetector regions during the control voltage edges leads to the flowing of adverse capacitive current pulses through supply contacts. In the detection mode, these pulses are superimposed on the photocurrent, and it causes false activations of photoreceiver circuit. To deal with this problem, we propose to generate a measurement signal using two device structures connected with a high-speed differential amplifier. Both structures have the same parameters, supply and control voltages, but only one device is attached to an optical waveguide and acts as a photodetector. It means that the output signal of the differential amplifier contains only the useful photoresponse component, and displacement currents of similar photodetector structures approximately compensate each other. The control voltage shutdown before the recombination of the most part of non-equilibrium charge carriers in the LTG layers induces the photocurrent surges, those amplitude is comparable with the photoresponse. The solution of this problem implies the adding of special carrier-holding LTG layers located between the control junctions and usual LTG layers and having the deepest quantum wells in the whole heterostructure. This work was supported by federal budget of Russia (project FENW-2020-0022).

1. B.G. Konoplev, E.A. Ryndin and M.A. Denisenko. "Circuit model for functionally integrated injection laser modulators". Russian Microelectronics, **46**, pp. 216–223, 2017.
2. K. Sun and A. Beling. "High-Speed Photodetectors for Microwave Photonics". Applied Sciences, **9**, art. № 623, 2019.
3. T. Ishibashi and H. Ito. "Uni-traveling-carrier photodiodes". J. Appl. Phys., **127**, art. № 031101, 2020.

Development of nanoantenna array technology for switching in 3-D integrated circuits

D.A. Serov[1], I.A. Khorin[2], H.V. Pershina[1], A.M. Aliev[1]
1. RTU MIREA-Russian Technological University, Moscow, Russia, E-mail: d.serov589@gmail.com
2. Valiev Instutute of Physics and Technology, RAS, Moscow, Russia, E-mail: khorin@ftian.ru

The introduction of three-dimensional integral components contributes to a multiple reduction in the cost of their production without complicating the manufacturing technology. Currently, the switching of crystals of such circuits is carried out using the Cu TSV technology. This technology has a several reliability issues such as cracking and delamination of the dielectric layer.

One of the possible ways to solve the problems described above is to use a nanophotonics element instead of copper compounds – an array of metal nanoantennas. Due to the potential introduction of such structures, the speed and volume of information transmission theoretically increases [1-3], and an urgent issue affecting the overheating of copper elements in three-dimensional integrated circuits is also solved.

However, to implement this technology, it is necessary to solve a number of tasks. One of them is to develop an optimal nanoantenna array manufacturing process route [4, 5]. In this paper, we consider one of the possible methods for obtaining complex nanostructures on the surface of a silicon wafer, which could later be implemented and applied in the development of a data reception and transmission system in three-dimensional integrated circuits.

In conclusion, the results of the conducted research are summarized and further tasks are set. The finding solutions for them will lead to manufacturing a working architecture of a nanophotonics receiving and transmitting device that allows switching in 3-D IC crystals.

1. Sri Harsha Gade, Shobha Sundar Ram, Sujay Deb, Millimeter wave wireless interconnects in deep submicron chips: Challenges and opportunities, Integration, **64**, 127-136, 2019.
2. Nabil Khalid, Naveed A. Abbasi, Ozgur B.Akan, Statistical characterization and analysis of low-THz communication channel for 5G Internet of Things, Nano Communication Networks, **22**, 258-268, 2019.
3. Muhammad Rehan Yahya, Ning Wu, Zain Anwar Ali, Yasir Khizar, Optical Versus Electrical: Performance Evaluation of Network On-Chip Topologies for UWASN Manycore Processors, Wireless Personal Communications, **116**, 963-991, 2019.
4. Songya Cui, Yisha You, Kangyi Zhao, Yongqi Fu, Shaoli Zhu, Experimentalstudy of metasurface-based nanoantennas array fabricated using heavy ion tracking for biochemistry sensing, Sensors and Actuators B: Chemical, **273**, 815-820, 2018.
5. D.Pavlov, S.Syubaev, A.Kuchmizhak. S.Gurbatov, O.Vitrik E.Modin, S.Kudryashov, X.Wang, S.Juodkazis, M.Lapine, Direct laser printing of tunable IR resonant nanoantenna arrays, Applied Surface Science, **469**, 514-520, 2019.

Long-term irradiation effects in p-MNOS structure: experiment results

E. Mrozovskaya[1,2], P. Chubunov[1,2], G. Zebrev[1]
1. National Research Nuclear University MEPhI, Moscow, Russia
2. The branch of JSC URSC – ISDE, Moscow, Russia,
e-mail: liza.mrozovskaya @mail.ru

The cumulative damage caused by ionizing radiation is a significant threat to space electronics. In order to monitor and control total ionizing dose (TID), the RADFETs are widely used in space applications. However, it is commonly known that RADFETs with thick oxide may be subject to the effect of ELDRS. So investigation of the dose-response dependence of RADFETs on dose rate is an important task for ensuring the reliability of monitoring results.

We study the dose-response of RADFETs based on p-MNOS-structure with different oxide thicknesses experimentally. The dose sensitivity of the p-MNOS was obtained by irradiation at a low dose rate (0.013 rad(Si)/s) and was compared with previously observed results [1, 2] (see figs 1a and 1b).

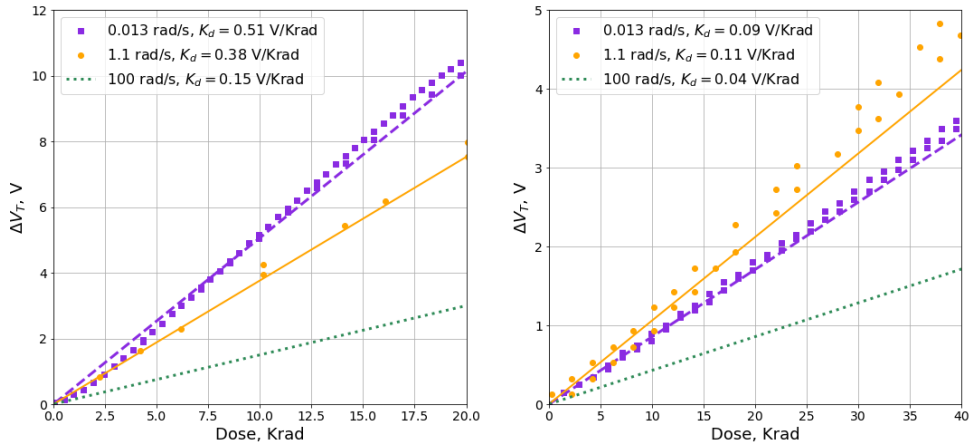

(a) (b)

Fig. 1. Comparison the dose responses of *p*-MNOS-structure irradiated at different dose rates. (a) The thickness of oxide is 500 nm, (b) The thickness of oxide is 150 nm.

As can be seen in figs.1, the dose sensitivity of *p*-MNOS (K_d) dependents on dose rate. For samples with 500 nm oxide, the dose sensitivity is grown with decreasing dose rate. For the 150 nm sample, the dose sensitivity also is increase with the change dose rate from 100 rad(Si)/s to 1 rad(Si)/s, but for low dose rates changes of the VD-slope are small and grow with increasing dose rate.

The obtained results correspond with works [3, 4, 5] and develop methods on-earth tests MOS-structure accounting ELDRS.

1. P. Zimin et al., "ELDRS in p-MOS and p-MNOS Based RADFETs with Thick Gate Insulators," a report accepted to RADECS 2018, Sweden, September 16th-21st, 2018.
2. E.V. Mrozovskaya et al., "Compact modeling of electrical characteristics of p-MNOS based RADFETs", Priceedings of SPIE – The International Society for Optical Engineering, 2019.
3. E.V. Mrozovskaya et al., "Simulation of annealing and the ELDRS in p-MNOS RadFETs", High Temperature Material Processes, **23**(4), pp 313-318, 2019.
4. G. I. Zebrev et al., "Compact Modeling of MOSFET I-V Characteristics and Simulation of Dose-Dependent Drain Currents," IEEE Trans. Nucl. Sci., **64** (8), pp. 2212-2218, 2017.
5. P.A. Zimin et al., "Calibration and electric characterization of p-MNOS RADFETs at different dose rates and temperatures", Nuclear Instruments and Methods in Physics Research, Section A: Accelerators, Spectrometers, Detectors and Associated Equipment, 2019, 940, pp. 307-312.

Influence of hydrogen diffusion and gettering on the radiation hardness of bipolar transistors

E.A. Polushkin[1.2], S.V. Nefediev[2], A.V. Kovalchuk[1], O.A. Soltanovich[1], S.Yu. Shapoval[1]
1. Institute of Microelectronics Technology and High Purity Materials RAS, Chernogolovka, Russia.
2. JSC Molecular Electronics Research Institute, Moscow, Russia, epolushkin@niime.ru

Degradation of semiconductor devices from ionizing radiation influence determines the service life and quality of operation of various devices in places with an increased background radiation. There are some ways to increase the permissible cumulative exposure without affecting the functionality of the device, for example, to use the wider-band materials or to update the construction of the device [1]. But these ways are not always economically affordable and / or technologically feasible.

Technological methods for increasing the radiation resistance of bipolar transistors and integrated circuits were tested in this work. As depicted in the studies [2, 3, 4], monatomic hydrogen is complexed with donors and acceptors. The experiment showed that hydrogenation of silicon p-n-junction devices reduces significantly the rate of degradation of the diffusion length and the recombination coefficient, thereby increasing their radiation resistance. Hydrogen passivation of defects and impurities was observed, as well as the radiation hardening. The effect of gettering together with hydrogenation on the radiation resistance of bipolar structures was also demonstrated.

Electron cyclotron resonance (ECR) plasma was used for effective diffusion hydrogen [5]. It is characterized by low operating pressures from 10^{-3} Torr to 10^{-5} Torr, a high degree of ionization of the plasma-forming gas, a possibility of applying a bias voltage to the substrate holder; all these properties make ECR plasma a good tool to introduce atomic hydrogen into various structures.

As a getter, we used polysilicon layer deposited on the back side of a silicon wafer.

The influence of the cumulative dose on the IC performance was determined by the change of the current gain β of the test bipolar P-N-P and N-P-N transistors located on the wafers from the corresponding groups, as well as by the yield factor of ICs

As a result of the experiments, a combination of hydrogen treatment in ECR plasma, rapid thermal annealing and gettering with polysilicon from the back side of the wafer make it possible to increase the radiation hardness of bipolar microcircuits and transistors.

Treatment in hydrogen ECR plasma leads to degradation of the transistors' the current gain, apparently due to the passivation of donors and acceptors, but it improves the dynamics of degradation of microcircuits and transistors under gamma irradiation.

Moreover, it is worth paying attention to the fact that these methods of the radiation hardness improvement of microcircuits do not require any modifications of transistors' and ICs' topology and fabrication methods. It is just enough to add some operations to the standard IC process flow.

1. Kobzev Yu.M., Frolov D.P., Enns A.V., Enns V.I., Osokin S.A. "Radiation-resistant analog-to-digital SOS ULA K1451BK1U: structure and design features." Trudy FGUP NPTSAP. Sistemy i pribory upravleniya [Proc. of the Federal state Unitary Enterprise "Science and Production Center on Automatics and Instrumentation Engineering". Control systems and device], 2010, no. 4,pp. 17-23. (in Russian).
2. Conyers Herring, N. M. Johnson, and Chris G. Van de Walle "Energy levels of isolated interstitial hydrogen in silicon" Phys. Rev. B 64, 125209 – Published 11 September 2001.
3. C. Herring and N. M. Johnson, "Hydrogen in Semiconductors", edited by J. I. Pankove and N. M. Johnson, Vol. 34 of *Semiconductors and Semimetals*, Treatise Editors R. K. Willardson and A. C. Beer ~Academic, Boston, 1991, Chap. 10.
4. J.I. Pankove, D. E. Carlson, J. E. Berkeyheiser, and R. O. Wance «Neutralization of Shallow Acceptor Levels in Silicon by Atomic Hydrogen» Phys. Rev. Lett. **51**, 2224, 1983.
5. S. Shapoval, V. Borodin, V. Gorbunov, A. Veretennikov 7th International Conference on Solid-State and Integrated Circuits Technology, Vol. 1, 571 2004.

Quantum drift-diffusion models for dual-gate field-effect transistors based on mono- and bilayer graphene

I. Abramov, V. Labunov, N. Kalameitsava, I. Romanova, I. Shcherbakova
Belarusian State University of Informatics and Radioelectronics, Minsk, Belarus, E-mail: nanodev@bsuir.edu.by

At present, a great deal of interest in device based on two-dimensional (2D) materials, especially graphene in the field of micro- and nanoelectronics is observed. Graphene has robust hoheycomb lattice structure and unique properties such as ambipolarity, high carrier mobility, high conductivity. Nevertheless the properties of mono- and bilayer graphene are different, and as a result significant difference in electrical characteristics of field-effect transistors (FETs) based on mono- and bilayer graphene was shown in few experimental works [1, 2]. Note, that FET on bilayer graphene has been demonstrated improved characteristics by contrast to FET on monolayer graphene [1]. Therefore necessity appears to create models specifically for FETs on bilayer graphene. In the FET a tunable band gap is observed, applying a perpendicular electrical field to the bilayer graphene channel [3].

In the paper quantum drift-diffusion model of FETs based on bilayer graphene is proposed. The model is combination of electrical and physical models [4, 5]. Mechanism of carrier transport along the bilayer graphene channel is considered. Electrostatic potential of the transistor channel is defined according to band gap. With using proposed model simulation of graphene dual-gate FET with length channel 4 μm. Calculation of electrostatic potential of investigated device structure was carried out.

Also with the using of model which means for simulation of FETs based on monolayer graphene [6, 7], a good agreement with the experimental data has been received for output characteristics of the investigated device. In the models different design parameters of FETs such as length channel, width channel, thickness of top- and back-gate dielectrics are supported.

The proposed models of device structures based on 2D materials were included in the nanoelectronic devices simulation system NANODEV [8, 9] developed at the BSUIR since 1995.

1. B. N. Szafranek, G. Fiori, D. Schall, D. Neumaier, H. Kurz. "Current saturation and voltage gain in bilayer graphene field effect transisrors", Nano Lett., **12**, N 3, pp. 1324-1328, 2012.
2. G. Fiori, D. Neumaier, B. N. Szafranek, G. Iannaccone. "Bilayer graphene transistors for analog electronics", IEEE Trans. Electron. Dev., **61**, N 3. pp. 729-733, 2014.
3. Y. Zhang, T.-T. Tang, C. Girit, Z. Hao, M. C. Martin, A. Zettl, M. F. Crommie , Y. R. Shen , F. Wang "Direct observation of a widely tunable bandgap in bilayer graphene", Nature, **459**, N 7248, pp. 820-823, 2009.
4. I. I. Abramov. "Problems and principles of physics and simulation of micro- and nanoelectronic devices. Part I. Basic positions", J. of nano- and microsystem technique, N 8, pp. 34-37, 2006.
5. I. I. Abramov. "Bases of micro- and nanoelectronic devices simulation", LAP LAMBERT Academic Publishing, Saarbrücken, Germany, 444 p., 2016. (In Russian).
6. I. I. Abramov, N. V. Kolomeitseva, V. A. Labunov, I. A. Romanova, I.Yu. Shcherbakova. "Influence of gate dielectrics of field-effect graphene transistors on cureent-voltage characteristics". Russian Microelectronics, **50**, N 2, pp. 118-125, 2021.
7. I. I. Abramov, V. A. Labunov, N. V. Kolomeitseva, I. A. Romanova, I.Yu. Shcherbakova "Simulation of device structures based on graphene using NANODEV system". Minsk: BSU, pp. 256-260, 2020. (in Russian).
8. I.I. Abramov, I.A. Goncharenko, S.A. Ignatenko, A.V. Korolev , E.G. Novik, A.I. Rogachev. "NANODEV: A nanoelectronic-device simulation software system". Russian Microelectronics, **32**, N 2, pp. 97-104, 2003.
9. I.I. Abramov, A.L. Baranoff, I.A. Goncharenko, N.V. Kolomejtseva, Y.L. Bely, I.Y. Shcherbakova. "A nanoelectronic device simulation software system NANODEV: New opportunities". Proc. of SPIE, **7521**, edited by Kamil A. Valiev, Alexander A. Orlikovsky, pp. 75211E1-1-11, 2010.

Monte Carlo simulation of picosecond laser irradiation photoresponse of deep submicron SOI MOSFET

A.V. Borzdov[1], V.M. Borzdov[1], V.V. Vyurkov[2]
1. Belarusian State University, Minsk, Belarus, borzdov@bsu.by.
2. Valiev Institute of Physics and Technology, Russian Academy of Sciences, Moscow, Russia, vvyurkov@gmail.com

The results of ensemble Monte Carlo simulation of deep submicron SOI MOSFET drain current photoresponse are presented. The photoresponse is simulated for picosecond laser pulses with 532 and 650 nm wavelengths at $5 \cdot 10^{10}$ W/m^2 intensity. The current decay and the dynamics of generated charge carriers in the transistor channel are studied.

The simulated SOI MOSFET is shown in Fig.1 (a). The SOI MOSFET structure is similar to that regarded as photodetector in [1]. Transistor dimensions used in our simulations are as follows: L_G = 50 nm, L_S = L_D = 50 nm. The width of the channel W_c = 50 nm, the buried oxide thickness W_b = 145 nm, the substrate thickness W_{sub} = 200 nm.

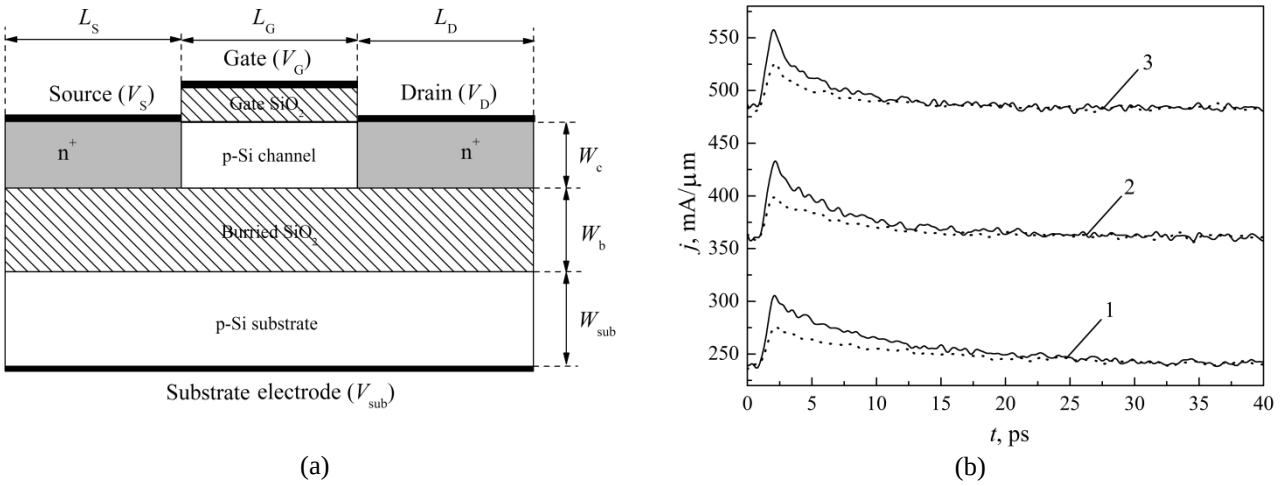

Fig. 1. The simulated SOI MOSFET (a) and photoresponse of the drain current (b). Solid curves – irradiation with 532 nm wavelength, dotted curves – irradiation with 650 nm wavelength. Curves 1 – V_D = 0.5 V, 2 – V_D = 0.75 V, 3 – V_D = 1 V

In the Fig. 1(b) photoresponse of the drain current is presented for several drain biases. The source, gate and substrate biases are zero. The lattice temperature is 300 K. It is supposed that laser radiation is switched on at t = 1 ps. The radiation intensity is uniform in space and time. Only gate area is under effect of radiation. For simplicity the gate electrode is supposed transparent for the radiation. Photon absorption with subsequent electron-hole pair generation is simulated according to intrinsic absorption coefficient taking into account multiple photon reflection from Si-SiO_2 interfaces. Optical properties of the materials are taken from [2, 3].

The simulation results show that the current decay is controlled by the processes in electron-hole plasma which is formed in the transistor channel under the gate dielectric. The long tail of current decay is mainly due to the lower rate of hole charge redistribution. Under the simulation conditions holes are accumulated near the gate SiO_2-Si interface.

1. W. Du, H. Inokawa, H. Satoh, and A. Ono. "Single-photon detection by a simple silicon-on-insulator metal–oxide–semiconductor field-effect transistor". Jpn. J. Appl. Phys., **51**, pp. 06FE01-1–06FE01-4, 2012.
2. D.E. Aspnes, A.A. Studna. "Dielectric functions and optical parameters of Si, Ge, GaP, GaAs, GaSb, InP, InAs, and InSb from 1.5 to 6.0 eV". Phys. Rev. B, **27**, pp. 985–1009, 1983.
3. H. Wang, X. Liu, Z.M. Zhang. "Absorption coefficients of crystalline silicon at wavelengths from 500 nm to 1000 nm". Int. J. Thermophys., **34**, pp. 213–225, 2013.

A universal approach to FET compact modeling: Case study for MESFETs and OFETs

D.S. Malich, G.I. Zebrev
National Research Nuclear University MEPHI, Moscow, Russia

Compact modeling is very essential for today's electronics as it allows you to link scientific research with circuit design [1]. Our purpose is to demonstrate a universal physic based approach for FET modeling. We have decomposed the FET modeling into two independent kinetic and electrostatic parts [2]. The former is based on solving of current continuity equation and leads to an explicit form of the I-V characteristic as a function of charge in the channel, which is universal for all field-effect transistors. The latter is based on solving of the electrostatic equation and specific for a particular device and configuration. The dependence of the current on the gate voltage is determined implicitly only through the charge density. This report discusses the applicability of this method using the example of OFET [3] and MESFET [4].

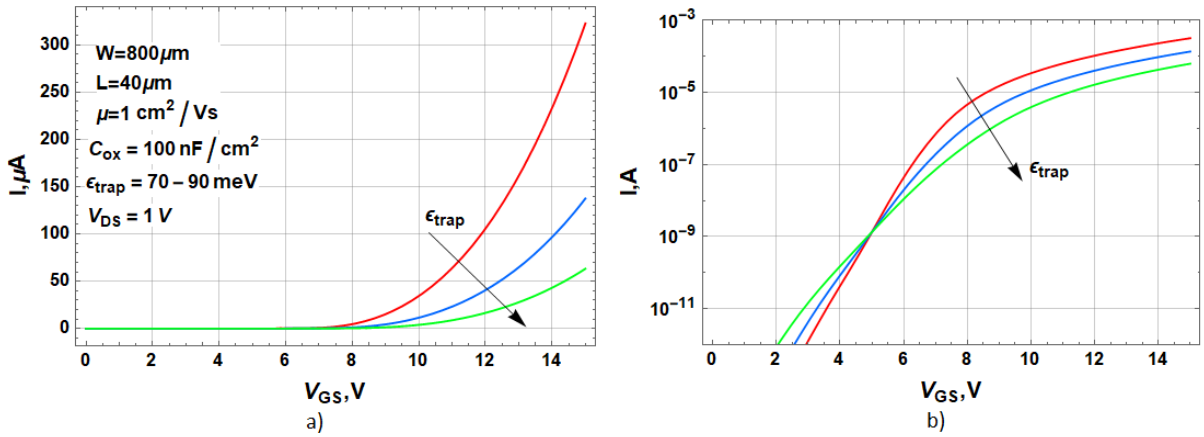

Fig. 1. Calculated I - V curves of OFET with different energy depths of the exponential spectrum (a) linear scale, (b) logarithmic scale.

We have considered two electrostatic equations specific to OFET and MESFET. Fig.1 shows the specific effect of deep tail states with an energy spectrum that grows exponentially closer to the edge of the band. The second is based on the specifics of the Schottky contact as a gate with modulation of the depletion region of the channel.

1. C. Hu. Compact modeling for the changing transistor “2013 International Conference on Simulation of Semiconductor Processes and Devices (SISPAD)”, 2013.
2. G. I. Zebrev. “Unified description of I-V characteristics in field-effect and bipolar transistors based on current density continuity equation solution,” Proc. SPIE, 94401C, Dec. 2014.
3. Kim C., Bonnassieux Y., Horowitz G. “Compact DC Modeling of Organic Field-Effect Transistors: Review and Perspectives,” IEEE Trans. Electron. Devices**, 61**, pp. 278–287, 2014.
4. M.M.Ahmed et al. “A Comprehensive Four Parameters I–V Model for GaAs MESFET output characteristics,” Solid-State Electronics, **51**, pp.511-516, 2007.

Modeling the assembly of a microinductor made by using residual mechanical stress

A. Babushkin, R. Selyukov
Valiev Institute of Physics and Technology of Russian Academy of Sciences, Yaroslavl Branch, Yaroslavl, Russia, artem.yf-ftian@mail.ru

Over the past few decades researchers and engineers have focused on miniaturizing electronic devices, improving their performance and reliability. Despite the great success in active electronics manufacturing, integrated silicon-based devices still require external auxiliary passive components to operate. However, they cannot be easily integrated into the flat surface of a silicon chip, so they are usually placed separately from the silicon chip on a printed circuit board. As a result, this limits the potential for further development of productivity and miniaturization. Therefore, new methods of the manufacturing of passive elements have to be compatible with silicon technology and applicable for mass production. The operating parameters of passive components are strongly dependent on their geometry and the physical properties of the surrounding objects. Therefore, for the most part, planar structures do not have satisfactory parameters. In recent years, there have been several attempts to fabricate three-dimensional passive components using bond-wire [1], liquid metals [2], 3D-printing [3] and special mechanical assembly [4]. However, these methods are complex and their sequential fabrication is not compatible with parallel mass production of semiconductor devices. One of the most promising approaches to solve these problems is the development of a technology for self-assembly of passive components. It involves the fabrication of two-dimensional patterns using conventional lithography and their subsequent transformation into three-dimensional structures. This opens up tremendous opportunities for designing devices and optimizing their performance.

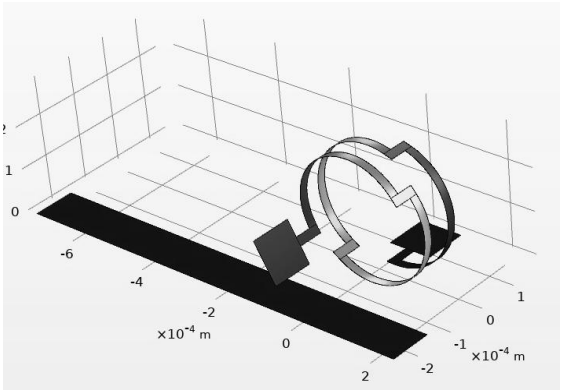

Fig. 1. Microinductor FEM model in the self-assembly process.

Figure 1 shows the FEM model of the self-assembly of a microinductor using residual stress. Microinductor is made of a Cr film 300 nm thick with stress gradient ~7 GPa/μm. It is possible to achieve such a large stress gradient by treating a Cr film in Ar plasma of the low-pressure RF induction discharge [5]. The solenoid shape is the most suitable for the inductor. The vertical orientation of the coils reduces losses due to the presence of eddy currents in the substrate compared to a planar design. Thin and wide coils reduce the negative effect of skin effect. Such a design leads to the increase of the quality factor and inductance.

The investigation was supported by Program no. 0066-2019-0002 of the Ministry of Science and Higher Education of Russia for Valiev Institute of Physics and Technology of RAS.

1. A. Moazenzadeh, N. Spengler, R. Lausecker, A. Rezvani, M. Mayer, J.G. Korvink and U. Wallrabe. "Wire bonded 3D coils render air core microtransformers competitive". J. Micromech. Microeng., **23**, 114020, pp. 1-11, 2013.
2. D.P. Parekh, C. Ladd, L. Panich, K. Moussa and M.D. Dickey. "3D printing of liquid metals as fugitive inks for fabrication of 3D microfluidic channels". Lab Chip, **16**, p. 1812, 2016.
3. S.-Y. Wu, C. Yang, W. Hsu and L. Lin. "3D-printed microelectronics for integrated circuitry and passive wireless sensors". Microsyst. Nanoeng., **1**, 15013, pp. 1-9, 2015.
4. Z. Yan, F. Zhang, F. Liu, M. Han, D. Ou, Y. Liu, Q. Lin, X. Guo, H. Fu, Z. Xie, M. Gao, Y.Y. Huang, J.J.J. Kim, Y. Qiu, K. Nan, J.J.J. Kim, P. Gutruf, H. Luo, A. Zhao, K. Hwang, Y.Y. Huang, Y. Zhang and J.A. Rogers. "Mechanical assembly of complex, 3D mesostructures from releasable multilayers of advanced materials". Sci. Adv., **2**, 1601014, pp. 1-11, 2016.
5. Babushkin A., Selyukov R., Amirov I. "Effect of Ar ion-plasma treatment on residual stress in thin Cr films". Proc. of SPIE, **11022**, 1102223, pp. 1-8.

Design of multi-electrode microprobe for silicon wet bulk micromachining

E. Gusev[1], A. Saryev[1], S. Malokhatko[1,2], O. Ageev[1,2]
1. Southern Federal University, Institute of Nanotechnologies, Electronics and Equipment Engineering, Taganrog, Russia, eyugusev@sfedu.ru
2. Research and Education Center "Nanotechnologies" of Southern Federal University, Taganrog, Russia, ageev@sfedu.ru

Microprobes, as an implantable part of the neural interface, are intensively used to study the neural activity of the brain. R&D in the field of invasive neural interfaces is focused on reducing the extent of the nerve tissue damage by lowering the diameter of implanted probes less than 100 μm [1]. Probe structures are formed by bulk micromachining by means of anisotropic etching of the wafer [2]. In this case, the size and shape of the probe is depended on etching conditions. The latter should be taken into account when designing the probe structure. The aim of the work is to establish dimension ranges of a silicon microprobe with a cross-sectional size less than 100 μm, taking into account the number of electrodes, as well as the conditions of anisotropic wet etching. Analytical calculations were carried out for the probe structure, represented by n-regions of various widths, carrying up to 2n-1 electrodes (fig. a). The dependences of the bottom width of the trapezoidal section of the probe and width of related mask on the thickness and top width of the probe are obtained. The permissible dimension ranges for several cases of one- to four-level microprobes have been established. The correction value of the mask size was estimated, reflecting the effect of etching conditions on the geometry of the probe. Modeling was carried out in an anisotropic wet etching simulator [3]. The geometric dimensions of the masks were chosen according the results of analytical calculations (fig. b). As the etchant was chosen KOH and values of the etching rate of silicon in the main directions were taken from [4]. Modeling made it possible to refine the results of the analytical calculations, refine dimensions of the silicon microprobe structure, the geometry of the masks, as well as the extent undercut effect, taking into account the conditions of KOH etching (fig. c). The obtained results could be used in development of silicon microprobes formed by anisotropic wet etching.

The reported study was funded by RFBR, project number 20-37-90087.

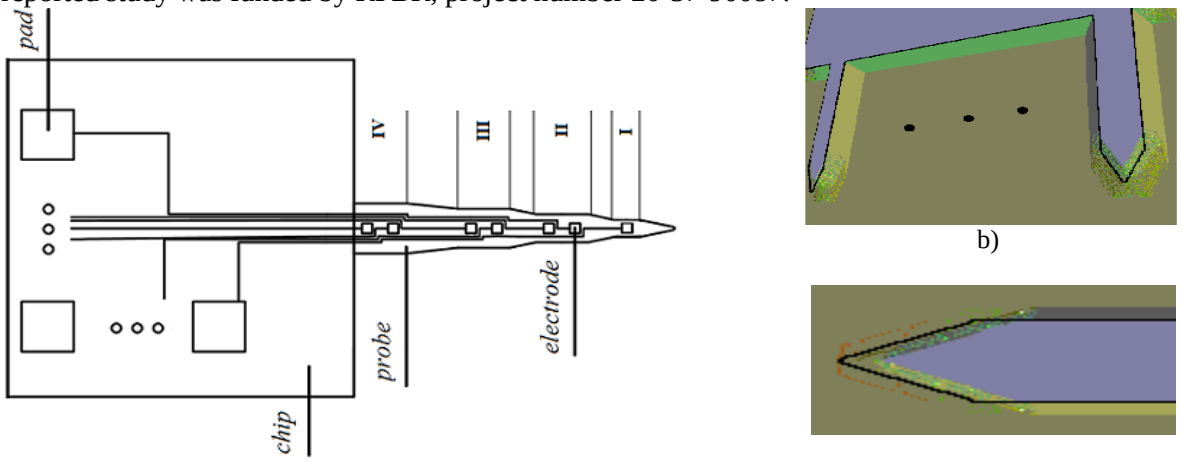

Figure. Schematic of multi-electrode microprobe (a) and features of anisotropic wet etching modeling (b,c).

1. N. Obidin, F. Tasnim and C. Dagdeviren. "The Future of Neuroimplantable Devices: A Materials Science and Regulatory Perspective". Advanced Materials, **32**(15), 1901482, 2019.
2. E.Yu. Gusev and J.Y. Jityaeva. "Process technology of multielectrode microprobe for a minimally invasive neurocomputer interface". Izvestiya SFedU. Engineering Sciences, **6**, pp. 61-70, 2019 (in Russian).
3. Z. Zhu and C. Liu. "Simulation of anisotropic crystalline etching using a continuous Cellular Automata algorithm". Computer Modeling in Engineering and Sciences, **1**(11), pp. 11-19, 2020.
4. H. Seidel, L. Csepregi, A. Heuberger and H. Baumgärtel. "Anisotropic Etching of Crystalline Silicon in Alkaline Solutions". Journal of the Electrochemical Society, **137**(11), pp. 3612-3625, 1990.

Beam power absolute measurements using calorimetric methods

V.P. Kudrya
Valiev Institute of Physics and Technology of the Russian Academy of Sciences, Moscow, Russia
E-mail address: kvp@ftian.ru

This work continues a series of our works devoted to the diagnostics of fast neutral particles beams (see, e.g. [1]). Calorimetric methods for measuring beam power are used to diagnose ion, neutral, electron, and photon (visible, IR) beams, that is, they are universal. Moreover, some of these methods are absolute since they do not require the use of calibration curves. This work is devoted to mathematical models describing the operation of calorimeters that provide absolute measurement of the beam power. We investigated the mathematical models of adiabatic, calibrated heat sink, and flow calorimeters.

For the adiabatic calorimeters a detailed analysis of the mathematical model is presented. A non-stationary solution of the appropriate heat conduction equation is given and its features are considered. Two definitions of the response time for adiabatic calorimeters are proposed. The calorimeter sensitivity is also defined. Based on these definitions a criterion of the receive plate material selection is proposed. A comparison with available published experimental and theoretical results is carried out.

Foe the calorimeters with a calibrated thermal sink a transient mode is analyzed. A simple one-dimensional model is proposed to calculate temporal dependencies of the temperature difference at the calibrated thermal sink. In addition, the limits of applicability of the widely used quasistationary approximation are determined.

For the flow calorimeters some results of the analysis of equations describing the operation of a flow calorimeter within the framework of a quasi-one-dimensional thermal model are presented. A consistent simplification of these equations is considered, which made it possible to obtain simple relationships for assessing the sensitivity, response time, and heating temperature of the receiving plate of the flow calorimeter. A thermal energy balance equation for a stationary mode of operation is obtained, expressed in terms of average temperatures. The functional dependence of the reduced value of the overheating of the channel shell of the flow calorimeter on the product of the value characterizing the heat transfer from the channel wall to the fluid flow and the calorimeter sensitivity is derived. In addition, within the framework of the proposed approach, a rough estimate of the lower boundary of the response time of the flow calorimeter was obtained.

1. V.P. Kudrya, Yu.P. Maishev. "Fundamentals of the fast neutral beams diagnostics". *International Conference on Micro- and Nanoelectronics 2016*. Eds.: V.F. Lukichev, K.V. Rudenko. Vol. 10224, Art. 10224-2C, 12 p., 2016.

Application of electron spectroscopy spectra interpretation methods to describe ions spectroscopy signals

V. Afanas'ev, L. Lobanova, D. Selyakov, M. Semenov-Shefov
National Research University «Moscow Power Engineering Institute», Moscow, Russia, v.af@mail.ru

Spectroscopy based on investigation samples properties via light ions (protons and helium ions) is widely used to study targets of complex composition (Ion Scattering Spectroscopy, Rutherford Back Scattering, Elastic Recoil Detection). To describe ions signals the OKG method [1] will be used, which has shown its high accuracy in describing electronic spectra [2, 3].

Analytical description of reflected ions energy spectra is traditionally based on the small-angle approximation, which is based on the "strong elongation" of the differential cross section for elastic scattering:

$$\omega_{el}(0) \gg \omega_{el}(\pi) \quad (1)$$

Condition (1) is met for ions in a wider energy range than for electrons. That means the high efficiency of the OKG method in Light Ion Spectroscopy [4]. The simplest process description of the ions elastic scattering is the Strait Line Approximation (SLA) [3, 4], which allows, for example, to interpret the Rutherford Back Scattering spectra of ions with MeV range energies. However, with a decrease in the energy of ions (which is necessary to determine layer-by-layer profiles with a higher resolution) special features appear in the spectrum, which the SLA approximation cannot explain. The use of the SLA approximation for the interpretation of Ion Scattering Spectroscopy spectra is even more problematic.

The method presented in the paper describes the spectra of homogeneous and multilayer targets on the basis of an analytical approach based on solving the boundary value problem for the transport equation by Ambartsumyan's invariant imbedding method. OKG method [1, 2, 3] allows using the Spherical Harmonics Method (MSH) to solve the obtained equations. The solution is determined by the parameters of the elastic scattering cross section, the stopping power, verification of which is discussed in detail in the work, and the parameters that determine the ion recharge process. Reflected protons energy spectra calculated on the basis of the presented technique are compared with experimental data from different works and obtained for both homogeneous and multilayer samples.

1. R. Oswald, E. Kasper, and K. Gaukler. J. Electron Spectrosc. Relat. Phenom., **61**, p. 251, 1993.
2. V. P. Afanas'ev, P. S. Kaplya, and E. D. Lisitsyna. Journal of Surface Investigation. X-ray, Synchrotron and Neutron Techniques, **10**, No. 2, pp. 326–331, 2016.
3. Afanas'ev V.P., Efremenko D.S., Kaplya P.S. Journal of Electron Spectroscopy and Related Phenomena, **210**, pp. 16-29, 2016.
4. Mashkova E.S., Molchanov V.A. Medium-Energy Ion Reflection from Solids. Amsterdam: North Holland, p. 422, 1985.

Uncertainty of a nano- object linewidth value at its control by a low-voltage SEM

Yu. Larionov[1], Yu. Ozerin[2]
1. A.M. Prokhorov Institute of General Physics, Moscow, Russia, luv@kapella.gpi.ru
2. Mikron, Zelenograd, Russia, yozerin@mikron.ru

The manufacture of nanostructures with sizes in the region of 1-10 nm or so demands the measurement of its values with uncertainty that should be in order of a single atom size. So the standard relief structures (SRS) that reproduce the linewidth sizes should have the ideal smooth surface. But angular fragments of SRS profile, which ordinary are edge pointers for measuring SRS parts, are really far from demanded sophistication in subnanometer range (even with ideal SRS surface) [1]. So in the capacity of such edge pointer one can propose the ideal surface itself instead of angular fragment of the profile. The linewidth of such SRS is a distance between couple of parallel ideal surfaces the value of which is averaged over a set of pairs of corresponding points disposed afar from the angles of the SRS profile [1].

SRS of this type exists already in the form of SCCDRM (NIST, USA) [2] and IVPS -100-(PTB, Germany) samples. These standards are produced by anisotropic etch of silicon plate that forms almost ideal smooth parallel sidewalls (SW) of SRS. Their linewidth is measured by a number of periods between silicon atoms that disposed inside RS edges. To do this the SRS edges and silicon atoms are imaged together by a transmission electron microscope (TEM) [2]. Further the value of standard linewidth is used for calibration of a radius of the cantilever apex of the special atomic force microscope which used for measuring critical dimensions (CDAFM) which is set on an optical interferometer. Because the apex radius is measured with subnanometer uncertainty it could be used as a secondary standard for calibration of working standards than can be applied in turn for calibration of a shop low voltage (LV) SEM. These standards and their certification tools were recommended by Working Group on Dimensional Nanometrology (WG-N) of consultative committee for length (CCL) BIPM as measuring instruments for reproduction at national metrology committees for measurement of linear sizes in nanorange [3].

The RS with the vertical SW but calibrated with a help of a certified cantilever apex can serve as a secondary measurement standard for a low voltage (LV) SEM in nanorange. Linewidth, as the only controlled parameter, can be defined by a direct method of measurement as a distance between a pair of selected points at video-signal (VS) formed by a LVSEM scanning the RS. The uncertainty of its value in order of some nanometers can facilitate the use of this standard in production. One of the obstacles to use this standard is a variation of linewidth value at inevitable in metrology repeated scanning its calibrated section [1]. The variation is turned to have some nanometers in value and a non –monotonic dependence on time and also depends on LVSEM scanning parameters and on the time interval between the series of scans. The reason for a value variation is the mobile electric charge in the film oxide layer on the silicon surface induced by the LVSEM beam [1].

The paper will present the influence of scanning modes of LVSEM on variation of linewidth values of the RS with a vertical SW. It was revealed that at the certain scanning mode, a linewidth variation can be noticeably reduced (up to 0.5 nm) or can disappear completely. An attempt is made to explain this phenomenon; the results of experiments confirming the proposed explanation are presented.

1. Yu. V. Larionov. «Geometry of structures developed by anisotropic etching in the nanometer range». Nano and Microsystems Technology, 22.№3. 131-138. 2021.
2. R. Dixon, W. Guffrei, M. Cresswell et al. “Single crystal critical reference material (SCCDRM): Process optimization for the next generation of standards”. Proc. Of SPIE. **6518**. 651815. pp. 1-11. 2007.
3**.** R**.** Dixon, H. Bosse. “Recommendations of CCL/WG-N on: Realization of SI metre using silicon lattice and Transmission Electron Microscopy for Dimensional Nanometrology”. Ver.1. CCL-GD-MeP-2 30/04/2019.

Qubit measurement based on a nonlinear quantum Josephson oscillator

D.S. Pashin[1], M.V. Bastrakova[1], A.M. Satanin[2], C.S. Kim[3]

1. National Research Lobachevsky State University of Nizhny Novgorod, Nizhny Novgorod, Russia, pashindmi@gmail.com.

2. All-Russian Research Institute of Automation named after N.L. Dukhov, Moscow, Russia, asatanin@gmail.com.

3. Department of Physics, Chonnam National University, Gwangju, Korea, cskim@jnu.ac.kr.

Josephson oscillators have actively studied recently due to the great interest in superconducting circuits. The Josephson junction with AC current is similar to a nonlinear pendulum excited by a moment of an external force. As is known, in the classical mode, under certain conditions, such a nonlinear oscillator can be in two dynamic equilibrium states with different amplitudes. In this case, the phase space of the oscillator consists of two stable foci separated by a separatrix. Since the process of capture to the region near the foci occurs almost randomly, it can be considered statistically. It was proved that with ohmic dissipation, the probability of capturing in one of the equilibrium states is determined by the area of the corresponding region that sweeps out by the separatrix in phase space [1].

A method for calculating the quantum dissipative dynamics of a Josephson oscillator was developed. The situation is studied when the oscillator is coupled with a boson thermostat, and its dynamics is described by the density matrix. In a certain range of parameters, such a system has two well-localized states that correspond to classical dynamic equilibrium states.

On the basis of the obtained calculations, a new effective method of nondemolition measurements of qubit states by a Josephson oscillator in a weakly dissipative regime is proposed. The bistable behavior of the Josephson oscillator is studied for various parameters of the external exciting force. The discrimination power of such a system has been determined. The influence of the measuring device on the control of the qubit state by Rabi technique was also analyzed.

The work was supported by the RFBR grant 20-07-00952. The work of M.V. was carried out with the support of the grant of the President of the Russian Federation (MK-2740.2021.1.2).

1. D.S. Pashin, A.M. Satanin and C.S. Kim. "Classical and quantum dissipative dynamics in Josephson junctions: An Arnold problem, bifurcation, and capture into resonance". Phys. Rev. E, **99**, p. 062223, 2019.

Towards receiving wide-band superconductor antenna unit technology

N. Kolotinskiy[1,2], D. Bazulin[3], V. Kornev[1]

1. Faculty of Physics, Lomonosov Moscow State University, Moscow, Russia, kolotinskij@physics.msu.ru

2. Quantum Technology Centre, Lomonosov Moscow State University, Moscow, Russia.

3. Former affiliation: Faculty of Physics, Lomonosov Moscow State University, Moscow, Russia.

Rapid growth of communication content and volume of information processing makes now them beyond possibilities of the semiconductor-based systems. Further progress in Big Data, IoT, cloud and streaming services, as well as, communication with remote regions and objects in outer space requires development and implementation of fundamentally new physical technologies including the ones based on quantum physics laws and effects.

The advanced software-defined receiving systems are based on direct broadband signal digitizing with high-performance analog-to-digital converters (ADC). Current progress in superconductive electronics based on macroscopic quantum effects in superconductors has yielded in highly sensitive broadband analog-to-digital converters (ADC) capable of providing high spurious free dynamic range of the signal conversion (up to 90 dB and even higher). However, the inferior linearity and dynamic range of antenna and following low noise semiconductor amplifier as compared to those of the superconductor ADC constrain the overall system performance. Therefore, one needs to develop and implement receiving antenna unit that does not degrade integral characteristics of the entire receiving system. Such a unit can be completely superconductive with using active superconductor antenna.

In the presentation, we report and discuss our achievements in development of both the physical and design bases of the superconducting active electrically small antennas (ESA) capable of providing high sensitivity and high dynamic range in ultra-wide frequency band ranged from several hertz to tens of gigahertz.

This work was supported by Russian Science Foundation Grant 19-72-10016.

Phase-locking phenomenon in series Josephson junction arrays with capacitive coupling

A.Yu. Levochkina[1], V.K. Kornev[1], N.V. Kolotinskiy[1,2]

1. Department of Physics, Lomonosov Moscow State University, Leninskie Gory, 1, 119991, Russia
2. Quantum Technology Centre, Department of Physics, Lomonosov Moscow State University, Leninskie Gory, 1, 119991, Russia

Series Josephson junction arrays with capacitive coupling circuits were studied using numerical simulation. In the simplest case of two-junction array, the study evidenced capability of mutual phase locking resulting either in in-phase or in anti-phase coherent Josephson oscillations, although the only latter was formerly predicted through analytic consideration of the two-junction array [1]. Frequency domains of the modes can overlap at moderate thermal fluctuations. Both the range of applicability of the analytic theory and the tolerable critical current margins representing locking range for these oscillation modes were determined numerically.

In case of a multi junction array, the use of pairwise capacitive coupling of the junctions cannot provide common mutual phase locking and coherent Josephson oscillations due to small coupling radius (of only two junctions). However, the use of a common capacitor connected in parallel to the array does provide mutual phase locking in two oscillation modes similar to the ones observed for the two-junction array. The anti-phase oscillations in two-junction system are transformed into a collectively anti-phase oscillation mode in the multi junction array, when the array voltage does not contain fundamental Josephson oscillation tone.

Experimentally measured IV-curves of Josephson junction arrays with shared coupling capacitor are presented and discussed.

1. A. K. Jain, K. K. Likharev, J. F. Lukens, and J. E. Sauvageau, «Mutual Phase-Locking in Josephson Junction Arrays», Physics Reports, **109** (6), pp. 311-426, 1984.

Dynamic processes in a superconducting adiabatic neuron with non-shunted Josephson contacts

Marina Bastrakova[1], Anastasiya Gorchavkina[1,2], Andrey Schegolev[3,4], Nikolay Klenov[3,4], Igor Soloviev[3,5], Arkady Satanin[2,5], and Maxim Tereshonok[4]

1. Lobachevsky State University of Nizhny Novgorod, Nizhny Novgorod 603950, Russia
2. Russia National Research University Higher School of Economics, Moscow 101000, Russia, gorchavkina5@outlook.com
3. Lomonosov Moscow State University, Moscow 119991, Russia
4. Moscow Technical University of Communication and Informatics, Moscow 111024, Russia
5. Dukhov All-Russia Research Institute of Automatics, Moscow 101000, Russia

Artificial intelligence is rapidly developing Computer Science field, which has already taken an important place in academia and business. In particular, neural networks are of the greatest interest, since they model the work of a neuron in the human brain. In this paper, we investigate the question of constructing a physical model of a neural cell based on superconducting circuits. We have developed the design of the basic cell of the neural network the sigmoid cell (S_C-neuron, see fig. 1) based on Josephson contacts without resistive shunting [1]. The advantage of this approach is the nonlinearity of the superconducting current in the system as a function of the phase difference on the Josephson junction. In addition, superconductivity ensures high computing speed and energy efficiency of processes.

Modeling of the state dynamics as a function of an external parameter (external magnetic flux) was performed by solving the system of Hamilton equations for S_C-neuron (fig. 1) and was implemented numerically by the Runge-Kutta method of the 4th order. The analysis of the obtained results allowed us to find the mode when the transfer characteristic of the element implements the "sigmoid" activation function (fig. 2 for l = 0.22). The stochastic approach to the analysis of the equations of motion based on the Monte Carlo method [2] revealed the influence of inertia (capacitances), dissipation, and temperature on the dynamic characteristics of the neuron. The presence of a finite temperature was taken into account using an ensemble of initial states with a Gibbs distribution.

As a result, a numerical model of neural cell was obtained. Furthermore, we established the set of parameters (capacitances, critical currents, inductances, resistances, temperatures) for which the transfer function of this system has the form of a sigmoid – one of the fundamental functions in the theory of neural networks.

The work was supported by the RFBR grant 20-07-00952. M.V. was carried out with the support of the grant of the President of the Russian Federation (MK-2740.2021.1.2)

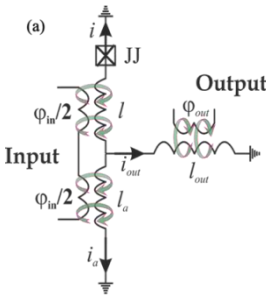

Fig. 1. S_C-neuron: the system under study.

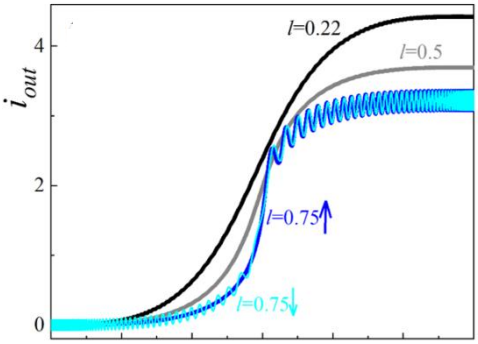

Fig. 2. The system's transfer function for different sets of physical parameters and fixed modeling ones.

1. A. E. Schegolev, N. V. Klenov, I. I. Soloviev, M. V. Tereshonok "Adiabatic superconducting cells for ultra-low-power artificial neural networks". Beilstein J. Nanotechnol, **7**, 1397, 2016.
2. A.A. Gorchavkina, M.V. Bastrakova, N.V. Klenov, A.M. Satanin, "Monte Carlo simulations of the switching processes in the superconducting quantron-based neuron". Journal of Physics: Conference Series. **1740** (1), 012063, 2021.

Aharonov-Bohm effect as a hylic phenomenon

V. Rubaev[1], L. Fedichkin[2]
1. NIX, Moscow, Russia, vladislav@nix.ru
2. Valiev Institute of Physics and Technology, Russian Academy of Sciences, Moscow, Russia, leonid@phystech.edu

Moving quantum charged particle may experience the influence of external vector-potential **A** even if in the region swiped by all possible particle trajectories there is no electromagnetic field. This phenomenon is usually called Aharonov-Bohm effect [1-3]. The fact that according to laws of quantum mechanics particle scattering cross section may happen to be nonzero even without action of any actual forces leads to numerous and sometimes bizarre interpretations.

In our work we provide the consideration of Aharonov-Bohm effect from different point of view. By investigating at quantum microscopic level the whole system comprising not only our particle but also the solenoid generating electromagnetic potential we show that the action on particle phase is physical natural phenomenon rather than spooky action at a distance as it may seem when solenoid is considered classically. We represent the electromagnetic potential as potential generated by many tiny magnetic dipoles. Each dipole interacts with the particle because field of particle acts on dipole. Dipoles are considered to be initially in quantum state which may be even entangled with environment. By properly taking path integral over particle trajectories accounting for force action between dipole and particle we arrive at expressions which are just the same as Aharonov-Bohm result. In contrast to previous attempts [4, 5] to explain Aharonov-Bohm effect as an action of charged particle magnetic field upon the source of magnetic vector potential our results are general and rigorous. We hope that our reverse approach to consideration of this effect paves the way for better understanding of physical processes behind Aharonov-Bohm effect and our alternative technique of calculations may occur to be useful for investigation of electronic transport in nanosystems.

1. Y. Aharonov, D. Bohm. "Significance of electromagnetic potentials in quantum theory". Physical Review, **115**, 485–491, 1959.
2. W. Ehrenberg, R.E. Siday. "The Refractive Index in Electron Optics and the Principles of Dynamics". Proceedings of the Physical Society, Series B, **62**, 8–21, 1949.
3. Y. Aharonov, D. Bohm. "Further Considerations on Electromagnetic Potentials in the Quantum Theory". Physical Review, **123**, 1511–1524, 1961.
4. L. Vaidman. "Role of potentials in the Aharonov-Bohm effect". Physical Review A **86**, 040101(R), 2012.
5. E. Santos and I. Gonzalo. "Microscopic theory of the Aharonov-Bohm effect". Europhysics Letters, **45**, 418–423, 1999.

On the features of various gas mixing regimes in $CF_4(C_4F_8)+O_2+Ar$ plasmas

A. Efremov[1], D. Bashmakova[1], D. Travkina[1], K.-H. Kwon[2],
1. Ivanovo State University of Chemistry & Technology, Ivanovo, Russia, amefremov@mail.ru.
2. Korea University, Sejong, South Korea, kwonkh@korea.ac.kr

Fluorocarbon gases are widely used in the microelectronic device technology for the dry patterning of silicon and silicon-based materials. Among these, the CF_4 is characterized by the highest F/C ratio and provides the domination of etching over the surface polymerization under typical reactive ion etching conditions. Oppositely, the C_4F_8 exhibits the lowest F/C ratio and is characterized by much higher polymerization ability. Accordingly, the corresponding etching process is featured by increasing etching residues, lower absolute Si and SiO_2 etching rates as well as by the maximum SiO_2/Si etching selectivity. The mechanism of last effect is connected with relative increase in the SiO_2 etching rate due to the lower fluorocarbon polymer film thickness on the oxygen-containing surface. Both etching and polymerization kinetics may be effectively adjusted by the mixing of fluorocarbon gases with Ar and/or O_2. Therefore, the correct choice of both fluorocarbon gas and additive component(s) is the real way to optimize output process parameters and thus, to obtain the advanced device performance.

In this work, we performed the comparative study of CF_4 + O_2/Ar and C_4F_8 + O_2/Ar inductively coupled plasmas under one and the same operating conditions with using different gas mixing regimes. Main goals were: 1) to compare the formation/decay kinetics for plasma active species and steady-state plasma compositions and efficiencies of both chemical and physical etching pathways; 2) to analyze the etching/polymerization balance (etching rates for target material and fluorocarbon polymer film, polymer deposition rate and polymer film thickness) using the set of gas-phase-related parameters; and 3) to study the fundamental differences in Si etching kinetics and mechanisms.

Plasma diagnostics and etching experiments were performed in the planar inductively coupled plasma (ICP) reactor. Plasma was excited using the 13.56 MHz power supply while another 13.56 MHz rf generator powered the bottom electrode in order to control the negative dc bias voltage, $-U_{dc}$. The process conditions were: total gas flow rate of 40 sccm, gas pressure of 10 mTorr, input ICP power of 700 W and bias power of 200 W. As the variable parameter, we used the initial composition of $CF_4(C_4F_8)$ + O_2 + Ar gas mixtures. In first experimental series, we substituted $CF_4(C_4F_8)$ for O_2 at constant y_{Ar} = 50%. Accordingly, experiments were started form 50% $CF_4(C_4F_8)$ + 50% Ar gas systems, and were finished with 12% $CF_4(C_4F_8)$ + 38% O_2 + 50% Ar one. In second experimental series, we substituted Ar for O_2 at constant fractions of $CF_4(C_4F_8)$ of 50%. As such, the starting point was also 50% CF_4 (C_4F_8) + 50% Ar while the final gas system combined 50% $CF_4(C_4F_8)$, 38% O_2 and 12% Ar. Langmuir probe diagnostics provided the data on electron temperature (T_e), ion current density (J_+) and total positive ion density (n_+). In order to determine the absolute densities and fluxes of plasma active species, we used the simplified global (zero-dimensional) plasma model. The input model parameters were experimental data on T_e and n_+ while the outputs include volume-averaged densities and fluxes of neutral and charged species.

The comparison of two gas mixing regimes in terms of electro-physical plasma parameters (electron temperature, electron density, ion energy flux) and gas-phase composition allowed one to conclude that a) both $CF_4(C_4F_8)/O_2$ and Ar/O_2 mixing ratios affect the electron-impact kinetics through changes in electron density and temperature; b) the O_2-rich gas mixtures provide noticeable changes in the F atom formation kinetics due to CF_x + $O/O(^1D)$ → $CF_{x-1}O$ + F, CF_xO + e → $CF_{x-1}O$ + F + e and CFO + $O/O(^1D)$ → CO_2 + F reaction pathways; c) opposite behaviors of F atoms densities in different gas mixing regime are due to either F atom formation kinetics (in the case of the CF_4-based plasma) or the F atom loss kinetics in a gas-phase (in the case of the C_4F_8-based plasma). The analysis of Si, SiO_2 and Si_3N_4 etching processes with model-predicted fluxes of active species allowed one to suggest their similar etching mechanisms (ion-stimulated chemical reaction with the domination of chemical etching pathway) as well as to attribute non-monotonic etching rates to opposite changes in F atom flux and effective reaction probability.

Low-energy etching of W and Mo films in halogen-containing plasma in continuous and atomic-layer etching mode

I.I. Amirov, M.O. Izyumov, A.N. Kupriyanov
Valiev Institute of Physics and Technology of Russian Academy of Sciences, Yaroslavl Branch, Russia,
E-mail ildamirov@yandex.ru

Refractory metals W and Mo are promising materials for metallization of sub-10 nm technology for manufacturing integrated circuits. Etching of metallization tracks in this technology should be carried out with nanometer accuracy in the mode of atomic-layer etching (ALE) [1]. Fluorides and chlorides of W and Mo are equally volatile, and the AlE etching process can be carried out in fluorine and chlorine-containing plasma. This paper presents the results of studying the etching of W and Mo metal films 40-50 nm thick in the plasma of RF inductive discharge in SF_6 /Ar, Cl_2 /Ar in the standard mode, depending on the ion energy (self-bias potential <60 V) and different Ar contents in mixture, as well as in ALE mode in the reactor detailed in [2]. The etching conditions were as follows p = 0.6 Pa, W = 200-700 W. The etching of the metal film was monitored by changing the signal of the laser beam (λ = 633 nm) reflected from the surface of the metal film. At the moment of etching off the metal film to the underlying SiO_2 layer, a sharp drop in the signal occurred, similar to that observed during the sputtering of the metal film [2]. This method of etching control made it possible monitoring the stages of formation of a fluoride and chlorinated metal layer. In Cl_2/80% Ar plasma, the Mo etching rate in the standard mode was much higher than W (Figure 1). This could indicate that the ALE process of these metals should be realized at different times of the ALE stages. Figure 2 shows the time variations of the signal of the laser beam during the W film etching in SF_6/Ar plasma in the ALE mode. On the stage I of the W fluorination in SF_6/Ar plasma at a low concentration of fluorine, the flat section indicates that etching of W does not occur. Etching of W occurs at stage II of the sputtering of the WF_x(x<6) layer at the energy 40 eV of ion Ar^+.

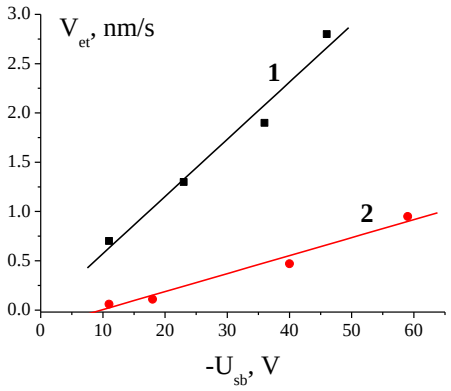

Figure 1. Dependence of the etching rate of Mo (1) and W (2) in a Cl_2/80%Ar plasma on the bias potential.

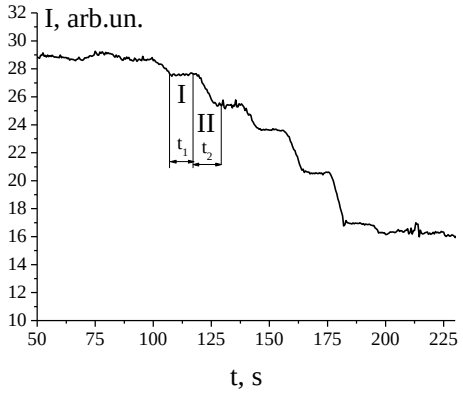

Figure 2. Time variations of the signal of the laser beam during of the W etching in ALE mode.

The conditions for the implementation of ALE etching of metals with a high synergy coefficient are discussed.

This work was supported by the Russian Foundation for Basic Research, project № 18-29-27017.

1. K.J. Kanarik, S. Tan, W. Yang, T. Kim, T. Lill, A. Kabansky, E.A. Hudson, et al. “Predicting synergy in atomic layer etching”. J. Vac. Sci. Technol. A. **35**, 05C302. 2017.
2. I.I. Amirov, M.O. Izyumov, V.V. Naumov, and E.S. Gorlachev. “Ion-plasma sputtering of Co and Mo nanometer thin films near the sputtering threshold”. J. Phys. D: Appl. Phys. **54**, 065204, 2021.

Study of inductively coupled plasma of fluorobromocarbons by Langmuir probe and optical emission spectroscopy

V.O. Kuzmenko[1], A.V. Miakonkikh[1], K.V. Rudenko[1]
Valiev Institute of Physics and Technology of Russian Academy of Sciences, Moscow, Russia, kuzmenko@ftian.ru

This work is devoted to the diagnostics of low-pressure inductively coupled plasma (ICP) of fluorobromocarbons (CF_3Br and $C_2F_4Br_2$), which can be used in microelectronics technology. CF_4 plasma was studied as a reference. One of possible application of $C_xF_yBr_z$ plasmas is low damage etching of low-k dielectrics for creation of metallization system of modern integrated circuits. Porous SiOCH is one of the common low-k dielectrics in the less then 90 nm technologic route. However, the microstructuring process of metallization system dielectric constant of SiOCH films increases due to plasma interaction. Various approaches to low-damage etching of low-k dielectrics are being investigated. Cryogenic etching in fluorobromocarbons ICP is one of possible approach to preserve their dielectric constant during etching. In this work plasmas applied for cryogenic etching of low-k dielectrics were studied in order to explain results observed earlier [1, 2].

Experiment was carried out in commercial PlasmaLab 100 Dual (OIPT) two-chamber ICP RIE cluster intended for processing of wafers up to 200 mm in diameter. Diagnostics of CF_4 and CF_3Br plasmas was conducted by Langmuir probe and optical emission actinometry. Langmuir probe studies were performed by Hiden Analytical ESPion Advanced Langmuir Probe. It provides information to determine positive ions and electron concentration, electron temperature and plasma potential in wide range of discharge parameters (p = 5-25 mTorr and W = 1000-2700 W). Neutral fluorine and bromine radical concentrations were determined using optical emission actinometry. Emission of neutral fluorine containing molecular particles was observed.

Obtained I-V characteristics of Langmuir probe were in quite good agreement with the Maxwellian electron energy distribution function. Electron temperatures in CF_3Br plasma are 1.5-3 eV in the studied value range of pressure and ICP power. CF_4 plasma has higher electron temperatures 2-4 eV. Optical emission actinometry showed that concentration of F radical is greater than the Br radical concentration. Emission of CF_x particles was observed in 200-280 nm (Figure 1).

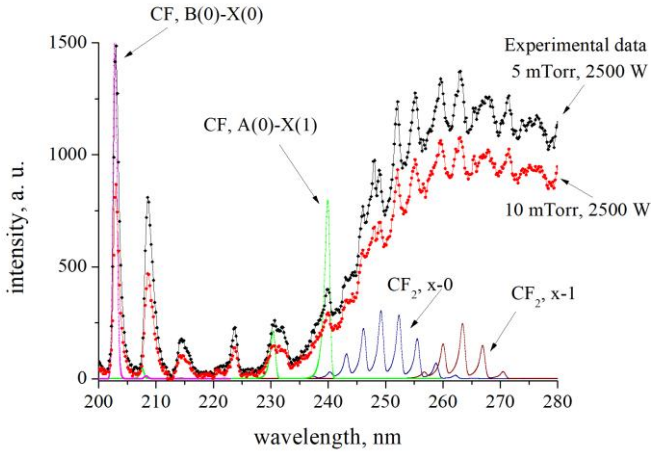

Figure 1. Emission spectra of CF_3Br (48 sccm)/Ar (2 sccm) plasma.

Results of this work can explain results of works devoted to cryogenic etching of low-k dielectrics in fluorobromocarbon plasma and can be modelling for this process.

The study was supported by Program no. 0066-2019-0004 for Valiev IPT RAS by RFBR (project № 18-29-27025).

1. A. Rezvanov, A. V. Miakonkikh, A. S. Vishnevskiy, K. V. Rudenko and M. R. Baklanov, "Cryogenic etching of porous low-k dielectrics in CF_3Br and CF_4 plasmas" J. Vac. Sci. Technol. B, **35**, p. 021204, 2017.
2. A. A. Orlov, A. A. Rezvanov and A. V. Miakonkikh, "Research on the process of lines formation in metallization system for technology nodes 28 nm and below" Nanoindustry, **S96-2**, pp. 684-687, 2020.

$C_2F_4Br_2$ plasma etching of nanoporous low-k dielectrics

A. Miakonkikh[1], V. Kuzmenko[1], A. Vishnevsky[2], A. Rezvanov[3], A. Orlov[3], K. Rudenko[1]
1. Valiev Institute of Physics and Technology RAS, Moscow, Russia, e-mail: miakonkikh@ftian.ru
2. Research and Education Center "Technological Center," RTU MIREA, Moscow Russia
3. Molecular Electronics Research Institute, Moscow, Russia

Low damage plasma etching is one of the key challenges for successful integration of porous low-k dielectrics in advanced interconnects of ICs. This problem is becoming even more important during the implementation of highly porous dielectrics with k < 2.5. Plasma processing degrades the low-k properties because of impact of chemically active radicals, ions and VUV photons. Increase of the k-value is caused by surface densification, changes in the chemical composition and bonds configuration, i.e. destruction of the hydrophobic Si-CH_3 bonds, forming the hydrophilic Si-OH and dangling silicon bonds with the following moisture adsorption. There are several approaches to protecting a porous structure during etching: 1) filling it with a polymer during etching, 2) using film-forming gases that deposit the polymer onto the surface from plasma, 3) condensation of etching products or plasma-forming gases in nanopores at a low temperature. Another option implied application of fromfluorine-containing plasma, in which radicals can spontaneously react with a dielectric to bromine-containing plasma with less active radicals. The last approach consisted in the use of gas CF_3Br which, in comparison with the reference CF_4, showed more damaging properties [1]. This was later explained [2] by the fact that in plasma CF_3Br the concentration of atomic fluorine turns out to be even higher than in plasma CF_4, in addition, calculations showed that at the temperatures used in [1], condensation does not yet occur. In this work, we used for the first time a gas with a more massive molecule $C_2F_4Br_2$, which, as the calculation shows, can condense in nanopores. The aim of this work is to study the degradation of a low-k dielectric during etching in plasma of $C_2F_4Br_2$ gas.

$C_2F_4Br_2$ is used as the etching gas; the sample temperature varies from -120°C to -20°C. The processes were performed in ICP etching tool (Plasmalab 100, OIPT) at pressure of 20 mTorr, with applied power of 1500 W with RF power of 52 W (DC bias ~140 V). As a test samples the organosilica glass with open porosity 30%, mean pore radius 1 nm and k-value 2.3 was used. Before and after etch the samples were heated up to 60°C in vacuum for 120 sec to remove atmospheric water or volatile etch by-products, and transferred to/from etching chamber without breaking the vacuum. After the etching step, the dielectric is thermally annealed for 30 minutes to remove the adsorbed substances and etching by-products. Langmuir probe and optical emission spectroscopy shows that plasma of $C_2F_4Br_2$, for the chosen parameters, has the same electron temperature (~ 1.5 eV), electron density (~ $2x10^{10}$ cm^{-3}), and approximately 1.5 times lower densities of fluorine and bromine radicals as plasma CF_3Br. In $C_2F_4Br_2$ the fluorine concentration also exceeds the bromine concentration by 1 order of magnitude. The chemical composition analysis of porous dielectric films was performed by Fourier transform infrared spectroscopy (FTIR) on annealed and pristine samples in room atmosphere. As a result of analysis, the IR spectra of the low-k dielectric before and after etching and subsequent annealing we observe low Si-CH_3 peak depletion and no change in 3800-3100 cm^{-1} region which attributed to water adsorption [1]. Also no products containing bromine were found on FTIR spectra after etching. Calculations based on FTIR peaks height shows that cryogenic processing in $C_2F_4Br_2$ plasma shows a non-monotonously decrease of the plasma induced damage with the decreasing the sample temperature. The films show significantly less damage at moderate cryo regime and remain hydrophobic (effective damaged layer (EDL) is about 12 nm after etch at -100°C). Thus, in this work, it was established that etching in plasma $C_2F_4Br_2$ in cryogenic leads to significantly less damage to the nanoporous dielectric, which is explained by the condensation of the plasma-forming gas in the nanopores. This can be used to develop low-damage etching processes for low-k dielectrics.

The investigation was partially funded by RFBR according to the research project # 18-29-27025.

1. A. Rezvanov, A. Miakonkikh, A. Vishnevskiy, K. Rudenko, M. Baklanov, J. Vac. Sci. Technol. B **35**, 021204 (2017).
2. V. Kuzmenko, A. Miakonkikh, Technical Physics Letters, 2021, **47** (1), pp. 99–102.
3. V. Kuzmenko, A. Miakonkikh, K. Rudenko, Journal of Physics: Conference Series, 2021, **1870** (1), 012006.

On the applicability of low-GWP $C_6F_{12}O$ gas plasma for the reactive-ion etching of Si and SiO_2

A. Efremov[1], K.-H. Kwon[2],
1. Ivanovo State University of Chemistry & Technology, Ivanovo, Russia, amefremov@mail.ru.
2. Korea University, Sejong, South Korea, kwonkh@korea.ac.kr

Gases from the fluorocarbon family with a general formula of $C_xH_yF_z$ have found numerous applications in the electronic device production industry for dry patterning of Si and SiO_2. The common feature of all conventional fluorocarbon gases are high values of their global warming potentials (GWP). The evident way to reduce the environmental pollution is to develop the eco-friendly dry etching processes where the conventional fluorocarbon gases are substituted for low-GWP compounds. One of suggested candidates is the dodecafluorooxepane $C_6F_{12}O$ which is featured by the GWP index of 1, exhibits low toxicity and keeps the liquid state at temperatures below 50 °C. The last feature provides the easier extraction of non-dissociated $C_6F_{12}O$ molecules from the output gas and thus, supports the recycling procedure. The idea of given study was to apply the comparative research scheme to $C_6F_{12}O$ + Ar/O_2 and CF_4 + Ar/O_2 plasmas. As the latter is well-know from many published works, it plays a role of the reference system for better understanding features of plasma physics and chemistry in the weakly-studied $C_6F_{12}O$-based plasmas.

Plasma diagnostics and etching experiments were performed in the planar inductively coupled plasma (ICP) reactor. Plasma was excited using the 13.56 MHz power supply while another 13.56 MHz rf generator powered the bottom electrode in order to control the negative dc bias voltage, $-U_{dc}$. Initial compositions of CF_4 + Ar/O_2 and $C_6F_{12}O$ + Ar/O_2 gas mixtures were set through individual flow rates of corresponding gases with equal values of 20 sccm. Therefore, each gas mixture was composed by 50% of fluorocarbon component and 50% of Ar or O_2. Variable processing parameters were the input RF power (W = 200–600 W that corresponded to the input power density of 0.02–0.06 W/cm^3) and the gas pressure (p = 4–12 mTorr). The constant bias power W_{dc} = 200 W produced the variable $-U_{dc}$ value, which changes oppositely to the positive ion flux. Langmuir probe diagnostics provided the data on electron temperature (T_e), ion current density (J_+) and total positive ion density (n_+). In order to determine the densities active species in the CF_4 + Ar/O_2 plasma, we used the simplified global (zero-dimensional) plasma model. The input model parameters were experimental data on T_e and n_+ while outputs include volume-averaged densities and fluxes of neutral and charged species. In addition, densities of F and O atoms in the $C_6F_{12}O$ + Ar/O_2 were evaluated using the actinometrical approach by optical emission spectroscopy (OES).

Plasma diagnostics data indicated that both gas systems are characterized by similar effects of process pressure and input power on plasma density (n_+ and n_e), ion bombardment energy and ion flux. Higher electron temperatures as well as lower n_+ and n_e values in $C_6F_{12}O$-based plasmas allow one to suggest higher fractions of smaller (less saturated) CF_x species which are characterized by lower cross-sections for excitation, dissociation and ionization. The possible reason is the multichannel electron-impact dissociation mechanism for $C_6F_{12}O$ molecules that provides the parallel formation of various C_xF_y fragments. Probably, this results in more effective production of CF_x radicals as well as causes the lack of oxygen atoms to transform these into CF_xO, FO and CO_x compounds. When analyzing chemistry of neutral species, it was found that $C_6F_{12}O$-based plasmas provide systematically lower densities of F and O atoms. An increase in both n_F and n_O vs. input power in both gas systems results from same changes in dissociation frequencies for corresponding source species. The similar effect of gas pressure is because of increasing amounts of fluorine- and oxygen-containing species coming with a feed gas. Etching experiments indicated a) the domination of chemical etching pathway; b) identical behaviors of Si and SiO_2 etching rates vs. processing parameters; and c) quite close SiO_2/Si etching selectivities of ~ 1.5. Principal features of $C_6F_{12}O$ + Ar/O_2 plasmas are lower absolute etching rates (that correlates with differences in F atom fluxes) as well as higher effective probabilities for Si + F and SiO_2 + F reactions. Perhaps, the last phenomenon is connected with heterogeneous processes involving oxygen atoms.

The principal conclusion is that the $C_6F_{12}O$ gas with low global warming potential may be the almost equivalent replacement for CF_4 in the reactive-ion etching of Si and SiO_2.

Biomimicry-gradient-based algorithm as applied to the inverse design of photonic devices

K. Edee, G. Granet, P. Bonnet, F. Paladian
Université Clermont Auvergne, Institut Pascal, CNRS, BP 10448, F-63000 Clermont-Ferrand, France

The classical adjoint-based topology optimization (TO) method, based on the use of a random continuous dielectric function as design variable distribution is known to be one of the timely efficient and fast optimization methods enable a very high performance functional optical devices [1]. It relies on the computation of the gradient of a figure of merit (FOM) with respect to the design parameters. The gradient of the figure of merit (FOM) may then be used to update the design vector element in several scenarios. One of the most common use scenario consists in updating simultaneously all the design parameter vector elements. In a linear problem case involving a simply convex FOM-function shape, utilizing the gradient information, it is a relatively easy and fastly to reach an optimal solution. In the case of constrained and non linear problems stated in an infinite and indeterminate design space, the conventional TO, a local optimizer, may require multiple restarts, with multiple initial points and multiple runs. The algorithm strongly depends on the initial conditions. We report in the paper, a global-like optimizer inspired by a wolves-pack hunting, enabling efficient design of metasurfaces through their geometrical parameters [2]. We apply the method to design a non periodic metasurface consisting of plasmonic metalenses, enabling a high energy flow focusing into a well-defined 2D focus spot. Numerical results show that the proposed inverse design method has a low sensitivity to initial conditions. In our design method of metalens.

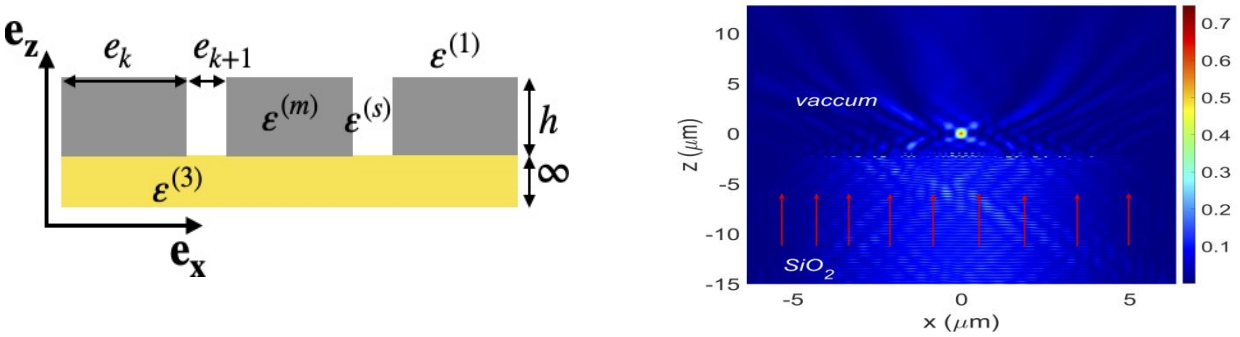

Figure 1 : Design of a plasmonic gold-flat-metalens of d = 12.75μm-wide and 400nm-height, made of 125 gold-nanoridges and air-gap focusing a normal incident TM-polarized plane wave at a wavelength λ = 0.637μm at a distance of 3λ. (Left): Schematic of dispersive metal film perforated with a non periodic subwavelength array of 1D nanoslits. (Rigth): Cartography of the normalized magnetic field intensity.

1. T. Phan, D. Sell, E. W. Wang, S. Doshay, K. Edee, J. Yang, and J. A. Fan, "High-efficiency, large-area, topology-optimized metasurfaces," Light. Sci. Appl., **48**, 2019.
2. K. Edee, "Biomimicry-Gradient-Based Algorithm as Applied to Photonic Devices Design: Inverse Design of Flat Plasmonic Metalenses", Appl. Sci., **11**, 5436, 2021.

Simulation of Various Nanoelectronic Devices Based on 2D Materials

I. Abramov, V. Labunov, N. Kalameitsava, I. Romanova, I. Shcherbakova
Belarusian State University of Informatics and Radioelectronics, Minsk, Belarus, E-mail: nanodev@bsuir.edu.by

The development of field-effect transistors (FETs), resonant-tunneling diodes (RTDs), vertical heterostructures and other device structures on the basis of 2D materials is one of the important tasks for producing a new element base for micro- and nanoelectronics.

The wave function formalism was applied in the development of numerical model of vertical heterostructures based on 2D materials [1, 2]. Combined self-consistent models [3, 4] were adapted for the case of taking into account vertical transport in the conduction zone. The influence of various factors on the electric characteristics of the vertical heterostructures based on graphene, h-BN and MoS_2 was investigated with the use of the developed model. The IV-characteristics of such structures were calculated for different number of layers of 2D materials that forms potential barriers and quantum wells. Comparison of the results of simulation of the investigated structures is carried out.

A numerical combined model based on a self-consistent numerical solution of the Schrödinger and Poisson equations in the active region of the device was used to calculate the IV-characteristics of GaN/AlGaN-based resonant tunneling diodes (RTDs) with vertical transport [5, 6]. The proposed model was used to study the effect of the aluminum concentration in the barriers on the IV-characteristics of the considered RTDs.

The developed quantum drift-diffusion model of field-effect transistors (FET) based on monolayer graphene was described in detail [7, 8]. The model is based on quantum drift-diffusion approximation of carrier transport. Graphene channel is located between top- and back-gate dielectrics. With the use of the model simulation of dual-gate FET with channel width 18 μm was considered. A good agreement with experimental data was carried out for number of applied voltages. Adequacy of the model is confirmed by these calculations.

The programs realizing the proposed models of were included in the nanoelectronic devices simulation system developed at the BSUIR since 1995 [9, 10].

1. I. I. Abramov. "Problems and principles of physics and simulation of micro- and nanoelectronic devices. Part I. Basic positions". J. of nano- and microsystem technique, **8**, pp. 34-37, 2006.
2. I. I. Abramov. *Bases of micro- and nanoelectronic devices simulation*. LAP LAMBERT Academic Publishing, Saarbrücken, Germany, 444 p., 2016. (In Russian).
3. I.I. Abramov, I.A. Goncharenko. "Combined numerical model of a resonant-tunneling diode". Telecommunications and Radio Engineering, **7**, N 3, pp.54-60, 2002. (In Russian).
4. Abramov, I. I., Kolomejtseva, N. V., Labunov, V. A., Romanova, I. A. "Simulation of resonant tunneling devices based on carbon nanomaterials," J. Nanotechnology: development and applications - XXI century, **9**, N 3, pp. 3-11, 2017. (In Russian).
5. I. I. Abramov, I. A. Goncharenko, N. V. Kolomeitseva. "A combined model of a resonant-tunneling diode," Semiconductors, **39**(9), pp. 1102-1109, 2005.
6. I. I. Abramov. "Problems and principles of physics and simulation of micro- and nanoelectronics devices. V. Resonant-tunneling structures," J. of nano- and microsystem technique, **3**, pp. 57-70, 2007. (In Russian).
7. I. I. Abramov, N. V. Kolomeitseva, V. A. Labunov, I. A. Romanova, I.Yu. Shcherbakova. "Influence of gate dielectrics of field-effect graphene transistors on cureent-voltage characteristics". Russian Microelectronics, **50**, N 2, pp. 118-125, 2021.
8. I. I. Abramov, V. A. Labunov, N. V. Kolomeitseva, I. A. Romanova, I.Yu. Shcherbakova. "Simulation of device structures based on graphene using NANODEV system". Minsk: BSU, pp. 256-260, 2020. (in Russian).
9. I.I. Abramov, I.A. Goncharenko, S.A. Ignatenko, A.V. Korolev, E.G. Novik, A.I. Rogachev. "NANODEV: A nanoelectronic-device simulation software system". Russian Microelectronics, **32**, N 2, pp. 97-104, 2003.
10. I.I. Abramov, A.L. Baranoff, I.A. Goncharenko, N.V. Kolomejtseva, Y.L. Bely, I.Y. Shcherbakova. "A nanoelectronic device simulation software system NANODEV: New opportunities". Proc. of SPIE., **7521**, edited by Kamil A. Valiev, Alexander A. Orlikovsky, pp. 75211E1-1-11, 2010.

Accounting for the body effect in the compact modeling of an "extrinsic" MOSFET drain current in the linear and saturation regimes

V. Turin[1], R. Shkarlat[2], V. Poyarkov[2], O. Kshensky[2], G. Zebrev[3], B. Iñiguez[4], M. Shur[5]
1. Orel State University after Ivan Turgenev, Orel, Russia, voturin@ostu.ru
2. JSC "Bolkhov Plant of Semiconductor Devices", Bolkhov, Orel region, Russia, oaobzpp@list.ru.
3. National Research Nuclear University "MEPHI", Moscow, Russia, gizebrev@mephi.ru.
4. Rovira i Virgili University, Tarragona, Spain, benjamin.iniguez@urv.cat.
5. Rensselaer Polytechnic Institute, Troy, NY, USA, shurm@rpi.edu

Compact MOSFET modeling requires smoothing functions describing the transition from the linear to the saturation regime. Our previously proposed smoothing function [1, 2] for an "intrinsic" MOSFET ensures a monotonic decrease of the differential conductance from the maximum value in the linear regime to the minimum value in the saturation regime. Later, we proposed a linear approximation for the "extrinsic" MOSFET drain current dependence on the drain bias in the saturation regime [3] and a nonlinear approximation for the drain current asymptote [4] when the drain bias tends to infinity. Finally, we combined the new smoothing function and the linear approximation for an "extrinsic" MOSFET drain current in the saturation regime to obtain an "extrinsic" compact model for a MOSFET operating in the above threshold regime [5]. In this paper, we generalize this approach to account for the body effect [6], i.e., for the threshold voltage dependence on the body bias applied between the source and the fourth (body) MOSFET terminal.

In earlier generations of MOSFETs, the body doping density was more or less uniform. In that case, the theory predicts that threshold voltage is a sublinear function of the body bias. Modern MOSFETs employ steep retrograde body doping profiles with light doping in a thin surface layer and very heavy doping underneath. The depletion-layer thickness is basically the thickness of the lightly doped region. As a result, modern transistors exhibit a nearly linear relationship between the threshold voltage and the body bias [6]. However, even for the earlier generations of MOSFETs, the threshold voltage dependence on the body bias can be still approximated by a linear function. In this work, we use the linear approximation for the threshold voltage dependence on the body bias and generalize the equations for an "extrinsic" MOSFET drain current dependence on the drain bias in the linear regime and the saturation regime by taking into account the body effect. By the way, we generalize the equation for "extrinsic" saturation current also.

Finally, following [5], we will combine the new smoothing function and the linear approximation for an "extrinsic" MOSFET drain current in the saturation regime, proposed in this work, to obtain an "extrinsic" compact model for a MOSFET operating in the above threshold regime with accounting for the body effect.

1. V.O. Turin, A.V. Sedov. G.I. Zebrev, B. Iñiguez and M.S. Shur. "Intrinsic compact MOSFET model with correct account of positive differential conductance after saturation". Proc. SPIE, **7521**, 75211H, 2009.
2. V. Turin, G. Zebrev, S. Makarov, B. Iñiguez and M. Shur. "The correct account of nonzero differential conductance in the saturation regime in the MOSFET compact model". Int. J. Numer. Model. El., **27**(5-6), pp. 863-874, 2014.
3. V. Turin, et al., "A linear "extrinsic" compact model for short-channel MOSFET drain current asymptotic dependence on drain bias in saturation regime", Proc. SPIE **11022**, 110220H, 2019.
4. V.O. Turin, et al., "A piecewise approximation for short-channel "extrinsic" MOSFET drain current dependence on drain-to-source bias including linear triode, linear saturation and asymptotic saturation regimes", ECS Trans., **90**(1), pp. 101-112, 2019.
5. V.O. Turin, R.S. Shkarlat, G.I. Zebrev, B. Iñiguez and M.S. Shur, "The "extrinsic" compact model of the MOSFET drain current based on a new interpolation expression for the transition between linear and saturation regimes with a monotonic decrease of the differential conductance to a nonzero value," 2020 4th IEEE Electron Devices Technology & Manufacturing Conference (EDTM), pp. 1-4.
6. C. Hu. *Modern Semiconductor Devices for Integrated Circuits*. N.J.: Prentice Hall, 2010.

Program for modeling of semiconductors devices characteristics for SPICE simulation of integrated circuits

M. Vidanov, O. Mikhailov, I. Gainullin
Physical Faculty of Moscow State University, Moscow, Russia, Ivan.Gainullin@physics.msu.ru

The simulation of integrated circuits is of great interest, because of the cost reduction of new circuits development. In SPICE (Simulation Program with Integrated Circuit Emphasis) modeling the compact models are used to describe electrical properties of each device in the circuit. The state-of-the-art models account many of physical factors, which adequately represent electrical properties of single devices. However, in some special cases the parameters for compact models should be precised. The physical measurement of semiconductor devices properties is relatively expensive. Moreover, not all properties or physical regularities of semiconductor devices can be measured directly. Hence, ab-initio modeling of semiconductor devices is of interest. For the ab-initio modeling of semiconductor devices so-called TCAD (Technology Computer Aided Design) programs are used. Modeling of semiconductor devices is rather well established field; there are some commercial TCAD solutions. However, to the best of the authors' knowledge, there are no free TCAD solutions which allow three-dimensional (3D) simulation of semiconductor devices. Moreover, modeling of ballistic transport in devices of ~10 nm topology size is under active investigation now.

We present prototypes of two TCAD programs for modeling of electro-physical properties of semiconductor devices. The first program implements drift-diffusion model [1], for modeling of devices with topological size greater than 100 nm. It uses finite elements method for discretization of drift-diffusion equations [2]. For obtaining of self-consistent solution for electrostatic potential and charge density, the Newton-Raphson iterations are applied. This program was written in C++ language for Linux operating system. We have applied the program prototype to the modeling of current-voltage characteristics of field effect transistor (FET), see fig. 1. The second program is designed to model ballistic transport in nanostructures. It implements NEGF (non-equilibrium Greens functions) method for calculating of electron density and current [3]. While the electrostatic potential accounts the atomic structure of device by means of DFT (Density Functional Theory) calculations. We applied this program for modeling of double-gate MOSFET with 5 nm channel size.

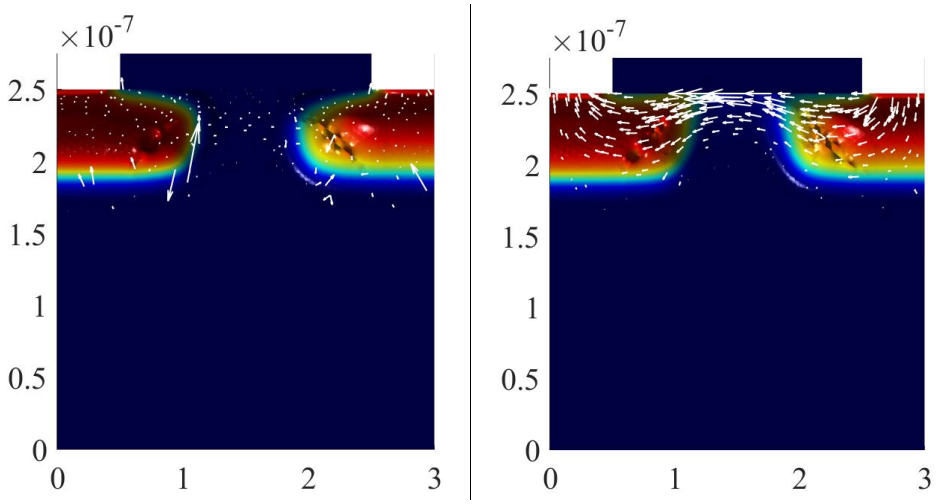

Fig. 1. Electron density distribution and electronic current for FET in closed (left) and open (right) states.

1. D. L. Scharfetter and D. L. Gummel. “Large signal analysis of a silicon Read diode oscillator”. IEEE Transaction on Electron Devices, **ED-16**, p. 64, 1969.
2. C. Tribbia. *3D transient drift-diffusion simulation of semiconductor devices in presence of impact ionization.* PhD thesis, 2016.
3. S. Datta. *Quantum transport: atom to transistor*. Cambridge University Press, Cambridge, 2005.

The influence of charge carrier quantum transport and isoenergy surface anisotropy on the high-frequency conductivity of a semiconductor nanolayer

O.V. Savenko[1], I.A. Kuznetsova[2]
P.G. Demidov Yaroslavl State University, Yaroslavl, Russia,[1]cryak92@mail.ru, [2]kuz@uniyar.ac.ru

In present work, we consider the task about the electrical conductivity of a semiconductor nanolayer placed in an ac-electric field. The nanolayer thickness can be less than the de Broglie wavelength of charge carriers. The quantum theory of transport phenomena is used for solving this problem, which consists in finding the density matrix by solving the Liouville equation. We assume that the charge carrier scattering is elastic and the carrier system deviation from the equilibrium state is small. In this case, the relaxation time can be introduced, which characterizes the volume charge carrier scattering. Surface scattering is viewed through the Soffer boundary conditions [1]. The constant energy surface of widely used semiconductors (silicon, germanium) is a system consisting of several ellipsoids of revolution. In this paper, we propose to consider the case of an ellipsoidal isoenergy surface.

An analytical expression is obtained for the integral conductivity as a function of the following dimensionless quantities: layer thickness, electric field frequency, isoenergy surface ellipticity parameter, chemical potential, and surface roughness parameters. The limiting cases of a degenerate and non-degenerate electron gas are considered. The analysis of the conductivity modulus and argument dependences on the above-mentioned quantities is carried out. We observe oscillations of the conductivity dependences on the layer thickness with a period equal to half the carrier de Broglie wavelength. Oscillations decay with growing surface roughness and thickness parameters. In the case of a nondegenerate electron gas, no oscillations are detected. We discover the oscillations of the conductivity argument dependences on the electric field frequency. In the event of the same roughness parameters, the oscillation period of the frequency conductivity dependences on the thickness is twice that of different roughness parameters.

We establish that the isoenergy surface anisotropy affects the behavior pattern of the conductivity dependences on the thickness and electric field frequency: with raising the ellipticity parameter, the oscillations period of the frequency dependence of the conduction phase decreases. We find that with increasing the ellipticity parameter, surface charge carrier scattering has a smaller effect on the conductivity. This is manifested that quantum oscillations of the conductivity dependences on the thickness are observed at large roughness parameters values.

The theoretical calculations are compared with experimental data for silicon films [2]. In the experimental thickness conductivity dependences, the conductivity of the films sharply drops at thicknesses of the order of 10 nm. This dependence character can be associated with decreasing the allowed energy states number, which can be accessed by charge carriers from the valence band to the conduction band. As a result, the charge carrier concentration declines, which leads to a conductivity decrease with reducing thickness.

1. S.B. Soffer. "Statistical Model for the Size Effect in Electrical Conduction", J. Appl. Phys., **38**, pp. 1710-1715, 1967.
2. V.G. Golubev, L.E. Morozova, A.B. Pevtsov, N.A. Feoktistov. "The conductivity of thin nanocrystalline silicon films", Semiconductors, **33**, pp. 66-68, 1999.

Magnetic properties and hyperfine interactions of iron-borate single crystals and nanoparticles

M. Chuev
Valiev Institute of Physics and Technology of Russian Academy of Sciences, Moscow, Russia, chuev@ftian.ru

Iron borate $FeBO_3$ is a canted easy-plane antiferromagnet with the Neel temperature of about 348 K, which displays specific magnetic, acoustic, optical, and resonance properties and can be used in magnetic memory, magneto-optical and magneto-acoustic transducers, etc. [1]. One of the most perspective applications is to use these crystals in the so-called 'synchrotron Mössbauer source' of a fully recoilless, highly collimated, linearly polarized and single-line radiation of almost natural linewidth [2].

Despite the fact that this material has been investigated for more than half a century, several fundamental problems involving the effects of type (ferro-, ferri- or antiferromagnetic) of the magnetism and morphology (crystalline or nanostructured) of materials are still under consideration [3-5]. In particular, the presentation of the 'synchrotron Mössbauer source' theory turned out to be amateurishly complex and incorrect up to omission of two additional lines in the Mössbauer spectrum [2], which naturally requires correction.

In this presentation we first discuss the development of a correct theory of Mössbauer spectra of an iron borate single crystal and start with a simple, but desperately needed technique of correction of any Mössbauer spectrum for the absorber (crystal) thickness. The corresponding, highly efficient procedure is developed on the basis of previous ideas of the transmission integral deconvolution [6] and the densest possible solution of a spectrum [7]. Then we describe the treatment of the Mössbauer spectra in the framework of the Hamiltonian of combined hyperfine magnetic and quadrupole interaction of nucleus in ground and excited states of nuclei ^{57}Fe. Due to the specific properties of the $FeBO_3$ crystal that the main axis of the electric field gradient is perpendicular to the direction of the hyperfine magnetic field on the nucleus, the solution of the secular equation inherent to the problem appears to be rather simple and reduced to a set of two quadratic equations for the spectral line positions and linear equations for the line intesities. This results in appearance of two additional spectral lines to a conventional magnetic sextet and describes the specific asymmetry of pairs of lines observed in low-temperature experimental spectra of $FeBO_3$ crystals. We discuss also the characteristic difference in the shape of Mössbauer spectra of the $FeBO_3$ single crystal and nanoparticles wherein the latter have been described within the model of magnetic dynamics of antiferromagnetic particles [3, 4].

Finally, we discuss the drastic difference in the shapes of magnetization curves of the $FeBO_3$ single crystal and nanoparticles in the framework of the generalized Stoner-Wohlfart ferromagnetic model [8] which is extended for antiferromagnetic nanoparticles. Such an approach allows one to develop an analytical technique for the numerical evaluation of the magnetic characteristics of the samples studied.

1. R. Diehl, W. Jantz, B.I. Nolang and W. Wettling. "Growth and properties of iron borate, FeBO3". In:, *Current Topics in Material Science*, pp. 241-386, Elsevier Science Publisher, 1984.
2. G.V. Smirnov. "Synchrotron Mössbauer source of 57 Fe radiation". Hyperfine Interact., **125**, pp. 91-112, 2000.
3. M.A.Chuev. "On the thermodynamics of antiferromagnetic nanoparticles by example of Mössbauer spectroscopy". JETP Lett., **95**, pp. 295-301, 2012.
4. M.A. Chuev. "Excitation spectrum of the Néel ensemble of antiferromagnetic nanoparticles as revealed in Mössbauer spectroscopy". Advances in Condensed Matter Physics, **2017**, 6209206 (15 pp.), 2017.
5. M.A. Chuev. "Novel models of magnetic dynamics for characterization of nanoparticles biodegradation in a body from Mössbauer and magnetization measurements". J. Magn. Magn. Mater., **470**, pp. 12-17, 2019.
6. D.G. Rancourt. "Accurate site populations from Mössbauer spectroscopy". Nucl. Instr. Meth. Phys. Res., **B44**, pp. 199-210, 1989.
7. A.M. Afanas'ev and M.A.Chuev. "Discrete forms of Mössbauer spectra". JETP, **80**, pp. 560-567, 1995.
8. M.A.Chuev, J.Hesse. "Nanomagnetism: Extension of the Stoner-Wohlfarth model within Néel's ideas and useful plots". J. Phys.: Condens. Matter, **19**, 506201 (18pp), 2007.

Control of the magnetic properties of metal oxide nanowires by electromagnetic field

K. Tsysar, D.I. Bazhanov, E. Smelova
Lomonosov Moscow State University, 119991, Leninskie gory 1, Moscow, Russia, smelova_k_m@mail.ru

Over the last decades one-dimensional (1D) magnetic nanowires (NWs) have attracted much attention for theoretical and experimental studies due to their unique physical properties [1]. Recent experiments revealed the formation of magnetic oxide nanowires on step edges of a vicinal metal surface [1]. These low-dimensional oxides are very attractive for investigations of their electronic, magnetic and magneto-optical properties. Moreover, oxide nanowires (NW) possess unusual optical properties such the most molecular systems. Thus, appears a new possibility of controlling the magnetic properties of magnetic nanowires using electromagnetic radiation. In present work we represent the results of theoretical study of magneto-optical properties of cobalt oxide nanowires formed at the vicinal platinum surface. Moreover, we investigate the influence of the oxygen concentration in the wire on their magnetic properties. To this purpose we considered two oxidized state of platinum surface: low (0.1 monolayer (ML) oxygen coverage) and high (0.4 ML oxygen coverage) oxidized states. All calculations in present work were made in two stages. At the first, the magnetic properties of oxide nanowires for both oxygen concentrations were studied within the framework of density functional theory in first principle code VASp [2] and then the optical properties of these magnetic systems were investigated following the formulation proposed by Gajdos et al. using the VASP code and the LOPTICS method [3].

Our study revealed that metal oxides wires in low oxidized state are ferromagnetic. However, the ground state of the wire is dependent strongly on the surface geometry. We found, that CoO NW on Pt(332) is FM with magnetic moments of the Co atom $1.5\mu_B$, however, the ground state of oxide wire on Pt(322) surface is antiferromagnetic (AFM) with the same value of magnetic moment of Co atom about $1.5\mu_B$. We found significant decrease of the magnetic properties, up to complete disappearance of magnetism in high oxidized state. Those the local magnetic moments of Co atoms decrease to $0.6\mu_B$ in CoO_2-Pt(332) system and the wire remains FM. In CoO_2 - Pt(322) system we found the complete disappearance of the magnetic properties with magnetic moment of Co atom $0.2\mu_B$, but AFM configuration remains more energetically preferable

Then we have studied the optical properties of CoO and CoO_2 wires on Pt(322) and Pt(332). Surface dielectric anisotropy (SDA) was measured in our work [4]. We found the difference between surface components of the dielectric tensor for FM and AFM oxide nanowires in terahertz range. Moreover, we observed the formation of a singular peak at energy 6eV for clean Pt surface in SDA spectra, the position and polarity of this peak are not specific and do not differ for the two types of step edges. The formation of this peak we associated with the optical response of the step edges as heterogeneities of Pt surface. The singular peak for the unoxidized CoNW-Pt(332) system shifted by 0.1eV to the low-energy region relative to a clean Pt(332) surface; for the CoNW-Pt(322) system, no peak shift was found. In low-oxidized state the small changes in SDA spectra were found. Strong oxidation in 0.4ML in case of CoO_2-Pt(332) system did not lead to a significant change in SDA spectra. At the same time, for the CoO_2-Pt(322) system we found the reverse of the polarity of the SDA peak, the position of the peak does not change in compare to low oxidized states. Thus, in the work, it is possible to find out the relationship between the magnetic and optical properties of nanowires.

1. L.-Y. Ma, et al., J. Phys. Chem. C, **117**, p. 18464, 2013.
2. J. Harl, et al., Phys. Rev. B, **76**, p. 035436, 2007.
3. M. Gajdoš, et al., Phys. Rev. B, **73**, pp. 045112, 2006.
4. D.E. Aspnes, et al., J. Vac. Sci. Technol. A, **6**, p. 1327, 1988.

Nanostructuring at oblique angle deposition

O.S. Trushin[1], A.A. Popov[1], A.N. Pestova[1], L.A. Mazaletsky[1], A.A. Akulov[2], A.A. Lomov[3]
1. Valiev Institute of Physics and Technology of RAS, Yaroslavl Branch,Yaroslavl, Russia, otrushin@gmail.com
2. P.G. Demidov Yaroslavl State University, Yaroslavl.
3. Valiev Institute of Physics and Technology of RAS, Moscow, Russia

A promising method for the formation of films with special properties is their nanostructuring during growth. One of the known technological methods allowing to ensure the growth of nanostructures is an oblique angle deposition. This method of producing films has attracted considerable interest in recent years, and many works are devoted to it [1, 2]. Highly porous conductive thin films might be a promising material for applications in nanocatalysis, nanosensors, as a promising material for ultradense magnetic recording and as an electrode in solid state accumulators. The main goal of this work was comparative study the growth mechanisms of thin films of different metals (Co and Al) by oblique angle deposition and finding optimal conditions for nanostructuring. Experiments on the deposition of metallic films on an inclined substrate were carried out on an Oratoria-9 electron beam evaporation unit. The deposition conditions were the following: base vacuum 4 10^{-6} Torr, electron beam voltage 8 kV, current 0.5 A (for Co films) and 1.2 A (for Al films). A standard single-crystal silicon wafer with a thermal oxide layer 300 nm thick was used as a substrate. As obtained the experimental samples were further subjected to various types of analysis. The cross section of the film and its surface was investigated by scanning electron microscopy (SEM, Supra 40). Besides that the surface morphology was studied using atomic force microscopy (AFM, SMM-2000). Magnetization reversal curves for Co films were measured using vibromagnetometer LakeShore VSM.

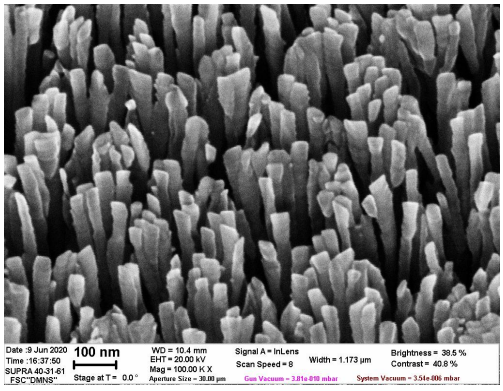

Fig. 1. Top view on the surface of Co film deposited at inclination angle φ=85°.

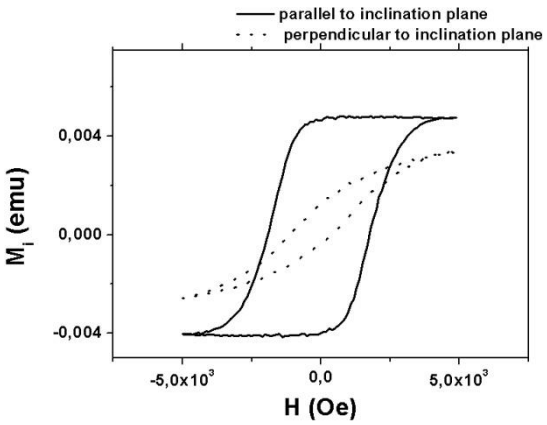

Fig. 2. Magnetization reversal curves for the external field parallel to the substrate surface. Angle of inclination of the substrate φ=80°.

Thus, as a result of the experiments, it was found that at large angles of inclination of the substrate (more than 70°), nanostructuring of aluminum[3] and cobalt films occurs. Optimal nanostructuring conditions are achieved at the substrate tilt angle of 85°.

Reported study was carried out under State Programs #0066-2019-0003 of the Ministry of Science and Higher Education of Russia on the equipment of the center for collective use of the scientific equipment «Diagnostics of micro- and nanostructures».

1. A. Barranco, A. Borras, A.R. Gonzalez-Elipe, A. Palmero, “Perspectives on oblique angle deposition of thin films: From fundamentals to devices”, Progress in Materials Science. **76,** pp. 59-153, 2016.
2. M.M. Hawkeye, M.T. Taschuk, M.J. Brett, *Glancing Angle Deposition of Thin Films*, UK: John Wiley & Sons Ltd, 2014.
3. O.S. Trushin, A. A. Popov, A. N. Pestova, L. A. Mazaletsky, and A.A. Akulov “Nanostructuring at Oblique Angle Deposition of Aluminum”, Technical Physics Letters, **47**, pp. 613–615, 2021.

Development of the four probes method for express diagnostics of unpatterned spin tunnel structures

O.S. Trushin, A.N. Pestova
Valiev Institute of Physics and Technology of RAS, Yaroslavl Branch, 150007, Russia, Yaroslavl, Universitetskaya, 21
otrushin@gmail.com, yablokowa-anastasia@yandex.ru

An experimental stand for express diagnostics of multilayer spin tunnel structures has been developed. The current-in-plane tunneling method (CIPT) requires no processing, is fast, and provides reliable data which are reflective of the deposition only [1]. The stand is based on the four-probe method for measuring resistance at external alternating magnetic field (Figure 1 a). This technique can be applied after only a short processing route, thereby saving time and resources, and reducing the potential for damaging the junction.
Measurements to control the magnetoresistive effects were carried out using probes with different distances between the contacts. The samples for measurements were standard spin tunnel structures provided by Crocus Nanoelectronics [2]. Their tunneling magnetoresistance (TMR) value was estimated using CIPT method on CAPRES equipment to be around 140%.
Figure 1 b shows resistivity versus magnetic field curves for the distances between the contacts of 2.5 mm measured for different orientations of external magnetic field. During the measurement in Figure 1 a, magnetization occurs along the easy magnetization axis. This result is confirmed by earlier studies of the magneto-optical Kerr effect of the same sample.

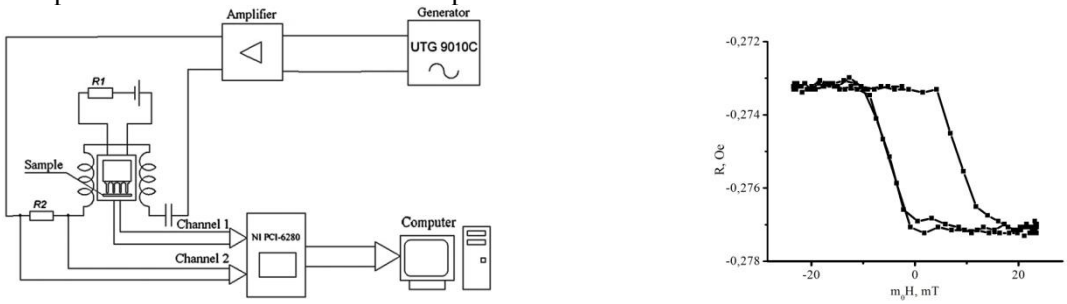

a b

Figure 1. a – Scheme of the stand; b – Hysteresis loop for external magnetic field along the easy axis

At the moment, the stand is designed, assembled and tested on a spin-tunnel structure. This stand has shown its efficiency. Thanks to it, it is possible to carry out express diagnostics of structures for the presence of magnetoresistive effects. Unlike the original version of CIPT method [1, 3] present realization uses relatively large probe spacing (about 1 mm) and high amplitude probe current (about 1A). The measurement of the signal for different sample orientations clearly shows the direction of the easy axis of the structure. It confirms possibility of magnetoresistance measurement at such conditions.

This work was carried out on the equipment of the centre for collective use of scientific equipment "Diagnostics of micro- and nanostructures" within the framework of the State assignment of the P.I. K.A. Valiev RAS Ministry of Education and Science of the Russian Federation on topic No. 0066-2019-0003 "Fundamental and applied research in the field of creating promising instrument nanostructures for storing information on new physical principles".
The work was carried out with the support of the Federal State Budgetary Institution "Fund for Assistance to the Development of Small Forms of Enterprises in the Scientific and Technical Sphere" (contract No. 14947ГУ/2019 dated 20.12.2019).

1. D. Worledge, D.L. Trouilloud. «Magnetoresistance measurements of unpatterned magnetic tunnel junction wafers by Current In-Plane Tunneling». App. Phys. Lett. **83**, P. 84–86, 2003.
2. O.S. Trushin, S.G. Simakin, S.V. Vasiliev, E.A. Smirnov. «Quality Control of a Multilayer Spin-Tunnel Structure with the Use of a Combination of Analytical Methods». Russian Microelectronics, **47**, No. 6, pp. 381–387, 2018.
3. C.L .Peterseny, R. Linz, D.H. Petersenz, P.F. Nielsenz. «Micro-scale sheet resistance measurements on ultra shallow junctions» 2006 14th IEEE International Conference on Advanced Thermal Processing of Semiconductors, 9431599, 2006.

Fabrication of Si structures with extremely angled sidewalls by the modified Bosch process in a controlled manner

O.V. Morozov, S.V. Kurbatov
Yaroslavl Branch of the Valiev Institute of Physics and Technology RAS, Yaroslavl, Russia, moleg1967@yandex.ru

The Bosch process is very popular for dry etching of grooves with close to vertical sidewalls (angle ~90°) to form various silicon microstructures. Although some applications require significant level of sidewall tapering the possibility of achieving much tapered sidewalls is limited. Slight tapering (sidewall angle lie in range 90-85 degrees) can be obtained by manipulating the parameters of the standard Bosch high aspect ratio etching process. But these recipes are poorly suited for etching freestanding structures.

There are few approaches to achieving a larger tapering. One of them is based on adding an isotropic etching step after a certain number of the standard Bosch process cycles. Sidewall angles of 90° to 54° can be reached, but a significant drawback is the specific "taper deviation" effect which is particularly pronounced in structures with larger tapering [1]. Another way is to transfer 3D photoresist patterns to Si. This method is to use the lateral erosion of the etching mask that results in a gradual shrinking of the mask structure. The 3D mask is often forming by grayscale lithography or by thermal reflow of patterned photoresist [2, 3]. Unlike adding an isotropic step precise control over etch selectivity is necessary when transferring method is used.

In this work transferring method is proposed which uses a mask formed by thermal reflow in combination with modified Bosch process to obtain a highly controllable etch selectivity. Modified Bosch process scheme is shown on figure 1. Adjustment of the lateral erosion (Δa) is achieved by adding an oxygen plasma step. If the lateral erosion is kept constant the correct taper like structure with sidewall angle θ may be produced.
Following this concept, we used the technique of process parameter ramping. Ramping the time of an oxygen step from long time to short time was used. Ramping recipes were developed based on our empirical models. Five recipes of parameter ramping was tested to achieve sidewall angle in range of 50° to 30°. As a result the correct taper like structures was obtained (fig. 2). The deviation of the sidewall angles from the model values is no more than ±1°. The ability to control etch selectivity in transferring method can become a powerful tool for developing arbitrary 3D silicon structures.

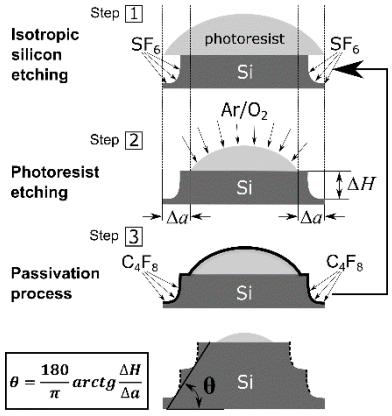

Fig. 1. The modified Bosch process sequence.

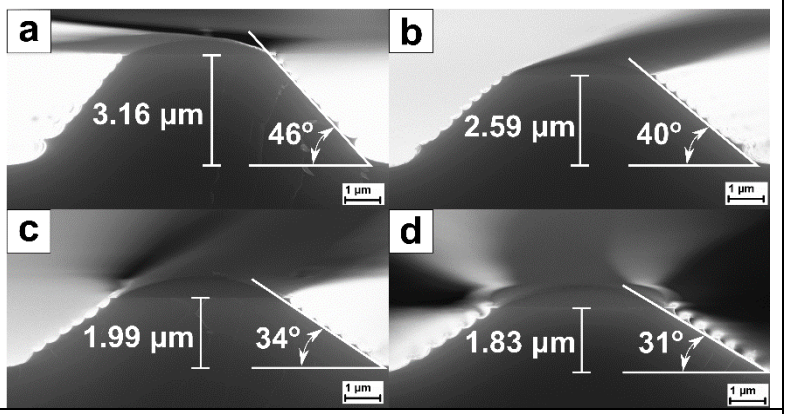

Fig. 2. SEM cross section of fabricated structure profile for target angles: a – 45°, b – 40°, c – 35°, d – 30°.

This work is supported by Program no. 0066-2019-0002 of the Ministry of Science and Higher Education of Russia for Valiev Institute of Physics and Technology of RAS and performed using the equipment of Facilities Sharing Centre “Diagnostics of Micro- and Nanostructures”.

1. Niclas Roxhed, Patrick Griss and Goran Stemme. "A method for tapered deep reactive ion etching using a modified Bosch process". J. Micromech. Microeng., **17**, pp. 1087–1092, 2007.
2. C.M. Waits, B. Morgan, M. Kastantin, R. Ghodssi. "Microfabrication of 3D silicon MEMS structures using gray-scale lithography and deep reactive ion etching". Sensors and Actuators A, **119**, 245–253, 2005.
3. A. Emadi, H. Wu, S. Grabarnik, G. de Graaf and R.F. Wolffenbuttel. "Vertically tapered layers for optical applications fabricated using resist reflow". J. Micromech. Microeng., **19**, 1-9, 2009.

Development and research of a micromechanical accelerometer sensitive element

V.V. Kalugin[1], L.R. Boev[1,2], E.S. Kochurina[1,2], S.A. Anchutin[1,2], A.S. Timoshenkov[1,2]
1. National Research University of Electronic Technology, Zelenograd, Russia, viktor118@mail.ru
2. LMD Ltd., Zelenograd, Russia, ekochurina@mp-lab.ru, leo.boev@mail.ru, step305@mail.ru, at@mp-lab.ru.

Microelectromechanical systems contain silicon sensitive elements (SE) and have a number of significant advantages over the known devices of the same functional purpose, made using traditional technology. The low cost of micromechanical sensors and systems based on them is explained by a high degree of integration, full automation of the manufacturing process based on existing technologies adopted in microelectronics, as well as the possibility of producing devices in large batches. In general, the technology of forming elements of micromechanical systems is based on operations that make up the technology of semiconductor, mainly silicon, devices and integrated circuits (ICs). But it has a number of significant features and problems that have to be taken into account when using typical technological processes for specific micromechanical structures and systems.

The paper describes the design of the developed SE of the micromechanical accelerometer (MMA). The MMA is a direct conversion device. Under the influence of acceleration, the values of the capacitances of the sensing element change. The use of only one technological operation (splicing) makes it possible to reduce technological errors and improve the metrological and operational characteristics of the developed MMA. The use of the anisotropic etching of silicon and modifications of the proposed design make it possible, to obtain sensors of various ranges, with small changes in the technological process (using an additional photomask) [1].

In the manufacture of the SE, in particular the protrusions that form the gap, errors occur due to the anisotropic etching of silicon. As a result of the study, an assessment was made of the influence of such errors on the MMA output signal.

To control the geometric parameters of the bulk parts of the SE after anisotropic etching of silicon, a non-contact method, for example, optical microscopy, can be used. This method allows you to control surface defects up to 1 micron (up to x500). Profilers can be used to control the surface. The information obtained during the processing of profilograms is used to calculate standard parameters and allows for a qualitative and quantitative assessment of the roughness of the investigated surfaces. [2].

1. A.S. Timoshenkov, S.A. Anchutin, E.S. Kochurina, A.S. Musatkin, M.S. Golovinskij, V.V. Kalugin, V.V. Puzikov, S.P. Timoshenkov. “Razrabotka i issledovanie mikromekhanicheskogo akselerometra”. Tekhnosfera, International Forum “Microeletronika 2019” 5th International Scientific Conference “Elektronnaya komponentnaya baza i mikroelektronnye moduli”, pp. 435-437 Collection of abstracts. 2019. (in Russian)
2. Yoshizawa T., Wakayama T, Takano H. Applications of a MEMS scanner to profile measurement. Proc. SPIE, **6762**, pp. 299-307, 2007.

RF MEMS switch with double-clamp and wafer level package with through silicon vias for integration RF MEMS in applications 5G and Internet of Things

A. Tkachenko, I. Lysenko
Southern Federal University, Design Center of the Microelectronic Component Base for Artificial Intelligence Systems, Rostov-on-Don region, Taganrog, Russia, alexeytkachenko@sfedu.ru

Reducing the complexity of the architecture of radio-frequency (RF) systems and subsystems of 5G mobile networks and Internet of Things (IoT) currently requires the presence of passive RF components with very high performance. Considering these requirements, the technology of RF microelectromechanical systems (MEMS) for the development of passive RF devices allows us to solve the corresponding tasks related to the requirements of 5G and IoT, concerning passive components and building blocks.

This work presents the development of one of the main passive RF components at the hardware level, namely a capacitive single-pole single-throw (SPST) RF MEMS switch with double-clamp and wafer level package with through silicon vias. The switch is schematically shown in Fig. 1 and consists of two series-connected capacitive RF MEMS switches with a hybrid contact type and a high capacitance ration [1, 2].

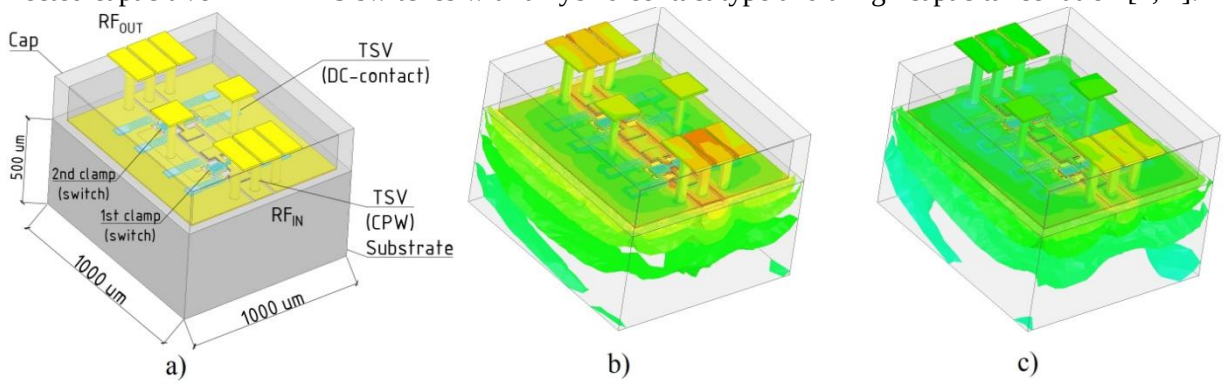

Figure 1. Schematic view of the developed RF MEMS switch with double-clamp:
a) 3D model; b) RF signal distribution in open-state; c) RF signal distribution in close-state.

The proposed RF MEMS switch provides high RF performance in the S-frequency band with isolation of more than -82.5 dB at 3.6 GHz in the close-state and low insertion loss of -0.23 dB at 3.6 GHz in the open-state, which corresponds to the main frequency range of 5G NR FR1 (below 6 GHz). In addition, the presented switch is characterized by a low activation voltage of 3.5 V and a switching time of 6.3 us.

Wafer level package using through silicon vias is used to redistribute electrical signals from the built-in passive RF MEMS device to other RF systems or subsystems, which makes such an integrated solution suitable for use in devices and systems of 5G mobile networks and IoT, as well as many wireless communication systems, space systems and satellites.

The work was carried out at the expense of funds, task No. FENW-2020-0022 for the implementation of scientific research carrying out scientific research at the expense of the Federal budget, in terms of scientific activities on the topic "Development and research of methods and means of monitoring, diagnostics and forecasting state of engineering objects based on artificial intelligence".

1. A.V. Tkachenko, I.E Lysenko. *High capacitance ratio radio-frequency micromechanical switch*. Problems of Advanced Micro- and Nanoelectronic Systems Development, **3**, pp. 237-243, 2020.
2. I.E. Lysenko, A.V. Tkachenko, O.A. Ezhova, D.V. Naymenko. *Designing high-performance radio-frequency micromechanical switches*. Nanoindustriya. Specvypusk 2020 (5s, v. 13 (102)). Mikrosistemy. Sensory i aktyuatory, pp. 527-541, 2020. (in Russian)

Reliability issues for electrostatically actuated MEMS switch

I.V. Uvarov, M.O. Izyumov, I.I. Amirov
Valiev Institute of Physics and Technology RAS, Yaroslavl Branch, Yaroslavl, Russia, i.v.uvarov@bk.ru

Microelectromechanical systems (MEMS) switches are attractive for advanced radio frequency and microwave systems due to their promising working characteristics [1]. However, low reliability limits the application of these devices. For two decades of research, many reliability aspects have been successfully overcome, but some of them received little attention. This work describes a failure mechanism of an electrostatically actuated MEMS switch due to the migration of adhesive material in a dielectric substrate. The phenomenon is demonstrated for the switch shown in Fig. 1. The movable electrode is a 100 μm long Al beam attached to the anchors by torsion hinges. The gate and drain electrodes are made of Au or Pt and located under the each arm of the beam. They are deposited onto the SiO_2 substrate with a 10 nm thick Cr adhesion layer. When the driving voltage is applied to the gate, the beam tilts under the electrostatic force and touches the drain, turning the switch on. When the voltage is removed, the beam returns to the initial state under the elastic force of the hinges. In case of stiction, the voltage is applied to the opposite gate, thereby creating an additional force that breaks the contact.

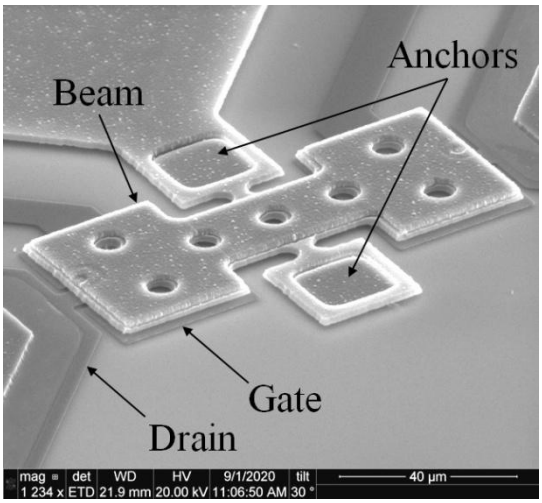

Fig. 1. SEM image of the switch.

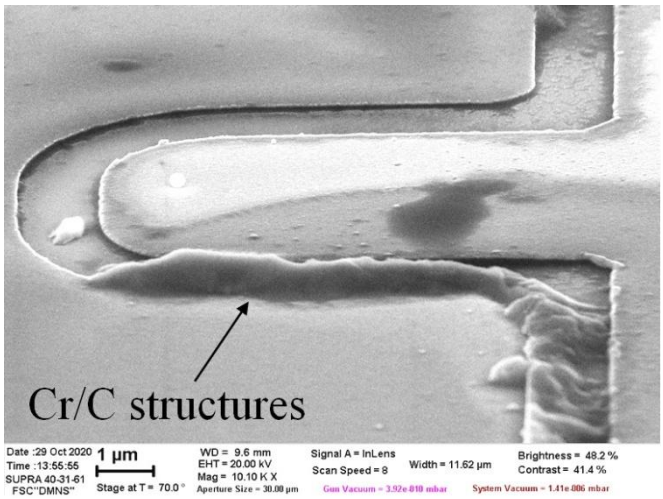

Fig. 2. The structures formed between the electrodes.

The switch fails after 10^2-10^5 actuation cycles due to stiction or short circuiting between the beam and gate, which was not observed previously [2]. The experiments performed at the samples with the removed beam revealed that nanoscale structures consisting of Cr and C appear at the gate. The structures grow and coalesce into micron-sized formations shown in Fig. 2. The beam touches them during operation and the device breaks down. The material transfer takes place not only in the gap between the electrodes, but also around the gate and its connecting line, where Cr and C agglomerate into spots and droplets. In addition, the adhesive material migrates under the Au and Pt films, causing the delamination of electrodes from the substrate. A possible explanation of the described effect is the drift of Cr at the SiO_2 surface under electric field. Chromium is widely used in microtechnology, but the field-induced migration was not reported previously. To all appearance, it became possible due to the features of the fabrication process. The conditions for the migration must be clarified in order to avoid this reliability issue for MEMS switches and other microfabricated devices.

This work was supported by the grant of President of the Russian Federation № MK-945.2021.4 and the program No. 0066-2019-0002 of the Ministry of Science and Higher Education of Russia for Valiev Institute of Physics and Technology of RAS. The study is performed using the equipment of Facilities Sharing Centre “Diagnostics of Micro- and Nanostructures”.

1. G.M. Rebeiz. *RF MEMS: theory, design, and technology*. John Willey and Sons, Inc., New Jersey, 2003.
2. I.V. Uvarov and A.N. Kupriyanov. "Stiction-protected MEMS switch with low actuation voltage". Microsyst. Technol., **25**, pp. 3243-3251, 2019.

A fast membrane actuator in the current stabilization regime

I.V. Uvarov[1], A.E. Melenev[2], V.B. Svetovoy[3]
1. Valiev Institute of Physics and Technology RAS, Yaroslavl Branch, Yaroslavl, Russia, i.v.uvarov@bk.ru
2. Research and Production Center "Research Institute for Microdevices", Zelenograd, Russia, timon_man@mail.ru
3. A.N. Frumkin Institute of Physical Chemistry and Electrochemistry RAS, Moscow, Russia, svetovoy@yandex.ru

Microfluidic systems require a compact and microtechnology-compatible actuator with low power consumption to drive pumps and valves. Electrochemical devices meet these criteria, but long time needed to terminate the gas makes them rather slow. Recently a novel actuator was demonstrated [1], which works several orders of magnitude faster than the conventional devices based on the DC electrolysis. The actuator is shown in Fig. 1. A main part of the device is a working chamber of 500 μm in diameter and 16 μm in height. The chamber is sealed by a 30 μm thick polydimethylsiloxane membrane and contains concentric titanium electrodes. Short voltage pulses of alternating polarity (AP) applied to the electrodes generate nanobubbles in the chamber. They push the flexible membrane up, and then disappear in milliseconds due to spontaneous combustion of hydrogen and oxygen. Periodic switching the pulses on and off creates reciprocating movement of the membrane with a frequency up to 1000 Hz. However, degradation of the electrodes suppresses the gas production and reduces the stroke in few minutes. This work describes a method to improve performance of the fast actuator.

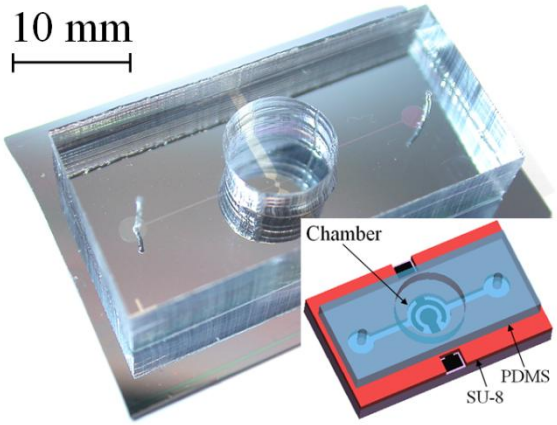

Fig. 1. A photo and schematic illustration of the fast electrochemical actuator.

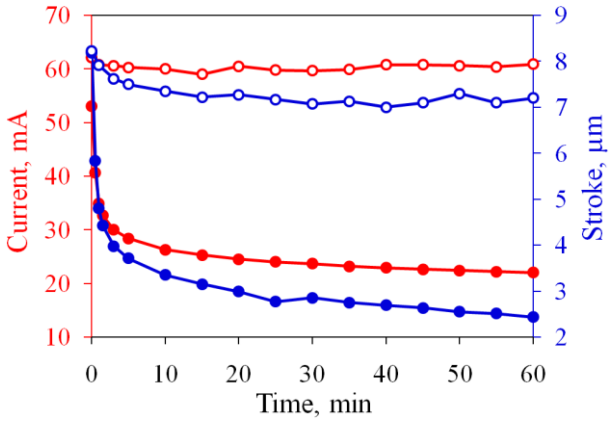

Fig. 2. Time dependence of the average current and stroke for standard and new working regimes (filled and open markers, respectively).

In a standard working regime, the voltage is turned off between the series of AP pulses. The electrodes are oxidized during operation, which reduces the current flowing through the electrochemical cell and the membrane deflection, as shown in Fig. 2. We propose a new regime, in which the passive time is filled with single polarity (SP) pulses [2]. A series of SP pulses reduces titanium from the oxide at the cathode. Thinning of the oxide layer lowers the resistance of the cell, which increases the current during the subsequent AP series. This regime is implemented using a specially developed generator of pulses. The generator applies a series of AP pulses to the electrodes, measures the average current and compares it to the target value. Then it adjusts the amplitude of SP pulses so that in the next series the current approaches this value. After a certain number of series, the current reaches the required level. As a result, the actuator keeps high performance during long-term operation, as shown in Fig. 2. However, the price for this is a certain increase in power consumption. In this work, a new regime is investigated in detail.

The study was supported by the Russian Science Foundation, Grant No. 18-79-10038, and performed using the equipment of Facilities Sharing Centre "Diagnostics of Micro- and Nanostructures".

1. I.V. Uvarov, M.V. Lokhanin, A.V. Postnikov, A.E. Melenev and V.B. Svetovoy. "Electrochemical membrane microactuator with a millisecond response time" // Sens. Actuators B, **260**, pp. 12-20, 2018.
2. I.V. Uvarov, A.E. Melenev, R.V. Selyukov and V.B. Svetovoy. " Improving the performance of the fast electrochemical actuator" // Sens. Actuators A, **315**, 112346, 2020.

Analysis of digital elevation models of silicon wafers and wafer-based structures

A. Dedkova[1*], I. Florinsky[2**], N. Djuzhev[1]

*1. National Research University of Electronic Technology (MIET), Zelenograd, Russia, *dedkova@ckp-miet.ru*

*2. Institute of Mathematical Problems of Biology Keldysh Institute of Applied Mathematics, Russian Academy of Sciences, Pushchino, Russia, **iflor@mail.ru*

Surface topography analysis of wafers and wafer-based structures with nano- and micrometer-range elevation differences is an important step in microelectronics production, because it allows one to determine their deformation, to estimate mechanical stresses, to assess quality of applied films, to analyze defects, etc. To get the most information about the objects under study, it is worth analyzing not only a digital elevation model (DEM) of the surface itself, but also variables calculated from a DEM, considering the wafer surface as a whole.

The aim of this research was to develop techniques for studying wafers and wafer-based structures using optical methods of measurement and surface analysis (in particular, optical interferometry) to calculate maps of various types of curvature and subsequent surface analysis using these maps.

We analyzed three approaches to calculation of wafer surface curvature from DEMs. The first approach is based on the analysis of wafer surface profiles using polynomial approximation; calculation of curvature and radius of curvature is based on the definition of a curve's curvature. The second approach is based on the derivation of the second partial derivatives from a DEM presented in the Cartesian or cylindrical coordinate systems. The third approach uses mathematical apparatus of differential geometry and experience of geomorphometry allowing one to determine convex and concave areas of a wafer surface and to perform an analysis of the complete system of surface curvatures.

For implementation of these approaches (Fig. 1), we used DEMs of circular wafers and wafer-based structures with diameters of 100 mm and 150 mm with an elevation difference ranging from 5 μm to 45 μm, as well as DEMs of parts of structures with sizes ranging from 47×63 μm and more with an elevation difference of nanometer range and higher. DEM grid spacing (resolution) ranges from 98 nm to 57 μm.

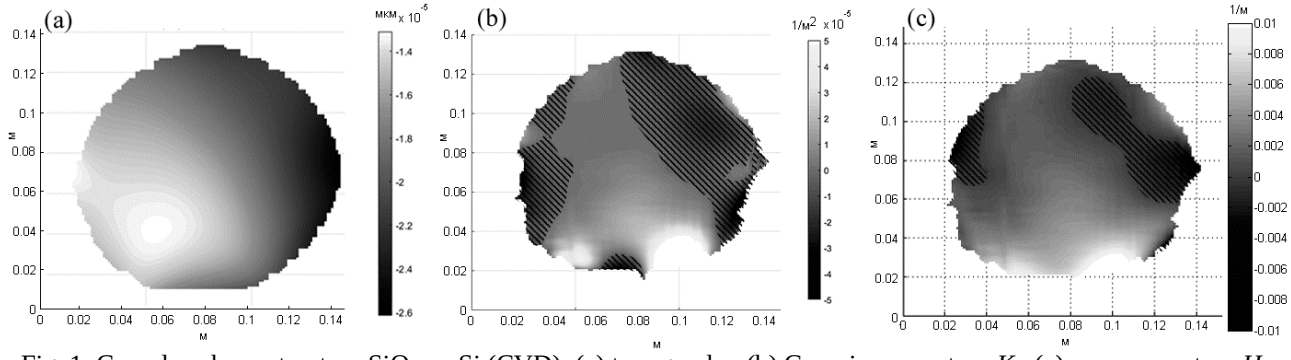

Fig. 1. Complex shape structure SiO_2 on Si (CVD): (a) topography, (b) Gaussian curvature K , (c) mean curvature H; hatching shows $K < 0$ (saddle area) и $H < 0$ (concave area).

Such studies are valuable for analyzing structures with complex shapes, quantifying and localizing irregularities, and subsequent calculations of mechanical stresses in films on wafers. The analysis of different types of curvatures allows one to analyze structures of complex (nonspherical) shape (Fig. 1), to better visualize areas of linear defects (folds and cracks), local convexities and depressions (including defects), and to visualize areas of cracking.

The study was performed with equipment of the R&D Center "MEMSEC" (MIET).

Monolayer and submonolayer films properties investigation using X-ray photoelectron spectroscopy

V. Afanas'ev, L. Lobanova, D. Selyakov, M. Semenov-Shefov
National Research University «Moscow Power Engineering Institute», Moscow, Russia, v.af@mail.ru

Results of theoretical and experimental surface layers (thickness ranges of 0.1-1 angstroms) investigation via X-ray photoelectron spectroscopy (XPS) peak shape analysis are presented. Direct application of traditional XPS methodology [1] and Straight Line Approximation [2] could significantly affect thickness determination measurement accuracy. XPS measurements of submonolayer gold coatings on silicon substrate were carried out on two installations: (1) SPECS installation with an energy analyzer capable of recording XPS spectra of photoelectrons emitted in the angular range from 27 to 75 degrees, and (2) KRATOS installation rotating the target to register XPS spectra at angles close to the normal and angles that are about 70 degrees with the normal.

The experimental data processing was carried out on the basis of the methods presented in the works [3, 4, 5]. Calculations consistently showed a decrease in coating thicknesses with an increase in the viewing angle relative to the normal. Similar measurements of the thicknesses of plane-parallel, uniform coatings led to the same thickness, independent of the viewing angle.

The observed effect is described on the basis of a parallelogram island coverage model. This model made it possible to observe the change in the path length distribution function (PLDF) of the emitted photoelectrons depending on the viewing angle. PLDF determines the intensity ratio of the coating and the substrate XPS signals.

Results obtained indicate that a series of experiments with angular resolution should be carried out to determine the average effective coating thickness. The value of the critical viewing angle, after which the thickness data are stabilized, is determined by the density distribution of the islands.

1. Hoffman S. Auger and X-Ray Photoelectron Spectroscopy in Material Science (Berlin, Heidelberg: Springer Berlin Heidelberg), p. 528, 2013.
2. Jablonski A., Zemek J. Overlayer thickness determination by XPS using the multiline approach, **41**, pp. 193–204, 2009.
3. Powell C., Jablonski A. Progress in Quantitative Surface Analysis by X-ray Photoelectron Spectroscopy: Current Status and Perspectives, Journal of Electron Spectroscopy and Related Phenomena, 2009.
4. Jablonski A. Surface Science, **688**, p. 14, 2019.
5. Afanas'ev V.P., Efremenko D.S., Kaplya P.S. Determination of the Thickness of Nanofilms Using X-Ray Photoelectron Spectroscopy. J. Surf. Invest.: X-Ray, Synchrotron Neutron Tech., **12**, pp. 1182–1189, 2018.

Modification of Bounded J-Ramp Method to monitor reliability and charge degradation of gate dielectric of MIS devices

D.V. Andreev[1], V.M. Maslovsky[2], V.V. Andreev[1], A.A. Stolyarov[1]
1. Bauman Moscow State Technical University, the Kaluga branch, Kaluga, Russia, vladimir_andreev@bmstu.ru
2. Moscow Institute of Physics and Technology (State University), Dolgoprudnyi, Moscow region, Russia, acdmaslovsky@mail.ru

Nowadays in order to monitor quality and defectiveness of the gate dielectric of metal-insulator-semiconductor (MIS) structures, methods of time depend dielectric breakdown (TDDB) are extensively used [1-5]. Under conditions of series manufacturing to monitor quality of the gate dielectric, quality control is normally implemented at semiconductor wafer stage what is in accordance with standards called wafer level reliability monitoring (WLR) [1, 2]. In that case a test procedure and corresponding test methods are usually chosen on the basis of JEDEC standards [2]. One of the suggested techniques is bounded J-Ramp technique. This method assumes to increase density of high-field injection current up to a set level (J_{bound}) and maintain it until the sample breakdown. In accordance with this method after the injection current reaches the set value, each subsequent step contributes approximately the same charge to the total value of charge injected until the breakdown (Q_{bd}) what significantly lowers a dependence of measurements on utilized test equipment. Because of these reasons, the method is the most appropriate to be applied for comparison of Q_{bd} values. One of the major disadvantages of bounded J-Ramp technique is a complexity in monitoring a change of charge state of the gate dielectric at steps corresponding to the current increase. Thus, modification of this method, aimed to enhance its functional capabilities and increase informativeness, is an important task for wafer-level testing of thin dielectrics.

This paper suggests a novel method to control quality and reliability of thin dielectric films of the gate dielectric. The proposed method is based on a modification of bounded J-Ramp. This technique, besides the control of charge injected into the gate dielectric until its breakdown, gives a capability to monitor a change of charge state of the gate dielectric during all the test procedure. In order to implement this, after ending of a test (current) step we switch the test current to the measurement current level (J_m) for a short time period and this allows to monitor the voltage change across MIS structure at the constant measurement current density. The current density J_m is chosen to meet the condition that at this level a significant charge degradation of the dielectric should not be observed. Besides, the switches to measurement level should not greatly influence on bounded J-ramp test procedure. The modified J-ramp method proposes to monitor amount of injected charge, at which irreversible degradation of MIS device characteristics takes place (Q_{deg}), and evaluate reliability of the dielectric film on the basis of statistical measurements of these quantities.

1. A. Strong, E. Wu, R. Vollertsen, J. Sune, G. Rosa, S. Rauch, T. Sullivan. *Reliability Wearout Mechanisms in Advanced CMOS Technologies*. IEEE Press Series on Microelectronic Systems. Wiley, 2009.
2. JEDEC Standard, JESD35–A: *Procedure for the Wafer–Level Testing of Thin Dielectrics*. (2001).
3. V.V. Andreev, G.G. Bondarenko, V.M. Maslovsky, A.A. Stolyarov, D.V. Andreev. "Control current stress technique for the investigation of gate dielectrics of MIS devices". Phys. Status Solidi C. **12**, pp. 299–303, 2015.
4. V.V. Andreev, V.M. Maslovsky, D.V. Andreev, A.A. Stolyarov. "Method of stress and measurement modes for research of thin dielectric films of MIS structures". Proc. SPIE, International Conference on Micro- and Nano-Electronics 2016, **10224**, p. 1022429 (1-8), 2016.
5. V.V. Andreev, V.M. Maslovsky, D.V. Andreev, A.A. Stolyarov. "Charge effects in dielectric films of MIS structures being under high-field injection of electrons at ionizing radiation". Proc. SPIE, International Conference on Micro- and Nano-Electronics 2018, **11022**, p. 1022429 (1-7), 2019.

Research methodic of the field transistors high frequency parameters using network analyzer

T. Krupkina[1], V. Losev[1], A. Khlybov[1], D. Rodionov[1], E. Kotlyarov[2], P. Timoshenkov[1]
1. National Research University of Electronic Technology (MIET), krupkina@miee.ru, dsd@miee.ru, alex1818@yandex.ru, denis.rodionov@gmail.com, cator@yandex.ru .
2.Molecular Electronics Research Institute (MERI), ekotlyarov86@gmail.com

Continuous increasing of the RF/MW device work frequencies and dynamic bands (3G, 4G, 5G, LTE) requires to use high precision metrological equipment for performance and parameters determination. Vector network analyzer (VNA) is one of the necessary devices. Today such analyzers are the most complex equipment for MW systems characterization. Modern VNAs combine the newest advantages in the fields of low-noise sources and receivers, matches MW paths, digital signal processing, sweep generators [1].

Radio frequency and microwave circuits characterization requires apply travelling wave approach to device under test. It's realized in VNA [2]. This approach required to know incident and reflected wave power values. The ratio of these power values allows to determine S-parameters matrix elements [3]. Modern VNAs allow to determine S-parameters in wide frequency bands (up to 120GHz), create Smith charts, measure amplitude and phase parameters of active and passive RF/MW devices.

Test transistor structure S-parameters measurement is used for get RF/MW integrated circuit dynamic characteristic. Measurement results allow to determine transistor frequency characteristics and to predict integrated circuit frequency characteristics. Transistor dynamic parameters characterized by maximum unity current gain (f_T) and maximum unity power gain (f_{MAX}). First value (f_T) determines as frequency where current gain is equal to 1. Second value (f_{MAX}) determines as frequency where power gain is equal to 1. Parameter S_{21} is power gain coefficient. Frequency with 0dBm S_{21} value is the transistor maximum power gain frequency on 50Ohm load.

Authors have got simple analytical expression that contains measured maximum frequency value and some other transistor parameters:

$$f_{MAX} = \frac{g}{2\pi(C_{gs} + 2C_{gd})} \cdot \left(2 - \frac{1}{gR_L}\right) \quad (1)$$

where: C_{gs} is the gate-source capacitance, C_{gd} is the gate-drain capacitance, R_L=50Ohm is the VNA ports input impedance; g is a transistor transconductance.

Authors have done S_{21} measurement of the double-gate *GaAs HEMT* test transistor with 150um overall gate width. Unity current gain frequency (f_{MAX}) value after this measurement shows good agreements with the value calculated using expression (1) (measurements – 26.32GHz, expression (1) – 27.42GHz).

It was shown that measured f_{MAX} value can be used for maximum unity current gain frequency (f_T) calculation. It was pointed that $f_{MAX} < 2f_T$. Authors formulate requirements for test transistor parameters for current f_{MAX} measurements.

The study was supported by a grant from the RFBR (project No. 19-07-00541).

1. M. Hiebel "Fundamentals of Vector Network Analysis", Rohde & Schwartz, 3rd edition, 2008.
2. R. B. Marks, D. F. Williams "A General Waveguide Circuit Theory", National Institute of Standarts and Technology, Boulder, CO 80303, 1992.
3. J. A. Dobrowolski "Microwave Network Design Using the Scattering Matrix", Artech House, 2010.

Calibration of step height standards in sub-micrometer range using three-dimensional reconstruction method in a scanning electron microscope

V.B. Mityukhlyaev, V.G. Maslov
Center for Surface and Vacuum Research (NICPV), Moscow, Russia, e-mail: vbm@nicpv.ru

Step height standards (SHS) are used for calibrating of stylus and optical profilometers and probe microscopes. In order to achieve the traceability of measurements in the process of calibration, probe microscopes combined with a laser interferometer are usually used. These measuring instruments are quite unique and expensive. We propose the alternative approach to solve the problem of SHS calibration, which is based on the use of the advanced three-dimensional reconstruction method (3D-SEM reconstruction method) using stereo images obtained in a scanning electron microscope (SEM).

The measurement method is based on the use of:
- a comparison measure from a single-crystal silicon, containing protrusions of approximately the same height as for the SHS;
- stylus profilometer D-600 for measurements in comparator mode;
- S-4800 scanning electron microscope for performing measurements in three-dimensional reconstruction mode, using specimen tilt of ±15°.

According to the proposed method, at first the ***K*** ratio of the step heights for the SHS and the comparison measure is measured using stylus profilometer D-600 in the comparator mode. Then, using 3D-SEM reconstruction method, the step height ***h*** of the comparison measure is determined. At last, the step height value ***H*** for the SHS is calculated by the equation

$$H = h \cdot K \qquad (1)$$

Conventional 3D-SEM reconstruction method, proposed in 1973 [1], deals with difficulties in processing of stereo images for precise measurements of SHS, since the high quality of surface treatment for this type of objects leads to the absence of contrasting elements in SEM images. So measurement of parallax value [2] in the process of 3-D reconstruction can be subjected to large error. Besides, apart from SEM magnification calibration, calibration of the specimen stage tilt is also necessary. To reduce the measurement error associated with the parallax measurement, a gold film of 2 nm thick was deposited on the comparison measure by magnetron sputtering followed by annealing in vacuum at a temperature of 300°C for 30 min to form contrast elements [3]. Calibration of the SEM magnification was carried out according to the method described in [4] and made it possible to achieve a relative error of magnification calibration of less than 0,14%.

For calibration of the tilt angle of the sample stage, a He-Ne laser, a flat mirror and a prism with a calibrated angle of 30° were used. An optical scheme for measuring the tilt of the sample stage with a nominal value of 30° is proposed, which made it possible to achieve the measurement error of the tilt angle of about 0,03°.

The calibration of SHS with a nominal height value of 450 nm was carried out; different sources of error were analyzed. It was shown that it is possible to achieve the measurement error less than 2 nm.

1. G.Piazzesi. "Photogrammetry with the scanning electron microscope" J. Phys. E: Sci. Instrum., **6**, pp.392-396, 1973.
2. F. Marinello, P. Bariani, E. Savio, A. Horsewell, and L. De. Chiffre. "Critical factors in SEM 3D stereo microscopy". Meas. Sci. Technol., **19**, pp.065705-1-065705-12, 2008.
3. A.Yu. Kuzin, A.L. Vasil'ev, D.A. Karabanov, V.B. Mityukhlyaev, A.A. Mikhutkin, M.Yu. Presnyakov, P.A. Todua, and M.N. Filippov. "Experimental study of three-dimensional reconstruction of relief structures from stereo images obtained in a scanning electron microscope". Measurement Techniques, **59**, pp.817-821, 2016.
4. R.V. Kirtaev, A.Yu. Kuzin, V.G. Maslov, V.B. Mityukhlyaev, P.A. Todua, and M.N. Filippov. "Calibration of scanning electron microscopes over a wide range of magnification". Measurement Techniques, **59**, pp.1245-1249, 2017.

Regularities of interaction of a silicon surface in a fluoroform medium

A. Efremov, D. Murin, S. Pivovarenok, D. Sitanov, A. Malyugin, A. Bobylev
Ivanovo State University of Chemistry & Technology, Ivanovo, Russia, dim86@mail.ru.

Currently, fluorine-hydrogen-carbon gas systems ($C_xH_yF_z$: CF_4, CHF_3, CH_2F_2, CH_3F) are promising plasma-forming media for etching semiconductors, in particular silicon. In this work, fluoroform, trifluoromethane or R-23 freon was used as a plasma-forming gas for silicon etching, which dissociates under plasma conditions with the formation of fluorine and hydrogen atoms. Fluorine atoms directly interact with the material, and the role of hydrogen particles is reduced to surface restoration and / or the so-called "polishing etching". Effective implementation and optimization of plasma processes requires knowledge of the relationship between the external parameters of the plasma, its parameters and composition. One of the main non-disturbing methods of obtaining such information is optical emission spectroscopy (OES). In addition, one of the important aspects of plasma-chemical etching is the quality index of the resulting surface. From the point of view of studying the relief, one of the most promising methods of surface control is atomic force microscopy.

The objectives of this work were: 1) control of the kinetics of plasma etching by the radiation of active particles and interaction products by the non-disturbing OES method; 2) identification of the regularity of changes in the surface roughness (as an indicator of the quality of processing) of silicon after etching in the HF plasma of freon CHF_3, for further application of the results obtained in the technology of forming the topology on the surface of semiconductors.

Experiments on the study of plasma parameters were carried out in a planar-type inductively coupled plasma (ICP) reactor (Platran-100KhT installation (13.56 MHz)). Freon R-23 (CHF_3) was used as a plasma-forming gas in this work. Freon R-23 (CHF_3) was taken from cylinders with the "pure" grade (MRTU 51-77-66), the main gas content was not less than 99.985%. The external (set) plasma parameters were the input power (200 ÷ 1250 W), the displacement potential (0 ÷ -107 V), the gas pressure (1 ÷ 10 mTorr), and the sample temperature (20 ÷ 300^{o}C). The etching time varied from 40 seconds to 3 minutes. Samples of the investigated semiconductor material were cut from a silicon wafer (S ~ 1 cm^2). Before being placed in the reactor, the surface of the samples was cleaned from oil, dust, and grease in toluene and acetone. The etching rate was determined by the gravimetric method by weighing the samples before and after treatment in plasma on an electronic analytical balance CAUW 120 D. Spectral measurements were carried out using fiber-optic spectrometers AvaSpec 2048 and AvaSpec 3648, operating wavelength range 200–1000 nm. The surface relief of the processed samples was monitored using a Solver P47-PRO atomic force microscope.

As a result of this work, we obtained and analyzed the emission spectra of the RF discharge plasma of the freon R-23 during silicon etching. It is shown that the radiation of an RF discharge plasma is represented by atomic and molecular components. It is assumed that the dependences of the intensities of lines and bands on the external conditions of the discharge are determined by the excitation of emitting states during direct electron collisions. Moreover, their behavior is in good agreement with the nature of the dependences of the etching rate under the same conditions. The analysis of the surface of the obtained samples was carried out using atomic force microscopy. The average roughness values of the investigated samples were calculated. The data obtained contribute to the development of modern plasma chemistry, namely, they establish the relationship between the external parameters of the plasma, its internal characteristics and composition; and propose the optimal modes of carrying out the processes of plasma-chemical and reactive-ion etching and the organization of non-disturbing spectral control methods.

The work was carried out within the framework of the state assignment for research, topic no. FZZW-2020-0007.

Bifurcations and catastrophes at the boundaries separating the phases of quantum correlations

M.A. Yurischev
Institute of Problems of Chemical Physics of the Russian Academy of Sciences, Chernogolovka, Moscow Region, 142432 Russia, E-mail address: yur@itp.ac.ru

When crossing the boundary from a region with a stationary optimal measurement angle (0 or $\pi/2$) to the region with a variable angle of optimal measurement ($0 < \vartheta < \pi/2$), quantum discord and one-way quantum work deficit experience a sudden change ('catastrophe') in their behavior [1]. The sudden change is accompanied by a splitting of the minimum characterizing stationary point of quantum correlation into two minima (i.e., bifurcation of the initial single minimum occurs). Such phenomena are analogous to phase transitions described within the Landau approach, or, more generally, by the mathematical formalism of catastrophe theory [2].

In the talk, both phenomena will be discussed using the example of a spin system in a state of thermal equilibrium.

This work was performed as a part of the program CITIS.

1. M.A. Yurischev. "Temperature-field phase diagrams of one-way quantum work deficit in two-qubit XXZ spin systems ". Quantum Inf. Process., **19**:110, 23 pp., 2020.
2. V.I. Arnold, Catastrophe Theory, Springer, Berlin, 1992.

On the control of the spread of quantum information in multiple quantum NMR spectroscopy of solids

V.E. Zobov[1] and A.A. Lundin[2]
1. Kirensky Institute of Physics, Federal Research Center KSC SB RAS, Krasnoyarsk, 660036 Russia
e-mail: zobov.ve@gmail.com.
2. Semenov Institute of Chemical Physics, Russian Academy of Sciences, Moscow, 117977 Russia
e-mail: ya-andylun2012@yandex.ru

The system of nuclear magnetic moments (spins) of a solid observed by NMR methods is a good example of a closed system. As is known, in a closed system, quantum information is stored with time. Wherein, in the process of time evolution, single-spin correlations turn into multiple-spin correlations due to dipole-dipole interactions. Multiple quantum (MQ) NMR spectroscopy of solids [1] allows us to observe this process and even control it by changing the duration of the intervals of forward and reverse evolutions in time. The form of the MQ spectrum describing the dependence of the intensities of the components on their coherence orders *M* is well described by the Gaussian distribution, the second moment $< M^2 >$ of which determines the average size $\bar{K}$ of the cluster of correlated spins $< M^2 >= \bar{K}/2$. Usually, the value $\bar{K}$ from the experimental MQ spectrum is determined through the value of the coherence order M_e, at which the MQ spectrum decreases by "*e*" times. For the Gaussian function $\bar{K} = 2M_e^2$. Crystalline solids such as adamantane and fluorite show rapid growth $\bar{K}$ over time, which is well described by an exponential function $\bar{K}(t) = \exp(at)$. At long times, growth slows down due to decoherence processes, in particular, due to the imperfection of the applied pulse sequence and the created effective Hamiltonian. The authors of [2] proposed introducing a controlled perturbation into the effective Hamiltonian. By changing the magnitude of the perturbation, experimenters were able to control the spread of quantum information and the average size $\bar{K}$. The estimation of the dependence of the stationary value of the size $\bar{K}$ on the magnitude of the perturbation was carried out in [3]. The authors proposed a model with diffusion growth of clusters, in which they took into account their size *K* distribution and the dependence on *K* of the rate of cluster degradation caused by perturbation. In [4] and in earlier works, we showed that, in addition to this contribution to degradation, it is important to take into account the contribution to cluster degradation, the rate of which is determined by the order of coherence *M*. Two such qualitatively different contributions to degradation were observed in adamantane in [5]. To assess the influence of the perturbation on the growth of clusters of correlated spins and on the observed MQ spectra, we implemented an expansion in terms of orthogonal operators, which made it possible to take into account the cluster size *K* distribution. A simple model with known amplitudes in the absence of perturbation we used for the calculations. The selected model led to exponential growth of $\bar{K}$ with time. Analytical estimates of the effects of perturbation [4] in the proposed report are supplemented by numerical calculations of the MQ spectra and the characteristics: $\bar{K}$, M_e, $< M^2 >$. The contribution to the degradation, which depends on the order of coherence, changes the shape of the MQ spectrum. As a result, the ratios of $\bar{K}$ with the values of M_e and $< M^2 >$ will change in comparison with those for the Gaussian function. In particular, with an increase in the preparation time, a narrowing of the MQ spectrum can occur while maintaining growth of $\bar{K}$. These changes must be taken into account when extracting the characteristics of the spread of quantum information from experimental MQ spectra.

1. J. Baum, M. Munovitz, A.N. Garroway, and A. Pines. “Multiple-quantum dynamics in solid state NMR”. J. Chem. Phys. **83**, pp. 2015-2025, 1985.
2. F.D. Domínguez, M.C. Rodríguez, R. Kaiser, D. Suter, and G.A. Álvarez. “Decoherence scaling transition in the dynamics of quantum information scrambling”. Phys. Rev. A, **104**, 012402, 2021.
3. F.D. Domínguez and G.A. Álvarez. “Dynamics of quantum information scrambling under decoherence effects”. arXiv:2107.03870, 2021.
4. V.E. Zobov and A.A. Lundin. “Effect of degradation processes caused by a small perturbation on the growth of the average cluster size of correlated spins in multiple quantum NMR spectroscopy of solids”. Appl. Magn. Res. **52**, pp. 879-892, 2021.
5. H.G. Krojanski and D. Suter. ”Scaling of decoherence in wide NMR quantum registers”. Phys. Rev. Lett. **93**, 090501, 2004.

Ideal transfer of zero-order coherence matrix and quantum state restoring

E.B. Fel'dman[1], A.N. Pechen[2,3], and A.I. Zenchuk[1]
1. Institute of Problems of Chemical Physics of RAS, Chernogolovka, Moscow reg., Russia, efeldman@icp.a.ru, zenchuk@itp.ac.ru
2. Department of Mathematical Methods for Quantum Technologies, Steklov Mathematical Institute of Russian Academy of Sciences, Gubkina str. 8, Moscow, Russia, pechen@mi-ras.ru, apechen@gmail.com
3. National University of Science and Technology "MISIS", Leninski prosp. 4, Moscow, Russia

The problem of state transfer goes back to Ref. [1] and is intensively studied during last decades. Such aspects as the perfect state transfer, high-probability state transfer, and remote state creation have been explored. Then, in Ref. [2], it was shown that the multi-quantum (MQ) coherence matrices of different order can evaluate independently provided that the Hamiltonian conserves the excitation number in the system. This allows us to transfer the MQ-coherence matrix from the sender to receiver without mutual interaction between them. This phenomenon was used to organize the block-scaled state transfer in Ref. [3], where the only deformation of the transferred state was scale factor ahead of the higher order MQ-coherence matrices. The information capacity of such transfer was not high: only one free complex parameter can be transferred by the MQ-coherence matrix of non-zero order. This stimulates development of state restoring protocol, which involves the extended receiver (i.e., the receiver and several nearest nodes) with unitary transformation into the process. Using this tool, the structural restoring of the nondiagonal part of the density matrix was proposed in Ref. [4], so that each nondiagonal element of the receiver density matrix differs by the scalar factor from the appropriate element of the sender density matrix. However, the diagonal elements can not be restored in the same way.

In this work, we turn to the problem of transfer of the zero-order coherence matrix. We find out such 0-order coherence matrix which can be perfectly transferred from the sender to the receiver in the case of the ground initial state of the whole chain except the sender whose state is to be transferred. At that we have to exchange position of two diagonal elements in the transferred state. We refer to the sate transfer with perfect transfer of the 0-order coherence matrix followed by restoring the elements of the higher order coherence matrix via the unitary transformation of the extended receiver as the optimal state transfer because deformation of the transferred state is minimized to the scale factors ahead of the elements of the higher-order coherence matrices. The possibility of encoding the free parameters in the nondiagonal part of the 0-order coherence matrix keeping perfect transfer of the diagonal part is also explored. We emphasize that the above mentioned scale factors and unitary transformation are universal objects which do not depend on a particular state to be transferred. They are defined by the interaction Hamiltonian and time instant for state registration. An example of optimal two-qubit state transfer is considered in details including two options for transfer of the 0-order coherence matrix.

This work was funded by Russian Federation represented by the Ministry of Science and Higher Education (grant number 075-15-2020-788).

1. S. Bose. *Quantum communication through an unmodulated spin chain*, Phys. Rev. Lett. **91,** 207901, 2003.
2. E.B.Fel'dman and A.I.Zenchuk. *Coherence evolution and transfer supplemented by sender's initial-state restoring*, JETP **125** (6), 1042, 2017.
3. Bochkin G.A., Fel'dman E.B., and Zenchuk A.I. *Transfer of scaled multiple-quantum coherence matrices*, Quant. Inf. Proc. **17**, 218, 2018.
4. Zenchuk A.I. *Partial structural restoring of two-qubit transferred state*, Phys. Lett. A. **382**, 3244, 2018.
5. E.B. Fel'dman, A.N. Pechen, and A.I. Zenchuk, *Complete structural restoring of transferred multi-qubit quantum state,* submitted to Phys.Lett.A, arXiv:2104.13762 [quant-p].

Investigations of multiple quantum NMR dynamics of spin dimer on a quantum computer

S.I. Doronin, E.I. Kuznetsova, E.B. Fel'dman, A.I. Zenchuk
Institute of Problems of Chemical Physics of RAS, Chernogolovka, Russia
Kuznets@icp.ac.ru

Dynamics of spin dimers in multiple quantum NMR experiment is studied on the 5-qubit superconducting quantum processor of IBM quantum experience for the both pure ground and thermodynamic equilibrium (mixed) initial states.

MQ NMR dynamics of a dimer at high temperatures [1] is investigated with the simple quantum circuit consisting of one rotation gate about the y-axis and one CNOT. Only two qubits are needed for realization of such circuit and four computational basis states |00>, |01>, |10>, |11> are used. The measurements yield probabilities of these states and these probabilities are connected with the intensities of MQ NMR coherences [1]. The results of quantum calculations are in a good agreement with the theoretical predictions [2].

In order to investigate MQ NMR dynamics at low temperatures we present the dimer's thermodynamic equilibrium state as a tensor product of 1-qubit states. Since we can simulate the evolution only of a pure state on a quantum processor it is necessary to purify the initial thermodynamic state. It is simple to show that one additional spin is enough to purify the thermodynamic state of a single spin. Therefore, the purification of a 2-qubit state yields the pure state of a 4-qubit system. Using an approach of Ref. [3], we perform the quantum circuit, which allows us to investigate MQ NMR dynamics of a dimer at low temperatures. We obtain the thermodynamic equilibrium state of the dimer tracing over two other spins of the properly prepared pure state of the 4-qubit system. Measurements on each spin of the dimer yield the probabilities of their states. These probabilities allow us to obtain the intensity of the MQ NMR coherence of zero order. The conservation law of the sum of the MQ NMR coherences [4] yields the intensity of the MQ NMR coherence of the second order. The obtained evolution of the MQ NMR coherences of the zero and second orders are in a good agreement with the exact theoretical predictions [5].

The work was partially supported by the Ministry of Science and Higher Education of the Russian Federation (Grant No. 075-15-2020-779).

1. J. Baum, M. Munowitz, A.N. Garroway, and A. Pines, "Computer-simulation of the multiple-quantum dynamics of one-, two- and three-dimensional spin distributions", J. Chem. Phys. **83**, p. 2015, 1985.
2. S.I. Doronin, "Multiple quantum spin dynamics of entanglement", Phys. Rev. A **68**, 05206, 2003.
3. G. Vidal and C.M. Dawson, "Universal quantum circuit for two-qubit transformations with three controlled-NOT gates" Phys. Rev. A, **69**, 010301(R), 2004.
4. E.B. Fel'dman and I.I. Maximov, "Multiple Quantum Dynamics in Linear Chains and Rings of Nuclear Spins in Solids at Low Temperatures", Journal of Magnetic Resonance **157**, pp. 106–113, 2002.
5. E.B. Fel'dman and A.N. Pyrkov, "Evolution of Spin Entanglement and an Entanglement Witness in Multiple-Quantum NMR Experiments", JETP Letters **88**, p. 398, 2008.

Determination of Wigner-Yanase skew information with multiple quantum NMR in solids

S.I. Doronin[1], E.B. Fel'dman[1], I.D. Lazarev[1,2]
1. Institute of Problems of Chemical Physics of Russian Academy of Sciences, Chernogolovka, Russia
2. Faculty of Fundamental Physical-Chemical Engineering, Lomonosov Moscow State University, Moscow, Russia, the.ilia.lazarev@gmail.com

Wigner-Yanase (skew) information [1] is an important quantity in quantum information theory. Wigner and Yanase introduced [1] the notion of skew information to quantify the information content of quantum states in the presence of conserved quantities, which was later identified as a paradigmatic version of quantum Fisher information. The skew information as well as the Fisher information allows the development of powerful methods for the investigation of entanglement, including many-particle entanglement [2-5]. Further investigations of the many-particle entanglement require the development of corresponding experimental methods. In particular, it was shown [6] that a lower bound on the quantum Fisher information coincides with the double second moment of the spectrum of multiple quantum (MQ) coherences. As a result, the lower bound on the quantum Fisher information can be found in MQ NMR experiments, in cold-atom experiments, including experiments with Bose–Einstein condensates, ultracold atoms in cavities, and trapped ions.

In this work we demonstrate that the Wigner–Yanase information in a spin system ($s = 1/2$) with the dipole–dipole interactions (DDI) in the MQ NMR experiment at the system temperature T equals the double second moment of the MQ NMR spectrum obtained at the temperature $2T$ [7]. Using the properties of the skew information we investigate many-spin entanglement on the basis of the MQ NMR spectroscopy. We perform a comparison of an estimation of the entangled cluster size obtained with Fisher information and Wigner–Yanase information. We use a nonspherical nanopore filled with a gas of spin-carrying atoms (for example, xenon) or molecules and a zigzag chain [8] in a strong external magnetic field as models for a comparison of the dependencies of numbers of the entangled spins on the temperature [7].

We acknowledge funding from the Ministry of Science and Higher Education of the Russian Federation (Grant No. 075-15-2020-779)

1. E.P. Wigner, M.M. Yanase. "Information Contents of Distributions", Proc. Nat. Acad. Sci. USA, **49**, 910-918, 1963.
2. S.I. Doronin, E.B. Fel'dman, I.D. Lazarev. "Many-particle entanglement in multiple quantum nuclear-magnetic-resonance spectroscopy", Phys.Rev.A, **100**(2), 022330, 2019.
3. I.D. Lazarev and E.B. Fel'dman. "Many-Spin Entanglement in Multiple Quantum NMR with a Dipolar Ordered Initial State", JETP, **131**(5), 2020.
4. G.A. Bochkin, et al. "Many-Spin Entanglement in zigzag spin Chain in Multiple Quantum NMR", Appl.Magn.Reson. **51**, 667–678 (2020).
5. Z. Chen. "Wigner-Yanase skew information as tests for quantum entanglement", Phys.Rev.A. **71**, 052302, 2005.
6. M. Gärttner, P. Hauke, and A.M. Rey. "Relating out-of-time-order correlations to entanglement via multiple-quantum coherences". Phys. Rev. Lett. **120**, 040402, 2018.
7. S.I. Doronin, E.B. Fel'dman, I.D. Lazarev. "Multiple quantum NMR in solids as a method of determination of Wigner-Yanase skew information", Phys. Lett. A **406**, 127458, 2021.
8. G.A. Bochkin et al. "H-1 NMR in a quasi-one-dimensional zig-zag spin chain of hambergite, $Be_2BO_3(OH)$", J. Magn. Res. **319**, 106816, 2020.

Quantum Hashing on the High-dimensional States

F. Ablayev[1,2], A. Vasiliev[1,2]
1. Kazan Federal University, Kazan, Russian Federation, fablayev@gmail.com
2. Kazan E.K. Zavoisky Physical-Technical Institute of the Kazan Scientific Center of the Russian Academy of Sciences, Kazan, Russian Federation, vav.kpfu@gmail.com

In [1] we have proposed a cryptographic quantum hash function and later in [2] provided its generalized version for arbitrary finite abelian groups based on the notion of ε-biased sets. Note that ε-biased sets are generally defined for arbitrary finite groups [3], but here we restrict ourselves to $\mathbb{Z}_q$. In this case a set $S \subseteq \mathbb{Z}_q$ is called ε-biased, if for any $x \neq 0$

$$\frac{1}{|S|}\left|\sum_{s\in S} e^{2\pi s x/q}\right| \leq \varepsilon. \#(1)$$

These sets are especially interesting when $|S| \ll \mathbb{Z}_q$ (as $S = \mathbb{Z}_q$ is obviously 0-biased). In their seminal paper [4] Naor and Naor defined these small-biased sets, gave the first explicit constructions of such sets, and demonstrated the power of small-biased sets for several applications.

Here we define a new version of the quantum hashing technique that is based on small-biased sets and high-dimensional states (qudits).

Let $S_1, S_2, \dots, S_m \subset \mathbb{Z}_q$ be the ε-biased subsets of $\mathbb{Z}_q$, and we denote $S_j = \{s_{j,1}, \dots, s_{j,d}\}$ for $j = 1, \dots, m$. Then for $x \in \mathbb{Z}_q$ we define a multiqudit quantum hash function in the following way:

$$\left|\psi_j(x)\right\rangle = \frac{1}{\sqrt{d}}\sum_{k=0}^{d-1} e^{2\pi s_{j,k} x/q}\,|k\rangle, \#(2)$$

$$|\psi(x)\rangle = \left|\psi_1(x)\right\rangle \otimes \cdots \otimes \left|\psi_m(x)\right\rangle \#(3)$$

The formula above gives the classical-quantum function that transforms a classical input into the quantum state composed of *m* qudits (*d*-dimensional systems). The same state can be constructed with appropriate number of 2-dimensional systems (qubits), however this would imply creating entangled states, which are harder to create and maintain.

According to [5] $|\psi(x)\rangle$ corresponds to the balanced $(d^m/q, \varepsilon^m)$-resistant quantum hash function, i.e. the probability of correct extraction of x from $|\psi(x)\rangle$ is bounded by d^m/q, while the collision probability is bounded by ε^m.

The research is supported by the Russian Science Foundation, project No. 19-19-00656.

1. F.M. Ablayev and A.V. Vasiliev. “Cryptographic quantum hashing”. Laser Physics Letters, **11**(2), 025202, 2014.
2. A. Vasiliev. “Quantum hashing for finite abelian groups”. Lobachevskii Journal of Mathematics, **37**(6), pp. 751-754, 2016.
3. S. Chen, C. Moore, and A. Russell. “Small-bias sets for nonabelian groups”. In *Approximation, Randomization, and Combinatorial Optimization. Algorithms and Techniques*, editors Prasad Raghavendra, Sofya Raskhodnikova, Klaus Jansen, and Jose D.P. Rolim, volume **8096** of Lecture Notes in Computer Science, pp. 436-451. Springer Berlin Heidelberg, 2013.
4. J. Naor and M. Naor. “Small-bias probability spaces: Efficient constructions and applications”. In *Proceedings of the Twenty-second Annual ACM Symposium on Theory of Computing, STOC '90*, pp. 213-223, New York, NY, USA, 1990. ACM.
5. F. Ablayev, M. Ablayev, and A. Vasiliev. On the balanced quantum hashing. Journal of Physics: Conference Series, **681**(1), 012019, 2016.

Quantum assisted unsupervised data clustering on the basis of neural networks

I.D. Lazarev[1,2], M. Narozniak[3,4], T. Byrnes[3,4,5,6,7], A.N. Pyrkov[1]

1. Institute of Problems of Chemical Physics of Russian Academy of Sciences, Acad. Semenov av. 1, Chernogolovka, Moscow Region, Russia, 142432, email: pyrkov@icp.ac.ru .

2. Faculty of Fundamental Physical-Chemical Engineering, Lomonosov Moscow State University, GSP-1, Moscow, Russia 119991.

3. New York University Shanghai, 1555 Century Ave, Pudong, Shanghai 200122, China.

4. Department of Physics, New York University, New York, NY, 10003, USA.

5. State Key Laboratory of Precision Spectroscopy, School of Physical and Material Sciences, East China Normal University, Shanghai 200062, China.

6. NYU-ECNU Institute of Physics at NYU Shanghai, 3663 Zhongshan Road North, Shanghai 200062, China.

7. National Institute of Informatics, 2-1-2 Hitotsubashi, Chiyoda-ku, Tokyo 101-8430, Japan

In the last years, the combination of big data and artificial intelligence produced a lot of impact on modern economy and a lot of people have referred to this as the forth industrial revolution [1, 2]. The contemporary artificial-intelligence methods based on neural networks have the potential to enhance the role of computers in science and engineering. Neural networks have evolved rapidly in recent years and nowadays are used almost everywhere from robotics to agriculture. On the other hand, a lot of algorithms for quantum machine learning were recently proposed [3]. Quantum machine learning protocols utilize such quantum phenomenon as quantum entanglement and quantum superposition for the tasks as linear regression, principal component analysis and so on. And at least from theoretical point of view, it is clear that the quantum machine learning approaches have the potential to outperform classical algorithms in many specific problems and get quantum speedup over classical ones. In particular, a lot of approaches for realization quantum neural networks were proposed recently [4].

Here, we consider a self-organizing feature map (SOFM) [5], a type of artificial neural network (ANN) that is trained in unsupervised manner. Self-organizing feature maps are used in many areas [6, 7] and in comparison with many other artificial neural networks they apply competitive learning and preserve the topological properties of the input space. The idea of our approach is based on the use of the Hamming distance as a distance metric for the training the SOFM that allows, in the quantum case, to reduce the number of distance calculations in the number of clusters and thus to speed up the original classical protocol. Furthermore, we optimize a circuit for the Hamming distance calculations by reducing number of one-qubit operations. We then apply the quantum assisted SOFM to a toy example of clustering paper abstracts and give a proof-of-concept realization of it on the IBM Q experience quantum computer and compare it to the original classical protocol.

1. LeCun, Y., Bengio, Y. & Hinton, G. Deep learning. Nature **521**, 436 (2015).
2. Schwab, K. The Fourth Industrial Revolution (Currency Press, Redfern, New South Wales, 2017).
3. Biamonte, J. et al. Quantum machine learning. Nature, **549**, 195 (2017).
4. Jeswal, S. K. & Chakraverty, S. Recent developments and applications in quantum neural network: A review. Archives of Computational Methods in Engineering **26**, 793 (2019).
5. Kohonen, T. The self-organizing map. Proceedings of the IEEE **78**, 1464 (1990).
6. Kohonen, T., Oja, E., Simula, O., Visa, A. & Kangas, J. Engineering applications of the self-organizing map. Proceedings of the IEEE **84**, 1358 (1996).
7. Corsello, S. M. et al. The drug repurposing hub: a nextgeneration drug library and information resource. Nature Medicine **23**, 405 (2017).

Quantum Version of Self-Balanced Binary Search Tree with Strings as Keys and Applications

K. Khadiev[1], S. Enikeeva[2]

1. Kazan Federal University, Kazan, Russia; Zavoisky Physical-Technical Institute, FRC Kazan Scientific Center of RAS, Kazan, Russia, kamilhadi@gmail.com

2. Kazan Federal University, Kazan, Russia, sumbel.enikeeva@gmail.com

There are many problems on string processing (text processing) which solutions use the "set of strings" data structure [1, 2]. Others use "map (or dictionary) with strings as keys" data structure. That is a mapping from some set of keys (strings) to another collection of objects. Such data structures are standard for programming languages like C++, Java and others. The main operations for these data structures are adding, removing and checking the existence of an element. In the classical (deterministic or randomized) case, we can use one of two data structures. The first one is a Self-Balanced Binary Search Tree [1] that can be AVL tree or Red-Black tree. In that case, the running time of the main operations is O(k log n), where k is the length of an inserted (removed or searched) string, and n is the number of elements in the set or map. The second data structure is the prefix tree (trie) [1, 3]. The running time of the main operations for trie is O(k). Trie is the best possible data structure for implementation of set or map for strings.

The authors of [2] have developed a quantum algorithm for comparing strings in $O(\sqrt{k})$. It allows them to implement the quantum version of set and map data structures using a Self-Balanced Binary Search Tree with $O((\log n)^2\sqrt{k})$ running time of the main operations.

In this paper, we implement quantum versions of set and map data structures with $O((\log n)\sqrt{k})$ running time of the main operations. We also use a Self-Balanced Binary Search Tree and the random walk algorithm with ideas from [4]. The quantum implementation from [2] works better than the best classical solution if $(\log_2 n)^4=o(k)$. Our quantum implementation has quantum speed-up if $(\log_2 n)^2=o(k)$. The situation $(\log_2 n)^2=o(k)$ opens us more opportunities for real-world applications.

To evaluate the complexity of a quantum algorithm, we use the standard form of the quantum query model [5]. Throughout this paper, by the running time of an algorithm we mean a number of queries to an oracle.

One of the applications is the "Online the Most Frequent String Problem". The problem is as follows. The input is $S=(s^1,...,s^n)$, where an integer n is the length of input and s^i is a binary string. Let $L=|s^1|+...+|s^n|$, here $|s^i|$ is the length of the string s^i. Let $\#_j(s)$ be the number of occurrences of a string s among $s^1,...,s^j$ for $1\leq j\leq n$. The problem is to find the sequence $y_1,...,y_n$. Here for $1\leq j\leq n$, the variable $y_j=s^{i(j)}$ where i(j) is the index of the most frequent string among $s^1,...,s^j$. In other words, $\#_j(s^{i(j)})=\max\{\#_j(s^z):1\leq z\leq n\}$. Many applications in packet routing, telecommunication logging, and tracking keyword queries in search machines are critically based on the problem [6]. The classical complexity of the problem is $\Omega(L)$, and the complexity of the quantum algorithm that uses our data structure is $O(L^{0.5}n^{0.5}\log n)$. If a significant part of strings (we mean O(n)) has length at least $\omega((\log n)^2)$, then we have quantum speed-up for the problem.

This work was funded by the subsidy allocated to Kazan Federal University for the state assignment in the sphere of scientific activities, project No. 0671-2020-0065.

1. T. H. Cormen, et al. *Introduction to algorithms*. MIT press, 2009.
2. K. Khadiev and A. Ilikaev. "Quantum algorithms for the most frequently string search, intersection of two string sequences and sorting of strings problems." International Conference on Theory and Practice of Natural Computing. Springer, Cham, 2019.
3. R. De La Briandais. "File searching using variable length keys." Papers presented at the the March 3-5, 1959, western joint computer conference. 1959.
4. U. Feige, P. Raghavan, D. Peleg, E. Upfal. "Computing with noisy information". SIAM Journal on Computing, **23**(5), pp. 1001-1018.
5. Ablayev F., Ablayev M., Huang J. Z., Khadiev K., Salikhova N., and Wu D. "On quantum methods for machine learning problems part I: Quantum tools". Big Data Mining and Analytics, **3**(1), pp. 41-55.
6. G. Cormode, G. and M. Hadjieleftheriou. "Methods for finding frequent items in data streams". The VLDB Journal, **19**(1), pp. 3-20.

Quantum Algorithm for the Shortest Superstring Problem

K. Khadiev[1], C.M.B. Machado[2]

1. Kazan Federal University, Kazan, Russia; Zavoisky Physical-Technical Institute, FRC Kazan Scientific Center of RAS, Kazan, Russia, kamilhadi@gmail.com

2. Kazan Federal University, Kazan, Russia, cmbosch2015@gmail.com

In the paper, we consider the "Shortest Superstring Problem"(SSP) or the "Shortest Common Superstring Problem"(SCS). The problem is as follows. For a positive integer n, a sequence of n strings $S=(s^1,...,s^n)$ is given. We should construct the shortest string t (we call it superstring) that contains each string from the given sequence as a substring.

The problem is connected with the sequence assembly method for reconstructing a long DNA sequence from small fragments [1]. There are two types of sequence assemble problems. The first one is Reference-guided genome assembly method that constructs an existing long DNA-string from the sequence S. For the problem, we should know the string t apriori and check whether we can construct it from S. The second one is de-novo assembly; in this problem, we do not have the string t and should construct it using all strings from S. The Shortest Superstring Problem is used as one of the main tools for solving de-novo assembly problems. The problem has applications in other areas such as virology and immunology (the SSP models the compression of viral genome); the SSP can be used to achieve data compression; in scheduling (solutions can be used to schedule operations in machines with coordinated starting times), and others. It is known that the Shortest Superstring Problem is an NP-complete problem and is typically solved by heuristic algorithms in practice. At the same time, researchers are interested in exact solutions also.

We present a quantum algorithm with running time $O^*(1.728^n)$. Here O^* notation does not consider a log factor; in other words, polynomials of n and the length of t. The algorithm is based on Grover's search algorithm [4] in a form with probabilistic oracle [5, 6] and the Dynamic programming approach for a Boolean cube [7]. To evaluate the complexity of a quantum algorithm, we use the standard form of the quantum query model [8]. Throughout this paper, by the running time of an algorithm, we mean a number of queries to an oracle.

The main idea is the following. As a first step we classically find the shortest superstring for all possible subsets of S of size (1-z)n/4 where z=0.055362. As a second step, quantumly using the Durr-Hoyer algorithm for minimum finding [9], we find the shortest superstring for all possible subsets of S of size n/4. Then, quantumly, we find the shortest superstring for all possible subsets of S of size n/2. Finally, we can construct the shortest superstring for S. Quantum steps are nested; that is why we can say that we use an oracle with constant error probability. So, we use the modification of Grover's search [5, 6].

This work was funded by the subsidy allocated to Kazan Federal University for the state assignment in the sphere of scientific activities, project No. 0671-2020-0065.

1. E. W. Myers, G. G. Sutton, A. L. Delcher, I. M. Dew, D. P. Fasulo, M. J. Flanigan, and Venter, J. C.. "A whole-genome assembly of Drosophila". Science, **287**(5461), pp. 2196-2204, 2000.

2. T. P.Gevezes, and L. S. Pitsoulis. "The shortest superstring problem." Optimization in Science and Engineering. pp. 189-227, 2014.

3. K.-J. Räihä and E. Ukkonen. "The shortest common supersequence problem over binary alphabet is NP-complete." Theoretical Computer Science **16**(2), pp. 187-198, 1981.

4. L. K. Grover, "A fast quantum mechanical algorithm for database search". In Proceedings of the twenty-eighth annual ACM symposium on Theory of computing, pp. 212-219, 1996.

5. P. Høyer, M. Mosca, and R. De Wolf. "Quantum search on bounded-error inputs". In International Colloquium on Automata, Languages, and Programming, pp. 291-299, 2003.

6. A. Ambainis, et.al. "Quantum Lower and Upper Bounds for 2D-Grid and Dyck Language". In 45th International Symposium on Mathematical Foundations of Computer Science (MFCS 2020), 2020

7. A. Ambainis, et.al. Quantum speedups for exponential-time dynamic programming algorithms. In Proceedings of the Thirtieth Annual ACM-SIAM Symposium on Discrete Algorithms, pp. 1783-1793, 2019.

8. Ablayev, F., Ablayev, M., Huang, J. Z., Khadiev, K., Salikhova, N., and Wu, D. "On quantum methods for machine learning problems part I: Quantum tools". Big Data Mining and Analytics, **3**(1), pp. 41-55, 2019.

9. C. Durr, and P. Hoyer, "A quantum algorithm for finding the minimum". arXiv preprint quant-ph/9607014, 1996.

The Quantum Version of Prediction for Binary Classification Problem by Ensemble Methods

K. Khadiev, L. Safina
Kazan Federal University, Kazan, Russia, kamilhadi@gmail.com, liliasafina94@gmail.com

In this work we suggest two algorithms to estimate an amplitude of a good state in a quantum register using the quantum amplitude amplification algorithm [1] and application them and the quantum amplitude estimation algorithms from [1] for binary classification problem by ensemble methods. The ensemble models use some small classifiers, where each from them predicts and returns a class for new input object, and after that the metamodel (an ensemble model) averages a result class by voting. The most popular models of ensemble methods are random forest and gradient trees boosting. We consider abstract small classifiers, they can be anything.

Let $O(T)$ be running time of prediction on one small classifier, it is the worst running time among all classifiers. To get a result from an ensemble model we need in $O(N \times T)$, where N is a number of classifiers.

We suggest using quantum computations to speed up this running time in case when a number of classifiers or a number of requires for prediction is large. The steps of our quantum prediction are next:

1. Set the quantum state using the Hadamard gate:
$$|res> = \frac{1}{\sqrt{2}}|Class_1> + \frac{1}{\sqrt{2}}|Class_2>$$
2. Let A be an algorithm of prediction. Each small classifier returns its own amplitude $\sqrt{p_i}$ of a good state. The result quantum state summarizes them: $\sqrt{p} = \frac{1}{\sqrt{N}}\sum_{i=1}^{N}\sqrt{p_i}$.

   Apply A:
$$|res> = A\,|res> = \sqrt{p}\,|Class_1> + \sqrt{1-p}\,|Class_2>,$$
   where p is a probability that an input object belongs the first class.
3. Estimate p using quantum amplitude estimation algorithms.
4. Return a result class:
$$Result\ class = \begin{cases} Class_1, if\ p \geq 0.5 \\ Class_2, otherwise \end{cases}.$$

To estimate p we can use the quantum amplitude estimation algorithms ***QSearch, Est_Amp*** from [1] or our quantum amplitude estimation algorithms based on the quantum amplitude amplification algorithm. It works in $O\left(\sqrt{N} \times T\right)$.

The first of our quantum amplitude estimation algorithms is next. We set $p = \frac{1}{2^j}, j = 1, 2, \ldots \in \mathbb{N}$ and run the quantum amplitude amplification algorithm. For $j \geq 3$ we can stop the algorithm and return $Class_2$, because $p \leq 0.125$.

The second algorithm is using the binary search approach to set $p = \frac{l+r}{2}$, where in the beginning $l = 0$ and $r = 1$, and also to run the quantum amplitude amplification algorithm from [1], after that l or r will be changed to p.

1. G. Brassard, P. Hoyer, M. Mosca, A. Tapp. “Quantum amplitude amplification and estimation”. Contemporary Mathematics, **305**, pp. 53-74, 2002.

Study of the effect of quantum noise on the accuracy of the Schrödinger equation simulation on a quantum computer using the Zalka-Wiesner method

N.A. Bogdanova, Yu.I. Bogdanov, D.V. Fastovets, V.F. Lukichev
Valiev Institute of Physics and Technology of Russian Academy of Sciences, Moscow, Russia
bogdanova_nadejda@inbox.ru

The study of the effect of quantum noise on the accuracy of modeling quantum systems on a quantum computer using the Zalka-Wiesner method is carried out. The efficiency of the developed methods and algorithms is demonstrated by the example of solving the nonstationary Schrödinger equation with allowance for quantum noise for a particle moving in the Pöschl–Teller potential. The analysis and prediction of accuracy for the Zalka-Wiesner method are carried out taking into account the complexity of the quantum system and the strength of quantum noise. In our opinion, the considered problem provides a useful test for assessing the quality and efficiency of quantum computing devices on various physical platforms currently being developed.

The obtained results are essential for the development of high-precision methods for controlling the technologies of quantum computations.

This work was supported by the Ministry of Science and Higher Education of the Russian Federation (program no. 0066-2019-0005 for the Valiev Institute of Physics and Technology, Russian Academy of Sciences), and by the Foundation for the Advancement of Theoretical Physics and Mathematics BASIS (project no. 20-1-1-34-1).

Software for analysis and comparison of quantum tomography methods

B.I. Bantysh, A.Yu. Chernyavskiy, D.V. Fastovets, Yu.I. Bogdanov
Valiev Institute of Physics and Technology, Russian Academy of Sciences, Moscow, 117218, Russia, bbantysh60000@gmail.com

Quantum tomography plays a key role in the control of quantum states and processes, in connection with which more and more new methods are constantly appearing. A side effect of this development is the difficulty in choosing the most appropriate methods for specific tasks. The reason for this difficulty is the lack of a general methodology for evaluating tomography methods, as a result of which various tests and metrics are encountered in different scientific papers. The variety of approaches to tomography does not allow obtaining general evaluations analytically.

In this work, we propose a general methodology for benchmarking tomography methods based on the simulation of their operation on a fixed set of test problems that are close to real experiments. This methodology has been implemented as open-source and easy-to-use software libraries (Matlab and Python), allowing researchers to easily compare existing and emerging quantum tomography methods. Benchmarking parameters corresponds to different resources (size of statistical sample, number of different measurements, computational time, etc.) needed to achieve the required accuracy.

In addition to developing a methodology, we present its approbation on more than 10 different methods of quantum tomography. An approach for evaluating the performance of tomography methods that require prior training (such as machine learning) is also presented.

This work was supported by the Ministry of Science and Higher Education of the Russian Federation (program no. 0066-2019-0005 for the Valiev Institute of Physics and Technology, Russian Academy of Sciences), and by the Foundation for the Advancement of Theoretical Physics and Mathematics BASIS (project no. 20-1-1-34-1).

Study of decoherence of a superposition of macroscopic quantum states by means the consideration of a multimode state of a Schrödinger cat

D.V. Fastovets, Yu.I. Bogdanov, N.A. Bogdanova, V.F. Lukichev
Valiev Institute of Physics and Technology of Russian Academy of Sciences, Russia
fast93@mail.ru

Quantum Schrodinger cat states are of great interest in quantum communications and quantum optics. These states are used in various scientific fields such as quantum computing, quantum error correction and high-precision measurements. The analysis of the Schrödinger cat states coherence is an important task for their complete practical application. Our developed approach makes it possible to estimate the coherence of the quantum Schrödinger cat state of arbitrary dimension, as well as to find the interference visibility of the state – an important optical characteristic. The obtained simple quantitative relationship between coherence and the Schmidt number, as well as the developed approach of reducing the multidimensional quantum cat state to a two-mode analog allow us to analyze macroscopic states formed by a large number of modes. Several explicit formulas for the reduced states that arise after measuring of some modes of the considered multimode system are obtained. The research results have significant application and can be used in the development of high-dimensional quantum information processing systems.

This work was supported by the Ministry of Science and Higher Education of the Russian Federation (program no. 0066-2019-0005 for the Valiev Institute of Physics and Technology, Russian Academy of Sciences), and by the Foundation for the Advancement of Theoretical Physics and Mathematics BASIS (project no. 20-1-1-34-1).

Linear optical circuits characterization with thermal states of light

G.V. Avosopiants[1], K.G. Katamadze[1,2], A.V. Romanova[1], Yu.I. Bogdanov[2], S.P. Kulik[1]
1. Quantum Technology Centre, Faculty of Physics, M. V. Lomonosov Moscow State University, Moscow, Russia
2. Valiev Institute of Physics and Technology, Russian Academy of Sciences, Moscow, Russia
avosopyantsgrant@gmail.com

Currently, linear-optical quantum chips are increasingly used in quantum informatics and quantum computing, which are seen as a good platform for building a universal quantum computer. Such chips consist of beam splitters with arbitrary transmission and reflection coefficients and phase shifters: by combining two such structural units, one can be performed arbitrary quantum operations.

In December 2020, quantum advantage was demonstrated on a 100x100 linear optical integrated chip: a group of Chinese scientists solved the boson sampling problem in just 200 seconds versus 2.5 billion years on the leading supercomputer in China [1]. And if the methods of manufacturing such chips are now actively developing, and many effective architectures for constructing a chip are known, then the methods of reconstructing the so-called transfer matrix describing the transformation are lagging behind.

We experimentally and theoretically investigate the proposed original approach for characterizing linear optical schemes based on correlation measurements of thermal fields [2]. The measured temporal cross-correlation functions make it possible to reconstruct the phases of the transfer matrix with high accuracy with short acquisition time and robustness against phase fluctuations.

This work was supported by the Ministry of Science and Higher Education of the Russian Federation (program no. 0066-2019-0005 for the Valiev Institute of Physics and Technology, Russian Academy of Sciences), by the Foundation for the Advancement of Theoretical Physics and Mathematics BASIS (projects no. 20-1-1-34-1 and 21-1-3-40-1), and Russian Foundation for Basic Research (project no. 19-31-27001).

1. Zhong H. Sen. et al., "Quantum computational advantage using photons", Science, **370** pp. 1460-1463, 2021.
2. K. G. Katamadze, G. V. Avosopiants, A. V. Romanova, Yu. I. Bogdanov, S. P. Kulik ,"Linear optical circuits characterization by means of thermal field correlation measurement", Laser Physics Letters, **18**, p. 075201, 2021.

High- fidelity tracking of the evolution of multilevel quantum states

N.A. Bogdanova, Yu.I. Bogdanov, Yu.A. Kuznetsov, V.F. Lukichev
Valiev Institute of Physics and Technology of Russian Academy of Sciences, Moscow, Russia
yurii.a.kuznetsov@gmail.com

The method of quantum tomography, which allows us to track with high accuracy the evolution of multilevel quantum systems (qudits) in Hilbert spaces of various dimensions, is presented. The developed algorithms for quantum control are based on the use of the spinor representation of the Lorentz transformation group [1]. In the simplest case of one-qubit states, it turns out that, in addition to three-dimensional rotations on the Bloch sphere, one can introduce four-dimensional Lorentz pseudorotations, similar to the transformations of the special theory of relativity.

We show that feedback through weakly perturbing adaptive quantum measurements turns out to be capable of providing high-precision control of the quantum system, while introducing only weak perturbations into the initial quantum state. It turns out that, together with the control of a quantum system through its weak perturbation, the developed algorithms for controlling the evolution of the state of a quantum system can be super-efficient, providing the higher measurement accuracy than any standard POVM (Positive-Operator Valued Measure) protocols. The results of the study are important for the development of optimal adaptive methods for quantum states and operations controlling.

The results obtained are essential for the development of high-precision control methods for quantum information technologies.

This work was supported by the Ministry of Science and Higher Education of the Russian Federation (program no. 0066-2019-0005 for the Valiev Institute of Physics and Technology, Russian Academy of Sciences), and by the Foundation for the Advancement of Theoretical Physics and Mathematics BASIS (project no. 20-1-1-34-1)

1. Bogdanov Yu. I., Bogdanova N. A., Bantysh B. I., Kuznetsov Yu. A. "The concept of weak measurements and the super-efficiency of quantum tomography", Proc. SPIE 11022, International Conference on Micro- and Nano-Electronics 2018, **110222O**, 2019.

Ion synthesis of SOI structures with silicate insulating layers

Ed.Yu. Buchin, Yu.I. Denisenko, S.G. Simakin
Yaroslavl Branch of the Valiev Institute of Physics and Technology, Institution of Russian Academy of Sciences, Yaroslavl, Russia, E-mail: den-yur55@mail.ru.

The SIMOX (Separation by Implanted Oxygen) process is one of the few industrial methods capable of mass production of thin-film SOI (silicon on insulator) structures. At the same time, the developers are constantly improving this technology in order to reduce the doses of implantation and energy costs during post-implantation annealing [1]. In this regard, we previously proposed an approach based on the synthesis of buried silicate layers instead of purely oxide ones [2]. In addition to the sub-stoichiometric dose of oxygen, a glass-forming agent was implanted into silicon wafers at the same depth, and boron ions were tested in this capacity. Studies have shown that in this way the energy consumption during annealing can be reduced by more than an order of magnitude, since the buried silicate layer of Si-O-B was formed rather quickly and at lower temperatures (1025÷1075 ^{o}C). The synthesized SOI structures have been successfully tested in MEMS technology.

In this work, lead ions were tested as a glass-forming agent. The experiments were carried out with n-type silicon wafers (4.5 Ohm·cm) with a crystallographic orientation (100). They were successively irradiated with molecular oxygen ions with a dose of $3\cdot10^{17}$ O_2^+/cm^2 (at an energy of 130 keV) and lead ions with a dose of $8\cdot10^{15}$ Pb^+/cm^2 (at an energy of 1150 keV), respectively. After implantation, silicon wafers were annealed in a mixture of argon and oxygen ambient under different regimes. The distribution profiles of oxygen and lead in the synthesized silicate layers were determined using methods SIMS and Auger spectroscopy. The electrical characteristics of the obtained SOI structures were evaluated using volt-ampere measurements and by the value of specific resistivity of the both insulator and device silicon layer.

A feature of the experimental structures was that the lead in the insulating layer was distributed non-uniformly with the depth. Its highest concentration was observed at the boundaries with silicon. This may be due to segregation of lead oxide into inhomogeneous regions between the contiguous phases, or spinodal decomposition of the PbO_x-SiO_x solid solution. In the course of the experiments, SOI structures with good insulating properties close to the parameters of the high-dose SIMOX material were obtained. At the same time, in comparison with the standard process, the use of lead ions as a glass former made it possible to somewhat reduce the dose of oxygen implantation, as well as to reduce the annealing temperature by 200 °C for the same duration of the process. This is due to the fact that lead in the form of pyramidal groups $[PbO_4]_4^-$ partially replace silicon ions in the nodes of the three-dimensional silicate network. Since the energy of the covalent Pb-O bond is several times lower than the energy of the Si-O bond, the combined silicate network can be formed under soft post-implantation annealing regimes. The resulting SOI structures with a lead-silicate insulator, in addition to reducing production costs, are mainly of interest as a new material. By changing the dose of implanted lead, it is possible to regulate their radiation resistance, as well as the optical properties of the buried silicate layer. These structures can be in demand by developers, as in the field of microelectronics and microphotonics.

1. Y. Hoshino, G. Yachida, K. Inoue, T. Toyohara, and J. Nakata. “Direct synthesis of ultrathin SOI structure by extremely low-energy oxygen implantation”. AIP Advances, **6**, 065313, 2016.
2. Ed.Yu. Buchin, Yu.I. Denisenko, S.A. Krivelevich, and R. V. Selyukov. “Diffusion and phase formation in ternary silicate systems framed by an ion bombardment”. Micro- and Nanoelectronics 2005, edited by Kamil A. Valiev, Alexander A. Orlikovsky, Zvenigorod, Russia, Proc. SPIE, V. 6260, 626007, 2006.

The shape of the relief of the insulating potential, created by ultrathin layers of the oxide

E.I. Goldman, I.A. Shusharin, G.V. Chucheva
Fryazino Branch of the Kotelnikov Institute of Radioengineering and Electronics of Russian Academy of Science, Fryazino, Russia, E-mail: gvc@ms.ire.mssi.ru

The insulating potential, created by ultra-thin (less than 5nm) oxide films has a more complex shape, than a rectangular one. Transition layers between plates and the oxide occupy at least 35% of the volume and largely determine properties of the insulator. Since there are no theoretical foundations that allow using the effective mass method to describe the wave function of an electron in a disordered material, the coordinate dependence of the potential in the insulating gap should be a certain function leading to the calculation results that coincide with experiment. This relief should be constructed from the experimental tunnel *I–V* characteristics of poly-n^+ Si-SiO_2-Si structures. This problem of inverting measurement data was solved earlier [1]. In this work, we will slightly change the previously developed apparatus and apply it to samples of poly-n^+ Si-SiO_2-Si structures, similar to those studied in [1], but with a pronounced asymmetry of tunneling *I–V* characteristics [2].

The inversion of the experimental dependence of the tunneling current on the voltage was obtained in [1]

$$\left[\frac{z_2(V)}{h}\right]^{3/2} - \left[\frac{z_1(V)}{h}\right]^{3/2} = \frac{2\overline{V}^{(1/2)}}{\pi}\int_V^{V_m}\left(V' - V\right)^{-(1/2)}\frac{d\ln\left[I\left(V'\right)/I_0\right]}{dV'}dV'$$

Where $z_{1,2}$ are coordinates of 1st and 2nd turning points, h is the thickness of the oxide, I_0 is the normalization constant, $\overline{V} = \left(9\hbar^2/32mh^2q\right)$, m is the mass of the tunneling electron, q is the elementary charge, V_m is the barrier removal voltage. From two branches of the dependence $I(V)$, depletion and enrichment Si, parametrically through functions $z_1(V)$, $z_2(V)$, successive approximations to the sought relief $U(z)$ were constructed. Calculations based on the trapezoidal potential with parameters providing the function $I(V)$ that is as close as possible to the experiment were used as a zero approximation (see curve 2 in Fig.). All actions were carried out for each of the 10 m values; the one at which the successive approximations converge in a single curve $U(z)$ in the best way was selected. The result for the relief (curve 1 in Fig.) corresponds to the 6th approximation and m=1.2m_0, where m_0 is the mass of a free electron. The barrier is much thinner than the insulating layer, its maximum is shifted towards the contact with the polycrystalline material, the potential drop towards the contact with Si is much more shallow than in the direction of poly n^+-Si, and the effective mass of the tunneling electron is greater than the value for a free particle.

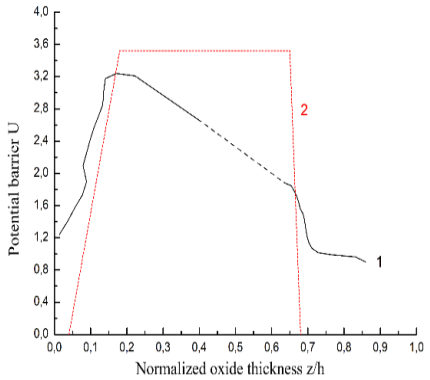

The work was carried out within the framework of the state task and partially supported by the Russian Foundation for Basic Research (projects No. 18-29-11029, No. 19-29-03042).

1. E.I. Goldman, A.G. Zhdan, N.F. Kukharskaya and M.V. Chernyaev. “Reconstruction of the Potential Profile in an Insulating Layer Using Current–Voltage Characteristics of Tunneling MIS Diodes”. Semiconductors, **42**, pp. 92-98, 2008. https://doi.org/10.1134/S1063782608010132.
2. E.I. Goldman, S.A. Levashov, and G.V. Chucheva. “Features of the Characteristics of Field-Resistant Silicon–Ultrathin Oxide–Polysilicon Structures”. Semiconductors, **53**, pp. 465–468, 2019. https://doi.org/10.1134/S1063782619040109.

Characterization of mobility in thin-films structures

E.G. Zaytseva, O.V. Naumova
Rzhanov Institute of Semiconductor Physics, Novosibirsk, Russia, zayceva@isp.nsc.ru

Mobility is a key quantity of carrier transport in hetero systems. The analysis of mobility and scattering mechanisms of free carriers is of great importance in the synthesis of new materials, development of thin-film technologies, and control over the fabrication of films and devices based on them [1, 2]. In thin films, the electrical potentials at the opposite interfaces of the film are interconnected ones, exhibiting the so-called coupling effect. As a result, the analysis of scattering mechanisms in thin-film structures becomes problematic, since the conditions at the two interfaces of the film will equally affect the value of the mobility [3, 4].

This study is devoted to the investigation of the dominant mechanisms of carrier scattering in thin films. For this, thin-film SOI MOS transistors with a silicon layer thickness of 30 nm were used. The value of the mobility was determined by varying the potentials at the heterointerfaces. The analysis of the dominant scattering mechanisms was carried out based on experimental temperature dependences of mobility and numerical calculations. The regularities of the behavior of the mobility depending on the conditions at the heterointerfaces have been established. A correspondence is drawn between the localization of charge carriers relative to the film interface and the dominant scattering mechanisms.

1. P. Dutta, Y. Gao, M. Rathi, Y. Yao, Y. Li, J. Martinez, V. Selvamanickam. "High mobility single-crystalline-like silicon thin films on inexpensive flexible metal foils by plasma enhanced chemical vapor deposition ". Acta Materialia, **147**, pp. 51-58, 2018.
2. S. B. Mitta, M. S. Choi, A. Nipane, F. Ali, Ch. Kim, J. T. Teherani, J. Hone, W. J. Yoo. "Electrical characterization of 2D materials-based field-effect transistors". 2D Mater., **8**, 012002, 2021.
3. S. Cristoloveanu, N. Rodrigues and F. Gamiz. "Why the universal mobility is not". IEEE Trans. Electron Devices, **57**, pp. 1327-1333, 2010.
4. S. Cristoloveanu, M. Bawedin and I. Ionica. "A review of electrical characterization techniques for ultrathin FDSOI materials and devices". Solid-State Electron., **117**, pp. 10-36, 2016.

Electron transport in quasi-2D array of *As* dopants in Silicon

M.A. Kolpakov[1,2], S.A. Dagesyan[1,2], V.S. Vlasenko[1,2], S.Yu. Ryzhenkova[1,2], V.V. Shorokhov[1,2], D.E. Presnov[1,2,3], V.A. Krupenin[1,2]

1. Department of Physics, Moscow State University, Moscow, 119991 Russia, E-mail address
2. MSU Quantum Technology Center, Moscow, 119991 Russia, E-mail address
3. Skobeltsyn Institute of Nuclear Physics, Moscow State University, Moscow, 119191 Russia, E-mail address

To increase the productivity of modern calculation systems it is necessary to decrease the sizes of its elementary nodes which leads to smaller energy dissipations and faster interactions. Therefore, idea to use an array of dopant atoms in a solid-state matrix to create artificial neural networks [1] appears very promising. A reservoir neural network assumes that there is a system of randomly connected neurons with fixed ("untrained") connections between them, which could be activated (or "trained") by the adjusting of external inputs of the reservoir. Previously, the systems based on a disordered array of nanoparticles [2] and dopant atoms in silicon [3] surrounded by several electrodes were demonstrated.

The main idea was to create a nanoscale system to be used as a solid-state reservoir neural network. To do this an original fabrication method was developed for a system with closely positioned (from 50 to 200 nm) electrodes that play the role of external connections to the reservoir. In the fabricated experimental structures, the tunnel conductivity was demonstrated through the array of dopant arsenic atoms located between the electrodes in the silicon (reservoir). The proposed fabrication method allows to control the density of the dopant atoms in the array by the doping level or by the additional etching of the near-surface silicon level [4]. Due to the small effective size (from nm 3 to 5 nm) of an arsenic atom in silicon it was expected that the developed structure will have a high operating temperature [5].

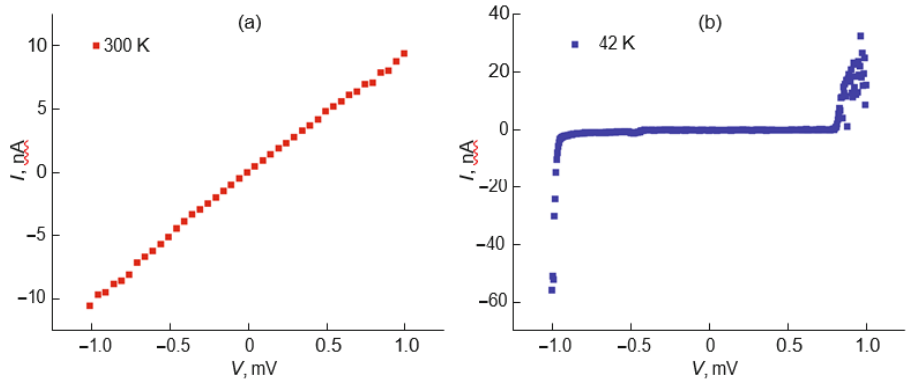

Fig. 1. The typical current-voltage characteristics of "etched-to-the-end" samples at (a) 300 and (b) 4.2 K.

The electric characteristics of the experimental structures were measured at temperatures of 4.2 and 300 K before and after the additional etching: before the additional etching of the upper silicon layer the fabricated structures had linear current-voltage characteristics both at room temperature and at a liquid-helium temperature corresponding to an almost "metallic" conductivity with a resistance below 100 kΩ at room temperature and growing with cooling. After additional etching procedure was applied to the sample the typical current-voltage characteristics of "etched-to- the-end" samples were measured as presented in Fig.1. At room temperature the dependence is close to linear and the characteristic resistance is approximately equal to 100 kΩ. At 4.2 K the greatest value of the Coulomb blockade exceeds 100 mV.

1. C. Gallicchio, A. Micheli, and L. Pedrelli, Neurocomputing, **268**, pp.87, 2017.
2. S. K. Bose, C. P.Lawrence, Z. Liu, et al., Nat. Nanotechnol. **10**, pp.1048, 2015.
3. T. Chen, J. van Gelder, B. van de Ven, et al., Nature (London, U.K.) **577**, pp.341, 2020.
4. S.A. Dagesyan, V.V. Shorokhov, D.E. Presnov, E.S. Soldatov, A.S. Trifonov, V.A. Krupenin, "Sequential reduction of the silicon single-electron transistor structure to atomic scale", Nanotechnology **28**, 225304 (pp.7), 2017.
5. V.V. Shorokhov, D.E. Presnov, S.V. Amitonov, Yu.A Pashkin, V.A. Krupenin, "Single-electron tunneling through an individual arsenic dopant in silicon" Nanoscale, **9**, pp.613-620, 2017.

Study of silicon carbide surface at different stages of doping by nitrogen atoms

M.Z. Andalashvili[1], D.E. Presnov[1,2,3], D.K. Minenbaev[1,2], A.E. Rogozin[4], A.V. Miakonkikh[4], A.V. Lubenchenko[5], I.I. Tsiniaikin[1,2], V.A. Krupenin[1,2], A.S. Trifonov[1,2]

1. Faculty of Physics, Moscow State University, 119991 Moscow, Russia, andalashvili.mz18@physics.msu.ru

2. MSU Quantum Technology Centre, Moscow, 119991, Russia artem.trifonov@physics.msu.ru

3. Nuclear Physics Institute, Moscow State University, 119991 Moscow, Russia, denis.presnov@physics.msu.ru

4. Valiev Institute of Physics and Technology, Russian Academy of Sciences, 117218 Moscow,Russia, rogozhin@ftian.ru

5.Department of General Physics and Nuclear Fusion, National Research University "Moscow Power Engineering Institute", 111250, Moscow, Russia, LubenchenkoAV@mpei.ru

Using the quantum properties of individual atoms as key elements of nanoelectronic devices is a very attractive idea, since atoms have a stable electronic structure and well-defined properties. Since the energy of the single-particle electronic valence level of the dopant can be comparable to the Coulomb energy of the system, for certain combinations of the crystal matrix and the dopant atom, the working temperature of the structure can reach high values [1, 2]. Prototypes of quantum bit and quantum logic gates based on single-atom single-electron tunneling devices have already been demonstrated.

The advantage of using silicon carbide (SiC) instead of silicon as a matrix from which nanoelectronic devices are made is that the band gap of SiC is almost three times larger (3.23 eV for the 4H polytype), which will significantly increase the operating temperature of the devices. Nitrogen atoms are used as classical doping donors for SiC.

Silicon carbide samples were doped with N_2^+ ions with energy of 8 keV at room temperature; the type of ions for irradiation was controlled by a separating magnet. Radiation dose varies in $5x10^{13}$-10^{15} см$^{-2}$ range. After doping, the samples were annealed in two stages at temperatures from 800 to 1250 °C, the duration of each stage was 100 sec. The X-ray photoemission spectroscopy (XPS) studies of the samples surfaces were performed with the help of the electron-ion spectroscopy module and shows that relative concentration of nitrogen atoms after doping is 7.7 % (Fig 1a, line #4).

The surface roughness (RMS) of silicon carbide after all processing stages was determined by scanning probe microscopy. RMS of initial SiC and after all stages was 0.7 ± 0.3 nm, which is acceptable for creating nanostructures on such a surface. Optimum surface conductivity (23 kOhm/□) was achieved at radiation dose $5x10^{14}$ cm^{-2} and annealing temperature 1250 °C.

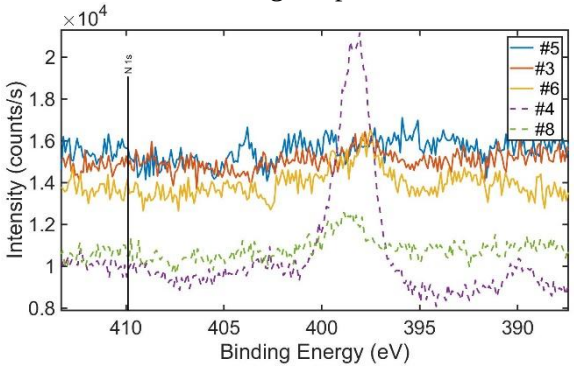

a)

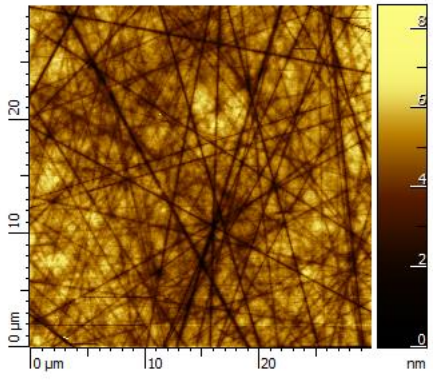

b)

This research has been supported by the Interdisciplinary Scientific and Educational School of Moscow State University «Photonic and Quantum Technologies. Digital Medicine».

1. G. Lovat, B. Choi, D.W. Paley, M.L. Steigerwald, L. Venkataraman and X. Roy, «Room-temperature current blockade in atomically defined single-cluster junctions». Nature Nanotechnology **12**, 1050, 2017. http://doi.org/10.1038/nnano.2017.156

2. S.J. Shin, J.J. Lee, H.J. Kang, J.B. Choi, S.-R. Eric Yang, Y. Takahashi, and D.G. Hasko. «Room-Temperature Charge Stability Modulated by Quantum Effects in a Nanoscale Silicon Island», Nano Lett. **11**(4), 1591, 2011. http://doi.org/10.1021/nl1044692

MBE growth of GaAs on modified silicon substrates

M. Eremenko[1], N. Shandyba[1], M. Solodovnik[1], S. Balakirev[1], N. Chernenko[1], O. Ageev[1,2]
1. Institute of Nanotechnologies, Electronics and Equipment Engineering, Southern Federal University, Taganrog, Russia, eryomenko@sfedu.ru
2. Research and Education Center "Nanotechnologies", Southern Federal University, Taganrog, Russia

The formation of high-quality III/V light-emitting sources on silicon remains one of the important modern tasks of optoelectronics and nanophotonics. The growth of the III/V polar semiconductor on a non-polar Si substrate leads to a decrease in the slope efficiency compared to native substrates. Despite the fact that a wide range of techniques is used to improve the structural and functional characteristics of the III/V optical components on Si, completely new approaches are required to reduce the defectiveness of the resulting structures. In this work, we investigated the effect of the implantation dose upon treatment with a focused ion beams and the growth rate on the morphology of the grown GaAs structures.

The studies were carried out on on-axis Si(001) substrates with local modification areas. The surface modification was carried out by local implantation of Ga ions into the Si substrate by the method of focused ion beams. The implantation dose varied from 1 to 21 pC/μm^2 and the current was 1pA. The growth rate varied from 0.1 ML/s to 1 ML/s. The removal of native oxide from the Si surface was carried out at 900°C in vacuum for 30 minutes. Then, a high temperature (600°C) GaAs buffer layer was deposited.

The effect of the dose of Ga implanted in Si was investigated and the degree of filling of the areas was calculated to reveal the optimal parameters of surface modification. At the lowest dose of Ga implantation equal to 1 pC/μm^2, the deposition of GaAs on modified areas occurs as separate crystallites with an irregular shape. An increase in the implantation dose leads to GaAs coalescence and further filling of the areas. At doses of 1, 3, 7, and 21 pC/μm^2, the degree of filling of the modified areas was 67%, 91%, 99%, and 95%, respectively. Analysis of the surface roughness showed that with an increase in the Ga ion implantation dose from 1 to 7 pC/μm^2, the roughness of the grown structures decreases (from 56 to 23nm). However, the roughness increases with an increase in the implantation dose from 7 to 21 pC/μm^2 (from 23 to 37 nm).

Studies have shown that an increase in the GaAs growth rate from 0.1 to 1.0 ML/s (Figure 1) with a constant As_4 flux leads to an intensification of the nucleation and growth processes of GaAs nanowires, regardless of the implantation dose. This behavior is due to the local accumulation of uncompensated Ga, which is associated with the presence of an excess of Ga atoms in the modified areas of Si. It should also be noted that outside the modification areas, an increase in the GaAs growth rate leads to a sharp increase in the density and size of GaAs crystallites, reducing the selectivity of nucleation and growth processes, which, nevertheless, does not lead to the formation of a continuous film. The best morphology with 99% coverage is observed with an implantation dose of 7 pC/μm^2 and growth rate 0.1 ML/s.

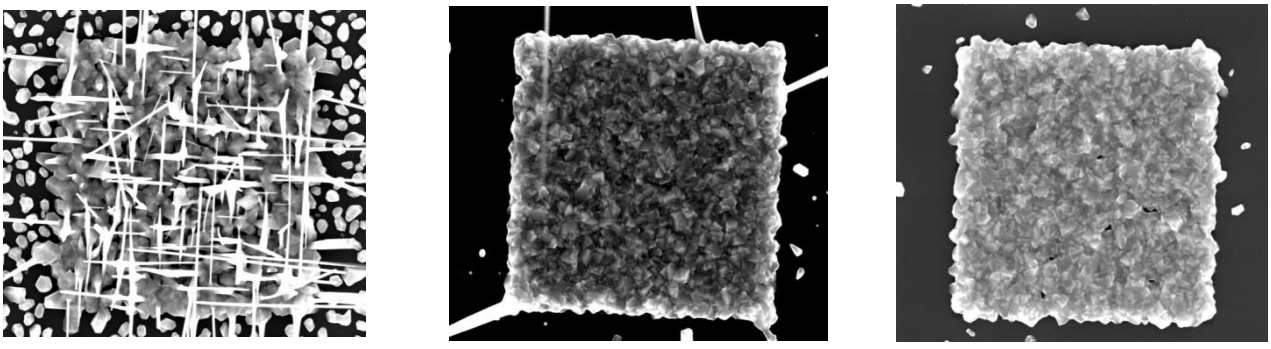

(a) (b) (c)

Fig. 1. SEM images of modified Si areas after deposition of 200 nm GaAs at T = 600°C with different growth rates: (a) v = 1 ML/s, (b) v = 0.25 ML/s, (c) v = 0.1 ML/s. The implantation dose and FIB current were 7 pC/μm^2 and 1 pA, respectively.

This work was supported by the Russian Science Foundation Grant No. 20-69-46076. The results were obtained using the equipment of the Research and Education Center "Nanotechnologies" of Southern Federal University.

In-situ MOVPE growth characterization of GaAs-based heterostuctures

N. Volkov
Sigm Plus, Moscow, Russia, Volkov_n_a@mail.ru

Measurement and characterization of semiconductor structures have always been critical for evaluation of MOVPE growth. Unfortunately results of traditional ex-situ measurements may significantly lag behind the end of growth process in which the structures were made. Although such delayed measurement results are tolerable for R&D facilities, production companies with non-stop growth cycles may be highly impacted by growth process disruption which can lead to severe losses.
Today MOCVD equipment production companies have in-situ measurement tools optionally available for their customers. One of such systems, EpiTT, which is available for Aixtron systems, is capable of measuring reflection of 3 wavelengths – 405nm, 633nm and 985nm. Light is generated by 3 LEDs and is transported to growth interface via optical fiber. The reflected light is collected in measurement head on top of the reactor lid and is transported back into detector unit. Besides temperature and thickness growth measurements, the EpiTT tool has less known feature of multiple wafers satellite rotation speed measurement. Although arbitrary growth speed is measured rather than real rotations per minute, comparative analysis can show relative speed of satellites in same process or complete stop of a satellite. Continuous stops normally lead to rejection of structures on stopped satellite and relative growth differences is something to watch for since different rotation speeds may lead to thickness fluctuations. The oscillations of 985nm light on GaAs growth interface is shown on Fig. 1. It is clearly seen that GaAs layer thickness difference of structures on satellite #3 comparing to neighboring satellites is increasing with time. Such thickness difference is attributed to lower speed and to occasional short stops of satellite #3.

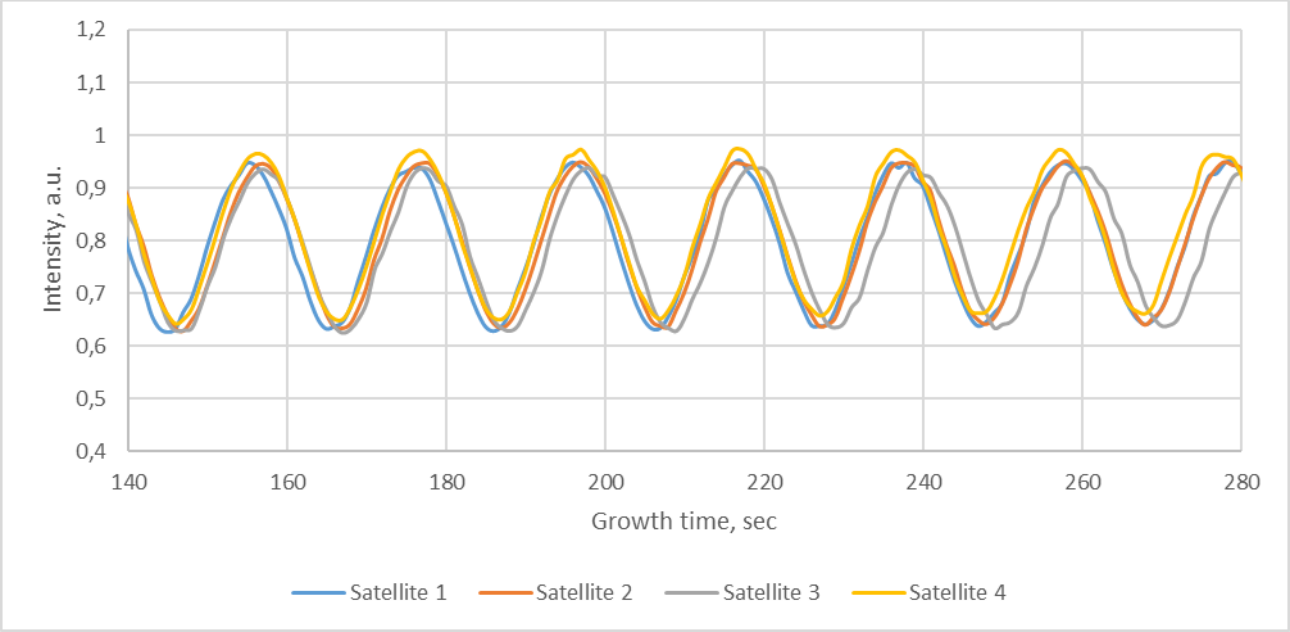

Fig. 1. 985nm light oscillation on GaAs growth interface for structures on 4 satellites in a MOCVD growth.

Luckily, in-situ characterization tools have built-in analitical software which can calculate thickness of such differently grown structures. In most cases decisions on wheather structures from various satellites can be passed to processing after growth can be made before the growth ends and great speed variations can indicate on growth tool malfunction.

Strain-compensated AlGaInAs/InP heterostructures for high-power laser diodes

V.N. Svetogorov, Yu.L. Ryaboshtan, M.A. Ladugin, A.A. Marmalyuk
Stelmach Research Institute Polyus, Moscow, Russia, bereg@niipolyus.ru

High-power laser diodes (LD) in the spectral range of 1.3-1.6 μm are widely used in many fields of modern science and technology. For their creation, as a rule, semiconductor heterostructures AlGaInAs/InP and InGaAsP/InP are used.

In comparison, It can be noted that the AlGaInAs/InP system has a large discontinuity in the conduction band $\Delta E_c = 0.72\Delta E_g$ compared to InGaAsP/InP ($\Delta E_c = 0.4\Delta E_g$), which means an increase in the depth of the potential well for electrons. High-power LDs based on this system of materials should have low threshold current and operate as higher temperatures without requirements for the use of thermoelectric coolers. As a result, the AlGaInAs/InP heterostructure becomes more preferable for creating high-power LDs.

The main negative effect on the LD parameters in the presented wavelength range is expected by an increase in the Auger-recombination intensity, which degrades the external quantum efficiency, lowers the output power level, and also causes a high temperature dependence of the output characteristics [1]. One of the methods to reduce it is the use of strain-compressive quantum wells in the active region of the LD. In this case, the magnitude of stresses in such quantum wells should not exceed critical values to prevent the generation of misfit dislocations.

In this work, a calculated estimate of the distribution of strain over the entire thickness of the active region of a high-power LD based on AlGaInAs/InP heterostructure is carried out [2, 3]. A modification of the computational model is proposed to clarity the nature of the strain distribution in the strain-compensated active region. To confirm the calculation results, photoluminescence studies of the active region of various configurations were carried out, which showed a twofold increase in the intensity of the photoluminescence signal.

Based on the results obtained, it was possible to create LD of the spectral range under consideration with an output power a continuous mode 4.2 W at 15 A and in a pulsed mode of 20 W (100 ns, 5 kHz) at a pump current of 80 A.

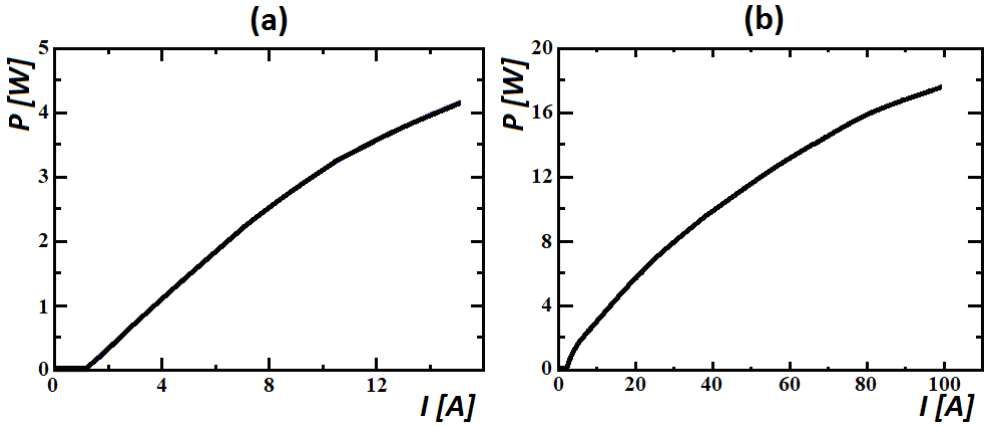

Fig. 1. Light-current characteristics of high power LD (a) continuous mode; (b) pulsed mode.

1. A.D. Andreev, G.G. Zegrya, *"Auger recombination in strained quantum wells"* Semiconductors, **31**, pp. 297-303, 1997.
2. Yu.B. Bolkhovityanov, O.P. Pchelyakov, S.I. Chikichev, *"Silicongermanium epilayes: physical fundamentals of growing strained and fully relaxed heterostructures"* Journal Physics-Uspekhi, **171**, pp. 690-715, 2001.
3. D.C. Houghton, *"Design criteria for structurally stable, highly strained multiple quantum well devices"* Applied Physics Letters, **64**, pp. 505-507, 1994.

Electrical properties of GaAs-based metal-oxide-semiconductor structures with HfO_2 insulating films

S. Koveshnikov[1], V. Kovalskiy[1], O. Soltanovich[1], M. Dorokhin[2], R. Kriukov[2], A. Zdoroveyshchev[2], and B. Zvonkov[2]

1. Institute of Microelectronics Technology RAS, Chernogolovka, Russia, general@iptm.ru

2. Research Institute of Physics and Technology, Lobachevsky State University, Nizhni Novgorod, Russia, nifti@nifti.unn.ru

Metal-oxide-semiconductor field effect transistors (MOSFETs) with III-V semiconductor based high mobility channels are strong candidates for advanced complementary metal-oxide semiconductor (CMOS) devices. The key advantage of these structures is a significant performance enhancement throughout device scaling as compared to traditional Si CMOS. Gallium arsenide, with five times higher electron mobility compared to silicon, is one of the most promising candidates for the role of high mobility channel material. However, the main obstacle in manufacturing these structures is the difficulty of achieving a practical enhancement-mode GaAs-based MOSFET due to poor interface quality between GaAs and gate dielectric films [1]. It is known that the GaAs surface and its interface with the gate oxide may contain partially saturated Ga- and/or As- dangling bonds which can induce midgap states leading to Fermi level pinning [2].

In this work, we investigated electrical properties of GaAs-based metal-oxide-semiconductor (MOS) structures with HfO_2 insulating films. The growth process of the samples consisted of the two stages: first, two 250 nm thick C-doped GaAs buffer layers with concentrations 10^{16} cm^{-3} and 10^{15} cm^{-3} were subsequently grown on the p^+-GaAs substrate by metal organic chemical vapor deposition (MOCVD) at 600°C; second, the sample were taken out from the MOCVD reactor chamber, cleaned and placed into the high vacuum chamber for electron beam evaporation of 15 nm thick HfO_2 film. Finally, 30 nm thick Au gate contacts with the diameter of 0.5 mm were fabricated.

The electrical properties of the fabricated MOS structures were studied by capacitance-voltage (C-V) technique in the frequency range from 1 kHz to 100 kHz using Keithley 4200A-SCS parameter analyzer. The C-V measurements demonstrated transition of the MOS structures from depletion to accumulation with voltage sweeping in the range from +1 V to -2V thus indicating effective modulation of the GaAs depletion layer width and the absence of the Fermi-level pinning effect. The distribution profiles of the elements and their chemical bonds were investigated using X-ray photoelectron spectroscopy (XPS). The obtained results showing the presence of GaO_x-rich layer at the vicinity of HfO_2/p-GaAs interface provides plausible explanation of the lack of Fermi-level pinning. This finding is in agreement with the data in Ref. [3] demonstrating no Fermi-level pinning due to passivation of the GaAs surface with the gallium oxide layer.

Thus, the results of our work imply that high quality GaAs/HfO_2 interface can be obtained without additional GaAs surface passivation layers.

1. M. Passlack, M. Hong, E. F. Schubert, J. R. Kwo, J. P. Mannaerts, S. N. G. Chu, N. Moriya, and F. A. Thiel. "In situ fabricated Ga_2O_3–GaAs structures with low interface recombination velocity". Appl. Phys. Lett., **66**, pp. 625-627, 1995.

2. T. Wang, N. Moll, K. Cho, and J. D. Joannopoulos. "Computational design of compounds for monolithic integration in optoelectronics". Phys. Rev. B, **63**, p. 035306, 2000.

3. Weichao Wang, Geunsik Lee, Min Huang, Robert M. Wallace, and Kyeongjae Cho. "First-principles study of GaAs (001)-β2(2×4) surface oxidation and passivation with H, Cl, S, F, and GaO". J. Appl. Phys., **107**, p. 103720, 2010.

Mechanical properties of p-type thermoelectric materials on the basis of Bi-Sb-Te system determined by nanoindentation

A. Yakubov, D. Pepelyaev, D. Murashko, A. Gerasimenko, D. Terekhov, I. Voloshchuk, M. Shtern, A. Sherchenkov

National Research University of Electronic Technology Moscow, Zelenograd, Russia, aa_sherchenkov@rambler.ru

An important role in the production and conversion of energy belongs to thermoelectricity. The main fields of application of thermoelectric devices are connected with cooling, temperature control and power generation. The characteristics of thermoelectric devices are determined by the properties of thermoelectric materials (TEM) used for their fabrication. Efficient low-temperature TEMs used for the manufacture of thermoelectric cooling devices and thermoelectric generators operating at temperatures up to 300 °C are solid solutions based on n-type Bi_2Te_3-Bi_2Se_3 and p-type Bi_2Te_3-Sb_2Te_3. However, in addition to the high efficiency, TEMs must have high mechanical strength in order to withstand mechanical and thermal loads, large temperature gradients, thermal cycling, which can be accompanied by the appearance of significant mechanical stresses that can even lead to the destruction of thermoelements. Therefore, the composition of the solid solution and the used dopants should provide not only a high thermoelectric figure of merit, but also the necessary mechanical strength of the TEM. In this regard, the purpose of this work was to study the mechanical properties of a solid solution based on p-type Bi_2Te_3-Sb_2Te_3 compounds of various compositions.

Mechanical properties were investigated for the following low-temperature TEMs: $Bi_{0.5}Sb_{1.5}Te_3$ + 3% Te + 0.09% Pb; $Bi_{0.5}Sb_{1.5}Te_3$ + 4% Te; $Bi_{0.5}Sb_{1.5}Te_3$ + 3% Te + 0.08% Pb; $Bi_{0.5}Sb_{1.5}Te_{2.91}Se_{0.09}$ + 1.5% Te + 0.27% Pb; $Bi_{0.5}Sb_{1.5}Te_{2.91}Se_{0.09}$ + 1.5% Te + 0.3% Pb; $Bi_{0.5}Sb_{1.5}Te_{2.91}Se_{0.09}$ + 1.5% Te + 0.35% Pb; $Bi_{0.5}Sb_{1.5}Te_{2.91}Se_{0.09}$ + 1.5% Te + 0.38% Pb.

Thermoelectric materials were synthesized by direct fusion of semiconductor-grade elements in sealed quartz ampoules in an argon atmosphere at a temperature of 950 K. The density of these materials was estimated using Archimedes method. The study of the mechanical properties of the synthesized materials was carried out on a NanoScan-4D Compact nanohardness tester. The parameters of hardness and Young's modulus were calculated using the Oliver-Pharr method [2]. The tests were carried out at applied loads of 30, 40, and 60 mN. The results of measuring the hardness and Young's modulus for TEM $Bi_{0.5}Sb_{1.5}Te_{2.91}Se_{0.09}$ + 1.5% Te with the different Pb concentrations of 0.27, 0.35, and 0.38 at.% are shown in Figure 1.

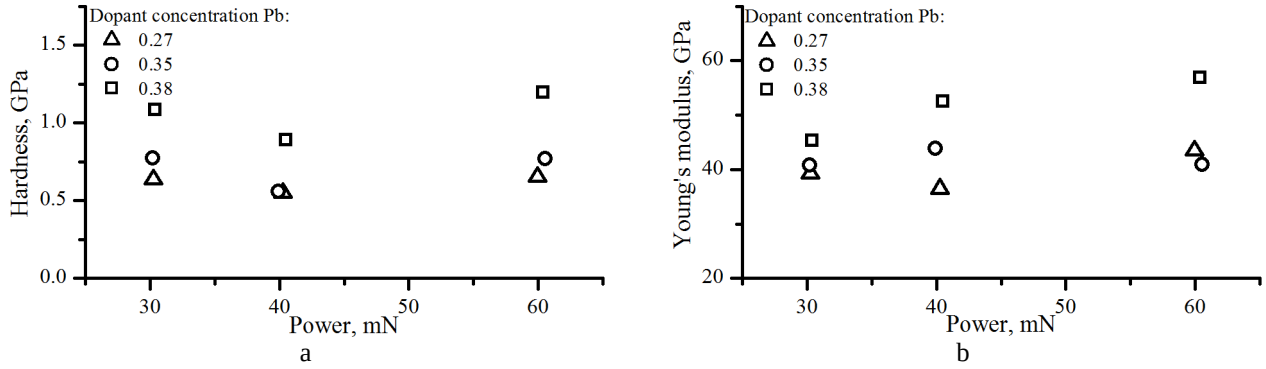

Fig 1. Dependences of hardness (a) and Young's modulus (b) on the applied load

As can be seen from the plots, the values of hardness and Young's modulus in most cases increase with an increase in the alloying concentration of lead. Thus, the values of hardness and Young's modulus were determined for different low-temperature thermoelectric materials. It is shown that the concentration of the dopant can have a significant effect on these characteristics. These parameters must be taken into account when developing a thermoelectric generator.

This work was supported by the Russian Science Foundation (project number 21-19-00312).

1. W.C. Oliver and G.M. Pharr. “An improved technique for determining hardness and elastic modulus using load and displacement sensing indentation experiments”. J. Mater. Res., **7**(6), pp. 1564-1583, 1992.

Investigation of the thermal properties for n-type thermoelectric materials on the basis of Bi-Se-Te system

Y. Shtern, M. Shtern, A. Sherchenkov, M. Rogachev, D. Pepelyaev, A. Babich
National Research University of Electronic Technology, Zelenograd, Russia, drent@yandex.ru

Thermoelectricity is one of the most promising and actively developing fields of science and technology. Thermoelectric generators (TEGs) using Seebeck effect are perspective as alternative energy sources for converting thermal energy into electrical one. A wide variety of heat sources can be used for operation of TEGs, including waste heat. However, low efficiency complicates their wide application.

Nowadays a new attractive field of TEG utilization is emerging. The development of the Arctic, Antarctic, hard-to-reach regions of the Far North of Russia is impossible without the use of autonomous energy sources, which include thermoelectric generators. For actively developed high-tech intelligent systems and sensors, devices for aerospace, military, computing and microwave technology, it is necessary to create highly efficient compact bulk, flexible and film thermoelectric microgenerators. However, flexible TEGs for wearable mobile devices are still at the stage of investigations and development of technology.

For successful practical application of all kinds of thermoelectric generators, in addition to high thermoelectric figure of merit Z, it is necessary to provide high stability of properties since the operation of TEGs is associated with using high temperature gradients, thermal cycling and other temperature treatments [1]. Although an important task is investigation of the specific heat of thermoelectric materials, since this allows to determine such an important parameter as thermal conductivity. It was shown that Bi-Se-Te materials are the best thermoelectric materials for the low temperature range [2]. In this regard a complex investigation of thermal properties and stability of such materials was the aim of this work.

The investigated materials were synthesized by direct alloying of the components taken as elements of semiconductor purity in stoichiometric ratio. Synthesis was carried out in sealed quartz ampoules in an Ar atmosphere at the temperature of 950 K. The furnace with ampoules was swinging continuously to homogenize the melt.

Then jaw crusher and knife mill were used for material processing. The average sizes of the particles after that treatment were about 0.5-1.0 mm. Next, obtained materials were placed in quartz ampoules and its directional crystallization was carried out by the method of vertical zone melting. After this, until the ampoules were depressurized, the materials were homogenized by annealing at a temperature of 650 K for 30 hours. Thus, the compositions of Bi-Te-Se system were obtained.

Scanning electron microscopy (Jeol JSM-6480LV) with energy dispersive spectrometry (Inca Energy Dry Cool) was used to study material compositions. The structure of obtained materials was studied by X-ray diffraction (Bruker D8).

It is important to understand what processes may occur in materials during heat treatment, as this directly affects the operation of the final device. In this regard, multiple measurements of investigated materials were carried out using differential scanning calorimetry (Netzsch 204 F1 Phoenix) and thermogravimetry (Netzsch STA F3 Jupiter). These methods complement each other perfectly and allow to obtain direct information about thermal processes in studied materials. Samples for thermal analysis were prepared as powders with the masses of about 10 mg, which were pressed in the aluminum crucibles. Empty aluminum crucibles were used as references. Measurements were carried out in the temperature range from 300 to 600 K at a heating rate of 10 K per minute in an argon flow with a flow rate of 50 ml per minute. Calorimeters were pre-calibrated using 6 different standards. For specific heat measurements synthetic sapphire standard was used for calibration. Five measurements of each sample were carried out. No thermal effects were observed on either the differential scanning calorimetry curves or the thermogravimetry curves up to 600 K. Thus, thermal cycling does not initiate any phase transitions.

This work was supported by the Russian Science Foundation (project number 21-19-00312).

1. Yu.I.Shtern. “A procedure to study thermo- and electrophysical properties of materials”. Inorg. Mater., **45**, pp. 1631-1634, 2008.

2. A.A. Sherchenkov, Yu.I. Shtern, R.E. Mironov, M.Yu. Shtern, and M.S. Rogachev. “Current state of thermoelectric material science and the search for new effective materials”. Nanotechnologies in Russia, **10**, pp. 827–840, 2015.

Investigation of nanoporous low-k dielectrics by spectral ellipsometry

R. Gaydukasov[1,2], A. Miakonkikh[1]
1. Valiev Institute of Physics and Technology of Russian Academy of Sciences, Moscow, Russia.
2. Moscow Institute of Physics and Technology (State university) (MIPT), Moscow, Russia.

From the topological size of 45 nm, metallization systems of ultra-large-scale integration (ULSI) are built on the basis of a porous dielectric with ultra-low relative permittivity to reduce capacitance between interconnections. Currently, low-k dielectrics are common, such as porous organosilicon glasses (OSG), which have a porosity of about 30% -40% and a permittivity close to 2.5, and an average pore size of 0.7-2 nm. These dielectrics are proposed to be used in sub-10 nm technological routes, therefore they are under intensive research. The control of the size of sub-nanometer pores in a dielectric material is a difficult experimental task. One of the approaches for determining the porosity and pore size distribution is ellipsometric porometry. This method is based on measuring the change of the refractive index of the film with an increase in the relative pressure of the adsorbate and its condensation in the pores. This makes it possible to measure the adsorption isotherm, which is the volume of the liquid condensed in the pores as a function of the vapor pressure. The adsorption isotherm should be described by an integral equation:

$$W = \int_0^{+\infty} z(r)K(r,p)dr, \quad (1)$$

where $z(r)$ is the pore size distribution, and $K(r,p)$ is the integral kernel. To describe the adsorption in pores whose radius is greater than 2 nm, the integral kernel has the form:

$$K(r,p) = \begin{cases} 1, r < r_0 \\ 0, r > r_0 \end{cases}, \quad (2)$$

where $r_0 = r_m + t$ is calculated using the Kelvin and BET equations [1], which must be taken into account during adsorption:

$$r_0 = \frac{2\sigma M}{\rho RT ln p}; \quad t = \frac{CKp}{(1-Kp)(1+(C-1)Kp)}; \quad (3)$$

where σ - surface tension of the liquid, R - molar gas constant, T - temperature, M - molar mass, ρ density, C - the constant describing the interaction of the adsorbent and adsorbate, K - coefficient for expanding the scope of the BET equation. For micropores, the integral kernel in (1) has the following form:

$$K(r,p) = \begin{cases} \exp\left(-\left(\frac{rRTlnp}{\beta k}\right)^n\right), r_0 - \delta < r < r_0 + \delta \\ 0, \quad r \notin \{r_0 - \delta, r_0 + \delta\} \end{cases} \quad (4)$$

where E - free energy of adsorption, n is a parameter depending on the adsorbent, β is the affinity coefficient and $r_0 = 6/E$ [2]. The number δ is chosen so that the difference $r_0 - r$ tends to zero. Equation (1) belongs to the class of ill-posed problems. As a rule, their solution by numerical methods is associated with the occurrence of instabilities and artifacts that lead to significant errors. We propose to implement the solution by the Tikhonov regularization method [3]. The method is based on the search for an approximate solution of ill-posed operator problems $Az = W$, by minimizing the Tikhonov functional:

$$M^\alpha(z) \equiv \left\|A^h z - u^\delta\right\|^2 + \alpha\|z\|^2 \to min;\ z \in Z;\ \alpha > 0 \quad (5)$$

This problem is reduced to solving a system of linear equations.

The experiment was performed by lab tool based on Woollam M2000X spectral ellipsometer. For this study, industrial samples of a porous OSG low-k dielectric with a thickness of 202 nm deposited on Silicon wafer were used. These samples were examined for porosity and pore size distributions. The work will present the results of calculating the pore filling curve of the sample according to the given model pore distribution (direct problem) and the reconstructed pore distribution obtained from it using our algorithm (ill-posed inverse problem), as well as the results of measuring the pore distribution on the studied samples.

This work was partially supported by the RFBR grant No. 18-29-27025.

1. S. Brunauer, J. Skalny, E.E. Bodor. "Adsorption on nonporous solids". Journal of Colloid and Interface Science, Vol. 30, № 4. P. 546–552, 1969.
2. M.M. Dubinin, H.F. Stoeckli. "Homogeneous and heterogeneous micropore structures in carbonaceous adsorbents". Journal of Colloid and Interface Science, Vol. 75, № 1. P. 34–42, 1980.
3. A.N. Tikhonov, V.Y. Arsenin. Solution of Ill-posed Problems. Washington: Winston & Sons, 1977.

Influence of low-energy Ar ion bombardment on the texture and resistivity of Ti films

R. Selyukov[1], M. Izyumov[1], V. Naumov[1], L. Mazaletskiy[2]
1. Yaroslavl Branch of the Valiev Institute of Physics and Technology, Yaroslavl, Russia, E-mail: rvselyukov@mail.ru
2. P.G. Demidov Yaroslavl State University, Yaroslavl, Russia.

Thin (001) textured Ti films are used as adhesive underlayers for Al, AlN, TiN, Pt, and ferromagnetic films. The Ti underlayer texture influences the properties of these films. Ion bombardment carried out during the deposition is widely used to control the film texture but a little is known about the influence of post-deposition ion bombardment on the film texture. In this work the influence of low-energy Ar ion bombardment on Ti film texture and resistivity is studied. 10-40 nm Ti films deposited on oxidized Si(100) were exposed to series of four 30 min ion-plasma treatments (IPTs) in an Ar rf inductively-coupled plasma at pressure 0.08 Pa. The bias 20, 25, and 30 V was applied to the films and the ion current density was 7.4 mA/cm^2. The specimen temperature didn't exceed 40°C during IPT.

As-deposited films have a mixed texture (100) + (001) and the (100) oriented fraction increases with film thickness. IPTs lead to the weakening of diffraction peak Ti (002) and the peak Ti (100) increases (fig. 1a). The relative intensity of the peak (100) $I_{100}/(I_{100}+I_{002})$ increases faster for thinner films (fig.1b) and for higher bias. Formation of (100) texture in the Ti films during IPT can be explained using the model according to which the compressive stress in the films originates due to atom migration into grain boundaries [1]. It was shown in [2] that IPTs carried out in similar conditions lead to the increase of compressive stress in Cr films. This result was explained by the increase of adatom mobility due to ion bombardment and their migration into grain boundaries. It's known that (100) texture in Ti films is stress-induced, thus the (100) texture formation can be explained by the increase of compressive stress caused by ion bombardment. Higher ion energy results in higher adatom mobility, thus amount of stress necessary for texture transformation is achieved faster for higher bias. Also grain reorientation occurs faster in thinner films due to smaller grain size. The current of atoms into grain boundaries is higher for thinner films due to larger grain boundary area. Interplanar distance d_{002} measured along the film normal increases for 20 nm film but does not change for 30 and 40 nm films during 30 V series. 20 and 25 V IPTs do not change d_{002} for 20-40 nm films but lead to the increase of d_{002} for 10 nm film. Increase of d_{002} indicates the increase of compressive stress. The decrease of film resistivity was observed after some 30 V IPTs. Resistivity decreases by 14% for 10 nm film after first two IPTs, and by 28% for 20 nm film after fourth IPT.

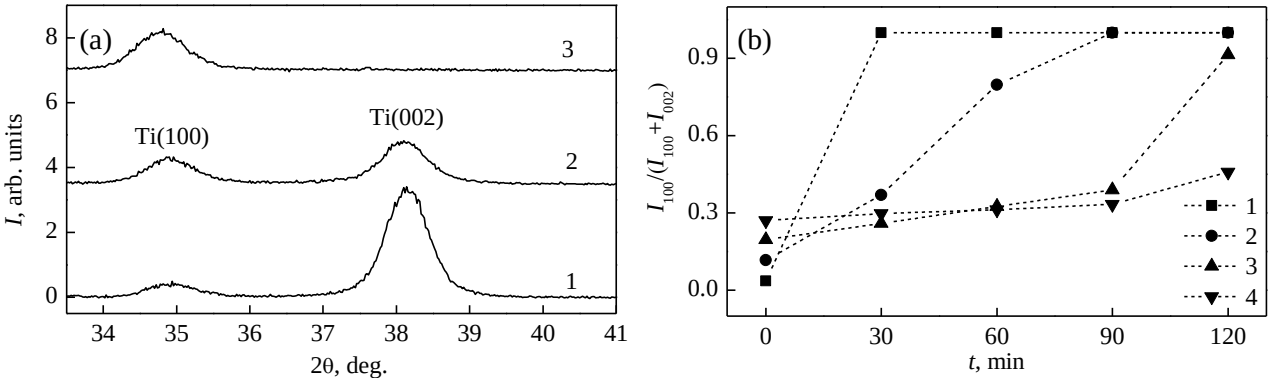

Fig. 1. (a) Diffractogram of 20 nm Ti film, as-deposited (1) and exposed to one (2) and three 30 V IPTs (3). (b) Relative intensity of the peak Ti (100) $I_{100}/(I_{100}+I_{002})$ vs. 30 V IPT time. 1 - 10 nm Ti film, 2 - 20 nm, 3 - 30 nm, 4 - 40 nm.

The investigation was supported by Program no. 0066-2019-0002 of the Ministry of Science and Higher Education of Russia for the Valiev Institute of Physics and Technology of RAS.

1. E. Chason, J.W. Shin, S.J. Hearne and L.B. Freund. "Kinetic model for dependence of thin film stress on growth rate, temperature, and microstructure". J. Appl. Phys., **111**, 083520, 2012.
2. A. Babushkin, R. Selyukov, I. Amirov. "Effect of Ar ion-plasma treatment on residual stress in thin Cr films". Proc. SPIE, **11022**, 1102223, 2019.

Investigation of the electrophysical and mechanical properties of metallization based on alloys W with Re, Ti, N for high-temperature silicon ULSI

A. Timakov, V. Shevyakov
National Research University of Electronic Technology, Moscow, Russia, aletimakov@yandex.ru

Currently, one of the priority directions for the development of the electronic industry both abroad and in our country is the creation of silicon semiconductor devices and ICs, which are able to operate at temperatures of 200 °C and above [1].

Since Russian researchers are only at the initial stage of exploratory research on the creation of a complex-functional high-temperature silicon micro- and nanoelectronics and there are few literature sources of foreign scientific research on this topic, there is a need for scientific research as well as applied development of basic technologies for high-temperature silicon element base.

In this work, it is shown that metallization is a critical unit of electronic products from the thermal stability point of view. New requirements involved with the reliability of the operation of devices as a whole are imposed on it. The currently used metallization materials are not able to meet the requirements for high-temperature products. In this sense, thin films of refractory metals (for example, tungsten) with increased electromigration resistance are suitable. To solve the problem of unsatisfactory mechanical properties and low adhesion ability of tungsten, the well-known "rhenium effect" is used worldwide, which manifests itself in a significant improvement in the plasticity of refractory materials: tungsten and molybdenum when rhenium is added to their volume (5-10%) [2].

It is noted that there is practically no scientific explanation for the function of this effect in the literature. This does not allow, in particular, to conduct a search for elements-analogues of rhenium. In this regard, the solution of the above problem is timely.

This work is devoted to the study of the electrophysical and mechanical properties of metallization based on alloys W with Re, Ti, N for high-temperature silicon ULSI.

The results of a study of the influence of technological (power, pressure, temperature, process time) and design factors (dopes of Re (5–15%), Ti (5–15%), N (5–15%) on the electrophysical and mechanical properties of tungsten films deposited by the magnetron method are presented. The optimal modes that provide the minimum resistance value are determined.

In the study of the mechanical properties of the films, it was found that the structures W (Re-5%) - Si or W (Ti-15%) - Si are characterized by a more than 5 and 3 times lower level of mechanical stresses, respectively, compared with W-Si. The force on separation of films W (Re – 5%) – Si or W (Ti – 15%) – Si exceeds the force on separation of the tungsten film (1200 G/mm^2) and amounts to 4800 G / mm^2 and 3750 G/mm^2. It is shown that metallization based on a tungsten alloys with rhenium or titanium has a significantly higher electromigration resistance compared to metallization based on an aluminum–copper–silicon alloy.

An approach (presentation) to the scientific substantiation of the "rhenium effect" when alloying with rhenium and its analogs of refractory metals is proposed, taking into account the effect of carbon as a background impurity in metals on the mechanical characteristics of films of refractory metals (built-in mechanical stresses, adhesive ability).

The results of the study confirmed the prospects of using these alloys of tungsten in high-temperature silicon micro- and nanoelectronics.

1. J. Watson and G. Castro. “High-Temperature Electronics Pose Design and Reliability Challenges”. Analog Dialogue, **46**, pp. 1-7, 2014.

2. V.I. Shevyakov et al. “Tungsten alloyed with rhenium as an advanced material for heat-resistant silicon ICs interconnects”. Proceeding of SPIE, **10224**, P. 10224-10, 2016.

Investigation of the deposition features and characteristics of diffusion barrier layers of Ti-TiN for metallization in MIS transistor structures with a vertical channel

V.S. Gornostay-Polsky, V.I. Shevyakov
National Research University of Electronic Technology, E –mail: vad00711@gmail.com

The main trend in the development of the IC's silicon element base is the reduction of topological norms and the design of new, more constructive versions of active elements. It provides a significant improvement in the characteristics of the IC. One of these elements is the MIS- transistor structure with a vertical channel. The peculiarity of its design is associated with the presence of metal contacts with a high aspect ratio to the source and gate regions buried in silicon. The metal contacts consist of Ti-TiN diffusion-barrier layers (DBL) located along the periphery of the trenches. These trenches are filled with a tungsten layer. The main problem is associated with such a structure is the conformity of the coating of their relief with Ti-TiN layers.

The analysis of modern methods of thin metal layers deposition is carried out. Physical (Ti deposition) and chemical (TiN deposition) methods are widely used to form DBL. The deposition was carried out on the AMAT ENDURA 5500 cluster tool. It was concluded that one of the most promising progressive method for increasing the conformity of film deposition on a relief surface is the method of chemical vapor deposition of an organometallic compounds (MOCVD) [1].

The paper presents the results of a study of methods for increasing the conformity of the coating of a silicon surface relief with a series of trenches with a width of 240 to 260 nm with Ti-TiN layers applied by physical and chemical deposition, respectively.

The results of the study of the influence of technological parameters (pressure, power, temperature) on the electrophysical properties of the PVD-Ti films are presented. The mode is determined that provides the minimum value of the volume resistance of Ti films with a thickness of ~15 nm. The pressure in the chamber was varied. Constant and variable DC and AC bias was applied to the target. The roughness of the obtained films was investigated by atomic force microscopy method, and the uniformity data of the thickness over the silicon wafer are indicated.

The results of the influence study of technological parameters on the electrophysical and mechanical properties of diffusion-barrier TiN films deposited by the MOCVD method from tetradimethylamide-titanium (TDMAT) are presented. The formation of TiN films was multistage. Each stage consisted of the deposition of a film layer with a thickness 5 nm and subsequent plasma treatment in a gas mixture N_2-H_2 *in-situ*. The number of stages in the process was determined by the required thickness of the TiN film. The multistage was due to the requirement to improve the conformity of the relief coating. The results were controlled by measuring the specific volume resistivity of the films. The goal was to minimize this parameter. During the deposition of a TiN film from TDMAT, carbon inclusions are formed in it. Plasma treatment promotes the reaction of hydrogen radicals in the gas with carbon impurities to form volatile hydrocarbons. The results of a study of the effect of the plasma treatment duration from 30 s to 45 s on the volume resistivity of the film are presented. A correlation was established between the values of the built-in mechanical stresses in the TiN film and the duration of the plasma treatment. We also associate it with the minimization of the residual level of carbon inclusions in the films.

Modes for DBL deposition were developed. The SEM data - analysis of cross-sections of the Ti-TiN films deposited on a relief silicon surface are presented. These results demonstrate a satisfactory conformity of the films deposition to the relief surface of trenches with a high aspect ratio. Passed functional control of the finished product confirms that the electrophysical parameters were in specifications.

1. Ju-Young Yun, Soo-Won Heo, Sang-Woo Kang. “A study on the real-time decomposition monitoring of a metal organic precursor for metal organic chemical vapor deposition processes”. Meas. Sci. Technol., **20**, pp. 1-6, 2009.

Copper filled contact plugs formation

S. Gorokhov[1, 2], S. Patyukov[2], V. Plaksin[2]
1. Moscow Institute of Physics and Technology, Dolgoprudny, Russia, sgorohov@niime.ru.
2. Molecular Electronics Research Institute, Moscow, Zelenograd, Russia.

The paper considered formation of contact plugs filled with copper instead of conventional tungsten. Copper has a lower resistivity than tungsten so its usage as conductive metal for contact plugs is desirable to increase IC performance. However, Cu atoms diffuse into the surrounding dielectric materials, doping Si with Cu leads to formation of deep energy levels in Si, and Cu also reacts with Si producing high resistance Cu_3Si states. In order to prevent a resulting deterioration of the devise's electrical performance the Cu plugs need to be isolated by reliable diffusion barrier layer.

The adhesive properties of copper to various materials such Ti, Ta, W, TiN, TaN were analyzed. Based on this analyze the suitable candidates were selected as barrier layers for the formation of contact plugs with copper. An experiment was carried out with the deposition of the selected layers on the wafer, followed by annealing at 410 °C 30 minutes, and measurements of the sheet resistance of stacks (Fig. 1) and surface roughness.

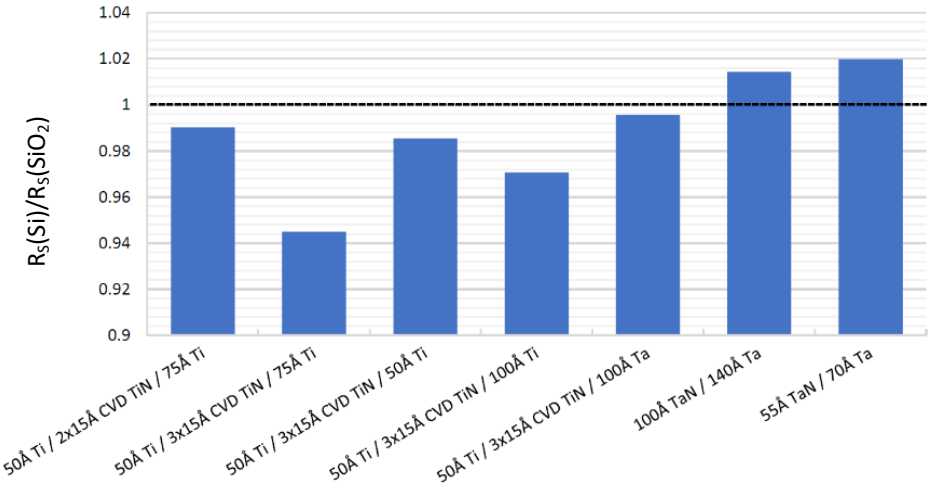

Figure 1. The ratio of sheet resistance of stacks on Si and on SiO_2.

Based on the results, multilayer structures with the best adhesive and barrier properties (Ti/TiN/Ti, Ti/TiN/Ta, TaN/Ta) were selected. After that, wafers with contact plugs were prepared, the influence of some parameters (deposition power, offset power) of the deposition processes of barrier layers and the seed layer of copper on the filling of contact plug with a large aspect ratio was studied. In result, working transistor structures with copper contact plugs were obtained, while the resistance of the contact chain, as well as the parameters of the transistors (leakage current, saturation current, threshold voltage) fully correspond to the specification.

1. G. Krasnikov, A. Valeev, N. Shelepin, O. Gushchin, K. Vorotilov, V. Vasil'ev, S. Averkin. Manufacturing method of multi-level copper metallization of VLSIC. Patent 2420827 RU.H01L 21/283. Date of filing: 11.01.2010. Date of publication: 10.06.2011. Bull. no. 16.
2. S. Gorokhov. "Calculating VLSI interconnect elements resistance". Nanoindustriya, **S96-2**, pp. 601-604, 2020.
3. A. Khandelwal, F. Wu, J. Or, K. Lai, J. Gelatos, M. Chang. "Evaluation of diffusion barriers for 32nm Cu contact metallization". Nanochip Technology Journal, **4**(3), pp. 2-5, 2006.

Structural and magnetic properties of nanostructured Co films fabricated by oblique angle deposition

D.M. Zakharov[1], A.A. Lomov[1], O.S. Trushin[2], L.A. Fomin[3]
1. Valiev Institute of Physics and Technology of RAS, Moscow, Russia, deniszakharovm@mail.ru
2. Valiev Institute of Physics and Technology of RAS, Yaroslavl Branch, Yaroslavl, Russia, otrushin@gmail.com
3. Institute of Microelectronic Technology and High Purity Materials, RAS, Chernogolovka, Russia.

A promising method for the formation of films with special properties is their nanostructuring during growth. One of the known technological methods allowing the growth of nanostructures is oblique angle deposition [1]. It is well known that by varying the angle of incidence one can change the direction of magnetic anisotropy [2]. Magnetic thin films with easy axis tilted to the substrate surface are of considerable interest as a promising material for ultra high density magnetic recording. Main goal of this work was to study structural and magnetic properties of nanostructured Co thin films fabricated by oblique angle deposition and finding optimal conditions for the formation of partial component of perpendicular magnetic anisotropy (magnetization vector tilted to the film surface). Experiments on the deposition of Co films on an inclined substrate were carried out on an Oratoria-9 electron beam evaporation unit. A standard single-crystal silicon wafer with a thermal oxide layer 300 nm thick was used as a substrate. Obtained experimental samples were further subjected to various types of analysis. Crystal structure of as deposited films was studied using SmartLab (Rigaku) X-ray diffractometer. Magnetization reversal curves for Co films were measured using vibromagnetometer LakeShore 7407. Magnetic Force Microscope (P-47 Solver NT MDT) was used to study magnetic domain structure. X-ray diffraction showed that Co thin films are growing polycrystalline, having preferable orientation (001) particles with the average size ~26 nm. Their magnetic properties were changing with inclination angle.

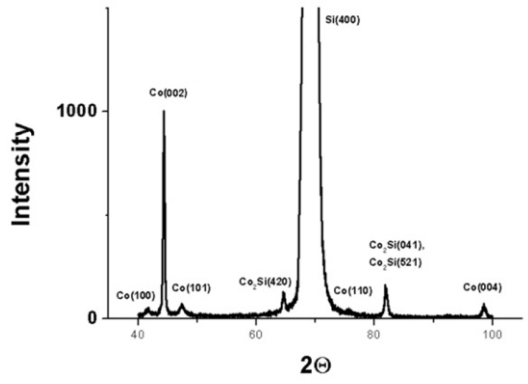

Fig. 1. X-ray difraction pattern for Co film deposited at inclination angle φ=80°.

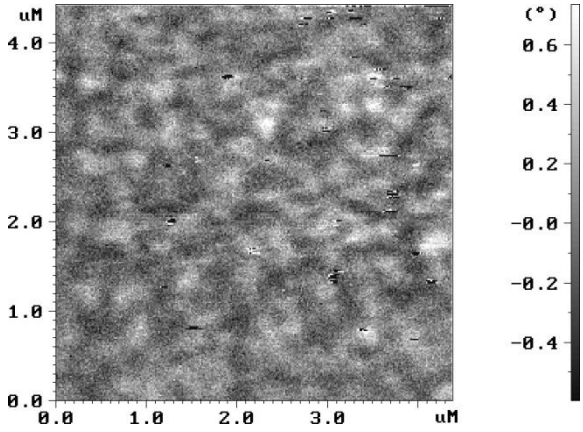

Fig. 2. Magnetic Force Microscope image of the sample at zero external field.

Thus, as a result of the experiments, it was found that optimal nanostructuring conditions are achieved at the substrate tilt angles more than 80°. In such conditions magnetic easy axis is oriented parallel to the inclination plane and nonzero component of magnetization normal to the substrate surface is appearing.

Reported study was carried out under State Programs #0066-2019-0003 and #0066-2019-0004 of the Ministry of Science and Higher Education of Russia on the equipment of the center for collective use of the scientific equipment «Diagnostics of micro- and nanostructures».

1. A. Barranco, A. Borras, A.R. Gonzalez-Elipe, A. Palmero, “Perspectives on oblique angle deposition of thin films: From fundamentals to devices”, Progress in Materials Science, **76**, pp. 59-153, 2016.
2. F. Tang, et.al “Magnetic properties of Co nanocolumns fabricated by oblique-angle deposition”, J. Appl. Phys. **93**, pp. 4194-4200, 2003

Features of the behavior of the resistance of thin Mo films during oxidation and weak antilocalization

V.A. Berezin, I.V. Malikov, L.A. Fomin
Institute of Microelectronic Technology RAS, Chernogolovka, Russia, fomin@iptm.ru

Currently, more and more attention is attracted to the study of the effect of the surface on the transport properties of conducting materials. In particular, it is of interest to study films of heavy metals in which the spin-orbit interaction is strong. In such two-dimensional systems, the Rashba and Rashba-Edelstein effects can manifest themselves, which make it possible to convert spin currents into charge currents during spin injection from a ferromagnetic material [1]. In this work, we paid attention to the behavior of the conductivity of Mo thin films. Having experience in growing perfect epitaxial films of refractory metals [2], we grew thin (~ 2 nm and thinner) Mo films on a sapphire substrate with metallic properties in the form of 0.2×0.2 mm^2 bridges. It was found that an increase in the resistance of the film per square (caused primarily by a decrease in the film thickness) leads to a change in the sign of the temperature coefficient of resistance in the temperature region from 50 to 300 K, but does not lead to a change in the characteristic increase in resistance at low temperatures. An important circumstance in the study of ultrathin films is the control of their continuity and uniformity in thickness. We carried out both control of the surface using a scanning probe microscope, which showed the continuity of the grown Mo films and the absence of planar defects (holes) larger than 5 nm, and measurements of the temperature dependence of the resistance of the film and control of its change with time. By controlling the conductive properties of the film as a function of time, one can judge how the bridge is predominantly oxidized. Four sections can be distinguished on the dependence of resistance on time. In the initial section, immediately after the preparation of the sample, the oxidation process is rather indefinite due to the smallness of the oxidized surface. After about 10 hours, the change in resistance reaches a logarithmic relationship. The third section also has a logarithmic dependence, but with a large coefficient. The change in the slope can be explained by the transition from a two-dimensional picture of the oxidation of a continuous film to a three-dimensional one, when the film is sour in places through and through and becomes "openwork". A further sharp increase in resistance is associated, from our point of view, with the complete oxidation of a part of the conducting channels in the "openwork" film and a corresponding decrease in the cross section of the conducting part of the film. In this case, the resistance of the bridge increases with decreasing temperature over the entire measured range. Thus, we can conclude that about 500 hours after spraying, the film is continuous and its oxidation occurs from the surface. The effect on the oxidation resistance along the grain boundaries in this area can be neglected, since their area is negligible compared to the lateral dimensions of the film. The measurement results show that in the low-temperature region, the resistance grows exponentially with decreasing temperature. This behavior is characteristic of the Kondo effect, weak localization, and jump conductivity. However, the numerical magnitudes of the effect are not typical for the first (high temperature of the onset of the effect) and the last case (weak change in resistance with a 20-fold change in temperature). A characteristic feature of weak localization is the dependence of the effect on an external magnetic field. We found that the magnetoresistance in the range of magnetic fields from -6 kOe to +6 kOe is positive and decreases with temperature, practically disappearing above 40K. This behavior is typical for antilocalization in relatively low fields; in high fields of ~ 3 - 4 T, a maximum is usually reached and then a decline is observed [3]. The presence of a maximum in the dependence upon antilocalization is explained by the competition between the magnetic disorder in the sample and the phase disruption due to the influence of the external magnetic field. In our case, an increase in magnetoresistance is observed up to the maximum field attainable for us of 8 T. We attribute these effects to antilocalization due to strong s-d scattering of electrons on the film surface.

1. T.H. Dang, J. Hawecker, E. Rongione, et.al. "Ultrafast spin-currents and charge conversion at 3d-5d interfaces probed by time-domain terahertz spectroscopy", Appl. Phys. Rev. **7**, p. 041409, 2020.
2. L.A. Fomin, I.V. Malikov, V.A. Berezin, et. al. "Probe Microscopy and Electron-Transport Properties of Thin Mo Epitaxial Films on Sapphire". Tech. Phys. **65**, p. 1748, 2020.
3. G. Bergman. "Weak localization in thin films: a time-of-flight experiment with conduction electrons". Phys. Rep. **107**, p. 1, 1984.

Formation of graphene structures on the surface of silicon carbide by the plasma ALE method

V.S. Klimin[1, 2], A.A. Rezvan[1], Yu.V. Morozova[1], I.O. Kessler[1], O.A. Ageev[2]

1. Southern Federal University, Institute of Nanotechnologies, Electronics, and Equipment Engineering, Department of Nanotechnologies and Microsystems, Taganrog, Russia, E-mail address: kliminvs@sfedu.ru

2. Southern Federal University, Research and Education Center "Nanotechnology", Taganrog, Russia, E-mail address: ageev@sfedu.ru

The prospect of using graphene in nanoelectronics is due to a number of advantages, the main of which are high carrier mobility and resistance to ionizing effects. The main method for obtaining graphene films on the SiC surface is thermal decomposition of the SiC surface. However, this method has a significant drawback, namely, annealing is required at very high temperatures, which can lead to the formation of high mechanical stresses in the structure. In this regard, an important task is to obtain graphene structures on SiC by a combination of methods of focused ionic and plasma-chemical etching.

This experimental work is aimed at considering the use of a combination of methods of focused ion beams and plasma-chemical etching to obtain field emission structures based on graphene films on a SiC surface. Experimental samples, which are plates of purified silicon carbide, were placed in the vacuum chamber of the focused ion beam module and oriented so that the flow of accelerated ions fell on the substrate in the normal direction. At the initial stage, experimental studies on the formation of nanoscale structures were carried out by the method of focused ion beams. For this purpose, a scanning electron microscope with an ion column Nova NanoLab 600 (FEI, Netherlands) was used. The built-in tools of the microscope control program formed templates for the subsequent etching of structures with a focused ion beam. The templates were formed in the form of a torus with an outer diameter of 2 microns and an inner diameter of 600 to 800 nm. These dimensions allow the performance of the resulting structure to be measured. The ion beam current was 30 pA. The accelerating voltage was 30 keV. The holding time at a point is 1 μs. The structures were then etched onto a silicon carbide substrate in accordance with these figures. To remove layers with embedded gallium ions, we used a two-stage atomic layer etching technique. In the first stage of the ALE process, the surface layer of silicon in the fluoride plasma was removed, in the second stage, the carbon layer on the surface in the oxygen plasma was removed. After the removal of defective layers with embedded gallium ions, as well as those containing surface defects in the plasma-chemical etching facility Semiteq STE ICPe68 (NTO, St. Petersburg, Russia), graphene structures were formed on the surface by removing silicon from the SiC lattice in a fluorine-containing plasma. The regimes of processing the structure during plasma-chemical etching are as follows. P = 2 Pa, gas flows N_{Ar} = 70 cm^3/min, N_{SF6} = 15 cm^3/min, the power of the capacitive plasma source was W_{RIE} = 20 V, the power of the inductively coupled plasma source was W_{ICP} = 300 V. The etching time was 1 minute. AFM images and current-voltage characteristics (CVCs) of the structures were obtained using an Ntegra probe nanolaboratory (NT-MDT, Russia). The SiC substrate was grounded and an HA_HR cantilever with a W_2C conductive coating was used. As a result, 10 CVCs were obtained at a voltage of 5 to 20 V, and, according to the results, an average CVC was built. Curve analysis was performed using Origin 8.1 software. AFM image processing was carried out using image analysis software. Analysis of the structures obtained shows that the diameter is 0.87 ± 0.15 μm. The study of the surface topology at each iteration was carried out using scanning electron microscopy. Electrical characteristics were measured using atomic force microscopy. It is shown that an increase in the voltage from 5 to 20 V leads to an increase in the current from 0.15 ± 0.03 nA to 6.3 ± 0.4 nA, and an increase in the electric field from 60 to 180 MV/cm leads to an increase in the current density with 96.32 ± 8.81 A/cm^2. The obtained dependences show that structures formed by a combination of methods of focused ion beams and plasma-chemical etching can have field emission characteristics. The presented technology can be used for the formation of modern vacuum microelectronic devices, as well as for the formation of pressure and gas sensors.

This work was supported by the Russian Foundation for Basic Research Project № 18-29-11019 mk. The results were obtained using the equipment of the Research and Education Center "Nanotechnologies" of Southern Federal University.

Influence of the duration of the oxygen-containing precursor supply on the carbon concentration during ALD

A. Fadeev[1], A. Miakonkikh[1], S. Simakin[2], E. Smirnova[1], K. Rudenko[1]
1. Valiev Institute of Physics and Technology, Russian Academy of Sciences, Moscow, Russia,
2. Yaroslavl Branch of the Valiev Institute of Physics and Technology, Russian Academy of Sciences, Yaroslavl, Russia.
E-mail: miakonkikh@ftian.ru

Atomic layer deposition is an indispensable approach for the formation of ultrathin films of dielectrics and metals in micro and nanoelectronic technology. It is especially useful for deposition on non-conforming surfaces. Since the method is based on the adsorption of metal-containing compounds (precursors) on the surface and subsequent oxidation/reduction with a second precursor, the films can be significantly susceptible to contamination, usually organics in the case of organometallic precursors or halogens in the case of halides. Studies have shown that with an increase in the dosage of the second precursor (time, pressure, plasma density), the degree of contamination decreases. We believe that when the second precursor acts on the surface of the deposited film, not only the surface layer is modified, but also deeper layers. The aim of this work is to study the distribution of carbon impurities over the depth of the film, as well as to search for optimal modes of achieving the minimum carbon contamination of the film during the deposition of oxides from organometallic precursors.

Earlier, a theoretical model was proposed [1] to explain the increase in the concentration of carbon impurities in the near-surface layers of films grown by the ALD method. An approach for controlling the concentration of carbon impurities during the ALD process has been proposed. The basic ideas of the method are: (i) an increase in the oxygen concentration in the earlier grown film monolayers during the ALD process; (ii) the interaction of oxygen with the remaining carbon impurity and the formation of CO/CO_2 molecules; (iii) the release of rapidly diffusing CO/CO_2 molecules from the growing film.

The deposition of Al_2O_3 films via ALD was performed in a commercial FlexAl system (Oxford Instruments Plasma Technology) at 300 °C with trimethylaluminum (TMA) and water as carbon and oxygen-containing precursors, respectively. In the basic recipe, the dosage time of TMA is 20 ms and water is dosed during 200 ms. Plasma-stimulated atomic layer deposition was used to deposit HfO_2. The organometallic precursor was tetraethylmethylaminohafnium (TEMAH), the second precursor was oxygen plasma, the duration of which varied from 1.5 sec to 15 sec. By varying the dosage time of water in different layers of the film, we obtained samples to test the stated theory.

Monitoring of film growth *in situ* was carried out on a spectroscopic ellipsometer (Woollam M-2000X). This method is very sensitive to weak effects at the interface (defects, adsorbed layers with a thickness of the order of monomolecular ones) [2].

One of the problems of the analysis of samples, which in our case had to be carried out with a break in the vacuum when moving the samples into the SIMS chamber, is the possibility of surface contamination with carbon. For this reason, research could be of little information. We have proposed the following experimental design: a layer of material is formed on the surface of a silicon wafer as a result of 100-150 ALD cycles at a constant dosage of the precursor, then the dosage is changed and another layer is deposited. This allows the transition areas to be buried under the layer of material and and to protect them from the influence of the atmosphere. The depth distribution of impurities was investigated using the method of secondary ion mass spectrometry. A characteristic feature of the distributions obtained in our experiment was that a constant impurity concentration was observed in the middle of the observed layers, while it increased towards the edges of the layer.

The model was used to analyze experimental data on the carbon contamination of thin oxide films by the ALD method with different duration of an oxygen-containing precursor supply. Qualitative agreement of the proposed model with the results obtained in the experiment is shown.

1. A.V. Fadeev, K.V. Rudenko. "Possibility of Controlling the Impurity Concentration in the Near-Surface Layers of Films Grown by the ALD Method". Russian Microelectronics, **48**, pp. 220–228, 2019.
2. A.V. Miakonkikh, E.A. Smirnova, I.E. Clemente. "Application of the Spectral Ellipsometry Method to Study the Processes of Atomic Layer Deposition". Russian Microelectronics, **50**, pp. 264–273, 2021.

Technology of the thin film flexible thermoelectric generator using low-cost photolithography

A. Terekhov, D. Pepelyaev, A. Sherchenkov
National Research University of Electronic Technology Moscow, Zelenograd, Russia, aa_sherchenkov@rambler.ru

Thermoelectric generators (TEG) are widely used in many fields of science and technology. One of the new and interesting directions is development of miniature flexible thin film TEGs as power sources for wearable electronics and flexible heat flow sensors. Miniaturization of TEG is associated with the need to introduce additional technological stages using photolithography. At the stage of developing the technology and design of flexible TEGs, the photolithography processes are the most expensive and time-consuming technological stages that require several iterations for the production of photomasks. In this regard, the purpose of this work was to develop setup for low-cost contact photolithography and technology of flexible thin film TEG with using of developed setup.

The developed setup for photolithography is based on a commercial high-resolution display module LS055R1SX04 providing a resolution of 2560×1440 pixels at 120960×68049 μm^2 aria. As a source of ultraviolet radiation, a matrix of LEDs with a wavelength of 395-400 nm and peak power of 100 W is used, which is mounted on a ventilated aluminum radiator. In operating mode, the power supplied to the LED matrix does not exceed 15 W, which provides low heating of the LED matrix and its long service life.

The developed setup was tested and used for the development of the technology of a flexible thin film TEG with a vertical arrangement of n- and p-type legs. TEG contained p- and n-type legs on the basis of $Ge_2Sb_2Te_5$ and B_2Te_3-Sb_2Te_3 thin films, respectively, deposited by magnetron sputtering. Flexible polyimide substrates were used. TEG consisted of 44 pairs of n- and p-type legs with the overall dimensions of the TEG 15×18 mm^2 and thickness of ~5μm. Size of each thermoelectric leg was 1.1×1.1 mm^2. Current-voltage characteristic of the fabricated TEG was measured. The developed technology of thin film thermoelectric generator consists of 6 stages of photolithography, including the formation of the topological pattern of the upper and lower contact systems, the formation of n- and p-type legs, and the formation of dielectric layers. As a photoresist, we used Ordyl Alpha 350 film negative photoresist providing a minimum track resolution of 50 μm and a gap of 60 μm, which, together with the display resolution, made it possible to obtain a track width of 50 μm and gap width of 100 μm. The formation of metallization and dielectric layers, thermoelectric legs of n- and p-types were carried out by explosive photolithography, which made it possible to completely eliminate the stages of etching the layers. Thus, the formation of layers was carried out on top of the developed photoresist with open windows, which made it possible to form films by magnetron deposition with a thickness of up to 3 microns using Ordyl Alpha 350 film photoresist. The alignment of the photomask and sample patterns was carried out using the marks located on the sample in the case of semitransparent samples, while for the opaque samples, the alignment was carried out using the marks on the photomask and on the edge of the sample with the help of a USB CMOS video camera with a resolution of 2 megapixels and a lens that allows focusing on plates with the different geometric dimensions.

Thus, a photolithography setup with using of display module allows to form and correct photomasks in real-time on a PC, which greatly accelerates the process and reduces the cost of prototyping the samples. In this work, widely available electronic and optical components were used, which provides minimal efforts for installation, tuning, completing to exploitation. Exposure technique was developed for negative film and positive liquid photoresists. The fabricated TEG is capable to generate ~1mV thermoEMF when touched with a finger. So, setup for the low-cost contact photolithography with a digital photomask and a minimum dot resolution of ~50 μm was developed. The setup was used for the development of technology and fabrication of flexible thin film TEG.

D.Yu. Terekhov expresses a special gratitude to the Grants Council of the President of the Russian Federation for scholarship support for scientific research.

This work was supported by the Russian Science Foundation (project number 18-79-10231).

3-D printing three-dimensional structures of millimeter size with submicron resolution

E.A. Polushkin, A.V. Kovalchuk, S.Yu. Shapoval
Institute of Microelectronics Technology and High Purity Materials RAS, Chernogolovka, Russia, epolushkin@niime.ru

For experimental verification of a particular idea in the field of structures of micron and submicron sizes, it is often required to create a model and an experimental sample. It is a common practice to use standard operations of microelectronics technology such as deposition of different layers, plasma and wet etching by using a photolithography mask [1]. These methods have good reproducibility, a wide range of equipment and they are ideal for commercial manufacture. However, to approbate an idea and to create experimental samples they are very expensive and time consuming. Moreover, the planar technology of microelectronics does not always allow to fabricate a certain three-dimensional structure.

Today technology of 3d printing of micron and nanometers size structures has come up. It gives a possibility to simplify and reduce costs of the process development of experimental and small-series structures. The process is based on the use of two-photon interaction effect [2, 3]. The radiation of a femtosecond laser at a wavelength of 780 nm is focused in the bulk of polymer material capable of being exposed to UV radiation. At the focusing point of the beam, a region with high intensity of laser radiation is formed. The probability of the process of two-photon absorption is greatly increased. Thus, the 780nm laser radiation inertly passes through the volume of the substance and the polymer is exposed at the focus of the beam due to the two-photon effect. The dimensions of this area depend on the intensity of the laser beam and determine the resolution with which the structure can be drawn (the minimum cross-sectional dimension can be 0.5 μm). Thus, by moving the focusing point of the beam over the volume of the corresponding polymer material in two or three coordinates, it is possible to form two and three-dimensional objects. The sizes of the objects are determined by the range of structure movements relative to the focusing point of the beam and can reach 100 mm. The drawing accuracy is determined by positioning accuracy and reaches a value of several nanometers.

This presentation discusses the installation of a three-dimensional printing Photonic Professional GT company Nanoscribe. Its principle of operation is based on the use of two-photon polymerization effect. Designated basic technological aspects 3D printing process micron size objects and examples are presented with their implementation [4, 5].

The use of the two-photon interaction effect to create various volumetric microstructures made it possible to expand significantly the range of technological capabilities of modern equipment. As shown by this work and by lots of others, Nanoscrib 3D printing equipment is used in various fields of the science and the technology, from photonic crystals to biological systems and makes it easy to create the objects that were technologically difficult before.

The work was performed as part of the state task.*STATE TASK № 075-00355-21-00

1. Zimin V.N., Salahov N.E., Chaplygin Yu.A., Shelepin N.A. "Precision integral pressure transmitters" ["Precizionnye integral'nye preobrazovateli davleniya"]. Izmeritel'naya tekhnika. 1995, no.1, pp. 20-21. (in Russian)
2. Ertugrul, Ishak, Akkus, Nihat, Aygul, Ebuzer, Yalçinkaya, Senai. “MEMS fabrication using 2PP technique based 3D printer”. International Journal of Architectural Computing. 12-17, 2020.
3. Kotz, F., Quick, A. S., Risch, P., Martin, T., Hoose, T., Thiel, M., Helmer, D., Rapp, B. E., Two-Photon Polymerization of Nanocomposites for the Fabrication of Transparent Fused Silica Glass Microstructures. *Adv. Mater.*, **33**, 2006341, 2021. https://doi.org/10.1002/adma.202006341
4. Shapoval S, Borodin, V.,Gorbunov V, Veretennikov A. “ECR-plasma equipment application for nanotechnology.” **1**, 571-574, 2004. 10.1109/ICSICT.2004.1435071.
5. Demenev A, Kovalchuk A, Polushkin E, Shapoval S. “Manufacturing by the method of three-dimensional femtosecond laser submicron lithography of spiral phase plates for the formation of photon beams with orbital angular momentum.” Bulletin of the Russian Academy of Sciences: Physics, **85**, pp. 212-219, 2021.

Investigation of the Au-Assisted Chemical Etching of Silicon for formation of Ethanol fuel cells

Olga Volovlikova*, Gennady Silakov
*National Research University MIET, Moscow, Russia,*5ilova87@gmail.com*

One of the most perspective trends in portable electrochemical energy generators is porous silicon fuel cell [1]. That devises based on ethanol electrooxidation on noble metal nanoparticles inside of pores. The advantages of those devices are their safety for humans and the environment, reproducibility in biosystems in unlimited quantities, etc [2].

The nature and structure of the electrode material play an important role in the electro-oxidation of ethanol. It is necessary to ensure the maximum value of the active surface of the catalyst. To date, the majority of the studies concentrate on Pt and Pt-based catalysts. At the same time, non-Pt catalysts are also of interest, including nanocomposite systems on the basis of Pd and Au [3].

In our work we have prepared por-Si/Au layers with different morphologies by the Au-assisted chemical etching of p-type Si wafers with specific resistivity's of 0.01, 1, and 12 Ω·cm. It was shown that with increasing Au deposition time, the thickness of the porous Si layer increases for the same etching duration, and the morphology of the por-Si/Au changes from porous to filamentary.

It was shown that the resulting por-Si/Au layers possess the capability of ethanol oxidation. Products such as H_2, CH_4, CO, O_2, CO_2, acetaldehyde $(CHO)^+$, and water vapor were detected by mass spectrometry analysis of the gases released when the por-Si/Au specimens were immersed in the ethanol solutions.

The J_{MAX} and Q_{EC} values are dependent on the por-Si/Au layer thickness, which affects the number of Au particles. The Q_{EC} is also affected by the specific resistivity of the Si substrate and the thickness of the mono-Si layer, due to charge carrier recombination. Also, it was shown that the non-uniformity in porosity and orientation of pores in the por-Si/Au layer caused by the change in etchant composition over time also affected the EEO parameters.

Among those studied in this work, the por-Si/Au structures formed on Si with a specific resistivity of 1 Ω·cm (7 min Au deposition) demonstrated the minimum values of J_{MAX} and Q_{EC} of 5 μA·cm^2 and 1.2 mC, respectively. The maximum values of J_{MAX} and Q_{EC} (31 μA·cm^2 and 82.3 mC, respectively) were observed for the por-Si/Au structures formed on Si with the same specific resistivity (5 min Au deposition).

This investigation was supported by the Russian Science Foundation (project No. 19-79-00205), State assignment 2020-2022 № FSMR-2020-0018.

1. P. Hoffman. *Tomorrow's Energy: Hydrogen, Fuel Cells, and the Prospects for a Cleaner Planet*. MIT Press, Cambridge, 2012.
2. U. Schmiemann et al. "The influence of the surface structure on the adsorption of ethene, ethanol and cyclohexene as studied by DEMS". Electrochimica Acta, **40**, pp. 99-107, 1995.
3. L. Wang et all. "In situ assembly of ultrafine AuPd nanowires as efficient electrocatalysts for ethanol electroxidation". Int. J. Hydrog. Energy, **46**, pp. 8549–8556, 2020.

Creation of nanoscale structures on the silicon surface by plasma chemical etching and focused ion beam

V.S. Klimin[1, 2], A.A. Rezvan[1], I.O. Kessler[1], Yu.V. Morozova[1], O.A. Ageev[2]
1. Southern Federal University, Institute of Nanotechnologies, Electronics, and Equipment Engineering, Department of Nanotechnologies and Microsystems, Taganrog, Russia, E-mail address: kliminvs@sfedu.ru
2. Southern Federal University, Research and Education Center "Nanotechnology", Taganrog, Russia, E-mail address: ageev@sfedu.ru

As of this moment, optical lithography reaches its limit in the region of deep ultraviolet radiation; therefore, the study of new methods for the formation of nanoscale structures on the surface of semiconductors is an urgent task. The size of electronic components for the needs of nanoelectronics is constantly decreasing, which leads to a decrease in energy consumption and an increase in productivity. One of the promising methods for obtaining a nanoscale profile on the surface of semiconductor wafers is a combination of methods of a focused ion beam and plasma-chemical etching. The focused ion beam method is based on the interaction of accelerated gallium ions with the sample surface. This method allows you to modify the material on the surface. The modified local regions serve as a mask for subsequent plasma-chemical etching.

The aim of this work is to obtain nanoscale structures on the silicon surface without using optical lithography.

The experimental technique was as follows: at the initial stage of experimental studies, templates in the .bmp format were formed to form an irradiated Ga^+ region on the sample surface. Further, the formation of local modified regions 5x5 μm in size was performed on the formed template on a scanning electron microscope with a Nova NanoLab 600 ion column (FEI, Netherlands) at an accelerating voltage U_{AV} - 30 keV and an ion beam current I_{IB} - 10 pA with a different number of beam passes (10, 25, 50, 75, 100) and various doses (2.5 pC/μm^2, 6.25 pC/μm^2, 12.5 pC/μm^2, 18.75 pC/μm^2, 25 pC/μm^2), respectively. At the next stage of experimental studies, the samples were processed in fluorine-containing plasma on a Semiteq STE ICPe68 plasma-chemical etching facility (NTO, St. Petersburg, Russia), with the following parameters: fluorine-containing gas N_{SF6} flow - 15 cm^3/min, argon flow N_{Ar} - 100 cm^3/min, pressure in the reactor P - 2 Pa, the power of the inductively coupled plasma source W_{ISP} - 200 W, the power of the capacitive plasma source WIT - 35 W, the bias voltage U_{bias} - 24 V, the processing time varied from 30 to 120 seconds. Investigations of the geometric parameters of the obtained structures were carried out on an Ntegra Vita scanning probe microscope (NT-MDT, Russian Federation). As a result of the studies, it was found that after plasma-chemical etching over the entire surface of the substrate, the locally modified region obtained by the focused ion beam method was higher than the level of the remaining substrate, which indicates a masking effect. The analysis shows that with the specified combination of modes, the locally modified region is characterized by a lower etching rate (V_{mSi} - 0.019 nm/sec) than the unmodified region of the substrate surface (V_{Si} - 2.21 nm/sec). The masking effect can be explained by the formation in the near-surface silicon layer of a locally modified region saturated with intercalated Ga^+ ions, which are characterized by a greater inertness with respect to fluorine-containing plasma ions than silicon atoms. It was also shown that the locally modified area after plasma-chemical treatment has a more developed surface relief (roughness 13.7 nm) in relation to the surrounding area (roughness 3 nm). This effect is due to the predominance in this area of the physical component of reactive ion etching. This technology can be used to form structures and functional layers of quantum and optical nanoelectronic devices that require high resolution, and the ability to control the parameters of the irradiated structures makes it possible to judge the high manufacturability of the process.

This work was supported by the Grant of the Russian Science Foundation № 20-69-46076. The results were obtained using the equipment of the Research and Education Center "Nanotechnologies" of Southern Federal University.

Optimization of OxiEtch process using time-resolved optical emission spectroscopy

V.O. Kuzmenko[1], A.V. Miakonkikh[1], S. Kolar[2], K.V. Rudenko[1]
1. Valiev Institute of Physics and Technology of Russian Academy of Sciences, Moscow, Russia, kuzmenko@ftian.ru.
2. Moscow Institute of Physics and Technology, Moscow, Russia

Deep silicon etching processes are required for different applications. One of them is formation of high aspect ratio structures for high capacity 3D integrated capacitors for DRAM. High aspect ratio structures have great surface area that allows you to create a high capacity capacitor on relatively small area on wafer. There are some well-known deep silicon etching processes, which have their pros and cons. Bosch process allows to achieve high selectivity but produces difficult to remove polymer dielectric film on the structure surface. Cryogenic etching process allows to control the inclination of the walls and to obtain structures with a relatively smooth wall surface but requires cryogenic equipment that complicates industrial applications. Another deep silicon etching process is OxiEtch process [1]. It is cyclic process, in which passivation step in oxygen plasma and etching step in SF_6 plasma are repeated. Structures produced in this process have typical wall roughness called scalloping like in cyclic Bosch process but does not have polymer film on the surface. Oxygen plasma does not allow the use of resist masks in OxiEtch process, so there is idea to use O_2/N_2 mixture for produce SiO_xN_y film for passivation.

OxiEtch process was investigated in commercial PlasmaLab 100 Dual (OIPT) two-chamber ICP RIE cluster intended for processing of wafers up to 200 mm in diameter. Modified cycle consisted from passivation step, which was conducted in O_2 and O_2/N_2 plasma, then it was short breakthrough step, when passivation layer was broken by applying DC bias in SF_6/Ar plasma and after it at etching step silicon was etched in SF_6 plasma without bias. This approach makes it possible to achieve high selectivity by preserving mask. There were two groups of samples: with SiO_2 (2 μm) mask and with resist mask (1.2 μm). Both patterns have holes and trenches 1-16 μm width. Monitoring of emission of different spectral lines by OceanOptics HR4PRO was used for optimization of process.

Emission of atomic line and molecular band were monitored in cyclic process (Figure 1). Rise of emission of fluorine line and increase of emission of SO band at the start of passivation step can be ascribed to transition processes in plasma, which increase fluorine concentration at the start of passivation step, when silicon surface is naked. That is why OxiEtch process was optimized by decreasing ICP power on transition step before passivation step, which should reduce transition processes. Optimized process with oxygen passivation showed good results on silicon etching with hard mask: structures with vertical walls and aspect ratios up to 11 were achieved; the selectivity to mask was more than 60. Using O_2/N_2 plasma for passivation makes it possible to achieve aspect ratio about 2 after etching with resist mask with selectivity up to 10.

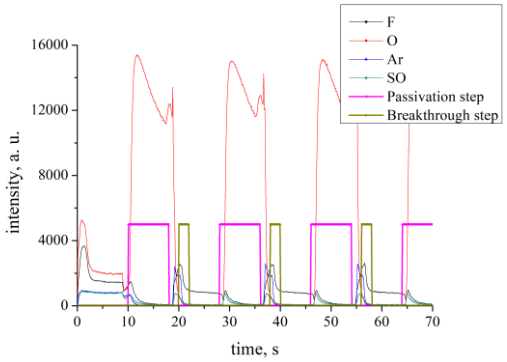

Fig. 1. Monitoring of intensity of plasma particles emission F* – 685.6 nm, O* – 777.4 nm, Ar* – 750.4 nm and SO* – integral over 254.74-257.57 nm.

The study was supported by Program no. 0066-2019-0004 for Valiev IPT RAS and by RFBR (project № 20-07-00832).

1. S. N. Averkin et al., "Method of anisotropic plasma etching of silicon microstructures in a cyclic two-step oxidation-etching process" Patent RU 2691758 C1, 2019.

Dynamics of trenches formation by moving ribbon ion beam

A.S. Rudy[1], A.N. Kulikov[2], V.I. Bacurin[1], E.A. Kozlov[2]
1. Valiev Institute of Physics and Technology of Russian Academy of Sciences, Yaroslavl Branch, Yaroslavl, Russia, E-mail address: rudy@uniyar.ac.ru
2. P.G. Demidov Yaroslavl State University, Yaroslavl, Russia, E-mail: rectorat@uniyar.ac.ru

In the early 2000s a method for the formation of a regular wavy nanorelief [1] by a moving ion beam was developed. A ribbon ion beam moving translationally at a constant rate was used to form an array of ordered waves. While moving the beam forms a trench with a slope in its front part (see Figure), where the local angle of bombardment $\Theta - \Theta_0$ may fall in the region of a wavy nanorelief existence. In this event an array of a coherent nanometer-size waves is formed at the bottom of the trench. It was supposed that by changing the speed of the ion beam, the fluence, or the angle of bombardment, it would be possible to obtain slopes of various steepness, thereby adjusting the wavelength. The analysis of mathematical model of surface erosion by translationally moving ion beam of a Gaussian shape is considered carried out in present paper and shows that this is far from the case.

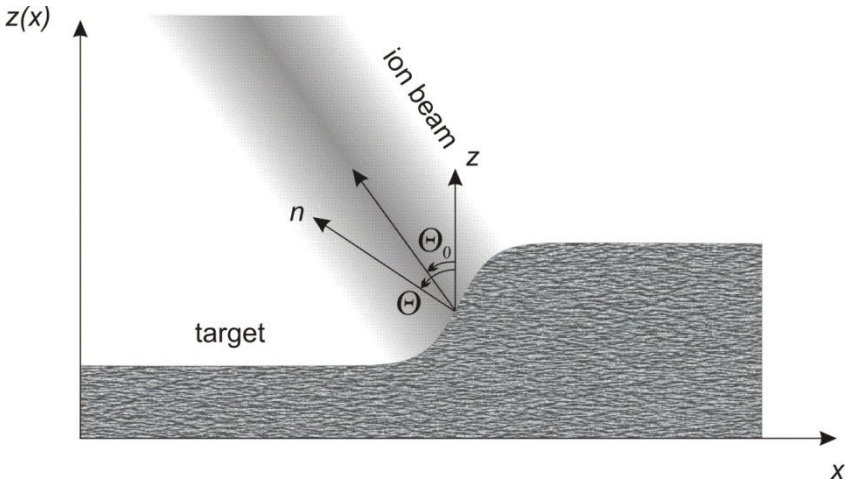

Side-view of flat surface sputtered by a moving ribbon ion beam

The solutions obtained in self-similar variables describe the states of equilibrium of the boundary value problem and their dependence on the sputtering parameters. It is shown that there are three areas of a generalized control parameter A in which only smooth, smooth and discontinuous and only discontinuous solutions exist. The most important for practical application result is the revealed relationship of wave's amplitude and control parameter value. According to this result trench's profile and depth may be controlled by A parameter adjustment, but only within a certain limit. With parameter A variation and compliance with the condition $A < A_1$ the trench depth varies monotonically. Within domain $[A_1, A_2]$ there are two feasible solutions $z(x)$: smooth and discontinuous. The results of the analysis do not answer the question which of the two solutions will be stable, i.e. which of the two sputtering regimes will occur in the real technological process. If one of the solutions is unstable, then during the trench formation, a spontaneous change in the sputtering regime can occur despite the fixed parameters of the ion beam. For example, the transition from a high sputtering rate at large angles Θ when a deep trench is formed, to a low sputtering speed with a small angle profile $z(x)$ and shallow trench is possible. And finally, at $A > A_2$, only one discontinuous solution remains, to which in practice correspond deep trenches.

1. V. Zhuravlev, D. S. Kibalov, G. F. Smirnova, V. K. Smirnov, Wavy surface nanostructures formed in amorphous silicon films by sputtering with nitrogen ions, Technical Physics Letters **29**, p. 949, 2003.

Investigation of the influence of the parameters of the temporary bonding and thinning operations on the bending of silicon wafers

N. Djuzhev, M. Makhiboroda, E. Gusev, M. Fomichev, A. Dedkova, P. Ivanin
National Research University of Electronic Technology, Moscow, Russia, fomichev@ckp-miet.ru., 124498, Moscow, Zelenograd, Shokina square, 1

The traditional method of downsizing components using lithography to maintain Moore's Law is becoming more complex and expensive. Manufacturing costs are growing faster than the income of the semiconductor industry [1]. 3D integration is a technology that serves to extend Moore's Law at a lower cost.

In this work, we study the influence of materials and parameters of temporary bonding and thinning operations required for 3D integration on the resulting bending of wafers and assemblies to reduce it. To perform the work, wafers with a diameter of 150 mm were used. The following results were obtained:
A. The effect of a significant decrease in the bow of a silicon wafer from 126 µm to 42 µm was found when the adhesive film was removed from it.
B. It is shown that as a result of bonding a thinned silicon device wafer without layers with a glass carrier wafer with functional layers, the bow of the resulting assembly becomes significantly larger than the initial one (from 42 µm to 129 µm).
C. It was found that when a silicon wafer is thinned as part of an assembly with a silicon or glass carrier wafer, its bow increases insignificantly (by 11.4 µm and 17 µm, respectively).

The following technological operations were carried out. 1. The first 950 µm Si device wafer was coated with a 22 µm BrewerBond 305-30 adhesive. 2. The second 675 µm Si carrier wafer was coated with 0.22 µm BrewerBond 530 release material. 3. The bonding of these wafers was carried out at a pressure of 1700 N/m^2 and a temperature of 200 °C. 4. The device wafer was thinned by grinding and polishing from 950 µm to 300 µm. 5. Mechanical debonding of two wafers was performed on the SUSS DB12T. 6. The adhesive film has been manually removed from the carrier wafer surface. 7. A 0.22 µm layer of release material was applied to a 500 µm Borofloat 33 glass carrier wafer. 8. A 35 µm thick adhesive layer was applied on top of the release layer on a glass wafer. 9. Bonding the wafer obtained in step 6 with the glass wafer with two functional layers from step 8. 10. The device wafer was thinned by the standard method from 300 to 144 microns. Relief measurements of manufactured structures following the operation number are shown in Figure 1.

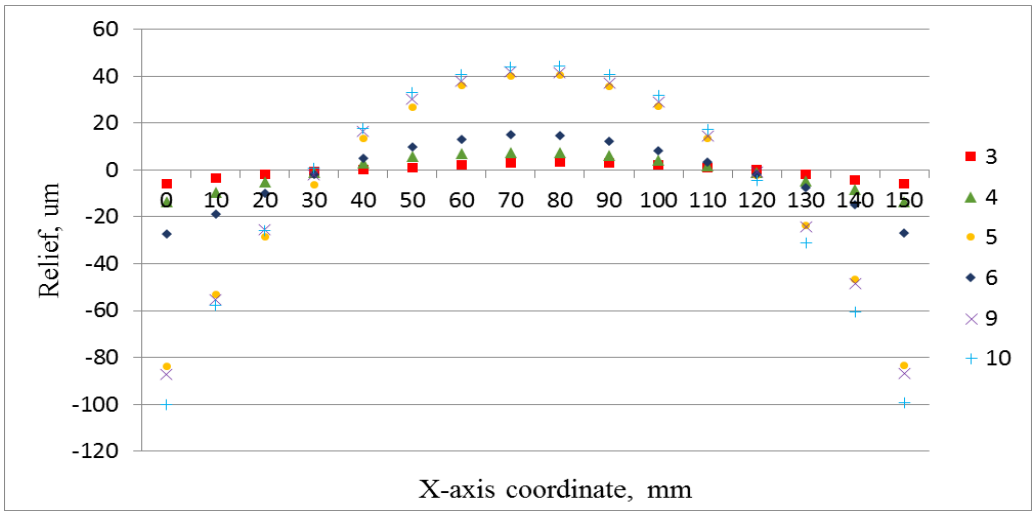

Fig. 1. Relief measurements of manufactured structures.

This work was carried out on the equipment of the R&D center «MST and ECB» MIET and supported by the Fund for the Promotion of Innovations under contract No. 418GR/57264 dated 26.12.2019.

1. D.C. Brock, Understanding Moore's Law: Four Decades of Innovation // Chemical Heritage Foundation, 2006, ISBN 0-941901-41-6, pp. 67–84.

Numerical study of aperture shape effects in deep cryogenic etching of silicon

M.K. Rudenko, A.V. Miakonkikh, V.F. Lukichev
Valiev Institute of Physics and Technology of RAS, Moscow, Russia, mikhail.rudenko@ftian.ru

Cryogenic etching of silicon in SF_6/O_2 plasma is the process of choice for fabrication of deep high aspect ratio structures for the fields of MEMS/NEMS, 3D integration of integral circuits and other applications with strict requrements for sidewall angle, surface roughness and contamination.

High aspect ratio structures employed in MEMS, X-ray optics, etc, combine features of various geometric shapes: trenches, holes, wedges, fins, pillars and grooves of various width and curvature. During the etching they are exposed to varying particle flux conditions, which results in differences in etch rate, aspect ratio dependence, sidewall angle and surface roughness. This makes optimization of etching process for fabrication of structures with different shape of aperture a challenging task.

A possible solution to this problem is three dimensional computer simulation of the etching process [1]. We propose a novel three dimensional Monte-Carlo model for complex structure cryogenic etching simulation as an aid in process optimization. It employs surface kinetics model tuned to SF_6/O_2 process in 2.5D geometry [2] and cubic voxel representations of simulation domain. Use of efficient online surface connectivity algorithm [3] together with hierarchical spatial data structure for raycasting allows to run simulations of as much as $5 \cdot 10^9$ voxels on a workstation-class PC. In turn, this makes possible to simulate etching of structures, containing both fine and coarse features, in a single simulation run, and perform extensive scans on both plasma and surface parameters.

Systematic research on cryogenic etching of various test structures (fig. 1) under varying plasma and surface conditions was performed. Aspect ratio dependent etching of various structures was simulated. ARDE effect was found to increase with increasing geometric shadowing. By varying ion energy and ion-to-neutral ratio, it was shown that under relevant conditions ARDE effect can be mostly attributed to the waning flux of neutrals to the bottom of structure rather than that of ions.

Sidewall angle of simulated profiles was researched under diverse temperatures, ion divergence angles and aperture width. Rising the process temperature above the optimal one leads to increasing mask undercut and positive slope. On the other hand, increasing ion divergence angle results in negative slope formation. Under certain conditions, these effects cancel each other. It was also found, that narrower trenches have more positive slope, and holes have more positive slopes than trenches of matching width. Unlike simple 2D models, our 3D model provides adequate means for researching sidewall roughness. It was found that the key factor leading to roughness is oxygen to fluorine flux ratio. The most pronounced roughness and nanopore formation is observed at flux ratio of 60% of optimal, decreasing for both higher and lower ratios.

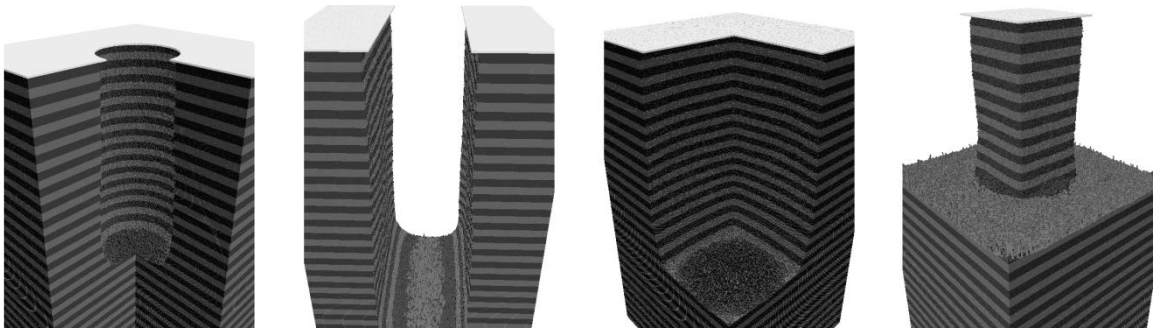

a) b) c) d)

Fig. 1. Some of the simulated structures: holes (a), trenches (b), corners (c), pillars (d).

1. C. M. Huard, Y. Zhang, S. Sriraman, A. Paterson and M. J. Kushner, "Role of neutral transport in aspect ratio dependent plasma etching of three-dimensional features". Journal of Vacuum Science &Technology A: Vacuum, Surfaces, and Films, **35**, p. 05301, 2017.

2. M.K. Rudenko, A.V. Myakon'kikh and V.F. Lukichev. "Monte Carlo simulation of defects of a trench profile in the process of deep reactive ion etching of silicon". Rus. Microelectronics, **48**, pp. 157–166, 2019.

3. Y. Shiloach and E. Shimon. "An on-line edge-deletion problem". Journal of the ACM, **28**, pp. 1-4, 1981.

High temperature sintering of Al_2O_3 sol-gel films for acoustic applications

S. Avdeev[1], D. Ryabova[1], S. Malokhatko[1,2], E. Gusev[1]

1. Southern Federal University, Institute of Nanotechnologies, Electronics and Equipment Engineering, Taganrog, Russia, savdeev@sfedu.ru

2. Research and Education Center "Nanotechnologies" of Southern Federal University, Taganrog, Russia, malohatko@sfedu.ru

Aluminum oxide films have thermal, chemical, corrosion and radiation resistance, have high dielectric constant, and are good electrical insulator. Due to these characteristics, aluminum oxide films are widely used in microelectronic devices and sensors (gate dielectric, antireflection and passivation coatings), as well as in acoustic devices (membranes) [1]. This work considers Al_2O_3 films prepared by the sol-gel method based on aluminum isopropoxide ($Al(OC_3H_7)_3$). Using this method and the possibilities of electron-beam heating [2] in local area up to high temperatures, it is possible to change the phase composition and morphology of the film. During high-temperature treatment, the films are modified due to sintering of the material and the transition into a stable monolithic film. The preparation of the film-forming solution was carried out according to [3]. For research, a phosphorus doped silicon wafer was used as substrate. The substrate surface was treated with a 10% solution of hydrofluoric acid, washed in distilled water, and dried at room temperature for several minutes. Then, the film-forming solution was applied to the substrate by centrifugation. The prepared series of samples was subjected to high-temperature treatment at temperatures of 200-800 ° C. The change in film thickness for several sintering temperatures is shown in Table.

Table. Effect of sintering temperature on the film thickness

Parameter	Temperature, °C				
	27	200	400	600	800
Thickness, nm	– (247±39)*	162±4 (225±18)	169±11 (202±6)	119±11 (185±20)	93±24 (180±36)

* – values of initial (as-synthesized) film thickness are given within brackets

It was found that due to high-temperature sintering, the average values of film thickness and surface roughness are reduced by about 2 times. It should be noted that at temperature of 200-600°C, the average roughness almost did not change (fixed at 8.26±0.03 nm), but at 800°C it decreased to 4.21 nm. Investigation of sintered films by nanoindentation has shown that the average hardness of the film obtained at 200°C was 7.81-2.32 GPa, and at 800°C - 8.71-2.40 GPa. Finally, the conditions for electron-beam processing of the sintered film are determined, which make it possible to obtain a homogeneous Al_2O_3 film.

The reported study was funded by RFBR, project number 20-37-90087. The work was done on the equipment of the Research and Education Center "Nanotechnology" of Southern Federal University.

1. Y.W. Kim, S.E. Sardari, M.T. Meyer, A.A. Iliadis, H.C. Wu, W.E. Bentley and R. Ghodssi. "An ALD aluminum oxide passivated Surface Acoustic Wave sensor for early biofilm detection". Sensors and Actuators B, **163**, pp. 136-145, 2012.

2. S.P. Avdeev, E.Yu. Gusev, D.I. Ryabova. "Improving the mechanical resistance of the glass surface for optoelectronic devices by electron beam processing". Journal of Physics: Conference Series, **1695**, 012191, 2020.

3. V.V. Vinogradov, A.V. Agafonov, A.V. Vinogradov, T.I. Gulyaeva, V.A. Drozdov and V.A. Likholobov. "Sol-gel synthesis, characterization and catalytic activity of mesoporous γ-alumina prepared from boehmite sol by different methods". Journal of Sol-Gel Science and Technology, **56**, pp. 333-339, 2010.

Induced bistability effect in the thermal reactor elements for a bistable mode of heat treatment of silicon wafers

V. Ovcharov, V. Prigara
Yaroslavl Branch of the Valiev Institute of Physics and Technology of the RAS, Yaroslavl, Russia.
Email:ovcharov.vlad@gmail.com

IR thermal processes are widely used in micro- and nanoelectronics. These are an epitaxial process, post-implantation annealing of semiconductor wafers, forming shallow p-n junctions, obtaining silicides, nitrides and oxides, fusing ohmic contacts, fire-polishing borosilicate and phosphor silicate glasses for VLSI/ULSI. For carrying out of these processes the equipment for Rapid Thermal Treatment (RTT) is used, the important part of which is a thermal reactor. During thermal treatment by powerful radiation fluxes and in conditions which are far from thermal equilibrium the following non-linear effects can be recorded: thermal bistability [1] and temperature oscillations of the wafer [2] under steady-state temperature values of a heater. Also experiments that are performed for switching the silicon wafer by a square wave impulse show that the mode of the wafer differs from one of the semiconductor samples that are switched by the use of a laser impulse [3]. To clarify the described non-linear effects, the thermal reactor with all its elements and a semiconductor wafer must be taken into account as a single thermodynamical system. Generally, the RTT reactor consists of a heater, quartz glass and water-cooled absorber of IR-radiation. The efficiency of the heater is defined by the heating current of the incandescence tubes of the heating block, and the efficiency of the absorber is defined by its temperature and a cooling water flow rate. Normally, as the temperature of the heater changes, there is a temperature change not only in a silicon wafer but also in the quartz glass and the absorber. As is shown in [4], bistable modes of the wafer leads to the bistable mode of the quartz glass (the effect of the induced bistability). This paper studies the influence of the bistable mode of the silicon wafer on the thermal mode of the water-cooled absorber during steady-state temperature values of the water cooling the absorber and its flow rate (regardless of the influence of quartz glass on the heat balance in the thermal system). The results obtained by different approximations are compared under simulation of the thermal modes of such a thermodynamical system. The refined calculations are also performed for the thermal mode of the quartz glass at the steady-state temperature of the absorber for the case of the bistable mode of the semiconductor wafer.

It is shown that as in the case of the thermodynamical system including a semiconductor wafer, quartz glass and an absorber is set at the steady-state temperature values, in the system without quartz glass but where the temperature of the absorber is varied, the effect of the induced bistability into the absorber of radiation is observed. The induced bistability in the absorber is revealed particularly vividly in the case of the real values of the emissivity of the heater made from tungsten material. The set of equations which describes the thermal mode of the thermodynamical system including a heater, a quartz glass, a semiconductor wafer and an absorber and temperatures of all elements of the system is derived. The set of equations makes it possible to plot complete series of the transfer characteristics for the thermodynamical system with a semiconductor wafer mounted in it.

1. V.I. Rudakov, V.V. Ovcharov, A.L. Kurenya, V.P. Prigara. “Bistable behavior of silicon wafer in rapid thermal processing setup ”. Microelectronic Engineering, **93**, pp. 67-73, 2012.
2. V. I. Rudakov, V.V. Ovcharov, A.L. Kurenya, V.P. Prigara. “Temperature oscillations in a silicon wafer under constant power of incoherent irradiation by heating lamps in a thermal chamber of RTP set up”. Proc. SPIE **8700**, 870006, 2013.
3. B. Segard and B. Macke. "Non critical slowing down in optical bistability." Le Journal de Physique Colloques, **49**, C2, pp. C2-115- C2-118, 1988.
4. V.P. Prigara, V.V. Ovcharov “Induced bistability into quartz glass by silicon wafer heat treatment in lamp-based reactor”. Proc. SPIE **11022**, 110221U, 2019.

Graph neural networks for quantum walks analysis

A.A. Melnikov[1], A.P. Deshpande[2], L.E. Fedichkin[1]
1. Valiev Institute of Physics and Technology, Russian Academy of Sciences, Moscow, Russia, melnikov@phystech.edu, leonid@phystech.edu
2. Birla Institute of Technology and Science, Pilani, India, ajinkya.deshpande56@gmail.com

Quantum walks represent a tool for studying various phenomena in quantum systems, including quantum transport in complex networks. For some complex network structures, quantum walks show advantages over classical random walks in node-to-node transport. The presence of quantum advantage is known on graphs with high symmetry: lines, rings, hypercubes, and glued trees. Nevertheless, the practical use of highly symmetric graphs is not apparent, in particular, due to the imperfection of quantum systems.

In our work we analyze non-symmetric, arbitrary graphs sampled uniformly, to find potential advantages in quantum transport. Direct computer simulation analysis of the dynamics of walks has its drawbacks: the computational complexity increases with the size of the graph, and an accurate physical model of the dynamics is also required. Our recent works [1-3] have developed an automated machine learning approach for quantum walks analysis. This approach is based on training a so-called quantum-classical convolutional neural network to perform binary classification. In our new work that we present here, we take state-of-the-art graph neural network approaches developed recently and compare their performance to the quantum-classical convolutional neural network.

1. A.A. Melnikov, L.E. Fedichkin, and A. Alodjants. "Predicting quantum advantage by quantum walk with convolutional neural networks". New Journal of Physics, **21**, 125002, 2019.
2. A.A. Melnikov, L.E. Fedichkin, R.K. Lee, A. Alodjants. "Machine learning transfer efficiencies for noisy quantum walks". Advanced Quantum Technologies, **3**, 1900115, 2020.
3. A.A. Melnikov, L.E. Fedichkin, A. Alodjants. "On training a classifier of hitting times for quantum walks". AIP Conference Proceedings **2241**, 020029, 2020.

Quantum entanglement in a family of Heisenberg models with the multiple components of Dzyaloshinsky-Moriya and Kaplan-Shekhtman-Entin-Wohlman-Aharony interactions

A.V. Fedorova and M.A. Yurischev
Institute of Problems of Chemical Physics of the Russian Academy of Sciences, Chernogolovka, Moscow Region, 142432 Russia, E-mail address: panna@icp.ac.ru

Quantum entanglement is one of the most important measures of quantum correlations. Recently [1], closed analytical formulas for the quantum entanglement has been derived for the four nine-parameter quantum states of two-spin-1/2 Heisenberg systems in an external magnetic field and with *multicomponent* Dzyaloshinsky-Moriya (DM) and Kaplan-Shekhtman-Entin-Wohlman-Aharony (KSEA) interactions.

In the talk, the family of found states and the structure of interactions in them will be discussed.

The work was performed as a part of the program CITIS # AAAA-A19-119071190017-7.

1. A.V. Fedorova and M.A. Yurischev. "Quantum entanglement in the anisotropic Heisenberg model with multicomponent DM and KSEA interactions". Quantum Inf. Process., **20:**169, 20 pp., 2021.

The effect of quantum noise on algorithmic perfect quantum state transfer on NISQ superconducting processors

D. Babukhin, W. Pogosov
Dukhov Research Institute of Automatics (VNIIA), 127055 Moscow, Russia

Quantum walks are an analog of classical random walks in quantum systems, which allow for advantage of quantum-walks-based algorithms on certain types of graphs. An important feature of quantum walks is that they are accompanied by the excitation transfer along the system nodes, and a moment of hitting the destination site is characterized by the maximum probability amplitude of observing the excitation on some node. It is therefore prospective to consider such problems as candidates for quantum advantage demonstration, since gate errors can smear out a peak in the transfer probability as a function of time, nevertheless leaving it distinguishable.

In this work, we investigated the influence of typical kinds of quantum noise in superconducting quantum processors (gate error noise, decoherence and crosstalk noise) on a hitting time and fidelity of the perfect state transfer over a chain of qubits (PST). We found that gate error noise and decoherence mostly smear out a peak in the fidelity of excitation transfer, while crosstalk noise between qubits mostly affect hitting time. We also found that as long as homogeneous and inhomogeneous gate error noise has equal intensity, there is no difference in their influence on the PST quality. Based on these findings, we proposed an error mitigation procedure, which we used to refine the results of running the PST on a simulator of a noisy quantum processor. This procedure incorporates a rescaling of the excitation range and a shift of dynamics time. This procedure uses only experimentally-available data to estimate effective influence of noise onto the dynamics of the PST and allows to correct the dynamics with a significant improvement.

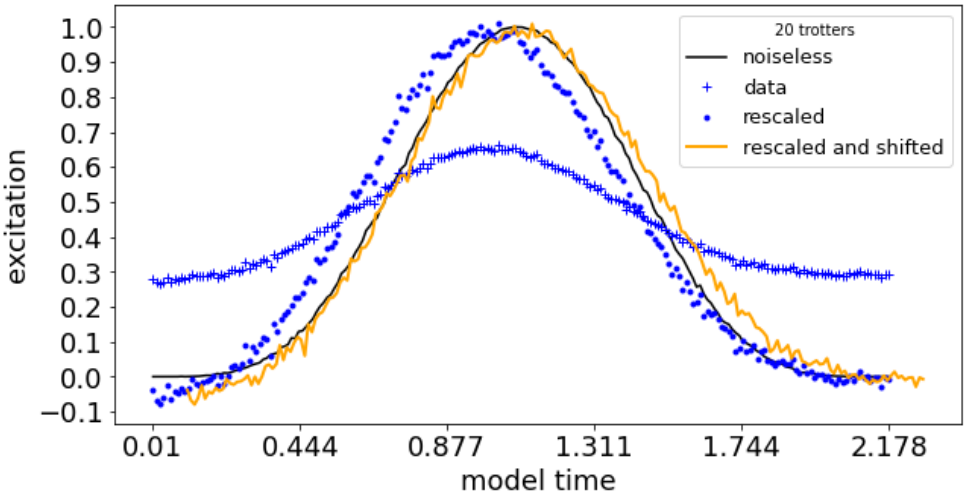

Figure 1. Dependencies of excitation dynamics over time on a target qubit of the qubit chain during the process of a state transfer. Here are provided a noisy excitation dynamics without postprocessing (crosses), excitation dynamics after rescaling (dots), excitation dynamics after rescaling and a time shift (orange line) and a noiseless excitation dynamics (black line).

The main result of our work is a demonstration that we only need to know the general properties of noise models without precise knowledge of noise parameters to mitigate its effect on the computation results. Using our post-processing error mitigation, we were able to sufficiently improve the quality of results for circuits of about 270 layers depth. Our results provide an example of post-processing error mitigation of quantum computing outcomes without precise knowledge of the quantum noise model.

Broadband biphoton source for quantum optical coherence tomography

A.V. Romanova[1], A.V. Pashchenko[1], K.G. Katamadze[1,2], S.P. Kulik[1]
1. Quantum Technology Centre, M. V. Lomonosov Moscow State University, 119991 Moscow, Russia.
2. Valiev Institute of Physics and Technology, Russian Academy of Sciences, 117218 Moscow, Russia
romanova.av15@physics.msu.ru

In some problems, the methods of classical microscopy do not provide high resolution due to the limited numerical aperture of the optical system. In this case, the method of optical coherence tomography (OCT) is often used [1]. Recently, quantum OCT methods have been developed, in which fields of correlated pairs of photons (biphotons) are used instead of coherent radiation [2].

The axial resolution of the OCT depends on the coherence length, which is inversely proportional to the spectrum width. However, with an increase in the spectral bandwidth, the axial resolution of the classical OCT becomes limited by the dispersion of light in the sample, while the QOCT has the property of odd-order dispersion cancellation [2].

In the present paper, a new method for obtaining biphoton fields with an ultra-broadband spectrum is proposed, based on strong focusing of the pump and the target mode in a crystal with a quadratic nonlinearity of the electric susceptibility. Due to the walk-off effect, the strongly focused modes overlap weakly, significantly limiting the effective length of the nonlinear interaction, which makes it possible to obtain broadband biphoton fields. According to calculations, a decrease in the spectral intensity proportional to the effective interaction length can be compensated by a multiple increase in the focusing strength.

The report will present the latest results of experiments on the implementation of a broadband biphoton field source based on the described principle.

This work was supported by the Ministry of Science and Higher Education of the Russian Federation (program no. 0066-2019-0005 for the Valiev Institute of Physics and Technology, Russian Academy of Sciences), and by the Foundation for the Advancement of Theoretical Physics and Mathematics BASIS (project no. 21-1-3-40-1).

1. Drexler W. “Optical Coherence Tomography”, Encyclopedia of the Eye. Elsevier, 2010. pp. 194–204.
2. Okano M. "0.54 μm resolution two-photon interference with dispersion cancellation for quantum optical coherence tomography", Sci. Rep., **5**, p. 18042, 2016.

Measurement of polarization quantum states under chromatic aberration conditions

Yu.I. Bogdanov, B.I. Bantysh, N.A. Bogdanova, M.I. Shakirov, V.F. Lukichev
Valiev Institute of Physics and Technology of Russian Academy of Sciences, Moscow, Russia
shakmark17@gmail.com

The wave plate is a basic device for transforming and measuring the polarization states of light. It is known that the transformation of light by means of two wave plates makes it possible to measure the state of polarization in an arbitrary basis. The finite spectral width of the light, however, leads to a chromatic aberration of the polarization quantum transformation caused by the parasitic dispersion of the birefringence of the plate material. This causes systematic errors in the tomography of quantum polarization states and significantly reduces its accuracy. This study is a development of our work [1], in which an adequate model for quantum measurements of polarization qubits under chromatic aberration was first formulated. This work includes a generalization of the results obtained earlier for the cases of two- and multi-qubit states. Along with examples of specific states, random states uniformly distributed over the Haar measure are considered. Using a matrix of complete information, it is quantitatively traced how the presence of chromatic aberrations under conditions of a finite spectral width of light leads to the loss of information in quantum measurements. It is shown that the use of the developed model of fuzzy measurements instead of the model of standard projection measurements makes it possible to suppress systematic errors of quantum tomography even when using high-order wave plates. It turns out that the fuzzy measurement model can give a significant increase in the reconstruction accuracy compared to the standard measurement model.

The results obtained are essential for the development of high-precision control methods for optical quantum information technologies.

This work was supported by the Ministry of Science and Higher Education of the Russian Federation (program no. 0066-2019-0005 for the Valiev Institute of Physics and Technology, Russian Academy of Sciences), and by the Foundation for the Advancement of Theoretical Physics and Mathematics BASIS (project no. 20-1-1-34-1)

1. B. I. Bantysh, Yu. I. Bogdanov, N. A. Bogdanova, Yu. A. Kuznetsov "Precise tomography of optical polarization qubits under conditions of chromatic aberration of quantum transformations", Laser Phys. Lett. **17**, 035205, 2020.

Comparative analysis of various protocols for high-precision tomography of ion-based qudits

Yu.I. Bogdanov, B.I. Bantysh, N.A. Bogdanova, K.B. Koksharov, V.F. Lukichev
Valiev Institute of Physics and Technology of Russian Academy of Sciences, Moscow, Russia
kirill.koksharov7@gmail.com

Quantum tomography is an important tool for obtaining information about the quantum state from experimental data. The practical implementation of tomography of ion-based multilevel quantum states (qudits) is noticeably complicated by the need to perform a large number of transformations on the qudit itself, herewith each of these transformations can reduce the accuracy of statistical reconstruction of the desired quantum state. In this study we carry out a comparative analysis of the quantum tomography protocol based on mutually unbiased bases (MUB) with an easier-to-implement protocol based on two-level transformations and swap operators. Using the universal distribution for the accuracy of statistical reconstruction of quantum states, we quantitatively trace the efficiency and complexity of quantum measurements for qudits of various dimensions as applied to a set of random states uniformly distributed over the Haar measure.

The results obtained are essential for the development of high-precision methods for controlling the technology of quantum computing on the ion platform

This work was supported the Program of activities of the leading research center "Development of an experimental prototype of a hardware and software complex for the technology of quantum computing based on ions" (Agreement No. 014/20), and by the Foundation for the Advancement of Theoretical Physics and Mathematics BASIS (project no. 20-1-1-34-1)

High-fidelity tomography of fluorescent ion qubits under conditions of limited discrimination between "bright" and "dark" levels

Yu.I. Bogdanov, B.I. Bantysh, N.A. Bogdanova, I.A. Dmitriev, V.F. Lukichev
Valiev Institute of Physics and Technology of Russian Academy of Sciences, Moscow, Russia
il.dmitryev@gmail.com

The present work is devoted to the development of a method for high-precision tomography of ion qubit registers under conditions of limited distinguishability of the states of a logical value 0 and a logical value 1. In the considered ion qubits, the identification of the quantum state is achieved by measuring the fluorescence of the ion by repeated excitation of the cyclic transition, which includes only the lower energy state that sets a logical value 0 and becomes "bright", but does not include the upper metastable state that remains "dark" and sets logical value 1. It is important to note that it is not always possible to achieve low levels of registration errors due to the finite lifetime of excited levels, photon scattering, dark noise, low numerical aperture values, etc. However, even under such conditions, with use of the model of fuzzy quantum measurements, it is possible to provide precise control of quantum states. We show that a model that is characterized by relatively high levels of errors under conditions, where we have a reliable statistical model of their occurrence, is more accurate than the case when the considered errors are small, but we do not have an adequate statistical model for the occurrence of these errors. In the given illustrative examples, we show that the factor of reducing the loss of accuracy with the use of the model of fuzzy measurements can reach values of the order of 1000 or more in comparison with standard measurements.

The obtained results are essential for the development of high-precision methods for controlling the technology of quantum computing on the ion platform.

This work was supported the Program of activities of the leading research center "Development of an experimental prototype of a hardware and software complex for the technology of quantum computing based on ions" (Agreement No. 014/20), and by the Foundation for the Advancement of Theoretical Physics and Mathematics BASIS (project no. 20-1-1-34-1)

Implementation of quantum operations in a transmon qubit by bipolar single-flux-quantum pulse sequence

M. Bastrakova[1], V. Vozhakov[2,3], I. Soloviev[2,3], N. Klenov[2,3], and A. Satanin[3,4]
1. Lobachevsky State University of Nizhny Novgorod, Nizhny Novgorod, Russia, mar.denisenko@gmail.com
2. Faculty of Physics, Lomonosov Moscow State University, Moscow, Russia
3. Dukhov All-Russia Research Institute of Automatics, Moscow, Russia
4. Russia National Research University Higher School of Economics, Moscow, Russia

Quantum computing is a fast developing frontier technology. Superconducting materials are shown to be one of the most promising physical basis for its implementation [1]. In most of the available superconducting quantum processors, the main element is a charge qubit of the transmon type. It is important that a small parameter of the anharmonicity of the transmon imposes a restriction on the duration and amplitude of microwave pulses [1]. Note, that for a typical qubit frequency corresponding to the transition between the levels, $\omega_{01}/2\pi \sim 5$ GHz, the control pulse duration providing a π rotation on the Bloch sphere (the quantum operation is NOT) with more than 99.99% fidelity is typically above 20 ns [2]. By using the derivative removal by adiabatic gate (DRAG) strategy proposed in [3], this time can be approximately halved.

An alternative developing approach to the implementation of quantum logic is the use of digital devices of superconducting electronics (SFQ) using a sequence of single quantum flux pulses – fluxon. The advantages of this technique are that by miniaturizing some equipment at room temperature and moving it closer to the quantum chip. This makes it possible to reduce the number of cables and connectors connecting room-temperature hardware with a cold chamber. Previously, this technique was successfully experimental applied and it was shown that a regular sequence of single quantum flux pulses [4] allows you to implement quantum operations at times of ~ 60 ns (NOT operation), which is comparable to the microwave technique. Further, it is demonstrated in [5] that the SCALLOP sequence allows accelerating operations up to ~ 24 ns with the same fidelity.

This work further develops the SCALLOP approach by introducing the pulses with negative polarity into the sequences. We consider the possible implementation of a bipolar SFQ pulse generator. Based on the Fourier analysis, we have studied the influence of the shape and duration of the vials on the accuracy of the quantum operations for single transmon qubit. We perform the optimization of the bipolar SCALLOP sequences by the numerical genetic algorithm developed by us aimed at the minimization of leakage from the computational subspace. When constructing pulses of a bipolar SFQ sequence, the input parameters in the algorithm are the qubit transition frequency, the anharmonicity parameter, the gate voltage and the clock frequency of the pulse generator. The control subsequences are readily amenable to storage in compact SFQ-based shift registers. We achieve high-fidelity (>99.99%) quantum qubit operations for a large number of discrete input parameters, as required for low-cross-talk control of a large-scale qubit array designed to implement the surface code. In addition, the control method proposed by us allows us to speeding up the implementation of quantum operations by about more than half, unlike the SCALLOP method [5], for example, the NOT operation for a bipolar sequence has a duration of ~ 10 ns, and the $Y_{\pi/2}$ operation with a duration of ~ 5 ns (for typical transmon frequency 5 GHz and an anharmonicity of 250 MHz).

The work was supported by the RFBR grant 20-07-00952.

1. P. Krantz et al. "A quantum engineer's guide to superconducting qubits". Applied Physics Reviews, **6**, 02131, 2019
2. J. Koch et al. "Charge-insensitive qubit design derived from the Cooper pair box". Phys. Rev. A, **76**, 042319, 2007.
3. J. M. Gambetta et al. "Analytic control methods for high-fidelity unitary operations in a weakly nonlinear oscillator". Phys. Rev. A, **83**, 012308, 2011.
4. R. McDermott and M. G. Vavilov. "Accurate Qubit Control with Single Flux Quantum Pulses". Phys. Rev. Appl., **2**, 014007, 2014.
5. K. Li and R. McDermott and M. G. Vavilov. "Hardware-Efficient Qubit Control with Single-Flux-Quantum Pulse Sequences". Phys. Rev. Appl., **12**, 014044, 2019.

Optical quantum memory in a $Tm^{3+}:Y_3Al_5O_{12}$ crystal waveguide

A.V. Pavlov[1], M.M. Minnegaliev[1], K.I. Gerasimov[1], R.V. Urmancheev[1], T.A. Rupasov[1], E.S. Moiseev[1], A.A. Kalinkin[2], S.P. Kulik[2], S.A. Moiseev[1]

1. Kazan Quantum Center, Kazan National Research Technical University n.a. A.N. Tupolev-KAI, 420111, Kazan, Russia, mansur@kazanqc.org

2. Quantum technology center and, Faculty of Physics, M.V. Lomonosov Moscow State University, 119991, Moscow, Russia

The creation of a quantum memory (QM) integrated into waveguide-resonator systems is a challenging issue for the practical application of quantum memory in quantum communications and computing. The use of waveguide structures in crystals doped with rare-earth ions is an interesting way in the development of an integrated QM. Using the femtosecond laser printing method we fabricated Type-III waveguide structures in a $Tm^{3+}:Y_3Al_5O_{12}$ crystal. The advantage of such waveguide structures is that light with arbitrary polarization can propagate through these waveguides. Moreover, it was shown [1] that in this crystal it is possible to create 2x2 and 3x3 waveguide beam splitters with different power dividing ratios, which makes it possible to manufacture an optical chip with a given logic on one crystal. Such chips are important for further usage in integrated QM circuits. Earlier, in the $Tm^{3+}:Y_3Al_5O_{12}$ crystal, an optical QM protocol was implemented in a revival of silenced echo (ROSE) scheme with addressable writing and reading of input optical signals [2].

In this work an optical QM protocol was implemented in a $Tm^{3+}:Y_3Al_5O_{12}$ crystal single-mode waveguide. Such parameters as an absorption coefficient, coherence time, inhomogeneous broadening of the optical transition line of thulium ions in the waveguide structure and in a bulk crystal were experimentally determined. Also an optical QM protocol was experimentally implemented for weak light pulses in a ROSE scheme. The storage of coherent optical pulses attenuated to the one photon level in the ROSE protocol has been achieved. To determine the transverse spatial structure of the light mode in this waveguide the principal mode was calculated by the finite elements method. The difference in the refractive index between the sections of the crystal treated with a femtosecond laser and untreated ones was estimated in the ranges $1^{*}10^{-3}$ - $3^{*}10^{-3}$. For these parameters the principal mode has a Gaussian shape with transverse half-widths at half maximum of ~ 5.1 μm. This made it possible to determine the effect of the spatial inhomogeneity of the laser beam intensity on the efficiency of the memory protocol under study and to understand the limits of the QM efficiency approachable in such waveguide systems.

This work was performed within the framework of the state assignment - agreement №. 02.03.2020 №. 00075-02-2020-051 / 1 register №. 78 КБК 01104730290059611.

1. N. Skryabin, A. Kalinkin, I. Dyakonov, S. Kulik, “Femtosecond laser written depressed-cladding waveguide 2 × 2, 1 × 2 and 3 × 3 directional couplers in Tm^{3+}:YAG crystal”, Micromachines 11, 1, 2020.
2. M. M. Minnegaliev, K. I. Gerasimov, R. V. Urmancheev, A. M. Zheltikov, S. A. Moiseev, “Linear Stark effect in $Tm^{3+}:Y_3Al_5O_{12}$ crystal and its application in the addressable quantum memory protocol”, Phys. Rev. B **103**, 174110, 2021.

Integrated multiresonator quantum memory

N. Perminov[1,2,*], S. Moiseev[1,2,**]

*1. Kazan Quantum Center, Kazan National Research Technical University n.a. A.N.Tupolev-KAI, 10 K. Marx, Kazan 420111, Russia. * qm.kzn@ya.ru*

*2. Zavoisky Physical-Technical Institute, Kazan Scientific Center of the Russian Academy of Sciences, 10/7 Sibirsky Tract, Kazan 420029, Russia. ** samoi@ya.ru*

The creation of a fully functional multi-qubit quantum computer using superconducting qubits is hampered by the relatively short lifetime of superconducting qubits of several hundred microseconds. In recent works, it has been shown that a system of coupled resonators with a given comb-like spectral structure of resonance lines is capable of playing the role of a highly efficient quantum memory and interface [1] when working with broadband pulses of an arbitrary temporal shape. For such multi-resonator systems, due to optimization, it is possible to provide highly efficient storage of light pulse with a wide spectrum. Moreover the storage time of the quantum memory can be controlled by dynamically switching the coupling constant between the multi-resonator system and external qubit [2].

In this work, a multi-resonator quantum memory scheme based on a system of four interacting resonators coupled through a common resonator with an external waveguide by means of switchable coupling is investigated. Using algebraic methods, the parameters of resonators (frequencies and coupling constants) are optimized, at which the possibility of highly efficient reversible transfer of photonic state into quantum memory with an arbitrary storage time due to reversible dynamics inside the resonator system is shown.

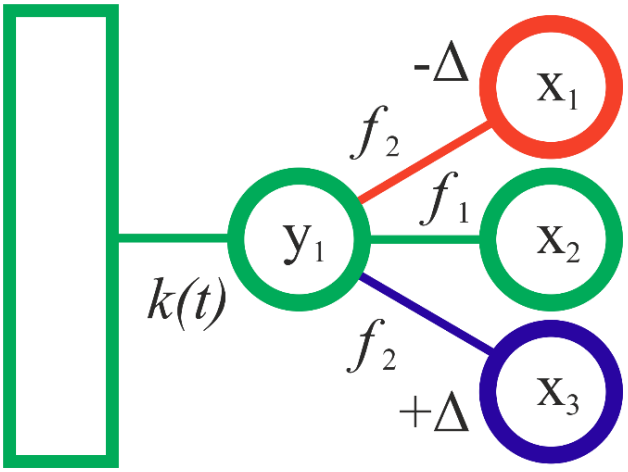

The figure shows a diagram of a four resonator quantum memory connected through a switch $k(t)$ to an external waveguide. When the coupling constant $k(t)\neq 0$ is switched on, the loading/unloading of the waveguide mode to the memory unit of four resonators is realized. With the coupling off $k(t)=0$, a cyclic energy exchange mode is obtained inside the memory unit between a common resonator mode $y_1(t)$ and three additional resonators $x_{1,2,3}(t)$.

In the present study, a matching condition is obtained, providing perfect operations of loading/unloading and storage stage from which it is possible to numerically find the required value of the switched coupling constant $k(t)$ depending on the remaining parameters of the resonator system for efficient loading/unloading of the field into the resonator system. The mode with constant optimal communication allows to ensure full loading and storage of the signal in a finite fixed time, and the use of the communication disabled mode allows the input field to be retained for a large number of storage cycles.

1. Moiseev S.A., et al. "Broadband multiresonator quantum memory-interface." Scientific Reports **8** (1), pp. 1-8, 2018.

2. Moiseev S.A. and Perminov N.S. "Multiresonator quantum memory with switcher." JETP Letters **111** (9), pp. 500-505, 2020.

Quantum memory on atomic frequency comb in a plasmon-polariton waveguide

N.M. Arslanov*, S.A. Moiseev**
*Kazan Quantum Center, Kazan National Research Technical University named after A. N. Tupolev, 420111 Kazan, Russia; * narkis@yandex.ru; ** samoi@yandex.ru*

The practical implementation of quantum information science leads to creation of quantum devices on a chip with integration of different physical qubits. Plasmon-polariton qubits are of great interest due to their strong spatial confinement, enhanced interaction with surface atoms and the possibility of significant acceleration in performing quantum operations. The achieved successes in quantum nanoplasmonics [1] make it relevant to develop nanoplasmonic quantum memory devices, the appearance of which will allow creating more complex quantum devices. We present a nanooptical version of quantum memory for surface plasmon-polariton modes based on their interaction with a Λ-scheme of quantum transitions of atomic ensemble, which is controlled by additional laser radiation acting on an adjacent atomic transition. The theoretical study of quantum memory was carried out for the periodic structure of the inhomogeneous broadening of the Raman atomic transition, using the developed approach in determining the optimal parameters of the nanoscale waveguide structures [2], allowing the propagation of low-losses plasmons.

The quantum memory scheme is not critical to the parameters of controlling laser fields and provides stable conditions for the efficient storage of plasmonic qubits at the condition of sufficiently strong interaction with resonant atomic qubits. The issues of experimental implementation of such memory and its integration into a chip containing single-photon sources and plasmon detectors are discussed.

This work was prepared as part of the state assignment – agreement № 02.03.2020 №00075-02-2020-051/1 registry №78 КБК 01104730290059611.

1. X.Xiong at al, Appl. Phys. Lett. **118**, 130501 (2021).
2. N.M. Arslanov, et al, Las. Phys. **27**, 025103 (2017).

Quantum transistor with multi-qubit memory in an integral waveguide-resonator scheme

Yu.A. Kharlamova, N.M. Arslanov*, S.N. Andrianov, S.A. Moiseev**
*Kazan Quantum Center, Kazan National Research Technical University named after A. N. Tupolev, 420111 Kazan, Russia: * narkis@yandex.ru; ** samoi@yandex.ru*

The modern development of integrated technologies leads to the creation of single-photon light sources, switchers and detectors on a single chip and successful implementation of basic operations with individual qubits. In this work, we present an integrated waveguide-resonator scheme of a quantum transistor with a multi-qubit memory, which could provide efficient realization of two-qubit gates on a system of stored photon qubits. The quantum transistor is realized in an atomic-photon molecule scheme in the form of a linear chain of three interconnected resonators, each of which contains one resonant three-level atom. The side resonators are connected through the waveguides to the quantum memory cells containing long-lived multi-atomic system capable of storage photonic qubits with an arbitrary temporal mode. The time reversible protocols of efficient loading photonic qubits from the quantum memory cells into the quantum transistor are considered by using the fast storage approach developed in [1]. After loading, the photon qubit is transmitted in a controlled manner between the side resonators and transfer into the quantum memory cell. Efficiency of performing a complete set of the operations is analyzed.

Advantages and experimental implementation of the proposed scheme are discussed.

This work was prepared as part of the state assignment – agreement № 02.03.2020 №00075-02-2020-051/1 registry №78 КБК 01104730290059611.

1. N. M. Arslanov, et al, Fast quantum memory on single atom in high-Q cavity Journal of Russian Laser Research **42**, 378–387 (2021).

Author Index

Author Index

Author Index

Author Index

Author Index

Author Index

Author Index

Author Index

Author Index

Научное издание

Труды международной конференции

МИКРО- И НАНОЭЛЕКТРОНИКА – 2021

Сборник тезисов

4-8 октября, 2021, г. Звенигород, РФ

Под редакцией:
В. Ф. Лукичева, чл.-корр. РАН;
К. В. Руденко, д-р. физ.-мат. наук
Составитель: *В. П. Кудря,* канд. физ.-мат. наук

Издание доступно на электронном ресурсе e-LIBRARY
и www.icmne.ftian.ru

Издательство «МАКС Пресс»
Главный редактор: *Е.М. Бугачева*

Напечатано с готового оригинал-макета
Подписано в печать 13.09.2021 г.
Формат 60x90 1/8. Усл.печ.л. 26,75.
Тираж 230 экз. Изд. № 133.

Издательство ООО “МАКС Пресс”
Лицензия ИД N 00510 от 01.12.99 г.
119992, ГСП-2, Москва, Ленинские горы,
МГУ им. М.В. Ломоносова, 2-й учебный корпус, 527 к.
Тел. 8(495)939-3890/91. Тел./Факс 8(495)939-3891.

Отпечатано в полном соответствии с качеством
предоставленных материалов в ООО «Фотоэксперт»
115201, г. Москва, ул. Котляковская, д.3, стр. 13.